*The dissolution of lime in iron silicate melts.*

GREEN, J.

Available from the Sheffield Hallam University Research Archive (SHURA) at:

http://shura.shu.ac.uk/19719/

A Sheffield Hallam University thesis

This thesis is protected by copyright which belongs to the author.

The content must not be changed in any way or sold commercially in any format or medium without the formal permission of the author.

When referring to this work, full bibliographic details including the author, title, awarding institution and date of the thesis must be given.

Please visit http://shura.shu.ac.uk/19719/ and http://shura.shu.ac.uk/information.html for further details about copyright and re-use permissions.

POLYTECHNIC LIBRARY
POND STREET
SHEFFIELD S1 1WB

Ref no. 244650

SHEFFIELD POLYTECHNIC
LIBRARY SERVICE

MAIN LIBRARY

Sheffield City Polytechnic Library

REFERENCE ONLY

Books must be returned promptly, or renewed, on or before the last date stamped above.
FAILURE TO DO SO WILL INCUR FINES
PL/17

ProQuest Number: 10697021

All rights reserved

INFORMATION TO ALL USERS
The quality of this reproduction is dependent upon the quality of the copy submitted.

In the unlikely event that the author did not send a complete manuscript
and there are missing pages, these will be noted. Also, if material had to be removed,
a note will indicate the deletion.

ProQuest 10697021

Published by ProQuest LLC (2017). Copyright of the Dissertation is held by the Author.

All rights reserved.
This work is protected against unauthorized copying under Title 17, United States Code
Microform Edition © ProQuest LLC.

ProQuest LLC.
789 East Eisenhower Parkway
P.O. Box 1346
Ann Arbor, MI 48106 – 1346

# THE DISSOLUTION OF LIME IN IRON SILICATE MELTS

JEFFREY GREEN B.Sc.

A thesis presented for the Degree of Doctor of Philosophy

Department of Metallurgy

Sheffield Polytechnic

NOVEMBER 1975

SHEFFIELD POLYTECHNIC
LIBRARY
669.961Q
GR
THESIS

76-01671

SHEFFIELD CITY POLYTECHNIC LIBRARY
POND STREET

## Preface

The work described in this thesis is submitted for the Degree of Doctor of Philosophy to the Council for National Academic Awards. It was carried out at Sheffield Polytechnic in the period January 1972 - December 1974.

During this period, the author has attended three modules of the MSc course in Industrial Metallurgy. These are:-

1. Process Metallurgy
2. Numerical Methods and Programming
3. Oxygen Steelmaking

In addition, the author attended a conference on 'Refractories for Oxygen Steelmaking' held by the British Ceramic Society in Sheffield in October 1974.

The work described herein is to the best of my knowledge original, except where reference is made to others, and no part of it has been submitted for an award at any college or university.

# Summary

A study has been made of the dissolution of lime in iron silicate melts. The experiments were carried out under an inert atmosphere of argon at 1300°C in a vertical tube furnace. A small cylindrical pellet of lime was preheated to the melt temperature before being immersed in the melt contained in an iron crucible. After a preselected period, ranging from 10 seconds to 9 minutes, the pellet and crucible were withdrawn and water quenched for microscopic examination and electron probe microanalysis.

The reaction between lime and fayalite produced two reaction products, solid dicalcium silicate and a liquid rich in iron oxide. As dissolution proceeded, the precipitated particles of $2CaO.SiO_2$ sintered together to form a tenacious layer between the two reactants.

The rate of dissolution was calculated from the volume loss of partially dissolved pellets. A kinematic model has been derived to fit the qualitative observations and the quantitative results. The rate controlling step was initially the transfer of lime to the liquid - $2CaO.SiO_2$ interface but later the transport of melt became rate controlling.

The effects of manganese oxide, calcium fluoride and boric oxide on the dissolution process were also examined. The presence of manganese oxide in the melt was detrimental to the dissolution of lime. Even though the $2CaO.SiO_2$ particles formed a porous layer, the overall kinetics were retarded by the increased viscosity of the melt. In contrast calcium fluoride and boric oxide accelerated the rate of dissolution by reducing melting points and viscosities.

The rate of dissolution was also increased when the pellet was rotated in the melt.

With large lime pellets, the dissolution rate was lower than that of corresponding smaller pellets in similar melts.

To ascertain whether these results were characteristic only of the dissolution of synthetic hard burnt lime, immersion experiments were carried out using commercially available lime.

# Table of Contents

Page

Preface

Summary

Table of Contents

1. Introduction 1

2. Literature Survey 2

2.1 Oxygen Steelmaking Processes 2

2.1.1 L.D. Process 2

2.1.2 Kaldo Process 4

2.1.3 Rotor Process 5

2.1.4 Bottom Oxygen Blowing Processes 5

2.2 Oxidation of the Metalloids 7

2.2.1 Silicon 7

2.2.2 Manganese 7

2.2.3 Carbon 8

2.2.4 Sulphur and Phosphorus 10

2.3 The Lime Addition 12

2.3.1 Chemical Properties 12

2.3.2 Physical Properties 13

2.3.3 The Quantity of Lime Required 14

2.3.4 The Size of the Lime 14

2.3.5 The Timing of the Addition 14

2.4 Slag Formation 16

2.4.1 The Change in Slag Composition during a Blow 16

2.4.2 Dicalcium Silicate 17

2.5 Possible Methods for Accelerating Slag Formation 19

2.5.1 Soft Burning of the Lime 19

2.5.2 Blowing Pulverised Lime 20

2.5.3 Temperature and Iron Oxide Content of the Slag 20

Page

2.5.4 Flux Additions 20

2.5.4.1 Fluorspar 21

2.5.4.2 Alumina 22

2.5.4.3 Magnesia 23

2.5.4.4 Iron Oxide 23

2.5.4.5 Borates 25

2.5.4.6 Manganese Oxide 26

2.6 Laboratory Techniques developed for studying Lime Dissolution 29

2.7 Reaction Kinetics 31

3 Experimental Work 33

3.1 Starting Materials 33

3.1.1 Lime Pellets 33

3.1.2 Dicalcium Silicate Pellets 36

3.1.3 Preparation of the Melt 38

3.2 Experimental Equipment 41

3.2.1 Cone Fusion Furnace 41

3.2.2 Hot Filament Microscope 41

3.2.3 Immersion Furnace 42

3.3 Experimental Procedures 44

3.3.1 Cone Fusion Studies 44

3.3.2 Determination of the Initial Liquidus Temperature 44

3.3.3 Immersion Experiments 45

3.3.3.1 Specimen Preparation for Microscopic Examination 46

3.3.3.2 Electron Probe Analysis 46

3.3.3.3 Determination of Bulk Volume and Surface Area 47

3.3.4 Penetration Experiments 49

Page

4. Experimental Results and Observations 50

4.1 Lime-Fayalite System 50

4.1.1 Cone Behaviour 50

4.1.2 Initial Liquidus Temperatures 52

4.1.3 Immersion Experiments 53

4.1.3.1 Small Lime Pellets 53

4.1.3.1.1 Electron Probe Analysis 55

4.1.3.2 Large Lime Pellets 56

4.1.3.3 Dissolution Kinetics 57

4.2 Lime-Fayalite + 10 Wt% Manganese Oxide System 58

4.2.1 Cone Behaviour 58

4.2.2 Initial Liquidus Temperatures 59

4.2.3 Immersion Experiments 59

4.2.3.1 Small Lime Pellets 59

4.2.3.1.1 Electron Probe Analysis 61

4.2.3.2 Large Lime Pellets 61

4.2.3.3 Dissolution Kinetics 62

4.3 Lime-Fayalite + Other Fluxes 63

4.3.1 Lime-Fayalite + 10 Wt% Calcium Fluoride System 63

4.3.1.1 Cone Behaviour 63

4.3.1.2 Initial Liquidus Temperatures 63

4.3.1.3 Immersion Experiments 63

4.3.1.3.1 Small Lime Pellets 63

4.3.1.3.1.1 Electron Probe Analysis 65

4.3.1.3.2 Large Lime Pellets 65

4.3.1.3.3 Dissolution Kinetics 66

4.3.2 Lime-Fayalite + 10 Wt% Boric Oxide System 66

4.3.2.1 Cone Behaviour 66

Page

4.3.2.2 Initial Liquidus Temperatures 66

4.3.2.3 Immersion Experiments 67

4.3.2.3.1 Small Lime Pellets 67

4.3.2.3.1.1 Electron Probe Analysis 67

4.3.2.3.2 Large Lime Pellets 67

4.3.3 Chemical Loss 68

4.4 Dicalcium Silicate - Fayalite System 69

4.4.1 Immersion Experiments 69

4.4.1.1 Electron Probe Analysis 69

4.4.1.2 Dissolution Kinetics 69

5. Discussion 70

5.1 The Dissolution of Small Lime Pellets in Fayalite 70

5.2. The Effect of Manganese Oxide 77

5.3 The Effect of Other Fluxes 81

5.4 The Effect of Pellet Rotation 83

5.5 The Effect of Pellet Size 85

5.6 Rate Controlling Mechanism 87

5.6.1 Small Lime Pellets 87

5.6.2 Large Lime Pellets 88

6. Conclusions 89

7. Suggestion for Future Work 91

8. Appendices 92

9. References 95

10. Acknowledgements 101

Tables

Figures

Plates

## 1. Introduction

With the advent of oxygen steelmaking and the accompanying shorter refining times, the early formation of a fluid basic slag is important in ensuring favourable desulphurisation and dephosphorisation. For this reason it is desirable that the lime addition is rapidly fluxed to promote slag formation. However despite the widespread use of basic oxygen furnaces (B.O.F.) slag formation is unpredictable with sulphur and phosphorus removal at variance. The reaction mechanisms accounting for the variations experienced are not fully understood nor are the singular and collective effects of the number of constituents (hot metal analysis, blowing practice, lime quality and quantity) involved. In order to explain the dissolution of lime in multicomponent systems, a knowledge of the phase relationships in the $CaO-FeO-SiO_2$ system is essential since these three components form the basis of steelmaking slags.

A study has been made of the dissolution behaviour of synthetic hard burnt lime pellets in an iron silicate ($2FeO.SiO_2$) melt. During reaction the lime becomes encapsulated by a precipitated layer of dicalcium silicate, which retards further dissolution. It is common practice in the B.O.S. process to add small amounts of fluorspar to accelerate slag formation. However this addition has become very expensive, consequently the steel industry is currently examining possible substitutes such as manganese ore and borates. To study the influence of fluxes, the immersion experiments were repeated with additions of manganese oxide, calcium fluoride and boric oxide made to the base melt.

# 2. Literature Survey

## 2.1. Oxygen Steelmaking Processes

Even though Bessemer produced patents covering the use of pure oxygen for steelmaking, it was not until the 1930's that tonnage oxygen (Linde Frankl Process) became a reality. Since those early days pneumatic injection has gone full circle from the original bottom air blown Bessemer, through the side blown Tropenas (1) and the top blown L.D. and Kaldo to the bottom blown oxygen converter (Q.B.O.P.). A number of books and articles have been published on these steelmaking processes (2,3,4) whilst others have examined the physico - chemical reactions taking place during refining (5,6).

### 2.1.1 L.D. Process

The initials L.D. stand for Linz-Donawitz the region in Austria where the process was developed. The expansion of the process during the last twenty years can be judged by the increase in converter capacity from the original 25-30 tonnes to the modern day 200-300 tonne vessels.

The refining vessel is pear-shaped with an open top, through which a water cooled lance is lowered towards the metal surface. Commercially pure (99.5%) oxygen is injected through the lance, leaving at supersonic speed through a single or multiholed nozzle (7). The use of oxygen gives a favourable heat balance such that up to 30% scrap can be used to make up the charge. (Air injection in the Bessemer process limits the scrap charge to 7% (4) ).

A material flow chart for the L.D. converter is shown (8) overleaf.

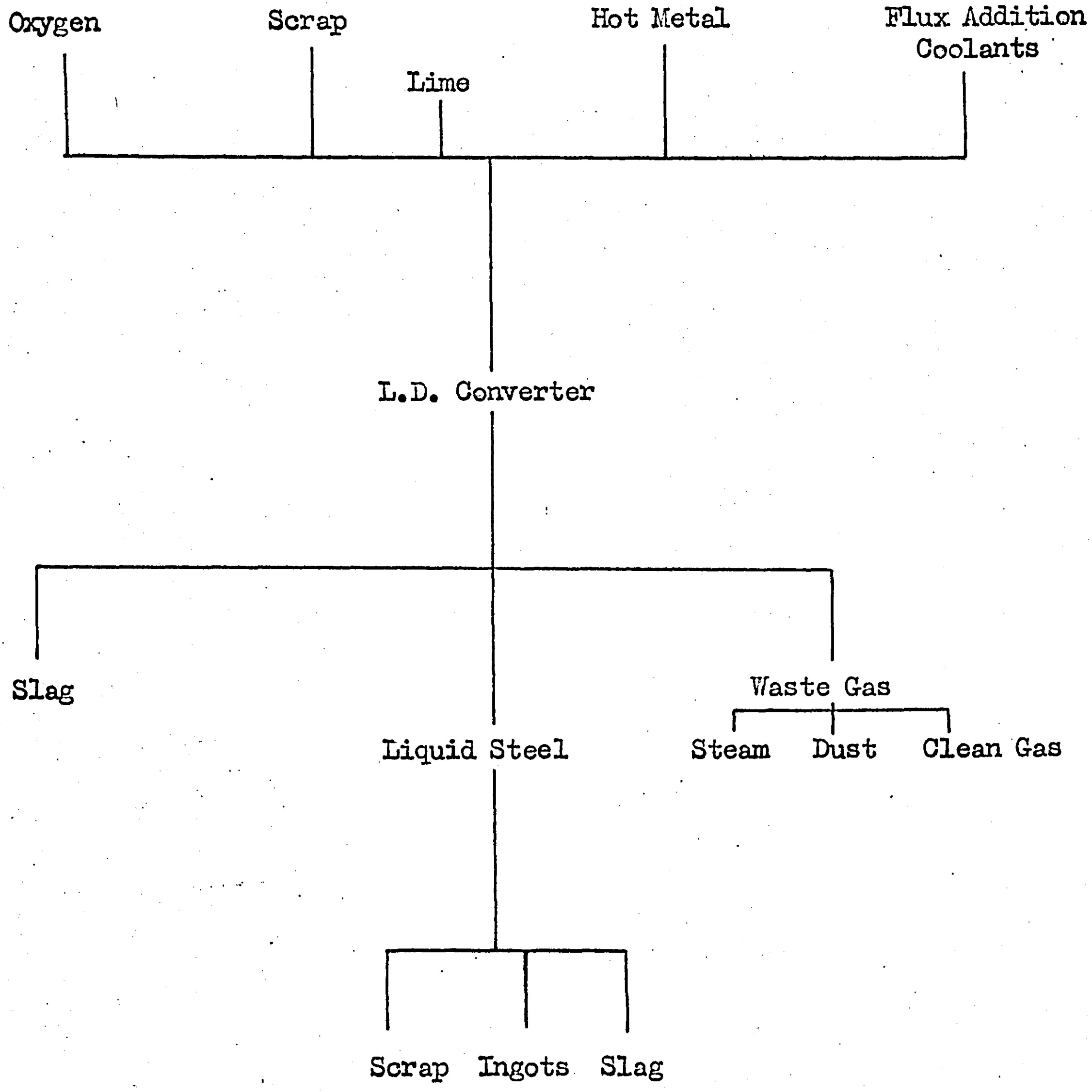
Oxygen
Scrap
Lime
Hot Metal
Flux Addition
Coolants
L.D. Converter
Slag
Liquid Steel
Waste Gas
Steam
Dust
Clean Gas
Scrap
Ingots
Slag

The charge varies from plant to plant, the differing proportions of hot metal, scrap and lime being dependant upon local conditions. From the initial successes achieved with Austrian low phosphorus iron, later trials proved that the process could be adapted for high phosphorus (1-2%) hot metal (9).

After rotating the vessel into the vertical position, oxygen is blown at the rate of 500 $m^3$ per minute. A typical blow on a 200 tonne heat lasts 20-25 minutes (10) during which approximately 10 tonnes of oxygen are consumed. The process requires no external fuel source since the thermal energy requirements are supplied by the hot metal and the oxidation of the metalloids (silicon, carbon, manganese and phosphorus). Because of the heat generated in the vessel, coolants have to be added to achieve the correct tapping temperature. Although scrap is the usual choice, this may be in short supply so that iron ore (11) or sponge iron (12) may be used.

New techniques are continually being developed to increase the potential of the L.D. process. An investigation in America (13) has demonstrated that the L.D. can operate with a 100% scrap charge provided that it is preheated and supplemented with additional fuel (100 kg of coke per tonne of scrap). At the time (1969) when the report was published, nitrogen pickup was limiting the possible applications of the steel.

A recent development of the L.D. refining technique is the Rotavert process. The converter is similar in shape to an ordinary basic oxygen furnace (B.O.F.) but it can rotate around its vertical axis at high speed (85 rpm). Results from heats carried out in a 6 tonne pilot vessel indicated that the speed and change of rotational direction increase the rate of slag-metal reactions (14). It remains to be seen whether these findings are repeated in a full scale converter. One rotating steel refining technique that has made the transition from pilot plant to commercial production is the Kaldo Process.

### 2.1.2 Kaldo Process

The process (15) was developed in Sweden specifically for refining local high phosphorus irons. The vessel is rotated up to 30 r.p.m. in an inclined position ($20^{\circ}$) so that the melt covers half of the back wall. This practice avoids overheating of the lining when carbon monoxide (from the oxidation of carbon) is burnt to carbon dioxide by a secondary oxygen jet above the bath.

Dephosphorisation is mainly dependent upon the oxidising potential (iron oxide content) of the slag. This can be increased either by (16)

a. Keeping the rotation speed low

or b. Blowing the oxygen jet more vertically onto the bath

In refining basic bessemer iron (1.76% phosphorus) at Domnarvet, it was found desirable to lower the carbon content from 3.5% to between 1%-2% before oxidising phosphorus. This was achieved by rotating the vessel at full speed at the beginning of the blow. The speed was then reduced to raise the iron oxide content of the slag for dephosphorisation and finally towards the end of the blow, the speed was again increased to obtain a low slag iron content. Although primarily developed for refining high phosphorus irons, the process will also produce high quality steel from raw materials of variable composition.

In 1966 Pearson et al (6) compared the operation of the L.D. and Kaldo vessels at Consett. They found that the L.D. was faster for the same size of unit (100-130 tonnes) as a result of the ability to inject greater volumes of oxygen without spillage. However the heat evolved by the combustion of carbon monoxide to carbon dioxide allowed a higher scrap charge (31-35%) in the Kaldo compared to 25% in the L.D.

### 2.1.3 Rotor Process

Although originally commisioned for pretreating blast furnace metal for final refining in the open hearth process, later investigations showed that the process could refine high and low phosphorus iron in a similar manner to the Kaldo. The first 60 tonne Rotor (17) had a tap to tap cycle time of 2 hours.

The furnace consists of a long cylindrical vessel, open at one end for charging and oxygen injection and at the other for tapping and waste gas removal. Oxygen is blown through 2 lances, primary oxygen is introduced beneath the metal surface for oxidation and stirring of the bath. The secondary lance blows oxygen or enriched air (4) above the metal surface where carbon monoxide is burnt to carbon dioxide.

Unlike the Kaldo, rotational speed (0-2 rpm) has no great influence on the refining process. The progress of a blow is controlled by the oxygen flow (primary and secondary) rates and the position of the lances in the furnace.

In the United Kingdom the two rotary processes never gained the popularity expressed by foreign authors, for both the Rotor and the Kaldo, rotation proved an expensive engineering innovation. In comparison, the strength of the L.D. process lies in its simplicity and its rapid rate of refining of imported low phosphorus irons.

### 2.1.4 Bottom Oxygen Blowing Process

The air blown Bessemer has continually been handicapped by a low scrap charge and a high nitrogen content in the hot metal. The replacement of air by oxygen was examined by Brotzmann (18). He found that the nozzles reacted with the oxygen, burning away in a few minutes. Water cooling was too dangerous and porous nozzles proved unsuccessful due to slag penetration.

Oxygen mixed with steam (1:1) as a cooling agent had been tried with some success (19) but the scrap consumption was limited to only 15 per cent. Renewed interest arose in the 1960's following a breakthrough in nozzle design. The refractories could be protected by enveloping the oxygen in a gaseous or liquid shield. In the converter, each of the tuyeres consists of an inner copper tube for the oxygen and an outer steel tube forming an annular passage for the coolant, (propane, natural gas or a liquid fuel oil) (20). Instead of generating heat (21) the fuel vapourises and cracks endothermically which creates increased cooling at the tuyere and greatly extends the life of the refractory bottom (one bottom per converter lining (22) ).

Scrap charges as high as 26% have been quoted for a 30 tonne converter (21) with a predicted 33% for a 200 tonne converter with lower heat losses. Even with a short refining time (tap to tap time of 30 minutes) the bath and slag were closer to equilibrium than in the L.D., whilst the improved sulphur removal was associated with better gaseous desulphurisation (22). Refractory consumption was low, only 5 kg per ingot tonne even with high phosphorus irons.

As of 1972 the total capacity of oxygen bottom blown converters was 9.75 million tonne, with U.S. Steel commisioning the world's largest at 200 tonnes (23). Although there appears to be some justification for modifying air blown Bessemers and replacing open hearth furnaces, there is still insufficient saving for the scrapping of modern LD plants.

## 2.2 Oxidation of the Metalloids

The object of steelmaking is to partially or completely remove the impurities present in the raw material, iron. Pig iron, the product of the blast furnace contains about 4% carbon (dissolved from the coke), up to 2% phosphorus (P), 2.5% silicon (Si), 0.1% sulphur (S) and 2.5% manganese (Mn) (24). The basic thermodynamic data for the oxidation reactions seems to be well documented (3, 25) and the predicted order of removal of the elements in terms of their oxygen potential has been calculated. The theoretical order of removal would be Si-C-Mn-Fe-P, however the actual sequence is Si-Mn-C-P-Fe. The change in concentration of the various elements is shown in Plate 1. The smooth curves shown, whilst generally true cannot be applied to any specific blow.

In the impingement zone, under the lance, oxygen goes into solution with some oxidation of the bath surface (26)

$$\tfrac{1}{2}O \rightleftharpoons [O]$$

$$Fe + [O] \rightleftharpoons (FeO)$$

$$2(FeO) + \tfrac{1}{2}O_2 \rightleftharpoons (Fe_2O_3)$$

### 2.2.1 Silicon

This is the first impurity to be oxidised

$$[Si] + 2[O] \rightleftharpoons (SiO_2)$$

$$[Si] + 2(FeO) \rightleftharpoons (SiO_2) + 2Fe$$

with complete oxidation occurring at about a quarter of the way through the blow (27).

### 2.2.2 Manganese

Like silicon, manganese forms an oxide more stable than iron oxide

$$[Mn] + [O] \rightleftharpoons (MnO)$$

$$[Mn] + (FeO) \rightleftharpoons (MnO) + Fe$$

The oxidation process can be divided into 3 stages. Initially manganese undergoes rapid oxidation. This is followed by a period of reversion due to the reduction of the slag during decarburisation, but as the carbon removal rate decreases towards the end of the blow, manganese is again transferred to the slag. The final distribution being dependent upon the temperature (28) and the iron oxide content of the slag. According to Welbourn and Kulig (106) there is an inverse relationship between oxygen combined with manganese in the slag and oxygen combined with iron as FeO and $Fe_2O_3$.

### 2.2.3 Carbon

Whereas silicon and manganese are transferred as oxides into the slag, carbon is removed as its gaseous oxide, carbon monoxide. Vasher and Hamilton (29) showed that at low carbon contents $\%C \times \%O = 0.0025$ at 1600°C. This work was extended by Marshall and Chipman (30) who found the product was not a constant at any given temperature but increased slightly with increasing carbon content.

With the low solubility of carbon monoxide in iron, the carbon-oxygen reaction has to take place at a gas-liquid interface. Although some carbon removal can and almost certainly does take place directly from the bath, by transfer to rising heterogeneously nucleated bubbles, this simple mechanism does not account for the high rate of transfer.

During plant investigations on a 200 tonne B.O.F., Meyer (31) found that slag blown out of the converter contained droplets of metallic iron. This led to the theory that the majority of refining was carried out in a slag-metal emulsion where the surface area for reaction could be $10^6$ $cm^2$ per tonne and up to 30% of the metal charge might be emulsified at any one time. Formation of the emulsion begins almost as soon as refining itself. The oxygen jet on striking the metal surface causes a depression and eventually if the momentum is increased sufficiently, splashing occurs with metal droplets being thrown up into the gas or slag. Meyer's concept of decarburisation was that oxygen was pumped into the metal droplets from the oxidising slag so that a carbon monoxide equilibrium pressure of up to 100 atmospheres or more can be built up. The droplet comes into contact with a carbon monoxide bubble into which its own carbon monoxide is unloaded,or by explosive nucleation within the droplet (32) or possibly by nucleation at a metal-solid interface.

At the beginning of refining, metal droplets containing not only carbon but also silicon and manganese exist in the slag. Therefore while some 'new' silicon-containing droplets are undergoing their first oxidation cycle, others are already into later cycles and are beginning to lose carbon. Thus, for the system as a whole, carbon, silicon and manganese are all being oxidised in different places simultaneously.

Since Meyer's work, Kootz and Altgeld (33) have published an alternative and conflicting mechanism. They found that in the oxygen converter and the basic Bessemer, decarburisation occurred even when the slag became so viscous that reactions in the slag-metal emulsions could no longer proceed. Their theory proposed that supersaturated iron is rapidly transported in a radial direction from below the lance. Bubbles of carbon monoxide are heterogeneously nucleated at the metal-slag interface, the reaction continuing as the metal circulates outwards towards the vessel wall. Price (34) has also concluded that the calculation of Meyer as to the amount of refining in the slag was an overestimation. Price's estimate of refining in the foam was about 35%, again placing more emphasis on the removal of carbon in the bath. His work, however only dealt with the second half of the blow. Unlike Meyer's technique of analysing slag overflow samples, Price's samples were obtained from the condensate on a bomb chain attachment. At this stage it is very difficult to say what proportion the differing mechanisms contribute to the overall decarburisation rate.

### 2.2.4 Sulphur and Phosphorus

The removal of these two elements presents a problem for the steelmaker since their oxides are less stable than iron oxide at steelmaking temperatures.

Ward (28) quoted an equation for predicting the sulphur level in the refined steel in terms of a series of parameters

$$\%\ [S] = 0.11 + 23.6\ S_1 - 0.003\ V - 0.003\ Fe - 0.00\,005T$$

$[S]$ = turn down sulphur content

$S_1$ = charged sulphur content of the metallic charge

$V$ = basicity ratio

$Fe$ = % iron in slag

$T$ = turn down temperature °C.

Desulphurisation, is therefore favoured by a high slag basicity, high temperatures and a high slag iron content. However the cost of controlling the slag iron content to the extent required is far in excess of that for lime control. Even with a highly basic fluid slag, sulphur elimination in the LD vessel is relatively inefficient (35). To achieve low sulphur levels, further desulphurisation can be carried out after tapping by adding a synthetic basic slag to the ladle. These slags are similar to white electric arc slags, but differ from them by lower basicity and the absence of fluorspar, the iron oxide content being 0.45% - 0.55%.

Whereas a basic slag may achieve a degree of desulphurisation of 40%, the degree of dephosphorisation may exceed 90 per cent (36).

The phosphorus reactions have been written as

$$2[P] + 5[O] \rightleftharpoons (P_2O_5)$$

$$(P_2O_5) + 3(O^{2-}) \rightleftharpoons 2(PO_4^{3-})$$

The strength of the attraction between the $PO_4^{3-}$ ion and the cation of the basic oxide is reflected in the high negative heats of formation, such that in basic slags, the activity coefficient of $P_2O_5$ can be as low as $10^{-18}$ (3). Generally low temperatures have been quoted as a condition for good dephosphorisation (25, 37) however laboratory experiments by Kurita et al (38) using a FeO-CaO slag indicated a positive dependance of the dephosphorisation rate on temperature. Although factors such as temperature are important, desulphurisation and dephosphorisation depend primarily upon the formation of a basic slag.

The relative dephosphorising power of the various divalent basic oxides is shown below (25)

| $Ca^{2+}$ | $Mg^{2+}$ | $Mn^{2+}$ | $Fe^{2+}$ |
|---|---|---|---|
| 30,000 | 1000 | 3 | 1 |

Of the above $Ca^{2+}$ (lime) contributes the most towards desulphurisation.

## 2.3 The Lime Addition

Although lime does not occur free in Nature, it can be produced easily by the calcination of limestone ($CaCO_3$). Above 900°C limestone breaksdown to give lime and carbon dioxide

$$CaCO_3 \longrightarrow CaO + CO_2$$

Today lime burning is carried out in rotary kilns, rotary hearth kilns and fluidised beds where the process time is 3 hours compared to 1-2 days with the older shaft kilns (39).

The required chemical and physical properties have been summarised by Anderson and Vernon (40).

### 2.3.1 Chemical Properties

The purity of the lime should be as high as possible, a typical specification is given below:-

$CaO > 95\%$
$SiO_2 < 1.0\%$
$MgO < 1.5\%$
$S < 0.05\%$
Loss on Ignition $< 3.0\%$

The silica and magnesia impurities arise from the original limestone deposit. A 2% silica content in the limestone becomes roughly 4% after calcination, consequently additional lime is required to achieve a satisfactory basicity. Although the quoted level of MgO was $< 1.5\%$, higher levels have been tolerated where the magnesia has proved effective in reducing lining wear (41).

[Also discussed in section 2.5.4.3]

Tait and Lewis (8) found that while 45% of the total sulphur load originated in the blast furnace, 15% came from burnt lime contaminated by the fuel during calcination. In Germany (42) the sulphur level is 0.02%S on lime from rotary kilns fired by natural gas compared to 0.06% - 0.09% found on lime from coal fired shaft kilns. The loss on ignition is the percentage weight loss which occurs on reheating the calcined lime. Although it can indicate underburning, it is usually associated with the evolution of $CO_2$ and $H_2O$ adsorbed from the atmosphere during transportation (43) and storage.

### 2.3.2 Physical Properties

The theoretical density of lime is 3370 kg $m^{-3}$ but soft burnt lime has only a bulk density of 1600 kg $m^{-3}$ (60% porosity). With increasing burning time or calcination temperature, the individual particles begin to coalesce so that the porosity decreases to 25 - 30 per cent. To assess the degree of burning, various reactivity tests have been developed (44, 45).

These are:-

1. The Coarse Grain Test
2. The A.S.T.M. Test
3. The German Test
4. The G.L.A.C. Test

The tests follow the kinetics of the reaction

$$CaO + H_2O \longrightarrow Ca(OH)_2$$

by the heat evolved or by titrating the hydroxide with acid. The results can be misleading as shown by the work of Eades and Sandberg (46).

| reactivity temperature rise after 60 secs. | surface area |
|---|---|
| 29°C | 5.14 $m^2$ $gram^{-1}$ |
| 30°C | 2.07 $m^2$ $gram^{-1}$ |

False results can occur when there is a thin layer of calcium hydroxide on the surface of the lime. Generally, whilst reactivity tests are used by the supplier, the receiver favours bulk density as a quality control check. Even so quoted porosity figures do not differentiate between the different forms of voidage, fissures, pores and microporosity.

### 2.3.3 The Quantity of Lime Required

The amount required for the formation of a basic slag (2:1 lime to silica ratio) is dependent upon the chemical analysis (sulphur, phosphorus and silicon) of the charge; the final figure being determined by melting shop experience. A basicity ratio in excess of 3(47) is usually aimed for, with the excess amount compensating for the lime which remains undissolved (48).

### 2.3.4 The Size of the Lime

Welbourn and Kulig (49) suggested that the lump size should have a marked effect on lime dissolution since the smaller the size, the greater the surface area to volume ratio. This reasoning would be justified if the lime had theoretical density but the actual surface area depends upon the voidage in each lump. Practical results have shown that the most suitable size range is 12 mm - 40 mm. Above 40 mm, lime becomes impractical to calcine and below 6 mm a large proportion is lost in the exhaust gases (50) of the refining vessel.

### 2.3.5 The Timing of the Addition

This varies from plant to plant, it can be either

1. at the beginning of the blow

or 2. in batches during the blow

In comparative trials, Nilles et al (51) found that lump lime had to be added progressively through the blowing period for efficient dephosphorisation. Investigators at C.A.P.L. have reported that a four fold increase in the lime addition at the start of refining less than doubled the amount dissolved after 5 minutes (52).

The importation of low phosphorus iron ore into Britain means that only a single slag is necessary to reduce the phosphorus level from 0.4% to 0.015 percent (28).

In Europe where the hot metal contains 1% - 1.2% phosphorus, a double slagging technique has been evolved. Before the phosphorus pentoxide content gets too high, the first slag is removed and a further addition of lime is made to the vessel. At the end of the blow, the final slag contains less than 6% $P_2O_5$ and 20 - 25% FeO (53). Because of the high FeO content, the slag is retained to promote lime dissolution in the next heat.

## 2.4 Slag Formation

Chemical analysis provides an easy technique for studying slag development during refining. However even though the main slag constituents are lime, iron oxide and silica, the ternary CaO - FeO - $SiO_2$ phase diagram cannot be used to plot slag compositions. This is because the oxygen potential and other minor oxides in the slag can appreciably extend the liquidus region of the simple three component system (10). From the basic ternary, Tromel and Gorl (54) developed the CaO - $SiO_2$ - (FeO + MnO + MgO) system for representing slag equilibria, later superseded by the quaternary CaO - FeO - MnO - $SiO_2$ and the quinternary CaO - FeO - MnO - MgO - $SiO_2$ (55).

Some investigators (26) dislike this method of representation saying that five component systems are too complex and difficult to manipulate. As a compromise Bardenheuer (56) produced a pseudo ternary ($CaO^1$ - $FeO^1$ - ${SiO_2}^1$) for a particular slag composition where the three main components make up 80% of the total composition. The major difference between the pseudo diagram and the CaO - FeO - $SiO_2$ diagram of Allen and Snow (57) is the contracted phase field of dicalcium silicate.

### 2.4.1 The Charge in Slag Composition During a Blow

After charging with scrap and hot metal, the LD vessel is turned up and further additions (lime and fluorspar) are made prior to blowing. Some of the silicon in the hot metal will have oxidised by reacting with the atmosphere, the balance along with manganese and some iron being oxidised in the first few minutes of blowing with oxygen.

These three oxides, FeO, MnO and $SiO_2$, contribute to an initial rapid solution of lime which moves the bulk slag composition away from the ${SiO_2}^1$ - $FeO^1$ binary (Fig. 1).

The iron droplets (rich in carbon) thrown up by the jet react with oxygen and the iron oxide component of the slag. The evolution of carbon monoxide causes the bath to foam (58). To prevent the slag overflowing the vessel, the lance is lowered which results in a decrease in the iron oxide content of the slag. If the lance is lowered too far, the reduction of iron oxide proceeds at a faster rate than the formation of fresh oxide. The resultant viscous slag becomes incapable of sustaining a high decarburisation rate.

With an increasing lime content, the slag composition enters the dicalcium silicate ($2\ CaO.SiO_2$) phase field which coincides with the appearance of maximum foaming (56). The precipitation of solid $2\ CaO.SiO_2$, and its effect on the surface tension and viscosity of the liquid slag (59, 60, 61) prevents the decantation or coalescence (collapse) of the emulsion (62).

Unlike the bottom blown process (3) carbon removal in the L.D. rapidly decreases towards the end of the blow. As a consequence, the foam starts to collapse and the slag composition moves towards the $CaO^1 - FeO^1$ binary (Fig. 1) due to the secondary oxidation of the bath and increased fluxing of the remaining lime.

The slag temperature climbs very rapidly, as shown typically by the data of Bardenheuer (56). For the last 80% of the blow, the slag temperature remains between 1550°C - 1650°C.

### 2.4.2 Dicalcium Silicate

At the beginning of refining, the concentration path between dissolving lime and the bulk ($FeO - MnO - SiO_2$) slag intersects the $2\ CaO.SiO_2$ + liquid phase field. When the saturation concentration is exceeded, a thin layer of $2\ CaO.SiO_2$ is precipitated around the lime. The shell does not directly adhere to the lime surface, but is separated from it by an oxide skin and very often a $3\ CaO.SiO_2$ layer as well (63, 64). Electron microprobe analysis of slag samples showed the precipitated layer to be a complex solid solution [$2\ CaO.SiO_2 - 3\ CaO\ P_2O_5$] with calcium partly substituted by iron and manganese, and the silica by phosphorus pentoxide.

Many experiments in steel plants (64) and laboratories (65) have shown that the formation of $2\ CaO.SiO_2$ retards the dissolution of lime, and as a consequence can lead to increased refractory wear in the converter. Even with enhanced slag resistance (impregnation of the basic refractories with tar-pitch mixtures) the magnesite and dolomite bricks are still vulnerable to chemical attack during the early period of refining when the slag is acid in nature. If the rate of lime dissolution is too slow, the acid slag will be neutralised by the lime and magnesia in the refractory lining.

## 2.5 Possible Methods for Accelerating Slag Formation

In order to produce a fluid basic slag earlier than occurs in the normal order of reactions in the converter, various modifications can be made to the lime addition and the blowing practice. When comparing these alternatives with flux additions, the improvement must be justified in terms of cost, process control and most important the removal of sulphur and phosphorus.

### 2.5.1 Soft Burning of the Lime

One method is to use lime with a large surface area. Behrens et al (48) concluded that soft burnt lime produced faster dephosphorisation and better desulphurisation as well as a cleaner blow with less slopping. However Gregory et al (47) found no advantage in using soft burnt lime, but this inconsistency may be due to the hard burnt lime being briquetted into pellets while the soft burnt lime was in the form of fragments. Reinders et al (66) came to the conclusion that any advantage from soft burnt lime dissolving faster, was not reflected in more favourable results at the end of the blow. They found no correlation between the degree of desulphurisation and the calcination of the lime.

Investigations by Obst et al (67) gave the explanation for the conflicting opinions. From laboratory experiments and later plant trials, they concluded that during the period of slag formation, recrystallisation and grain growth of soft burnt lime occurs very rapidly. The porous lime became dead burnt within 10 minutes at 1600°C. This became very apparent when making certain carbon steels, the soft burnt lime became hard burnt at a faster rate than it was being dissolved. If dissolution is impaired ($2\,CaO.SiO_2$ layer) charging soft burnt lime produces no advantage.

### 2.5.2 Blowing Pulverised Lime

The problem of lime burning can be overcome to some extent by reducing the size of the lime. In contrast to normal LD practice of adding lump lime (10 - 40 mm) the L.D.A.C. process (68, 69) uses crushed lime (0.5 - 1.5 mm) which is progressively injected into the refining vessel. The process can utilise lime of very different compositions and physical properties because blowing it in the oxygen stream gives a remarkable reactivity whatever the nature of the lime (70).

Lime injection has not been restricted to L.D. vessels, it has also reduced the refining time in the open hearth (71) and bottom blown processes (72). In recent years several steelplants in Britain have stopped using the L.D.A.C. process (73). This has coincided with the importation of low phosphorus iron ores.

### 2.5.3 Temperature and Iron Oxide Content of the Slag

Referring to the $CaO^1 - FeO^1 - SiO_2{}^1$ phase diagram (Fig. 1), effective dephosphorisation has been found to occur only below the $2\,CaO.SiO_2 - FeO^1$ join (56, 74). To avoid the retarding influence of encapsulation, the slag composition can either go over or around the $2\,CaO.SiO_2$ + liquid phase field. Schürrman et al (75) found that in the open hearth process, lime dissolution was improved by increasing both the temperature and iron oxide content of the slag. In the LD process, these two parameters can be changed by adjusting the lance height. As the lance is raised, the oxygen jet becomes softer and less penetrating with only the surface layers being oxidised (52). However this method has certain disadvantages, noteably a lower metal yield and increased refractory wear.

### 2.5.4 Flux Additions

This has been the most widely used technique forpromoting slag formation. The fluxes can enhance lime solution by several different mechanisms:-

1. Alter the phase equilibria in the slag system such that dicalcium silicate shell formation is limited
2. Lower the melting point of $2\ CaO.SiO_2$
3. Change the physical form of the $2\ CaO.SiO_2$ encapsulating layer.

Fluorspar ($CaF_2$) has been the major flux addition in the past, but future supplies may be insufficient to meet the demand. Consequently steelplants are carrying out a wide ranging search for an alternative. Possible substitutes are alumina, magnesia, iron oxide, borates and manganese oxide.

### 2.5.4.1 Fluorspar ($CaF_2$)

There are three reasons for the increasing demand for fluorspar (76) :-

1. The rapid rise in basic oxygen and electric arc steelmaking capacity. These two processes consumed 2 million tonnes of fluorspar in 1972.
2. The high growth rate in world aluminium production
3. A further increase in the production of fluorocarbon products.

The effect of fluorspar is to depress the slag melting point, by forming low melting point eutectics (77, 78). Generally the amount added does not exceed 8 kg per tonne of steel (36). However this figure can be reduced by using lime-fluorspar briquettes (79). Fluorspar briquetted with mill scale and ferromanganese blast furnace downcomer dust has been used for a number of years by the United States Steel Corporation (80).

Holappa (11) found that fluorspar produced an instantaneous increase in slag fluidity, but its effect was of short duration. For the best results, fluorspar had to be added in small amounts , 1 kg per tonne of steel at a time.

There are a number of disadvantages associated with fluorspar:-

1. Primarily its use increases refractory wear in the same way as it improves slag formation
2. Economically, the finishing slag cannot be sold as fertiliser because calcium fluoride renders the phosphate insoluble.

#### 2.5.4.2 Alumina ($Al_2O_3$)

During World War II, aluminium dross was reported to be a satisfactory substitute for fluorspar (81). In more recent times other alumina-bearing materials have been suggested such as bauxite, red mud and alumina grinding residues (82). In comparative trials carried out by Holoppa (11), the results indicated that bauxite (6 kg per tonne of steel) was not as effecient as fluorspar but its influence was more permanent.

Successful laboratory trials (83) have been reported using lime pelletised with red mud[overall composition 42.2% CaO 21.6% $Al_2O_3$]. Later the pellets were used in a 6 tonne converter replacing one third of the normal lime addition. The addition of the pellets accelerated lime solution when compared with a normal lime charge.

In 1972 Nikkai Sangyo (84) built a plant to produce a fluorspar substitute based on red mud. The product known as "Alblack" contains 40-45% alumina, 20-25% iron oxide and 8-10% silica. No figures are available on its effectiveness as a lime flux.

### 2.5.4.3 Magnesia MgO

Initially magnesia was added to the slag in order to increase the service life of the lining (44, 45). During a heat, the slag absorbs up to 6% MgO, but if magnesia is added in the form of doloma (dolomitic lime), there is a corresponding decrease in refractory attack. At Jones and Laughlin (85) the policy is to aim for a concentration of 7.4% MgO in the slag by adding dolomitic lime. Despite the increase in slag MgO, data analysis revealed no evidence that desulphurisation was adversely affected. Similar results have been reported by Russian workers (86) who aimed for MgO levels of 4-7% in the finishing slag. The effect of magnesia in terms of accelerating slag formation was such that the fluorspar addition could be halved. The iron oxide content of the slag dimished, increasing the metal yield and metal desulphurisation.

In contrast,Harhai and Dukelow (87) reported that with a 8.5% level in the slag, magnesia was detrimental to sulphur removal because of high slag viscosity and the low desulphurising potential of magnesia relative to lime. Magnesia (50) was also a problem at the Voest steelplant where the dolomitic lime had a varying MgO content. When lime (10% MgO) was used, the wear resistance of the lining decreased by 5%, this was due to increased fluxes necessary for lime dissolution. On the basis of their findings (over a 8 month period) a maximum permissible MgO level of 3.5% was fixed for the lime.

### 2.5.4.4 Iron Oxide $FeO_x$

Iron oxide is one of the most effective fluxes of lime, for in both the FeO - CaO and $Fe_2O_3$ - CaO systems the initial liquidus temperature is below 1300°C (77).

One way of adding iron oxide is to recharge the dust from L.D.

collectors. This practice is used in Finland (11). Because of the addition, the high lance practice in the initial period of the blow was found to be unnecessary nor were additional fluxes (fluorspar) required.

The agglomeration of L.D. dust with limestone into briquettes and pellets prior to calcination has been tried in Germany (79). Compared with heats using only lime, the charging of the special lime pellets resulted in a considerable acceleration of dephosphorisation. Another advantage of prefluxed pellets is the low rate of hydration when compared to soft burnt lime (88, 89). Millscale is another iron oxide flux (90). By calcining limestone in the presence of millscale (c.f. case-carburising) a 10mm thick layer of dicalcium ferrite (1400°C mpt.) is formed on the surface of the lime.

Swedish iron ore (86.3% $Fe_2O_3$ — 9.8% FeO) has been proved to be a good lime flux (91). However additions of more than 26% did not result in a proportional increase in dissolved lime. When the ore was added in the first quarter, slopping generally occurred after 50% of the blowing time compared to 75% when the ore was added in the second quarter. Even so there was no trouble with phosphorus or sulphur removal. Iron oxide forms the major proportion of ilmenite (52% $FeO_x$, 33% $TiO_2$) currently being marketed as a replacement for fluorspar (92). Although it has a high melting point, laboratory tests showed it was superior to fluorspar for lime dissolution. However in trials carried out at Bethlehem Steel, ilmenite was less effective than fluorspar even with a 2:1 replacement ratio (93).

### 2.5.4.5 Borates $B_2O_3$

In the refractory industry, it is well known that low concentrations of boron oxide reduce the hot strength of basic bricks by forming low melting point compounds. It is this particular property which now makes boron compounds attractive as fluxes for lime.

Flintkote of America (94) carried out the initial laboratory work on the fluxing power of certain boron compounds. Their effectiveness on the dissolution of lime in a (FeO - MnO - $SiO_2$) slag was reported in a subsequent patent. Some of the results are presented below

| | dissolution time |
|---|---|
| standard slag | 16 secs. |
| + $Na_2B_4O_7$ | 0.8 secs. |
| + $H_3BO_3$ | 0.8 secs. |
| + $B_2O_3$ | 0.7 secs. |

Other possible borates are colemanite (2 CaO.3 $B_2O_3$.5 $H_2O$) and hydroboracite (MgO.CaO.3 $B_2O_3$.6 $H_2O$) (95). Using 1 kg (per tonne of steel) of colemanite, Hollappa (11) found that its influence was very rapid and more lasting than fluorspar. It did however have a tendency to stabilise the emulsion so that foaming persisted after the blow.

From Germany, Oberhauser et al (96) reported that there was a substantial difference in slag formation during blowing when colemanite replaced fluorspar. Shortly after the first charge of colemanite, the slag collapsed in exactly the same way as with fluorspar. After the addition of fluorspar, the slag quickly foamed again at a considerably lower lance position, but when colemanite was added, a foam could only be maintained by placing the lance in a higher position. Even so there was no adverse effect on desulphurisation or dephosphorisation. A problem with using boron compounds is the possibility of boron pickup by the steel. In all the trials (where colemanite was charged in amounts up to 35 kg per tonne of hot metal) no boron was reduced from boric oxide dissolved in the slag. However if slag is carried over into the teeming ladle, boron reversion can occur when the steel is deoxidised (97).

### 2.5.4.6 Manganese Oxide MnOy

Theoretically manganese oxide should promote slag formation, since increasing amounts contract the 2 $CaO.SiO_2$ phase field in the $CaO - FeO - MnO - SiO_2$ system (98). In the presence of MnO, however saturation with lime is no longer possible. As a saturation phase, a ternary solid solution of CaO - FeO - MnO must occur, the activity of the lime being dependent upon the relative amounts of the other two oxides (78).

In practice, excellent results have been reported in Russia (36) while American workers (80) found iron oxide to have a greater influence on lime dissolution. Boichenko (99) considered manganese oxide only participated in lime dissolution when a sufficient amount of iron oxide was present in the slag. The conflicting results may be associated with variations in the manganese content of the hot metal. Kohler et al (100) carried out a study of the refining of high phosphorus irons with various manganese contents. They found the manganese level influenced the oxidation of carbon during the early stages of refining. High manganese levels (1.0 - 1.5%) inhibited carbon removal, this resulted in high slag irons and accelerated slag formation. When low - Mn irons were produced in the blast furnace, (36) it was claimed productivity improved (in the B.F.) with reduced raw material and hot metal costs. However in the converter, slag formation proceeded more slowly, (than normal Mn irons) delaying desulphurisation and dephosphorisation. Even with an addition of fluorspar, the basicity remained low. These poor results were reversed when 31 kg (per tonne of steel) of manganese ore was added at the beginning of the blow. The reduction of manganese oxide during the blow reduced the consumption of ferromanganese required for deoxidation.

At the Highveld steelplant (43) a slag rich in manganese oxide (derived from a nearby ferroalloy producer) is used for inducing rapid slag formation with very low manganese hot metal. Without the addition, desulphurisation effeciency deteriorated particularly with lime of medium or low reactivity.

With 0.8 - 0.9% manganese in the hot metal (101), additions of manganese ore and fluorspar ensured progressive lime dissolution, but without the fluorspar, slag formation underwent a marked deterioration. However if the manganese ore was preroasted, slag formation was completely satisfactory without the fluorspar addition. The only problem was the high silica content of the ore (20% $SiO_2$) which required additional lime for neutralisation.

In Britain, laboratory experiments (102) have shown manganese oxide to be superior to fluorspar in its ability to flux lime (discussed in section 2.6). Following these encouraging results, a plant trial (103) comparing 5 kg (per tonne of steel) additions of fluorspar and manganese ore, was carried out in a 10 tonne electric arc furnace. With manganese ore, the melt out temperature was higher with some indication that refractory wear had increased. This result is contrary to the laboratory findings of Beecham and Steger (104). They reported manganese oxide to be a less corrosive addition than fluorspar after carrying out erosion tests on pitch impregnated burnt magnesite. In further comparative trials carried out in an L.D. converter (105) no difference could be detected in slag formation, desulphurisation, dephosphorisation, or refractory wear. Contrary to the Russian practice of adding the ore at the start of blowing, the optimum time was found to be after two thirds of the blowing period. Earlier additions caused uncontrollable foaming. Similar results have been reported by investigators at C.A.P.L. (106) where the optimum time appeared to be after a quarter of the blowing time, any later additions caused very sudden slag collapse. Along with other investigators (101, 103) they found that an addition of manganese ore produced a more than equivalent reduction in the iron oxide content of the slag.

In the majority of reported trials, manganese oxide was added as ore, but calcined limestone containing 11.2% Mn has been successfully tried in Russia (107). However, due to the high silica content (10% $SiO_2$) the special lime had to admixed with normal lime to achieve the best results noteably improved slag formation and lining life.

## 2.6 Laboratory Techniques Developed for Studying Lime Dissolution

It is very difficult to simulate the operating conditions found inside a L.D. vessel. As a compromise a number of investigators have studied lime dissolution by immersing synthetic pellets in a slag at steelmaking temperatures (65, 99, 108). The slags were melted under an inert atmosphere to keep the iron oxide in the divalent state which is compatible with liquid iron. The choice of atmosphere is important because the lower the partial pressure of pxygen, the larger the 2 $CaO.SiO_2$ phase field (10). In the L.D. vessel, considerable differences exist in the oxygen partial pressure between parts in contact with the oxygen jet and those through which pass bubbles of carbon monoxide.

As an alternative method, Limes and Russell (109) devised the crucible test, in which 3 grams of lime (-5 + 6 mesh) are mixed with 1 gram of slag (19% $Fe_2O_3$ - 56% $SiO_2$) in a crucible before being placed in a furnace at 1480°C. After a fixed reaction time, the crucible is withdrawn for microscopic examination and free lime determination of the slag. For this particular test, free lime does not appear to be a satisfactory parameter for measuring the reaction kinetics, since the analysis cannot distinguish between unreacted lime and lime precipitated on cooling.

To avoid the precipitation of lime, investigators at the British Steel Corp. used equal proportions (by weight) of lime and slag. Two investigations were carried out specifically to study the influence of different fluxes on lime dissolution (102, 110). The chosen slag was fayalite (2 $FeO.SiO_2$) which was mixed with the lime before being placed in a furnace at either 1300°C or 1400°C. However if the tests were carried out inan identical manner to the Limes and Russell method (i.e. in air) fayalite would oxidise into two separate components, silica and iron oxide, which require a fusion temperature above 1600°C. This may account for the abnormal increase in lime solubility obtained with a manganese oxide addition in the slag which has not been confirmed by other investigators (99, 108) who melted under argon.

Instead of using a muffle furnace, Schürrman et al (75) used a hot stage microscope to study lime-slag reactions. From the hot stage microscope Derge and Shegog (111) developed the hot filament microscope in which the thermocouple serves as a heating element and thermometer at the same time. By locating the thermocouple loop on a microscope stage, the investigators could observe the dissolution of fused lime (0.025 cm dia.) in a molten slag adhering to the filament.

## 2.7 Reaction Kinetics

The great majority of metallurgical reactions are heterogeneous and can be classified into the following groups.

gas - solid
gas - liquid
liquid - liquid
liquid - solid

The dissolution of solids in liquids (metallic and non-metallic) may be controlled by one of three processes:-

1. The rate of chemical attack at the solid-liquid interface
2. Diffusion of reactants to, or products from the interface
3. A function of (1) and (2) - termed intermediate.

The kinetics of oxygen steelmaking have been reviewed by a number of German investigators (112, 113, 114). Oeters (113) found that generally the rate determining step in refining was the resistance to transfer in the diffusion layer of the metal phase, however the dissolution of lime could become rate controlling where silicate slags were involved.

Two analysis (chemical (65) and gravimetric (108) ) techniques have been used to measure the amount of lime that has dissolved in a slag or melt. The accuracy of both methods must be questioned. The results from chemical analysis may be in error because the saccharine solution (used for leaching free lime) does not dissolve lime with iron oxide in solid solution. Measuring the weight loss of a reacted lump or pellet would be adequate if the lime had theoretical density. In practice, the weight loss (by dissolution) is counterbalanced by a weight gain due to the slag infiltrating the pore system. In complete contrast Russian workers have used a cold model to study the heat and mass transfer involved in the dissolution of lime. Pure water and 2.8 mm. dia. balls of ice were used to model the heat transfer process while a 20% aqueous solution of $NaNO_3$ and 2.9 mm dia. balls of the same salt modelled the mass transfer process (115).

## 3. Experimental Work

Commercial lime was considered unsuitable for this investigation because of the physical and chemical inhomogeneity found in natural limestone. Instead analytically pure reagents (calcium carbonate and calcium hydroxide) were used in the preparation of lime pellets with reproducible properties. To model an early steelmaking slag, fayalite was chosen for the base melt. Fayalite is an iron silicate ($2\,FeO.SiO_2$) with a congruent melting point at 1205°C.

In addition to the immersion experiments, the deformation behaviour (c.f. Seger Cones) and the initial liquidus temperatures of mixtures prepared from the oxide components of the different lime-melt systems were also examined. The results were important for later work where no ternary or quaternary phase data was available.

## 3.1 Starting Materials

### 3.1.1 Lime Pellets

In 1951 Williams (116) successfully sintered lime pellets. The calcium oxide used was -300 mesh powder calcined at 1700°C. To obtain a uniform packing density, paraffin (8% by weight) was mixed with the powder before compaction. The pellets were made by compressing the powder under a pressure of $68.94\ MN.m^{-2}$ in a cylindrical die. After firing for 1 hour at 1800°C., the pellets had a bulk density of $2820\ kg.m^{-3}$ (the theoretical density of lime is $3370\ kg.m^{-3}$).

Twenty one years later Dickinson (117) tried to produce cylindrical pellets by compacting lime (from calcined calcium carbonate) in a 20 mm diameter die and sintering at 1500°C. Unfortunately all the compacts spalled during firing in a muffle furnace. The author extended this work by varying the following parameters:-

compacting pressure $8 \longrightarrow 200\ MN.m^{-2}$

withdrawl speed 1 $\longrightarrow$ 5 mm. min$^{-1}$

heating rate 0.5 $\longrightarrow$ 3°C. min$^{-1}$

Like the previous results, every fired compact was rejected, because of splitting around the circumference or a conical defect in the top surface.

Following these unsuccessful attempts, a new series of experiments was carried out. Lime was prepared from calcium hydroxide calcined for 16 hours at 1100°C., ground in an agate pestle and mortar, and sieved through a 120 B.S.S. mesh. The results were exactly the same as before, the specimens spalled before reaching the firing temperature (1250°C).

Subsequent attempts to calcine and sinter 20 mm diameter pellets of calcium hydroxide in one operation, failed due to the pellets exploding on heating. This was associated with the evolution of 'water' during calcination

$$Ca(OH)_2 \longrightarrow CaO + H_2O\uparrow \qquad \text{above } 360^\circ C.$$

However it was found that by reducing the die diameter to 10 mm and thereby doubling the surface area to volume ratio, sintered pellets could be produced. Even so, the change was not a complete success, since the fired pellets were distorted ('banana' shaped) with small surface cracks. These defects were caused by variations in the packing density and an uneven temperature distribution during the heating of the pellets. These defects ceased to appear when shorter pellets were fired. However distortion would still occur if a specific procedure in relation to the placing of the pellets in the hot zone were not followed. The furnace used was of standard design, built around a horizontal alumina tube (1 m long 25 mm o.d. 20 mm i.d.) and heated by four silicon carbide heating elements.

## Compaction of 10mm Pellets

The calcium hydroxide powder (approx. 3 grams) was compacted in a 10 mm. die under a pressure of 76 $MN.m^{-2}$ transmitted through the top plunger. Both theload and the withdrawl speed, 1mm. $min^{-1}$, were controlled accurately on an Avery hydraulic compression/tensile machine.

## Sintering

The compacts (two at a time) were fired in a platinum boat charged into a cold tube furnace. The heating schedule used was:-

100°C per hour from cold to 600°C

200°C per hour from 600°C to 1250°C

The slower rate prevented spalling during calcination. After holding at 1250°C for 3 hours, the pellets were furnace cooled. Compacts before and after firing are shown in Plate 4.

## Properties

During calcination and sintering, the weight of the pellets decreased by 24 per cent. The diameter of the sintered pellets was 7.42 mm. The bulk density of the pellets was measured by the mercury balance technique (118). The pellets were weighed in air and in mercury. A stirrup - like holder (Fig. 2) was used to keep the specimens submerged in the mercury.

$$\text{Bulk Density}\ \text{kg.}\ m^{-3} = \frac{\text{wt in air. density of mercury}}{\text{wt in air + wt in mercury}}$$

$$\text{True Porosity}\ \% = 1 - \frac{BD}{TD} \cdot 100$$

To determine the percentage of closed pores, the evacuation method prescribed in B.S. 1902:1952 was used with paraffin instead of water as the immersion liquid.

The porosities of the pellets, before and after firing, are given below:-

| | | | |
|---|---|---|---|
| $Ca(OH)_2$ | pellet | 45 ± 1% | |
| CaO | pellet | 25 ± 1% | (mercury) |
| CaO | pellet | 25 ± 1% | (paraffin) |

### 20 mm diameter Pellets

Twenty millimetre diameter pellets were successfully produced for some of the later experiments. To compact the powder using the same pressure, as per the 10 mm pellets, a load of 2.4 tonnes would be required. Compacts (approx. 10 grams) pressed under this load exploded due to the high internal gas pressure. By trial and error, the most suitable load was found to be 0.6 tonnes.

### Sintering

The green compacts (two at a time) were fired in a platinum boat charged into a cold muffle furnace. To prevent excessive temperature gradients, the charge was 'cocooned' inside an insulating brick coffin.

The furnace was heated at 50°C per hour to 1450°C, the higher temperature being required to offset the low compacting pressure (19.3 $MN.m^{-2}$). After soaking for 3 hours, the pellets were cooled with the furnace.

### Properties

The sintered pellets were 13.42 mm in diameter with porosities of 25 ± 2 per cent.

### 3.1.2 Dicalcium Silicate Pellets

Some experiments were carried out using dicalcium silicate pellets (section 4.4). Dicalcium silicate has 4 enantiotropic forms, alpha $\overset{(\prime)}{\alpha}$ beta $\beta$ and gamma. $\gamma$ . The $\alpha \rightarrow \alpha'$ inversion occurs at 1425°C and the $\alpha' \longrightarrow \beta$ at 675°C (119). When the $\beta$

form changes to $\gamma$ during cooling, the volume increases by 12%, causing the so called 'dusting' of materials in which 2 CaO.$SiO_2$ is an ingredient. It has been found that a number of substances [ $Cr_2O_3$, $B_2O_3$, $V_2O_5$, $P_2O_5$, $As_2O_5$, $Mn_2O_3$ ] prevent this inversion by stabilising the $\beta$ phase down to room temperature (120).

Preparation of Stabilised Dicalcium Silicate

Samples weighing 20 grams were made up from calcium carbonate and precipitated silica. These components were mechanically tumbled before being repeatedly fired at 1500°C and ground until no trace of $SiO_2$ or CaO could be detected by X ray diffraction.

Five gram portions of the prepared material were mixed with differing weight percentages of $B_2O_3$, $Cr_2O_3$ or $V_2O_5$. Each mixture was fired at 1500°C for 6 hours, cooling each half hour for grinding to -120 B.S.S. mesh.

The results are tabulated below:-

| $B_2O_3$ | | $Cr_2O_3$ | | $V_2O_5$ | |
|---|---|---|---|---|---|
| Quantity Wt% | Result | Quantity Wt% | Result | Quantity Wt% | Result |
| 1 | dusting | 1 | no dusting | 1 | dusting |
| 2 | " | 2 | " | 2 | no dusting |
| 5 | partial melting | 3 | " | 3 | " |
| | | 4 | " | 4 | " |
| | | 5 | " | 5 | " |

To reaffirm the results, compacts of $Cr_2O_3$ and $V_2O_5$ stabilised dicalcium silicate (2 CaO.$SiO_2$) were heated to 1500°C. After soaking for 3 hours, the $Cr_2O_3$ stabilised material dusted oncooling in air, however specimens of $V_2O_5$ stabilised 2 CaO.$SiO_2$ did not disintegrate.

The structure of the pellets consisted of sintered 2 $CaO.SiO_2$ with an isolated second phase, the latter forming a continuous film around the grains as the amount of $V_2O_5$ increased. Therefore compacts were prepared with the lowest $V_2O_5$ (2%) addition which would prevent dusting.

### Compaction of 10 mm Pellets

During the initial experiments, a number of compacts laminated during removal from the die. Therefore to prevent any reoccurence, the internal bore and plunger were coated with zinc stearate suspended in acetone. The 2 $CaO.SiO_2$ powder (approx. 3.5 grams) was compacted under the same conditions as the 10 mm lime specimens viz. a compacting pressure of 76 $MN.m^{-2}$ and a withdrawl speed of 1mm. $min^{-1}$.

### Sintering

In the absence of a calcination reaction, the compacts were heated at 300°C per hour to 1500°C. After soaking for 6 hours, the pellets were cooled with the furnace.

### Properties

Sintering reduced the porosities from 40 ± 2% to 33 ± 2%, the new pellet diameter was 9.5 mm.

### 3.1.3 Preparation of the Melt

Fayalite was prepared from fused silica flour and ferrous oxalate. Although successful with the use of the oxalate, the yield of ferrous oxide was low due to the high weight loss associated with the evolution of $CO$, $CO_2$ and $H_2O$ during heating.

In subsequent preparations calcined G.P.R. ferric oxide was used along with electrolytic iron fillings and silica flour. A mixture calculated to yield a melt corresponding to fayalite

$$Fe_2O_3 + Fe \longrightarrow 3\ FeO$$
$$2\ FeO + SiO_2 \longrightarrow 2\ FeO.SiO_2$$

was induction heated to 1500°C for complete fusion in a carbon susceptor (prepared from electrode carbon). To minimise oxidation both heating and cooling were carried out under an argon atmosphere (99.995% pure).

When cold, the fayalite was crushed to -120 B.S.S. mesh in a Glen Creston mixer mill. Any particles of iron and magnetite were removed by a magnet. The chemical analysis was 65% FeO, 5% $Fe_2O_3$ and 30% $SiO_2$; X ray analysis also confirmed the material as fayalite (Table 1.)

## Additions to the Melt

### Manganese Oxide

Manganese oxide can be obtained either by reducing a higher oxide or by heating the metal oxalate or carbonate out of contact with oxygen. The latter was the easier technique with manganese carbonate being the most economical material. This was confirmed when 2 grams of $MnCO_3$ were heated under flowing argon on a Stanton massflow balance. The resulting weight loss and chemical analysis showed that the atmosphere was sufficient to maintain the manganese component in the desired oxidation state.

Following this, 15 gram batches of $MnCO_3$ were heated in a controlled atmosphere tube furnace. After holding for 1 hour at 850°C., the charge was furnace cooled, again under argon.

To prevent oxidation and hydration, the manganese oxide was stored in a vacuum dessicator.

## Other Additions

Experiments were also carried out using additions of calcium fluoride and boric oxide. These materials were supplied as G.P.

reagents by British Drug Houses Ltd. Both chemicals were dried at $350^\circ C$ for 16 hours prior to use.

## 3.2 Experimental Equipment

### 3.2.1 Cone Fusion Furnace

The fusion points were determined in a horizontal furnace with a maximum operating temperature of 1500°C. The furnace consisted of an alumina work tube heated by eight silicon carbide heating elements. Using a Variac controller, the furnace temperature was raised at a steady rate of 5°C per minute from 600°C to the maximum temperature. While some cones were heated in air, the majority were heated in argon. The inert gas (0.5 litres per minute) was introduced into the furnace through an inlet in the back seal.

### 3.2.2 Hot Filament Microscope

The classical quench method (122) of measuring liquidus temperatures is very tedious and time consuming. An alternative technique described by Welch (123) offers a quick and accurate method which can be applied to slags. The initial liquidus temperatures were determined on the hot filament microscope (Telecommunication Instruments Ltd.) shown in Plate 5. It comprises a microscope with light source, a gas tight cell and a Pt - 5% Rh, Pt - 20% Rh thermocouple. The 'V' shaped thermocouple acted as a heating element and a crucible. By using a high speed relay, it was possible to heat the couple (and hence the sample) and read the temperature at virtually the same instant. Before studying the lime-fayalite system, experience was gained with potassium sulphate which possesses a sharp melting point at 1072°C, undergoes a polymorphic transition at 580°C with minimum bifringence at 420°C. With practice, these temperatures were reproducible to within ± 10°C.

### 3.2.3 Immersion Furnace

During the design stage, it was estimated that the maximum temperature required would be 1550°C, accordingly platinum was chosen for the furnace element. But after only limited operation to 1300°C, difficulties were encountered with pronounced thinning of the windings; requiring the furnace to be dismantled for welding or rewinding. Finally with the windings failing every other week, a new furnace was constructed around a tubular Crusilite D.M. type element (Plate 6). The general arrangement is shown in Plate 7 and the furnace section is shown in detail in Fig. 3.

An open ended alumina tube (1m long 59 mm o/d 50 mm i/d) was inserted inside the heating element, protruding above and below the furnace. Fitted to both ends were water cooled aluminum heads sealed to the tube with 'O' rings. The top head had a centre bore through which a refractory tube was inserted and rotated if required. The bottom head supported an alumina tube (25 mm dia.) with a ceramic plug on which rested the crucible in the hot zone.

#### Temperature Control and Measurement

The power input to the furnace was governed by a Eurotherm 070 Mark II thyristor drive controller (0-25 amp with current limit); the temperature being controlled by means of a thermocouple (Pt 5% Rh-Pt 20% Rh) placed close to the heating element.

Temperatures in the hot zone (75 mm long) were measured with a Pt - Pt 13% Rh thermocouple inserted through the bottom head and located in the ceramic plug. Initially the thermocouple was connected to a Honeywell millivolt recorder (calibrated in °C) but this was found to be inaccurate at high temperatures due to an induced e.m.f. Above 1000°C the thermal emf was measured with a Cambridge Portable Potentiometer.

## Crucibles

The melts were held in iron (.06 carbon) crucibles suspended by stainless steel wire from the top head. The crucibles were 40 mm dia. high x 40 mm in diameter.

## Furnace Atmosphere

To prevent the oxidation of the crucible and melt, high purity argon (99.995%) was passed through the furnace at a flow rate of 0.3 litres a minute. Every week, the exit gas was sampled and checked for oxygen (leaks) using a Fison's Gas Chromatograph.

## 3.3 Experimental Procedures

### 3.3.1 Cone Fusion Studies

Cones were prepared from mixtures of lime and fayalite (-120 + 150 mesh). To ensure homogeneity the two components were mixed together for 2 hours in an air tight container. The powder together with a binder ( 1 Wt % $NH_4$ CL and alcohol) was pressed into a triangular mould. Each cone was mounted onto an alumina cement base (Plate 8) so that when inserted into the furnace, the vertical face was parallel to the longitudinal axis of the tube.

After flushing with argon, the furnace was heated at 150°C per hour to 600°C, after which the temperature was increased by 5°C per minute. During heating, the behaviour of the cones was observed through a cross-wire cathetometer viewing through a silica glass window in one end of the furnace tube (Plate 9).

### 3.3.2 Determination of the Initial Liquidus Temperature

To confirm whether the initial deformation of the cones coincided with the start of melting, a small quantity of each mixture was heated in the hot filament microscope.

To load the sample onto the thermocouple, the tip was moistened with alcohol. After making the electrical connections, the cell was flushed with argon. Whilst maintaining an inert atmosphere, the temperature was slowly increased until the crystals started to dissolve between the arms of the thermocouple.

Since the melts contained FeO and MnO, it was thought these might contaminate the thermocouple junction and give rise to errors in the temperature measurements. After cleaning a number of thermocouples in boiling hydrofluoric acid, subsequent redetermination of the melting point of a standard substance (potassium sulphate) showed no such contamination has occurred. However as a precaution the thermocouple was renewed after each measurement.

### 3.3.3 Immersion Experiments

All the experiments were carried out at 1300°C because this represents the average hot metal temperature at the beginning of the blow in a L.D. converter. The cone fusion results (Section 4.2.2) confirmed that all the melt compositions (except 20 Wt% MnO) would be molten at this temperature under an inert atmosphere.

The pellet assembly is shown in Plate 10. The pellet was attached by stainless steel wire to an alumina tube (6 mm o/d 4 mm i/d). This 50 mm long tube was securely fastened between two halves of a partially split spindle (alumina tube 12 mm o/d 8 mm i/d) supported by a stainless steel sleeve.

Sixty grams of the required melt were placed in the crucible, before being lowered into the reaction tube. To prevent spalling on immersion, the pellet was held just above the crucible (but still in the hot zone), however a few tests were carried out with large pellets preheated to 1000°C and 600°C. [ At 600°C - 10 runs produced only 4 results - in the others the pellets spalled ] .

After flushing out the system with argon for 30 minutes, the furnace temperature was slowly increased over a 6 hour period to 1300°C. The temperature in the hot zone was allowed to equalise for 1 hour, before the pellet was immersed for the required time. The bulk densities of 6 pellets (2 of each size) increased by a very small amount ($<1\%$) after refiring for 1 hour at 1300°C.

In the initial experiments, the partially dissolved pellets were withdrawn and air cooled, but the reaction zones shattered due to the inversion of dicalcium silicate. The outer layers were retained after quenching in water, but the observation of magnetite dendrites indicated that the surface had oxidised. Both problems were overcome by fastening the crucible to the top head so that the whole assembly (crucible + pellet) could be withdrawn and quenched.

In the dynamic experiments, a stirrer motor (Gallenkamp Variable Speed) was utilised to rotate the pellet upon immersion in the melt. The motor could not be connected directly to the top of the spindle because the assembly had to be withdrawn very quickly for quenching. Instead the two were connected by a length of polythene tubing which allowed the motor to be placed at 90° to the spindle and approximately 15 cm. away from the top head (Plate 11). The choice of 141 cm. per minute for the rotational speed was purely arbitary, the number of revolutions (60 rpm for the small and 33 rpm for the large lime pellets) being measured by a hand tachometer and checked with a stop watch.

### 3.3.3.1 Specimen Preparation for Microscopic Examination

After removing the bottom of the crucible by surface grinding, the remainder was mounted in a cold setting resin, (Metserv Metset FT). To prepare a section for examination, the specimen was ground on silicon carbide papers (150 and 600 grades only) followed by polishing on a disc impregnated with 1/4 micron diamond paste. Two etchants were used for the specimens:-

1. 2% nitric acid in alcohol (Nital)
2. 5% aqueous copper sulphate solution

### 3.3.3.2 Electron Probe Analysis

In the field of refractories, microanalysis has been used to study the distribution of elements in magnesite bricks (124) and the composition gradients formed during slag and glass corrosion (125). In this investigation, the migration of oxides to and from the dissolving lime was followed using an updated Cambridge Microanalyser Mark IIA possessing two spectrometers.

A cross-section 1/4" in diameter and 1/8" thick was trepanned from the lime-melt reaction interface of the mounted specimens. After repolishing to 1/4 micron finish, the surface was coated with evaporated carbon to allow the current from the beam to flow away to earth. After finding a suitable area in the attached optical microscope, the specimen was rotated under the electron beam. The analysis was made at an accelerated potential of 25 kilovolts with a probe current of 8 millimicroamps. Poloroid photographs were taken of the electron backscatter from the selected area along with X ray images of calcium, iron, silicon and manganese (if present). Numerous attempts using the available crystals, Stearate and K.A.P., failed to detect fluorine (atomic number 9) or boron (atomic number 5).

The concentration profiles were produced by taking a 10 second integrated count of the element's radiation in a 38 micron square, then repeating the procedure across the interface.

The intensity of the radiation from the specimen was calibrated against a known standard. The calculation of the true concentration from the measured intensity ratio, involved a series of corrections (dead time, background noise, secondary fluorescence, adsorption and the atomic number effect) (126).

### 3.3.3.3 Determination of Bulk Volume and Surface Area

#### Bulk Volume

The methods used previously to monitor the dissolution of lime are discussed in section 2.7. In this investigation bulk volume was considered a suitable reaction parameter for the following reasons:-

1. The uniformity (size and porosity) of the pellets
2. Any adhering melt would be removed by the 2 $CaO.SiO_2$ inversion.

The main disadvantage was that all the immersion experiments had to be duplicated for qualitative and quantitative examination.

The bulk volume was calculated from the weight of the pellet + holder in air and in a density bottle containing paraffin. Plate 12 shows the two density bottles (originally large boiling tubes) mounted on Araldite MY750 resin bases. For the stoppers, sintered glass connectors were filled with resin, through which a fine hole was drilled down the centre.

Following immersion, the reacted specimen was quenched very quickly in agitated brine, this fractured the melt layer, thus allowing the 2 $CaO.SiO_2$ inversion to occur . After removing both the pellet and holder from the spindle, a plastic film ($\leq$.001 grams) was sprayed onto the pellet to prevent paraffin infiltrating the pores.

calculation of the volume of pellet + holder

weight of [ bottle + paraffin ] + pellet + holder in air —
(weight
(weight of [ bottle + paraffin ] + weight of [ pellet + holder]
in paraffin)

= equivalent weight of paraffin

$$\text{volume} = \frac{\text{equivalent weight of paraffin}}{\text{density of paraffin}}$$

volume of pellet lost during reaction =

volume of [ pellet + holder ] - volume of [ pellet + holder ]
before immersion after immersion

This technique was satisfactory for the following systems:-

$CaO - 2\ FeO.SiO_2$

$CaO - 2\ FeO.SiO_2 + MnO$

$CaO - 2\ FeO.SiO_2 + CaF_2$

$2\ CaO.SiO_2 - 2\ FeO.SiO_2$ (referred to in section 4.4.1.2)

However it could not be used for the $CaO$-$2\ FeO.SiO_2 + B_2O_3$ system because the melt overflowed the crucible and the solidified layer around the lime did not shatter on quenching ($B_2O_3$ is a $\beta$ $2\,CaO.SiO_2$ stabiliser).

Surface Area

If 'h' is the mean length of the pellet attacked and the average diameter along this length as determined by a micrometer is

$$\bar{d} \text{ where } \bar{d} = \frac{\bar{d}_1 + \bar{d}_2}{2}$$

$\bar{d}_1$ and $\bar{d}_2$ are the mean diameter before and after dissolution then the area of pellet surface attacked is given by

$$A = \pi \bar{d} h + 1/4 \pi d^2$$

where $d$ is the mean diameter of the lower face of the pellet.

### 3.3.4 Penetration Experiments

It was hoped that these experiments would provide an insight into the penetration of liquid oxides into porous lime. A hole (5 mm in diameter and 5 mm in depth) was drilled in one end of a large lime pellet. The cavity was filled with powdered fayalite, after which the pellet was fired at 1300°C for a preselected time (varying from 5 minutes to 1 hour). On cooling down, the lime-melt interface shattered due to the dicalcium silicate inversion. This phase transformation could not be prevented even by quenching in water, consequently the experiments were abandoned.

## 4. Experimental Results and Observations

These are reported for the following combinations of pellet and melt.

1. Lime - Fayalite
2. Lime - Fayalite + Manganese Oxide
3. Lime - Fayalite + Other Fluxes
4. Dicalcium Silicate - Fayalite

For each system the results and observations are subdivided into:-

1. Cone Behaviour
2. Initial Liquidus Temperatures
3. Immersion Experiments

### 4.1 Lime-Fayalite System

The main constituents of steelmaking slags are lime, iron oxide and silica. The appropriate equilibrium diagram is that for the CaO-FeO-$SiO_2$ system (Plate 2) where the oxide phases are in equilibrium with metallic iron. The main feature to note is the 2 CaO.$SiO_2$ + liquid phase field which forms a high temperature ridge between lime and fayalite.

### 4.1.1 Cone Behaviour

During heating the cone changes from a porous heterogeneous solid into a viscous liquid, never reaching (except during slow heating) chemical or physical equilibrium. Deformation begins when sufficient liquid has formed for flow to occur under gravity continuing as the temperature is raised until an arbitary end point is reached.

Two temperatures were recorded:-

1. The temperature at which the cone tip started to bend
2. The temperature at which the specimen had completely collapsed.

In addition to tabulating the initial and final collapse temperatures

(Table 2), the results are superimposed on the CaO - 2 $FeO.SiO_2$ isopleth (Fig. 4). The isopleth is a section through the $CaO-FeO-SiO_2$ ternary showing the liquidus and solidus temperatures of phases intersected by a line from the CaO corner to the 2 $FeO.SiO_2$ composition on the $FeO-SiO_2$ binary (Fig. 5).

At the 2 $FeO.SiO_2$ end of the isopleth, both temperatures were reduced by an addition of 10 Wt% CaO. But as the CaO content increased above this value, the initial collapse temperature increased sharply. The equilibrium liquidus temperature follows a similar trend across the isopleth. Initially there is a small decrease (from 1204°C to 1150°C), but after 8 Wt% CaO the remaining portion of the liquidus curve increases sharply as the section intersects the FeO + liquid and 2 $CaO.SiO_2$ + liquid phase fields.

In the range 0 → 30 Wt% CaO the deformation of the cones was continuous from the onset of bending to the final collapse. With higher CaO compositions, deformation appeared to cease after the initial bending of the tip and it did not resume until 20°C before the final collapse temperature.

Although the isopleth can give useful information it cannot be used to calculate the amount of liquid present at any particular temperature for any composition along the CaO-2 $FeO.SiO_2$ join. These were calculated from the ternary diagram and are plotted in Fig. 6. The most interesting feature of this plot is the difference in the ratio

$$\frac{\text{increase in \% liquid}}{\text{unit increase in temperature}}$$

for various compositions at equilibrium. For compositions up to 30 Wt% CaO, the ratio is high (i.e. the graph of % liquid against temperature is steep). This means that a small increase in temperature produces a large increase in the liquid content. For compositions richer than 30 Wt% CaO, the ratio is low indicating that a large increase in temperature produces only a small change in the amount of liquid.

Changing the atmospheric conditions inside the furnace (from argon to air) produced a marked increase in the melt collapse temperatures. The results are tabulated in Table 3 and plotted on a section from the CaO-$SiO_2$-$Fe_2O_3$ phase diagram (Fig. 7). At low concentrations of CaO, both collapse temperatures were reduced but this trend was reversed as the proportion of CaO exceeded 40% by weight. Cones with a high proportion of CaO collapsed in a similar manner to those heated in argon i.e. a period of very little observed movement after the initial bending of the tip. Again this can be associated with the percentage liquid-temperature relationship(Fig. 8).

### 4.1.2 : Initial Liquidus Temperature

The temperature range in which a liquid was formed for each composition (4 runs on each) determined by the hot filament microscope technique is shown in Tables 2 and 3 and plotted in Figs. 4 and 7. These results support the hypothesis that the initial deformation of the cones coincided with the formation of a liquid phase. Continuous heating above these temperatures gave some qualitative indication of the melting range of the various lime-melt mixtures. Here again, melt rich compositions were soon completely molten while those enriched in lime had a longer melting range. Similar behaviour was observed when the mixtures were heated in air. However it was only compositions above 40% lime which had long melting ranges.

With the good correlation between the experimental results and the liquidus and solidus temperatures across the isopleth, experiments were carried out with additions of manganese oxide, calcium fluoride and boric oxide to lime-fayalite mixtures.

### 4.1.3 Immersion Experiments

### 4.1.3.1 Small Lime Pellets

Microscopic examination of immersed specimens revealed five distinct zones

| $2 FeO.SiO_2$ | $2 CaO.SiO_2$ | $FeO$ | $CaO + FeO$ | Unreacted $CaO$ |
|---|---|---|---|---|
| liquid | solid | liquid | solid+<br>liquid | solid |

with the products of the heterogeneous reaction

$2 FeO.SiO_2 + 2 CaO \longrightarrow 2 CaO.SiO_2 + 2 FeO$ separating the pellet from the melt (Plate 13). The solid $2 CaO.SiO_2$ etched dark by 'Nital' lies vertically down the centre of the plate. The white phase, rich in iron oxide, separating the CaO from $2 CaO.SiO_2$ was liquid at 1300°C. During infiltration of the porous solid, the iron oxide liquid dissolved the sintered necks between the lime grains (Plate 14). Inside the infiltrated pore system there were two other phases, metallic iron and tricalcium silicate ($3 CaO.SiO_2$). The presence of metallic iron in the microstructure (revealed by the precipitation of copper from copper sulphate solution) (Plate 15) illustrated the difficulty in differentiating between isothermal and athermal reaction products. Although the $CaO-FeO-SiO_2$ ternary system has no metallic iron phase field, it is a component of the Ca-Fe-Si-O system. Fleischer and Fischer (68) put forward the following reaction to account for its presence, $3 FeO + 2 CaO \longrightarrow 2 CaO.Fe_2O_3 + Fe$. (Lime in contrast to silica stabilises the ferric state). But iron is also a product of the athermal decomposition of wustite $4 FeO \longrightarrow Fe + Fe_3O_4$ (77).

Tricalcium silicate can also be precipitated isothermally or athermally. The $3 CaO.SiO_2$ crystals formed on cooling from the liquid state, were easily recognised by their needlelike shape. Both types were present in the microstructure of a pellet immersed for 6 minutes (Plate 16). The coarse isothermal crystals were redissolving at the reaction temperature of 1300°C.

N.B. Under equilibrium cooling $3\ CaO.SiO_2$ decomposes into CaO + $2\ CaO.SiO_2$.

With only brief immersion times the iron oxide rich liquid solidified as a single phase (Plate 13). However with longer times, a eutectic could be resolved between the wustite dendrites (Plate 17).

After only 10 seconds immersion, the precipitated particles of $2\ CaO.SiO_2$ were observed to be agglomerating into small groups (Plate 18). This process continued until a compact layer was formed around the pellet (Plate 13). As the immersion time increased, there was a gradual transition from a planar to a corrugated $2\ CaO.SiO_2$ rim with large aggregates breaking away into the liquid phase (Plate 19). An average rim width was calculated from readings taken around the specimen's circumference, the results (Table 4 Fig. 9) show a maximum thickness after 4 minutes. Examination of a specimen immersed for this period of time (Plate 20) revealed dissolving crystals of $3\ CaO.SiO_2$ adjacent to the $2\ CaO.SiO_2$ rim.

To assess the reaction mechanism for the formation and growth of a solid product, inert markers have been used to estimate the relative diffusion rates of the reacting species (127). In this investigation, however it would have been extremely difficult to devise an accurate experimental technique since the $2\ CaO.SiO_2$ layer was separated from the pellet by a liquid phase. But an insight into the reaction mechanism can be gained from the microexamination of a specimen immersed for 7 minutes (Plate 21). The microstructure shows the precipitated layer to have moved inwards as the pellet receded during dissolution.

Initially the melt solidified as fayalite + eutectic (Plate 13), but as it became enriched in CaO, primary wustite (Plate 22) and the eutectic CaO-FeO-$SiO_2$ (Plate 26) occurred as phases in the solid state. Rotating the lime pellet produced a corrugated melt - 2 CaO.$SiO_2$ interface (Plate 23) with a thicker 2 CaO.$SiO_2$ layer on the convex part (viewed from the pellet side). As the immersion time increased the 2 CaO.$SiO_2$ precipitate appeared as a solid mass between the pellet and the melt (Plate 24) although some liquid had penetrated through to the melt. The maximum width of the precipitated layer (Table 4 Fig. 9).occurred on a specimen immersed for 4 minutes. On the same specimen (Plate 25) aregion of melt was observed in the liquid phase. The corrugations and liquid extrusions along the isolated melt region - 2 CaO.$SiO_2$ interface resembled those along the bulk melt boundary.

After 4 minutes, the 2 CaO.$SiO_2$ layer had decreased in thickness (Plate 26), however it still remained corrugated. The tenacity of the 2 CaO.$SiO_2$ particles was clearly visible from the specimen immersed for 5 minutes. Besides sintering into small groups (Plate 28) the particles formed a coherent network inside the CaO-FeO - liquid phase (Plate 27).

### 4.1.3.1.1 Electron Probe Analysis

Plate 29 shows a series of scanning images (electron and X ray) of a section of the reaction interface from a specimen immersed for 5 minutes. As expected, the concentration of calcium gradually decreased from bottom right to top left i.e. moving from the reacted pellet towards the melt. In contrast the distribution of silicon was highest in the melt with a sharp drop occurring at the 2 CaO.$SiO_2$ -

liquid interface. Along this interface, there was a zone depleted in iron, but the distribution increased in the regions surrounding the lime grains. Concentration profiles (Fig. 10) for calcium, iron and silicon (expressed as oxides) were plotted across the lime-melt reaction zone. These profiles do no give the true composition of phases because some overlap in the area under the electron beam nearly always occurred.

The important feature of Fig. 10 is the sudden decrease in the $SiO_2$ concentration at the 2 $CaO.SiO_2$ layer ($<$ 1 Wt% in the iron oxide - lime liquid). A separate analysis of the 2 $CaO.SiO_2$ produced the following composition 30 Wt% $SiO_2$, 68 Wt% CaO, 2 Wt% FeO, this agrees with the findings of Obst et al (42) who found that iron could substitute for calcium in the 2 $CaO.SiO_2$ shells surrounding partially reacted lime extracted from an LD vessel.

The concentration of iron oxide gradually decreased from the bulk melt towards the pellet, but there was a sudden increase in concentration inside the 2 $CaO.SiO_2$ rim. The concentration of lime showed a reverse trend to iron oxide i.e. gradually decreasing from the 2 $CaO.SiO_2$ rim towards the bulk melt.

Another way of illustrating the profiles was to plot the results on the 1300°C isotherm of the $CaO-FeO-SiO_2$ ternary (Fig. 11). From the melt composition on the $FeO-SiO_2$ binary, the concentration path moved along the 30 Wt% $SiO_2$ isoconcentration line into the 2 $CaO.SiO_2$ + liquid phase field. This was followed by a sudden change towards the FeO corner before the compositions moved finally towards the CaO-FeO binary.

### 4.1.3.2 Large Lime Pellets

Although the microstructures resembled those observed around small static pellets, there was one major difference. This was the athermal precipitation of 2 $CaO.SiO_2$ dendrites around the 2 $CaO.SiO_2$ particles present at 1300°C (Plate 30). The particles which were present at the reaction temperature formed a thin cohesive layer (Table 5 Fig. 12) between the melt and the lime-iron oxide liquid (Plate 31). Similar microstructures were observed when the pellets were rotated (Plates 33, 34). Although the 2 $CaO.SiO_2$ layer remained very close to the lime surface, isolated regions of melt were found in the lime-iron oxide liquid (Plate 35) after long immersion times.

### 4.1.3.3 Dissolution Kinetics

The results of the quantitative experiments are tabulated in Tables 6 and 8 and presented graphically in Fig. 13 and 14 where the volume loss per unit area is plotted against the immersion time. The graphs for the small pellets show a change in dissolution rate after a reaction time of 3-4 minutes in both the static and dynamic experiments. With short immersion times, the influence of preheat temperature can be seen from Table 10 and Fig. 15. The delay in dissolution was almost certainly due to the build up of a frozen layer of melt on the pellet immediately upon immersion.

It was evident that pellet rotation increased the dissolution of lime, this was true for the two sizes of pellet immersed in the different melts. A visual comparison of the dissolution rates in the various melts (2 $FeO.SiO_2$, 2 $FeO.SiO_2$ + MnO, 2 $FeO.SiO_2$ + $CaF_2$) can be made from Plates 36 to 39. The actual dissolution rates obtained from the linear portions of the graphs are given in Table 11.

### 4.2 Lime-Fayalite + 10 Wt% Manganese Oxide System

Although very little is known about the $CaO-FeO-MnO-SiO_2$ quaternary system, a number of studies have been made on the three binary systems (77)

$MnO-FeO$ ) These are not true binary systems because manganese like
$MnO-CaO$ ) iron can exist in a number of oxidation states ($Me^{2+}$ $Me^{3+}$
$MnO-SiO_2$ ) etc) depending upon the oxygen potential

Manganese oxide (MnO) is very similar to wustite (FeO) in its reaction with silica, forming a silicate $2\,MnO.SiO_2$ with a congruent melting point. However the two oxides react differently with lime, FeO forms two solid solutions with a minimum at 1108°C., whereas MnO forms a complete solid solution series with the solidus never falling below 1700°C. In air, both MnO and FeO react with oxygen to form

$$Fe_2O_3 \quad Fe_3O_4$$
$$Mn_2O_3 \quad Mn_3O_4$$

Ferric oxide ($Fe_2O_3$) begins to dissociate at 1200°C in air. The dissociation at first increases regularly and at a steadily increasing rate with the temperature, corresponding to the formation of $Fe_3O_4$ and a solid solution between it and the remaining $Fe_2O_3$ (128).

In the manganese-oxide system, the temperature of equilibrium co-existence of $Mn_2O_3$ and $Mn_3O_4$ is 870°C in air (129).

#### 4.2.1 Cone Behaviour

A 10 Wt% addition of MnO increased both the initial and final collapse temperatures of compositions along the $CaO-2\,FeO.SiO_2$ isopleth (Table 12, Fig. 16). With a further increase to 20 Wt% MnO (Table 13 Fig. 17) both the collapse temperatures at the melt rich end were higher, but for compositions with a CaO to $2\,FeO.SiO_2$ ratio of 3:7, 4:6 and 5:5, the final collapse temperature remained constant at 1460°C. In air, manganese oxide was particularly effective in reducing the initial and final collapse temperatures of the pure melt and lime rich compositions (Tables 14 and 15, Figs. 18 and 19).

### 4.2.2 Initial Liquidus Temperatures

Compared with the results from the CaO- 2 $FeO.SiO_2$ system, manganese oxide (Tables 12 and 13, Figs. 16 and 17) produced an increase in the temperature at which a liquid phase appeared. But in air, the oxide addition reduced the initial liquidus temperatures (Tables 14 and 15, Figs. 18 and 19).

### 4.2.3 Immersion Experiments

#### 4.2.3.1 Small Lime Pellets

The reaction zone around a specimen immersed for 1 minute (Plate 40) resembled that between lime and fayalite (Plate 13). However there was less penetration of the porous pellet by the liquid oxides. The difference can be clearly seen by comparing the microstructure of reacted pellets (Plates 41 and 14) which were immersed for 3 minutes. Even after 6 minutes there was still a substantial amount of direct bonding between the lime grains (Plate 42).

The presence of the two reaction products (liquid oxides and solid 2 $CaO.SiO_2$) indicated that the lime-melt isopleth still intersected the 2 $CaO.SiO_2$ + liquid phase field. As the immersion time increased the transition from a planar to a corrugated rim was again evident, however significant differences were observed in the spatial distribution of 2 $CaO.SiO_2$ along the rim (Plate 43). Whereas only a thin layer had precipitated along the peaks (viewed from the lime side) there was a large number of 2 $CaO.SiO_2$ particles at the base of each trough. With increasing immersion time, the troughs became V shaped with 2 $CaO.SiO_2$ particles breaking away from the reaction interface (Plate 44). The peak thickness of the 2 $CaO.SiO_2$ layer (Table 4 Fig. 9) occurred on a specimen immersed for 4 minutes.

This was also the time when liquid breakouts were observed in the melt (Plate 45). Microexamination (and later Electron Probe Analysis) of a large extrusion (Plate 46) showed no 2 $CaO.SiO_2$ barrier between the breakout and the melt but there was a large precipitation of 2 $CaO.SiO_2$ around the breakout point. Considering the breakout was originally liquid from inside the 2 $CaO.SiO_2$ layer, the two had different structures on cooling. The white colour of the single phase breakout was similar to that of magnetite or wustite after etching in Nital, while the inner liquid had a eutectic-type structure.

As the number of breakouts increased (Plate 47), it was only a short time before two of them became connected, thereby isolating a region of melt (Plate 48). Whereas 2 $CaO.SiO_2$ had precipitated at the new melt-liquid interface, only one side of the isolated melt region had a 2 $CaO.SiO_2$ layer. However the microstructure of a specimen immersed for 8 minutes, showed a continuous 2 $CaO.SiO_2$ rim around isolated regions of melt (Plate 49).

During microscopic examination of all the specimens, only a small number of 3 $CaO.SiO_2$ crystals were observed near the 2 $CaO.SiO_2$ layer (Plate 49) and in the infiltrated pore system of the lime pellets (Plate 42).

Rotating the pellets produced a corrugated 2 $CaO.SiO_2$ layer (Plate 50). As the reaction time increased, the corrugations became more accentuated with a large number of 2 $CaO.SiO_2$ particles forming on the convex portion of the melt-liquid oxides interface (Plate 51). In some areas, the precipitation of 2 $CaO.SiO_2$ was so large that small regions of liquid became isolated from the parent phase (Plate 52). After reaching a maximum after 4 minutes, the thickness of the 2 $CaO.SiO_2$ layer started to decrease (Table 4 Fig. 9). With longer immersion times, liquid breakouts and isolated regions of melt

(Plates 53 and 54)

were observed in the reaction zone surrounding partially dissolved pellets. It was during the later stages that horseshoe shaped crystals of 3 $CaO.SiO_2$ were observed close to the 2 $CaO.SiO_2$ - liquid oxides interface (Plate 55).

### 4.2.3.1.1 Electron Probe Analysis

A section of the reaction interface from a specimen immersed for 5 minutes is shown in Plate 56, along with the X ray images for calcium, iron, manganese and silicon. Manganese was detected on both sides of the 2 $CaO.SiO_2$ layer and like iron it could replace calcium in 2 $CaO.SiO_2$ (1.04 Wt% MnO). The calculated concentration profile (Fig. 20) shows that MnO increased in concentration in the liquid region between the precipitated layer and the dissolving pellet.

To represent the compositions on a ternary diagram, the concentration of the oxides of calcium, iron and silicon were recalculated to 100 percent (Fig. 21). Compared to the lime-fayalite system, the concentration paths were very similar except for a shift towards the FeO corner.

Of particular interest in the MnO series of experiments were the breakouts of liquid oxides from inside the 2 $CaO.SiO_2$ layer. A section of interface containing one breakout (Plate 46) was prepared for the microprobe. Plate 57 shows the electron and X ray images for the four elements calcium, iron, manganese and silicon. It was apparent that the breakout contained a high concentration of iron and manganese with very little silicon. Microanalysis gave the breakout's composition to be 79 Wt% FeO, 9 Wt% MnO, and 14 Wt% CaO.

### 4.2.3.2 Large Lime Pellets

In contrast to the broken 2 $CaO.SiO_2$ rim observed around small specimens, the precipitated layer was thin (Table 5 Fig. 12) and continuous around large static pellets (Plates 58 and 59). Even when the pellets were rotated, the layer still remained intact (Plates 60, 61 and 62). These observations suggested that the occurrence of breakouts was related to the radius of curvature of the pellets. If breakouts only occur below a certain size, then a longitudinal groove with a small radius of curvature should promote extrusions on a large pellet.

To test this hypothesis a small groove was filed in two large pellets, one immersed in the base melt, the other in fayalite + 10 Wt% manganese oxide. With the base melt there was no difference between the melt - 2 $CaO.SiO_2$ interface around the pellet and that inside the groove (Plate 63). With manganese oxide in the melt, liquid breakouts had occurred,but only along the melt - 2 $CaO.SiO_2$ interface inside the groove (Plate 64).

### 4.2.3.3 Dissolution Kinetics

The results from the static and dynamic experiments are tabulated in Tables 6 and 8 and plotted in Figs. 13 and14. There is some similarity (inflexion points) between these results and those obtained from specimens immersed in fayalite. The major effect of the addition was to decrease the solution rates (Table 11) of lime. However this trend was reversed in one situation, the dissolution of small pellets after 4 minutes immersion under conditions of natural convection.

### 4.3 Lime-Fayalite + Other Fluxes

In order to assess the fluxing power of manganese oxide, experiments were carried out using the following melts:-

1. Fayalite + 10 Wt% Calcium Fluoride
2. Fayalite + 10 Wt% Boric Oxide ( a possible fluorspar substitute).

#### 4.3.1 Lime-Fayalite + 10 Wt% Calcium Fluoride System

The physical and chemical properties of slags containing calcium fluoride have been reviewed by Sommerville (130) and Davies (131). Both authors agree there is very little data on ternary and quaternary systems with $CaF_2$ as a component. What information is available, relates mainly to the $CaO-SiO_2-CaF_2$ ternary where $CaF_2$ forms a eutectic with CaO (18%) and 2 $CaO.SiO_2$ (36%) with a minimum liquidus temperature at 1360°C and 1110°C respectively.

##### 4.3.1.1 Cone Behaviour

The addition of calcium fluoride reduced the softening range of the lime-fayalite mixtures (Table 16 Fig. 22). The cones collapsed very rapidly after the initial bending of the tip. Even with a high lime to fayalite ratio of 6:4, the final collapse temperature was only 1290°C.

##### 4.3.1.2 Initial Liquidus Temperatures

The main effect of calcium fluoride was to lower the initial liquidus temperature of fayalite (Table 16 Fig. 22). For lime-fayalite mixtures, the addition produced only a small change in the temperatures at which a liquid phase appeared.

##### 4.3.1.3 Immersion Experiments

###### 4.3.1.3.1 Small Lime Pellets

Although the addition of $CaF_2$ produced a fluid melt, it did not prevent the precipitation of 2 $CaO.SiO_2$ in the lime-melt reaction zone (Plate 65). The microstructure of a specimen immersed for 15 seconds (Plate 66) showed 2 $CaO.SiO_2$ as a number of individual particles, which could not be regarded as a coherent interfacial layer. The other reaction product (an iron oxide rich liquid) had quickly penetrated the pore system where it became enriched in lime (increasing proportion of lime-iron oxide eutectic towards the centre of the cross section)(Plate 67). The differential etching of the lime grains along the same axis indicated varying amounts of iron oxide in solid solution.

During solidification, iron oxide dendrites and laths had precipitated around the particles of 2 $CaO.SiO_2$ (Plate 66). With longer immersion times, additional 2 $CaO.SiO_2$ had crystallised from the liquid phase on cooling (Plate 68). This indicated a higher $SiO_2$ content in the liquid phase than in the two previous systems.

The melt solidified as a two phase structure, but with increasing reaction time, wustite dendrites also appeared in the solid state. The wustite adjacent to the melt boundary, was associated with another phase (etched lighter than 2 $CaO.SiO_2$) (Plate 69). Using oil immersion to improve phase contrast, this other phase (grey in colour) had a honeycombed structure which suggests it was undergoing resolution after precipitation at 1300°C.

The dissolution process occurred so rapidly with rotated pellets, that very little solid lime remained after 30 seconds. With an immersion time of 15 seconds, a large number of 2 $CaO.SiO_2$ particles were observed along the melt - 2 $CaO.SiO_2$ interface (Plate 70). Even so there was no evidence of agglomeration, in fact a large proportion were redissolving in the lime-iron oxide liquid phase. From the lime-iron oxide liquid, dendrites of 2 $CaO.SiO_2$ had precipitated during cooling (Plate 71).

### 4.3.1.3.1.1. Electron Probe Analysis

Plate 72 shows a section of lime-melt interface from a specimen immersed for 30 seconds. Since fluorine could not be detected on the microprobe, the X ray images refer to iron, silicon and calcium. The distribution of silicon was important because it showed the element on both sides of the 2 $CaO.SiO_2$ layer (analysed 4.8% FeO). The concentration profiles (Fig. 23) clearly showed a silica compostional gradient towards the lime.

The concentration paths plotted on the ternary (Fig. 24) differ from those of the two previous systems in that the compositions were closer to the lime corner.

### 4.3.1.3.2. Large Lime Pellets

After a reaction time of 30 seconds, the area between the melt and the pellet contained a large number of 2 $CaO.SiO_2$ and 3 $CaO.SiO_2$ particles redissolving in the lime-iron oxide liquid phase (Plate 73). This liquid had already penetrated through to the centre of the pellet (Plate 74) whereas free lime still existed inside a pellet after 4 minutes immersion in pure fayalite.

The only microscopic difference between succeeding specimens (Plates 75 and 76) was the increasing amount of wustite precipitated from the melt during solidification.

The reaction zone between a rotated pellet and the melt is shown in Plate 77. The microstructure showed particles of 2 $CaO.SiO_2$ and 3 $CaO.SiO_2$ redissolving in the lime-iron oxide liquid phase.
At high magnification (Plate 78) the parallel twinning of 2 $CaO.SiO_2$ (associated with the $\alpha'$ to $\beta$ transition) can be clearly seen.
The dissolving particles of 3 $CaO.SiO_2$ (Plate 79) were the sites for hetrogeneous nucleation and growth processes taking place during cooling from 1300°C.

#### 4.3.1.3.3 Dissolution Kinetics

The addition of calcium fluoride to fayalite increased the dissolution of lime (Tables 7 and 9 Fig. 13 and 14). The results show that in the case of small static pellets, the dissolution rate was increased by a factor of ten (Table 11) while with large pellets the rate was only increased by a factor of four. Both rates were increased still further by rotation.

### 4.3.2 Lime-Fayalite + 10 Wt% Boric Oxide

At present there is no phase diagram for the $B_2O_3$-CaO-FeO-$SiO_2$ system. However information is available (77) regarding the phase assemblage in the following systems:-

$B_2O_3$ - CaO - $SiO_2$
CaO - $SiO_2$
$B_2O_3$ - CaO
$B_2O_3$ - $SiO_2$

Both the $B_2O_3$ - CaO and the $B_2O_3$ - $SiO_2$ phase diagrams show that $B_2O_3$ is a powerful flux for the other component. The same may be true in the $B_2O_3$ - FeO system, but this will have to be confirmed by investigation.

#### 4.3.2.1 Cone Behaviour

Boric oxide was very similar to calcium fluoride in reducing the softening range of the lime - fayalite cones (Table 17 Fig. 25). The additive also reduced the initial deformation temperature from 1100°C to 800°C as the proportion of lime increased.

#### 4.3.2.2 Initial Liquidus Temperatures

The initial liquidus temperature varied between 1050°C and 800°C depending upon the ratio of lime to fayalite in the mixture (Table 17 Fig. 25). As soon as the first liquid appeared, it rapidly fluxed the rest of the sample.

### 4.3.2.3 Immersion Experiments

#### 4.3.2.3.1 Small Lime Pellets

The pellets dissolved very quickly in the melt, even though 2 $CaO.SiO_2$ was precipitated in the reaction zone. However there was a considerable difference in the distribution of 2 $CaO.SiO_2$ along the melt-liquid interface. It varied from an almost monolithic layer (Plate 80) to a thin broken rim (Plate 81).

After only 15 seconds immersion, there was considerable wetting of the lime by the liquid phase (Plate 82). This liquid had also penetrated and dissolved parts of the 2 $CaO.SiO_2$ monolithic rim. After a reaction time of 30 seconds, it was evident that the melt was also dissolving the precipitated layer (Plate 83). The dissolution of 2 $CaO.SiO_2$ could account for the isolated regions of melt observed in the lime-iron oxide liquid phase (Plate 84).

##### 4.3.2.3.1.1 Electron Probe Analysis

Plate 85 shows the lime-melt interface of a specimen immersed for 45 seconds. Like fluorine, boron (Atomic Number 5) could not be detected on the microprobe, so the accompanying X-ray images relate only to the distribution of calcium, iron and silicon.

The precipitation of 2 $CaO.SiO_2$ did not prove to be a barrier for iron (oxide) which can be seen around the lime grains.

The distribution of silicon was very similar to that found with the first two systems i.e. a sharp drop in concentration at the 2 $CaO.SiO_2$-liquid interface (Fig. 26). Consequently the concentration paths (Fig. 27) showed a sudden change toward the FeO corner.

#### 4.3.2.3.2 Large Lime Pellets

Large eqiuaxed particles of 2 $CaO.SiO_2$ were observed along the melt-liquid interface (Plate 86) of a specimen immersed for 15 seconds. As the reaction time increased, there was a gradual transition from a planar to a corrugated rim (Plate 87). Along the melt boundary, there was extensive wetting and resolution by the melt and the lime-iron oxide liquid. In some regions the liquid had broken through to the melt (Plate 88).

### 4.3.3 Chemical Loss

Since both additives are volatile at high temperatures, separate checks were made on samples of melt after heating to 1300°C for 1 hour. Instead of 10 Wt% $B_2O_3$, the analysis was 8.7 Wt% $B_2O_3$ and instead of 10 Wt% $CaF_2$, the final analysis was 7.4 Wt% $CaF_2$.

## 4.4 Dicalcium Silicate - Fayalite System

During probe analysis of the reaction zones, there was no discernible concentration gradient of silicon (silica) from the bulk melt towards the 2 $CaO.SiO_2$ layer. The absence could be associated with the redistribution of oxides during solidification. However a similar result could be produced if two concentration profiles (one towards and the other away from the 2 $CaO.SiO_2$ layer) were superimposed one upon the other. To clarify the situation, synthetic pellets of stabilised 2 $CaO.SiO_2$ were immersed in 2 FeO. $SiO_2$ at 1300°C.

### 4.4.1 Immersion Experiments

With no solid reaction product, the melt rapidly infiltrated the pore system of the pellets (Plate 89). Within a short time (15 seconds) a large number of twinned grains (horseshoe shaped) were entirely surrounded by the melt (Plate 90). After 30 seconds (Plate 91) very little solid 2 $CaO.SiO_2$ remained.

#### 4.4.1.1 Electron Probe Analysis

Both the scanning images (Plate 92) and the concentration profiles (Fig. 28) showed compositional gradients for lime and iron oxide, while the silica concentration remained constant across the reaction interface.

#### 4.4.1.2 Dissolution Kinetics

The results are tabulated in Table 18 and plotted graphically in Fig. 29. They indicate a very high dissolution rate even though the partially dissolved pellets still had a thin layer of solidified melt adhering to the surface.

## 5. Discussion

The detailed discussion of the results and observations is given for the purpose of convenience under the following headings:-

1. The Dissolution of Small Lime Pellets in Fayalite
2. The Effect of Manganese Oxide
3. The Effect of Other Fluxes
4. The Effect of Pellet Rotation
5. The Effect of Pellet Size
6. The Rate Controlling Mechanism

### 5.1 The Dissolution of Small Lime Pellets in Fayalite

At 1300°C, the solid + liquid phase field of $2\ CaO.SiO_2$ extends almost to the FeO corner of the CaO - FeO - $SiO_2$ ternary system. This means that CaO can never be at equilibrium with a melt of composition 70 Wt% FeO - 30 Wt% $SiO_2$. The only liquids which can coexist with CaO at equilibrium are those along the line Le - Lf in Fig. 30. Although the isothermal section can provide useful information on phase assemblage, it cannot predict the spatial arrangement of the phases. This inability is illustrated by the position of dicalcium silicate relative to that of lime. While the isothermal section shows that the phase field of tricalcium silicate + liquid separates the two phase fields at 1300°C; in practice the two phases were separated by a liquid rich in iron oxide (Plate 13). Within this limitation, the 1300°C isothermal section will be used to illustrate how the composition of the various phases change during the dissolution of lime.

During the initial reaction between lime and fayalite, the interfacial liquid composition moves from $2\ FeO.SiO_2$ towards $L_b$ (Fig. 30) along the $2\ FeO.SiO_2$ - CaO isopleth. When the composition of the reaction product has a CaO to $SiO_2$ molar ratio of 2:1, $2\ CaO.SiO_2$

is precipitated between the pellet and the melt. Initially the molar ratio of 2:1 occurs very close to the CaO - 2 $FeO.SiO_2$ interface but as dissolution proceeds, the solid reaction product is precipitated some distance away from the receding pellet. The precipitation of solid 2 $CaO.SiO_2$ causes the composition of the interfacial liquid to move towards the FeO corner as it becomes enriched in the remaining components. The heterogeneous reaction can be summarised as

$$2\,CaO + 2\,FeO.SiO_2 \longrightarrow 2\,CaO.SiO_2 + L_c \text{ (fig. 30)}$$

It is the iron oxide rich reaction product which infiltrates and reacts with the porous pellet. The first iron oxide will be taken into solid solution in the CaO structure. But after 10 Wt% FeO, the solubility limit is exceeded and any additional amount causes the formation of a liquid phase. Inside the 2 $CaO.SiO_2$ layer, the liquid composition moves towards the CaO corner along $L_c - L_d$. Although the liquid compositions are very close to the CaO - FeO binary (Fig. 30) there is still sufficient silica in solution to react with lime (in solution) to precipitate prismatic crystals of 3 $CaO.SiO_2$ in the infiltrated pore system (Plate 16). Liquid compositions along $L_c - L_d$ (Fig. 30) cannot coexist with these along $L_b - L_c$. This means that where the two are in contact, 2 $CaO.SiO_2$ is precipitated along the interface. Because of their small size ($<$2 microns) the precipitated particles have a large surface area to volume ratio. To reduce their high surface energy (and surface area) the particles sinter together (Plate 18). Necks form at points of interparticle contact and an interconnected pore structure developes as the particles impinge upon one another (Plate 13).

From an examination of consecutive specimens (Plates 13, 19 and 21 ), it is apparent that the precipitated layer gradually moves inwards, keeping pace with the receding pellet - liquid interface. This observation contradicts the findings of Scheel and Oeters (132). After studying the dissolution of sintered lime pellets (trepanned from limestone) in a melt consisting of 76% FeO, 14% CaO and 10% $SiO_2$, the investigators stated that the zone of 2 $CaO.SiO_2$ precipitation moves outwards into the melt. If this was the case, the precipitation of 2 $CaO.SiO_2$ onto the outside of that already formed, would be accompanied by a high concentration of FeO at the melt - 2 $CaO.SiO_2$ interface. Electron probe analysis of the reaction zone between CaO and 2 $FeO.SiO_2$ (Fig. 10) shows that a compositional gradient for FeO exists from the bulk melt towards the lime with a sudden increase in concentration inside the 2 $CaO.SiO_2$ shell.

Scheel and Oeters said that the reason for the outward growth of the precipitate was that the diffusion coefficient of CaO is greater than that of $SiO_2$. In all diffusion processes, electrical neutrality must be preserved. If the diffusion coefficients of the various ions are different, they will influence the rate of diffusion of each other i.e. slower ions will tend to be accelerated and faster ions retarded. At the othosilicate composition, the diffusing species in the melt are $Fe^{2+}$ and $SiO_4^{4-}$. Therefore the diffusion rate of the silicate ion will be increased while that of the $Fe^{2+}$ ion will be retarded (cannot consider the ions in isolation). Since the 2 $CaO.SiO_2$ layer moves inwards, the components of the melt have to get to the reaction interface i.e. the inside surface of the 2 $CaO.SiO_2$ shell. A schematic representation of the reaction zone between CaO and 2 $FeO.SiO_2$ is shown overleaf:-

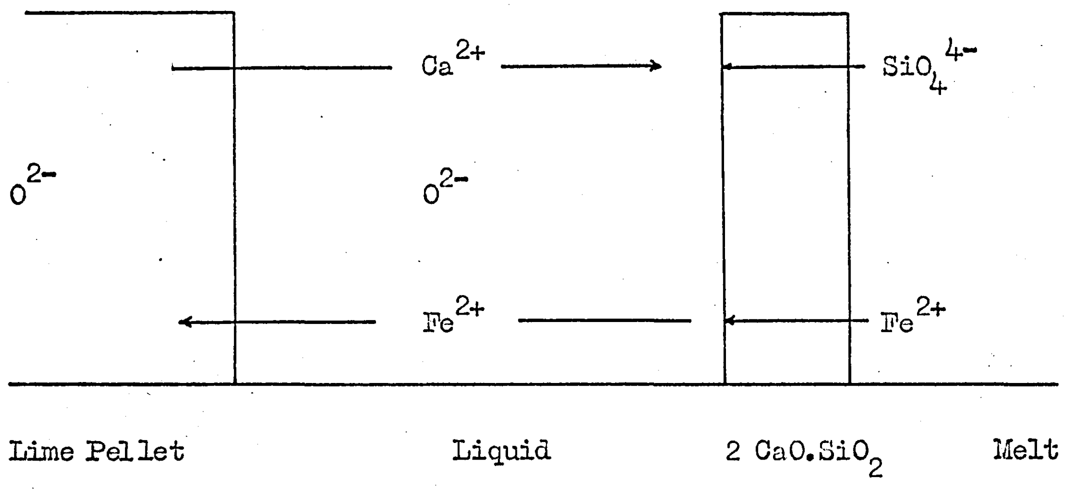

The transport of $2\ FeO.SiO_2$ to the reaction interface can be achieved by ionic diffusion through $2\ CaO.SiO_2$. This transport process is unlikely to be the main transport mechanism considering the dissolution rate of the lime pellet, the size of the $SiO_4^{4-}$ ion and the complex arrangement of atoms in the orthorhombic $2\ CaO.SiO_2$ lattice. The main transport route appears to be via the interconnected pore system in the $2\ CaO.SiO_2$ rim.

Although diffusion plays a major role in mass transfer, transport by thermal and density gradients must also be considered. Lee and Gaskell (133) have published a large quantity of data on the density of liquid melts in the $CaO-FeO-SiO_2$ system. When CaO replaces FeO in 2 (FeO, CaO) $SiO_2$, the liquid density decreases so that a density gradient exists between the bulk melt and that adjacent to the $2\ CaO.SiO_2$ layer. As dissolution proceeds, the low density liquid will rise, to be replaced by melt of higher density (and iron oxide content). This type of density gradient gives rise to inverted cone shaped specimens as shown in Plates 36 to 39. (Even without thermal or density gradients, this type of profile would be produced because dissolution occurs on two surfaces around the bottom edge of the pellet).

Besides the normal thermodynamic and density gradients, the melt and liquid phases are also under hydrostatic and capillary suction forces. The effect of these two forces is to force and draw liquid into the pore system of the pellet. The hydrostatic pressure occurs whenever a solid is immersed in a liquid. The body is under a force on all the immersed faces as the liquid (or melt) tries to lift the body. The other force, capillary suction is dependant upon the size of the pores and the degree of wetting of the solid by the liquid. If the pellet is composed of a series of uniform cylindrical straight capillary tubes of radius 'r', the magnitude of the pressure 'P' for a contact angle $\theta$ is given by $P = \frac{2\gamma \cos \theta}{r}$ (134, 135)

$\gamma$ = surface tension of the liquid

As $\cos \theta \rightarrow 1$ $\theta \rightarrow 0$ wetting tendency increases.

As the melt is drawn through the 2 $CaO.SiO_2$ layer, the FeO component is displaced by CaO. The change in free energy for the reaction $2\ CaO + 2\ FeO.SiO_2 \longrightarrow 2\ FeO + 2\ CaO.SiO_2$ is - 83 kJ $mole^{-1}$ at 1300°C (Fig. 31). The FeO released by reaction is transported down a thermodynamic gradient towards the lime. At the CaO - liquid interface, the FeO dissolves the remaining solid. The dissolved CaO migrates down a thermodynamic gradient in the direction of the 2 $CaO.SiO_2$ layer.

The first liquid reaction product ($L_c$) is at equilibrium with 2 $CaO.SiO_2$. But with an increasing proportion of CaO, the liquid has the potential to dissolve 2 $CaO.SiO_2$. However in the initial stages, the lime rich liquid reacts with the melt being drawn through the precipitated layer

$$L_d + L_b \longrightarrow 2\ CaO.SiO_2 + L_c$$

Although $L_c$ has no potential for dissolving 2 $CaO.SiO_2$, it can dissolve further CaO.

After a period of 3 -4 minutes, there is insufficient melt at the reaction interface. This deficiency is caused by compositional gradients forming in the bulk melt and/or the physical restraint of the thick precipitated layer. The result is that the lime rich liquid starts to dissolve 2 $CaO.SiO_2$

$$L_g + 2\ CaO.SiO_2 \longrightarrow Lh$$

Throughout the immersion period, fayalite was also dissolving 2 $CaO.SiO_2$.

$$2\ FeO.SiO_2 + 2\ CaO.SiO_2 \longrightarrow L_b \quad \text{(Fig. 30)}$$

Although there is no visual evidence of the latter reaction, the experiments using synthetic pellets and the base melt (section 4.4) showed how reactive 2 $FeO.SiO_2$ is with 2 $CaO.SiO_2$. However it must be remembered that 2 $CaO.SiO_2$ was the only solid phase present in the experiments whereas in the CaO - 2 $FeO.SiO_2$ system, a layer of 2 $CaO.SiO_2$ has to exist to separate compositions along $L_b - L_c$ from those along $L_c - L_d$ (Fig. 30).

In some respects, the compact 2 $CaO.SiO_2$ rim surrounding a lime pellet is analogous to the oxide layer which forms on a metal substrate. For in both cases, one is formed by the consumption of the other. During growth of an oxide layer, stresses (due to volume differences, point defects and recrystallisation etc) may be generated, and if these are of sufficient magnitude, the scale would buckle and eventually spall. In the CaO - 2 $FeO.SiO_2$ system, the layer of 2 $CaO.SiO_2$ will be in compression as it moves inwards to replace the consumed CaO. When the layer cannot withstand the pressure generated, it buckles in the hoop direction (Plate 19). If the process continued, the rim would eventually rupture. However this situation is prevented by the sintering of the precipitated particles into a strong coherent layer. Although there is some similarity, it must be remembered that unlike an oxide layer, 2 $CaO.SiO_2$ is being dissolved and reprecipitated during the immersion period.

## 5.2 The Effect of Manganese Oxide

During the initial stages (Plate 40) there was no visual evidence to suggest that MnO had been added to the melt. The presence of the addition became apparent only after the 2 $CaO.SiO_2$ envelopes had started to buckle. Large numbers of 2 $CaO.SiO_2$ particles were observed at the base of each trough along the interface (Plate 43) and in contrast to the CaO - 2 $FeO.SiO_2$ system there was no evidence of sintering.

These observations suggest that MnO alters the wetting characteristics of the melt and liquid phases such that densification of 2 $CaO.SiO_2$ is inhibited. Baker et al (102) reported similar qualitative results from laboratory tests carried out in B.S.C.'s Research and Development Department. They found that in the presence of manganese oxide, the 2 $CaO.SiO_2$ shells were noticeably looser around CaO particles. However they failed to give any details of the atmospheric conditions used in the experiments.

The increased wetting could account for the unexpected collapse of the cones with a high CaO content (Fig. 17); it could also explain the sudden collapse of the dynamic foam in a B.O.F. vessel after an addition of manganese ore (136). It is well known that some oxide additions can change the wetting of a refractory solid by a liquid phase. Jackson (137) studied the effect of a $Cr_2O_3$ addition on the size of the dihedral angle formed between periclase grains surrounded by a silicate rich liquid. The effect of the addition was to reduce the wetting of the periclase by the liquid.

In the CaO - 2 $FeO.SiO_2$ + MnO system, the variation in the amount of 2 $CaO.SiO_2$ precipitated along the interface cannot be completely explained by increased wetting. However if the melt and/or the liquid phase wets the solid phase such that a thin film covers the 2 $CaO.SiO_2$

particles, only a small force is necessary to fracture the precipitated layer. Earlier it was stated that hydrostatic and capillary suction forces are acting upon the melt and liquid phase during immersion. It is these forces which break open the protective shell of $2\ CaO.SiO_2$ at the base of each trough, thereby allowing a continuous reaction to occur between the melt and liquid phase. Along the interface peaks, these forces help to consolidate the thin solid layer.

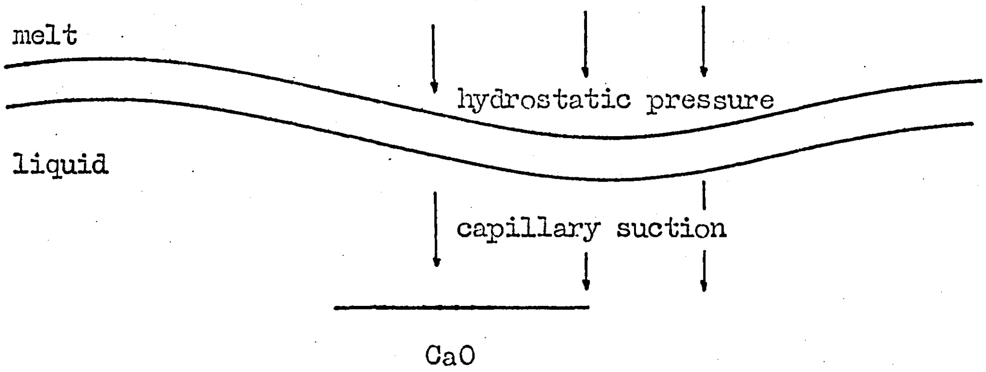

Although the hydrostatic pressure will exist as long as any solid lime remains in the melt, capillary suction will decrease as the iron oxide rich liquid penetrates the pores and channels of the pellet. After complete interpenetration, the net result is that the liquid phase is in the compression between the lime and the $2\ CaO.SiO_2$ layer. The compression may also be augmented by an additional pressure if the volume of the reaction products inside the $2\ CaO.SiO_2$ envelope is greater than the sum of the volumes of the reacting species (CaO and FeO - MnO liquid). This constraint was not a problem in the early stages when it could be relieved by the liquid infiltrating the porous pellet. But after complete interpenetration, the pressure is such that breakouts of liquid begin to occur along the peaks in the $2\ CaO.SiO_2$ layer (Plate 45).

The droplets present in the melt in the regions of liquid breakout (Plate 46) could be the result of intermittent bursting of liquid through the 2 $CaO.SiO_2$ layer and/or liquid-melt immiscibility. The second proposal seems unlikely as immiscibility is generally associated with liquids containing large quantities of silica. Without immiscibility, one would expect 2 $CaO.SiO_2$ to be precipitated by reaction at the liquid breakout-melt interface. The microstructure of a specimen immersed for 5 minutes (Plate 46) showedone liquid extrusion where the structure was different from that of the parent liquid inside the 2 $CaO.SiO_2$ layer. This observation together with electron probe analysis (Plate 57) indicates that 2 $CaO.SiO_2$ had precipitated from the liquid during breakout. By precipitation the composition of the remaining liquid (breakout) moves back along the base of the 2 $CaO.SiO_2$ saturation field towards the $FeO-MnO-SiO_2$ ternary face of the $CaO-FeO-MnO-SiO_2$ tetrahedron.. (There is no information available on the effect of MnO on the FeO + liquid phase field in the quaternary system).

Although breakouts do influence the lime dissolution rate (the breakouts help to maintain a steep concentration gradient of FeO from the melt to the 2 $CaO.SiO_2$ (Fig. 20) ) the total amount of CaO dissolved was still less than that in the CaO - 2 $FeO.SiO_2$ system. The difference is associated with an increase in melt viscosity. In 1949 Kozakervitch (138) published iso-viscosity lines for the system $FeO-MnO-SiO_2$ at 1400°C (Fig. 31). From a highly fluid zone in the FeO corner, the viscosity increases with MnO content.

Viscosity plays an important role in mass transport processes as can be seen from the Einstein equation

$$D = \frac{R\,T}{N}\left[\frac{1}{6\pi\ r\eta}\right]$$

$\eta$ = viscosity

D = diffusion coefficient

where the diffusion coefficient is proportional to the reciprocal of the viscosity at constant temperature. It is very difficult to compare the quantitative results with those obtained by Baker et al (110). Besides possible atmospheric differences the investigators used reaction temperatures of 1400°C and above. However they did report that a 10% manganese oxide addition did produce a slight inhibiting effect on the dissolution of lime by an iron silicate slag at 1400°C. But the dissolution rate constant was increased by a factor of 3.5 when the manganese oxide was prefluxed with the base slag (102). It is worth noting that in addition to manganese oxide, the prefluxed iron silicate slags also contained 4% - 6% alumina.

## 5.3 The Effect of Other Fluxes

As expected both $CaF_2$ and $B_2O_3$ increased the dissolution rate of lime. The principal effect of these additions is to lower the fusion point of the 2 $FeO.SiO_2$ melt as indicated by the cone fusion results. The result of lower melting points and decreased viscosities is a reduction in the thickness of the boundary layer, which coupled with more effective mixing produces a higher rate of mass transfer.

Both melts were very reactive with CaO and the 2 $CaO.SiO_2$ precipitate. An examination of immersed specimens showed that the iron oxide rich liquid penetrates very rapidly into the pore system of the pellets. Once inside, the liquid quickly dissolves the direct bonding between the sintered particles.

Although liquid FeO and solid 2 $CaO.SiO_2$ are the reaction products of $2\ CaO + 2\ FeO.SiO_2 \longrightarrow 2\ CaO.SiO_2 + 2\ FeO$, it is surprising that there was such a large difference in the relative amounts. This suggests that once 2 $CaO.SiO_2$ is precipitated, it is almost immediately redissolved either by the melt or by the CaO-FeO liquid. An extensive discussion of the unknown phase observed between the melt and 2 $CaO.SiO_2$ in the CaO - 2 $FeO.SiO_2$ + $CaF_2$ system cannot take place until the $CaO\text{-}CaF_2\text{-}FeO\text{-}SiO_2$ quaternary has been fully investigated.

Besides influencing viscosity, fluorine (as fluorspar) also increases the diffusion coefficients of ions in liquid slags. Johnson et al (139) has shown that in $Al_2O_3\text{-}CaO\text{-}SiO_2$ slags, fluorine nearly trebles the diffusion coefficient of the calcium ion. A similar effect was observed with the diffusion of iron when a small addition of wustite was added to the slags. Their findings regarding the acceleration of normally slow moving ions could explain the rapid transport of silicon ($SiO_2$) from the 2 $CaO.SiO_2$ layer towards the dissolving pellet (Fig. 23). For although both additions produced similar effects (lower melting points) it was only with calcium fluoride that 2 $CaO.SiO_2$ precipitated from the liquid phase during cooling.

The two systems also differ in the spatial arrangement of the 2 $CaO.SiO_2$ precipitate between the pellet and the melt. With an addition of $CaF_2$ (Plate 65) the precipitate appears as individual particles which contrasts with the monolithic layer (Plate 80) formed in the $CaO$ - 2 $FeO.SiO_2$ + $B_2O_3$ system. The latter structure however became more 'open' after an immersion period of 30 seconds (Plate 83) when the melt was observed to have penetrated the 2 $CaO.SiO_2$ rim. The ability to penetrate the precipitated layer is almost certainly associated with the interfacial melt becoming very fluid due to lime enrichment. As the concentration of lime increases in the melt, the initial melting temperature gradually decreases to below 900°C (Table 17).

## 5.4 The Effect of Pellet Rotation

A comparison of the static and dynamic dissolution rates (Table 11) clearly indicates that even slow rotation i.e. a relative velocity of 141 cm $min^{-1}$ has a pronounced effect on the solution rates in the systems studied. The effect of rotation is to decrease the thickness of the boundary layer and to increase the concentration gradients across such a layer (140). The boundary layer thickness is also a function of the kinematic viscosity of the melt. If the melt is viscous, the increase (in solution rate) will not be as high as in a low viscosity fluid. The effect of viscosity is seen below:-

| melt system | increase in static rate | |
|---|---|---|
| $2FeO.SiO_2+CaF_2$ | x 2 | |
| $2FeO.SiO_2$ | x 1.5 | increasing |
| $2FeO.SiO_2+MnO$ | x 1.2 | ↓ viscosity |

It is worth noting that while investigators have stated that the precipitation of $2\ CaO.SiO_2$ inhibits the solution of lime (64, 65); the dissolution rates increased even though the precipitated layers were thicker than in the static experiments. The increase must be associated with the physical disruption of the $2\ CaO.SiO_2$ rim by centrifugal forces. During rotation the liquid is forced out through channels in the precipitated layer (Plates 24 and 25). Like the breakouts observed with MnO in the melt, the liquid extrusions in the $CaO - 2\ FeO.SiO_2$ system appeared as droplets with no solid precipitate at the droplet - melt interface. This means that the interfacial melt composition must be enriched in lime (the composition having moved from $2\ FeO.SiO_2$ to beyond $L_j$ in Fig. 30) such that the reaction path between the droplet and the interfacial melt composition ($L_c$-$L_j$) does not intersect the FeO + liquid phase field.

Besides affecting the melt and the 2 $CaO.SiO_2$ layer, rotation also accelerated the reaction between the pellet and the iron oxide rich liquid. The effect was such that after 4 - 5 minutes, there was insufficient reacting species ($Fe^{2+}$, $SiO_4^{4-}$) at the 2 $CaO.SiO_2$ - liquid interface to precipitate 2 $CaO.SiO_2$ with all the lime in solution. This resulted in a decrease in the width of the precipitated layers (Fig. 9) and inflexions in the dissolution graphs (Fig. 13).

## 5.5 The Effect of Pellet Size

The most striking feature observed in the reaction zone surrounding the large pellets was the narrow width of the 2 $CaO.SiO_2$ layer (Fig. 12). Even with an immersion time of only 1 minute, the precipitated layer was being redissolved by the CaO-FeO liquid phase. These observations suggest that the transport of reaction species from the bulk melt to the 2 $CaO.SiO_2$ - CaO.FeO liquid interface was insufficient to precipitate 2 $CaO.SiO_2$ with all the CaO in solution.

Another structural difference between the two sizes was that the 2 $CaO.SiO_2$ layer always remained very close to the large pellets. This is consistent with a slow rate of dissolution and a reduced rate of CaO transfer from the pellet to the CaO.FeO liquid - 2 $CaO.SiO_2$ interface. The equation for the rate of mass transfer of CaO from the bulk CaO.FeO liquid to the 2 $CaO.SiO_2$ rim is given by:-

$$\frac{dn}{dt} = \frac{D}{\delta} (C_b - C_i) \qquad \text{per unit area of interface}$$

$C_b$ = bulk concentration of CaO in the liquid phase

$C_i$ = interfacial concentration of CaO at the 2 $CaO.SiO_2$ rim

$$\left.\begin{array}{ll} D = & \text{Diffusion coefficient} \\ \delta = & \text{thickness of the boundary layer} \end{array}\right\} \text{same for both sizes of pellet}$$

$$\therefore \text{rate of transfer} \propto (C_b - C_i)$$

$C_b$ will be higher with small pellets because of the faster dissolution rate

$C_i$ will be lower for small pellets because the CaO is consumed as soon as it reaches the CaO.FeO liquid - 2 $CaO.SiO_2$ interface. The net effect is a lower rate of transfer of CaO in the liquid surrounding the large pellets.

With a lower rate of dissolution (compared to the small pellets) it is curious that 2 $CaO.SiO_2$ precipitated from the melt adjacent to the 2 $CaO.SiO_2$ layer on cooling. This is probably due to the higher heat capacity of the large pellets. Because the interfacial melt cools more slowly, sufficient time is available for the precipitation of 2 $CaO.SiO_2$.

No liquid breakouts were observed around large specimens immersed in 2 $FeO.SiO_2$ with a MnO addition. Whereas the liquid phase had penetrated to the centre of small pellets after 4 minutes, there was still unreacted CaO present in large specimens after an immersion time of 7 minutes. Consequently the liquid was still under capillary suction.

The reason for no breakouts around rotated specines is a lower centrifugal force (the magnitude being dependant upon the reciprocal of the pellet radius).

An interesting feature seen in one large specimen is the structure inside an infiltrated crack (Plate 32). The entrapped liquid had come to partial equilibrium with CaO because the narrow opening of the crack prevented melt renewal. [ Penetration Experiments (section 3.3.4) were always unsuccessful.]

## 5.6 Rate - Controlling Mechanism

The dissolution of lime pellets in 2 $FeO.SiO_2$ is envisaged to take place in the following manner. FeO and $SiO_2$ diffuse from the bulk melt to the 2 $CaO.SiO_2$ - liquid interface where they react with CaO (in solution) to precipitate 2 $CaO.SiO_2$. The 2 $CaO.SiO_2$ in turn dissolves in the melt, allowing CaO and $SiO_2$ to diffuse from the interface into the bulk melt. In this mechanism there are several possible rate - controlling stages:-

1. The transport of melt to the 2 $CaO.SiO_2$-liquid interface
2. The transport of FeO from the 2 $CaO.SiO_2$-liquid interface to the pellet
3. Reaction between CaO and FeO
4. The transport of CaO to the liquid - 2 $CaO.SiO_2$ interface
5. Reaction between CaO and the melt to form 2 $CaO.SiO_2$
6. Dissolution of 2 $CaO.SiO_2$ by the melt
7. Transport of CaO from 2 $CaO.SiO_2$ into the bulk melt.

### 5.6.1 Small Lime Pellets

The increase in the dissolution rate under conditions of forced convection indicates that the rate-limiting stage is a transport process. An essential feature of diffusion controlled dissolution is the formation of concentration gradients. The concentration profiles for CaO into the melt and FeO into the pellet were very steep. These two transport processes are not thought to be rate controlling since the CaO - 2 $FeO.SiO_2$ system can never come to equilibrium [ the ratio of 2 $FeO.SiO_2$ to CaO was 60:1 by weight ] . This leaves two possible stages namely 1 and 4. In Fig. 13 there is an inflexion in the graphs which coincides with the peak thickness of the 2 $CaO.SiO_2$ layer (Fig. 9). These results and observations indicate that in the early stages CaO transport is rate controlling but later melt transport to the reaction interface becomes rate controlling. Support for this mechanism is provided by the observation of $3\ CaO.SiO_2$ crystals precipitated on the $2\ CaO.SiO_2$ layer surrounding a specimen immersed for 4 minutes (Plate 20).

Although an addition of manganese oxide to the melt reduced the dissolution rates, it did not affect the position of the inflexion in the dissolution graphs (Fig. 13) nor the timing of the peak thickness of the $2\ CaO.SiO_2$ layers (Fig. 9). These two observations suggest that the same rate controlling stages were operating in the CaO - $2\ FeO.SiO_2$ + MnO system.

With calcium fluoride in the melt, the most likely rate controlling stage is melt transport. Visual confirmation of this mechanism is provided by the observation of horseshoe shaped particles of $2\ CaO.SiO_2$ dissolving in the lime-iron oxide liquid phase.

Without quantitative measurements, it is difficult to predict the rate controlling stage(s) for dissolution in melts containing boric oxide. However the qualitative evidence suggests melt transport is probably rate controlling.

### 5.6.2 Large Lime Pellets

With large lime pellets, there was no inflexion in quantitative results from the static and rotational experiments. This fact coupled with the photomicrographs showing $2\ CaO.SiO_2$ dissolving in the lime-iron oxide liquid phase, suggests that in the four melt systems, the rate controlling stage is melt transport to the reaction interface.

## 6. Conclusions

The investigation of the dissolution of small lime pellets in static and dynamic contact with an iron silicate melt at 1300°C under an argon atmosphere leads to the following conclusions.

1. The reaction between lime and fayalite produced two reaction products, solid 2 $CaO.SiO_2$ and a liquid rich in iron oxide. As dissolution proceeded, the precipitated particles of 2 $CaO.SiO_2$ sintered together to form a tenacious layer between the two reactants.

2. Initially the dissolution of lime was controlled by the transport of lime to the liquid - 2 $CaO.SiO_2$ interface but at a later time the rate controlling stage was the transport of the reacting species of the melt (iron oxide and silica) from the bulk melt to the 2 $CaO.SiO_2$ - liquid interface.

3. The presence of manganese oxide in the melt was detrimental to the dissolution of lime. Even though the 2 $CaO.SiO_2$ particles formed a 'porous' layer, the overall kinetics were retarded by the increased viscosity of the melt and liquid phases.

4. In contrast, additions of calcium fluoride and boric oxide accelerated the dissolution of lime. The increase being associated with a decrease in melting points and viscosities.

5. In the systems examined (except fayalite + boric oxide) the rate of dissolution increased significantly when a relative velocity was applied between the lime and the melt. The actual increase being dependent upon the viscosity of the melt.

6. With large lime pellets, the static and dynamic dissolution rates were lower than those of the corresponding smaller pellets dissolving in similar melts. Visual evidence suggested that the reaction was under melt transport control.

7. No comparison can be made between the dissolution rates for the

two sizes of pellet. The reason being that in the initial stages dissolution is controlled by different transport processes. By the time dissolution was controlled by melt transport, large concentration gradients would have formed around the small pellets.

## 7. Suggestions for Future Work

Besides slag composition, the influence of slag temperature and oxygen potential on lime dissolution cannot be ignored. The slag temperature increases from approximately 1300°C to above 1600°C during the oxygen blow. In the LD vessel considerable differences exist in the partial pressure of oxygen between parts in contact with the oxygen jet and those through which pass bubbles of carbon monoxide. In the $CaO - FeO_x - SiO_2$ system, the $2\,CaO.SiO_2$ + liquid phase field moves towards the $CaO - SiO_2$ binary with increasing temperature and oxygen potential (10). In addition to studying the effect on lime dissolution, the influence of each parameter on viscosity can be determined using a Haake Viscometer (recently acquired by the Metallurgy Department). In the last few years a number of minerals such as ilmenite have been promoted as lime fluxes. Industrial - scale trials of each flux would be expensive in terms of time and manpower. Laboratory scale experiments using the immersion apparatus would provide a quick method for screening the large number of suggested fluorspar substitutes.

An obstacle to the understanding of the effect of different fluxes has been a lack of knowledge of the phase relationships involved. To study phase assemblages using the vertical tube furnace (Plate 7) the bottom head would have to be replaced with an oil quenching bath. By quenching equilibrated samples, the high temperature microstructure can be retained for examination at room temperature.

## 8. Appendix 1

### Immersion Experiments using Commercially Available Lime

Throughout the investigation, only pure components were used. For the lime pellets in particular the starting material was Analar calcium hydroxide. After calcination, the lime analysed 99+% CaO, which is higher than that quoted for commercial soft burnt lime (96+% CaO).

To ascertain whether the results and observations (in particular the liquid extrusions with MnO in the melt) were characteristic only of the dissolution of synthetic hard burnt lime, immersion experiments were carried out using commercially available lime. The soft burnt lime (kindly supplied by CAPL), was in the form of lumps (25 - 75 mm) with a porosity of 60 per cent. Because of the difference in porosity and size (compared to the synthetic pellets) the as received lime was fired for 2 hours at 1550°C (reducing the porosity to 35%) and then machined into cylinders approximately 10 mm in diameter and 20 mm long.

The immersion experiments and subsequent specimen preparation were carried out using the same procedures as per the synthetic pellets.

Photomicrographs of the reaction zone between CaO and

1. 2 $FeO.SiO_2$ are shown in
   Plate 93 - 2 minutes immersion
   Plate 94 - 4 minutes immersion
   Plate 95 - 4 minutes immersion
   Plate 96 - 6 minutes immersion
2. 2 $FeO.SiO_2$ + 10 Wt% MnO are shown in
   Plate 97 - 2 minutes immersion
   Plate 98 - 4 minutes immersion

Plate 99 - 6 minutes immersion

Except for the athermal precipitation of 2 $CaO.SiO_2$ the structures of the lime - melt reaction zones were very similar to those surrounding small synthetic pellets.

In the CaO - 2 $FeO.SiO_2$ system, the 2 $CaO.SiO_2$ layer had buckled, however no discontinuities were observed along the melt boundary. An interesting feature seen in the microstructure of a specimen immersed for 4 minutes,was the corrugated surface of the lime particles inside the reacted pellet. This suggests that the individual particles were inhomogeneous in composition.

In both systems, the liquid phase quickly penetrated to the centre of the lime pellets. With an addition of MnO in the melt, liquid breakouts were observed after an immersion period of 4 minutes (Plates 98 and 99). However it is possible that the breakouts were beginning to occur after 2 minutes, as indicated by the white phase at the melt - 2 $CaO.SiO_2$ interface (Plate 97). But being so small it is difficult to say whether this phase had formed isothermally or athermally.

## Appendix 2

### Errors in the Immersion Experiments

### 1. Temperature

At 1300°C, the thyristor 'drive' controlled the furnace temperature to ± 10°C. The actual temperature inside the furnace was measured by a Cambridge Potentiometer with an accuracy of 0.5 per cent.

### 2. Time

The immersion time was measured by a stop watch. The unknown time error is the time taken to withdraw the assembly from the furnace and quench it to below the minimum reaction temperature.

### 3. Rotational Speed

The speed of the rotating pellet dropped slightly with the additional drag at the start of the experiment. An immediate correction to the voltage of the drive motor increased the speed to 141 cm $\text{min}^{-1}$.

### 4. Pellet Volume

The volumes of irregular shaped bodies determined by the immersion technique were within 1% of the volume derived from the ratio of mass to density.

### 5. Pellet Diameter

Each micrometer measurement was in error by less than 0.03 mm, this was reduced to negligible proportions by averaging.

## 9. References

1. J. R. Robinson Steel Furnace Monthly 1973 8 515-520.
2. W. J. B. Chater and J. L. Harrison Recent Advances with Oxygen in Iron and Steelmaking 1964 Butterworth
3. C. Bodsworth and H. B. Bell. Physical Chemistry of Iron and Steel Manufacture 1972 Longman.
4. R. A. Hacking Iron and Coal Trades Review 1960 181 1107-1114
5. J. P. Coheur and P. Nilles C.N.R.M. 1967 No. 12 43-56
6. T. F. Pearson et al Journal of Iron and Steel Inst. 1966 204 997-1006.
7. Heat and Mass Transfer in Process Metallurgy ed by A.W.D. Hills 1967 Inst. of Mining and Metallurgy
8. T. Tait and J. T. Lewis The British Steelmaker 1969 35 16-20
9. A. Decker and P. Metz Iron andCoal Trades Review 1960 180 521-528
10. B. Trentini Trans. Met. Soc. AIME 1968 242 2377-2388
11. L.E.K. Holappa and P.A. Kostano Scan. J. of Metallurgy 1974 3 56-60.
12. J.M. Pena and D. Radke J. of Metals 1971 23 27-32
13. J.C. d'Entremont and R. E. Moon J. of Metals 1969 21 53-56
14. A. Ramaciotti Proceedings of Conference Iron and Steel Inst. of Japan 1971 297-300
15. T. O. Dormsjo Iron and Steel Engineer 1959 36 67-77
16. B. Kalling and F. Johansson J.I.S.I. 1959 192 330-338
17. R. Graef J. of Metals 1957 9 1435-1439
18. K. Brotzmann Technik Forschung 1968 21 718-720
19. M. C. Harrison and P. Trusscott J.I.S.I. 1961 198 341-352
20. Short Note C.R.M. 1972 March 43-44
21. P. Leroy Iron and Steel Engineer 1972 49 51-55

22. P. Nilles and M. Boudin Ironmaking and Steelmaking 1974 1 22-27
23. Anon. J. of Metals 1972 24 31-37
24. R. H. Parker An Introduction to Chemical Metallurgy 1967 Pergamon
25. R. G. Ward Introduction to the Physical Chemistry of Iron and Steelmaking 1962 Arnold.
26. R. D. Walker and D. Anderson Iron and Steel 1972 June 271-276 Aug. 403-407 Oct. 497-501
27. A. Kuznetzov et al Steel in USSR 1972 2 516-517
28. M. D. Ward J.I.S.I. 1970 208 445-449
29. H. C. Vasher and E. H. Hamilton Trans A.I.M.E. 1931 95 215
30. S. Marshall and J. Chipman Trans American Soc of Metals 1942 30 695
31. H. W. Meyer J.I.S.I. 207 1969 781-789
32. E. W. Mullholland et al J.I.S.I. 1973 211 632-639
33. T. Kootz and A. Altgeld Proc. of Conf. J. of Iron and Steel Inst. Japan 1971 527-531
34. D. J. Price Ph.D. Thesis Brunel Univ. 1972
35. M. G. Frohberg Proc. of Conf. on Chem. Met. 1972 139-143
36. S. G. Afanasev et al Stal in English 1969 620-625
37. W. O. Philbrook Open Hearth Proceedings 1961 44 376-400
38. M. Kurita Proc. of Conf. J. of Iron and Steel Inst. Japan 1971 236-238
39. V. V. Smoktii et al Stal 1971 2 118-120
40. L. C. Anderson and J. Vernon J.I.S.I. 1970 208 329-335
41. B. Ruzicka Hutnik 1971 98-101
42. K - H Obst et al Reaction Parameters of Lime 173-192 ASTM 1970
43. A. A. Hejja J. of S. African Inst. of Min. and Met. 1973 249-257

44. K - H Obst and J. Stradtman Blast Furnace Steel Plant 1969 57 933-937
45. B. Ruzicka Hutnik 1971 184-187
46. J. L. Eades and P. A. Sandberg Reaction Parameters of Lime 3-24 A.S.T.M. 1970
47. J. A. Gregory J.I.S.I. 1965 203 886-891
48. K. F. Behrens J. of Metals 1965 17 776-784
49. B. C. Welbourn and R. Kulig BISRA. Report SM/AL/118/70
50. J. Eibl and F. Hubner Berg - Hutten Monatsh 1970 115 231-239
51. P. Nilles et al J. of Metals 1967 19 18-23
52. B. C. Welbourn and R. Kulig C.A.P.L. Report SM/A/28/73
53. O. Cuscolesca and K. Rosner J.I.S.I. 1959 192 147-153
54. G. Tromel and E. Gorl Stahl and Eisen 1963 83 1035-1051
55. G. Tromel et al Proc. of Conf. Iron and Steel Inst. Japan 1971 511-515
56. F. Bardenheuer Blast Furnace Steel Plant 1970 58 401-407
57. W. C. Allen and R. B. Snow J. Am. Ceram. Soc. 1955 38 264-280
58. F. Bardenheuer and P. G. Oberhauer Stahl and Eisen 89 988-994
59. P. Kozakevitch J. of Metals 1969 21 57-67
60. C. F. Cooper and J. A. Kitchener J.I.S.I. 193 1959 48-55
61. P. Nilles and E. H. Dennis J. of Metals 1969 21 74-79
62. P. V. Riboud et al C.D.S. Circ. 1970 (4) 987-998
63. K - H Obst and J. Stradtman J. of S. A. Inst. of Mining and Met. 1972 158-164
64. G. Tromel and E. Gorl Inst. of Conf. on Oxygon Steelmaking Le Touquet 1963
65. W. J. Schlitt and G. W . Healy Ceram. Bull. 1971 50 954-957
66. F. Reinders et al Stahl and Eisen 1969 89 57-63
67. K - H Obst et al Stahl and Eisen 1970 90 460-465

68. H. J. Fleischer and W. A. Fischer Arch. Eisen 1967 38 185-190

69. B. Trentini et al J.I.S.I. 1959 192 143-147

70. B. Trentini et al J. of Metals 1962 14 570-583

71. S. F. Efimenko et al Stal 1972 43-44

72. F. Schenouda et al Iron and Steel 1971 167-172

73. G.C.R. Mathieson J.I.S.I. 1968 206 337-344

74. R. O. Russell J. of Metals 1967 19 104-106

75. E. Schurrman et al. Arch Eisen 1968 39 815-821

76. D. Engledow B.S.C. Report SM 6501/-/71/D

77. Phase Diagram for Ceramists Levin et al 1964

78. J. White Ironmaking and Steelmaking 1974 1 115-117

79. K. - H. Obst et al J.I.S.I. 1970 208 450-456

80. A. W. Hutnik and J. Buzdov Open Hearth Proceedings 1973 56 377-383

81. V. W. Jones Open Hearth Proceedings 1944 27 220-224

82. L. D. Newsletter No. 58 Kaiser Engineers 1971

83. K - H Obst et al Tonind - Ztg 1968 92 348-352

84. Anon. Industrial Minerals 1972 No. 60 34-35

85. R. K. Iyengar and F. C. Petrilli J. of Metals 1973 25 21-26

86. N. I. Yaroshenko et al Steel in the U.S.S.R. 1971 1 690-692

87. J. G. Harhai and D. A. Dukelow J. of Metals 18 833-835

88. B. C. Welbourn B.S.C. Report SM/A/121/70

89. M. Timucin and A. E. Morris Reaction Parameters of Lime 1970 A.S.T.M. 25-30

90. N. I. Rogovtsev et al. Steel in the U.S.S.R. 1972 2 518-520

91. B. C. Welbourn and R. Kulig B.S.C. Report CAPL/SM/A/53/73

92. Anon. 33 Magazine 1973 11 42-43

93. S. K. Sharma and T. W. Miller Open Hearth Proceedings 1974 57 178-188

94. B.P. 1218805

95. H - K Obst et al Stahl and Eisen 1972 92 260-262

96. P. G. Oberhauser et al Stahl and Eisen 1974 94 136-143

97. H. P. Haastert et al Stahl and Eisen 1972 92 255-259

98. E. Gorl et al Arch Eisen 1969 40 959-967

99. B. M. Boichenko Steel in the U.S.S.R. 1971 1 204-205

100. W. Kohler et al Stahl and Eisen 1967 87

101. V. M. Servetnik et al Stal in English 1969 1041-1042

102. K. L. Baker et al B.S.C. Report PC/5632/4/69/A

103. K. L. Baker et al B.S.C. Report PC/5632/6/70/A

104. C. R. Beecham and R. E. Steger Ceram. Bull. 1973 52 194

105. K. L. Baker et al B.S.C. Report PC/SM/6023/1/70/D

106. B. C. Welbourn and R. Kulig B.S.C. Report CAPL/SM/A/58/73

107. S. S. Volkov et al Izv VUZ Chern Met 1965 52-58

108. G. S. Yershov Izv VUZ Chern Met 1966 71-73

109. R. W. Limes and R. O. Russell Reaction Parameters of Lime 1970 A.S.T.M. 161-172

110. K. L. Baker et al B.S.C. Report PC/5632/5/69/A

111. G. Derge and J. R. Shegog Reaction Parameters of Lime 1970 A.S.T.M. 132-142

112. T. Kootz and A. Altgeld Trans Thyssen Forschung1970 2 171-181

113. F. Oeters Arch Eisen 1966 37 209-219

114. K. W. Lange Arch Eisen 1971 42 233-241

115. M. Ya. Medzhibozhskii et al Izv UVZ Chern Met 1973 41-45

116. A. E. Williams Trans Brit Ceram Soc. 1951 50 215-224

117. S. Dickinson B.Sc Project Sheffield Polytechnic 1971

118. D. R. Ashworth J. of Brit. Ceram. Soc. 1969 6 70-72

119. M. A. Bredig J. of Am. Ceram. Soc. 1950 33 188-192

120. E. S. Newman and L. S. Wells Nat. Bur. of Standards 1946 36 137-158

122. G. A. Rankin and F. E. Wright Am. J. Sci. 1915 39 1-79

123. J. H. Welch J. Sci. Inst. 1954 31 458-463

124. D. G. Jones and D. A. Melford Trans Brit Ceram Soc. 1969 68 241-247

125. G. Shaw and E. Vago Proceedings Brit Ceram Soc. 1969 13-14 1-27

126. P. Waudby Ph.D. Thesis Sheffield Polytechnic 1974

127. P. Kofstad High Temperature Oxidation of Metals 1966 Wiley and Co.

128. J. White J.I.S.I. Carnegie Scholarship 1938 1-38

129. E. A. Otto J. of Electrochem. Soc. 1964 111 88-92

130. I. D. Sommerville Univ. of Strathcylde Met. Journal 1972 No. 21 53-60

131. M. W. Davies Proc. of Int. Conf on Met. Chem. Sheffield I.S.I. 43-51

132. F. Oeters and R. Scheel Arch Eisen 1974 45 575-580

133. Y. E. Lee and D. R. Gaskell Met Trans 1974 5 853-860

134. J. E. Comeforo and R. K. Hursch J. of Am. Ceram. Soc. 1952 35 142-148

135. R. Scheel and F. Oeters Arch Eisen 1971 42 769-777

136. R. Baker B.S.C. Report CAPL/SM/A/31/74

137. B. Jackson Ph.D. Thesis Sheffield University 1965

138. P. Kozakevitch Rev. Metall 1949 46 505-516

139. R. F. Johnson et al Ironmaking and Steelmaking 1974 1 220-227

140. Physical Chemistry of Melts in Metallurgy F.D. Richardson 1974 Academic Press

## 10. Acknowledgements

In presenting this thesis, the author has pleasure in expressing his gratitude to Dr. G. Briggs and Dr. R. Baker for their guidance, advice and criticism during their supervision of the work.

Thanks are due to the technical staff of the Department of Metallurgy, especially Mr. D. O. Latimer, Mr. P. J. Roebuck and Mr. G. A. E. Williams for their assistance in the building of apparatus and preparation of materials.

My thanks are also due to my fellow post graduates noteably Robin Acheson and John Jordan for all their interest and help.

The author is indebted to Mrs. S. Davenport for her considerable patience and skill in the typing of this thesis.

Acknowledgement is also made to Sheffield Education Authority for providing financial support during the period spent at Sheffield Polytechnic.

## Table 1

## Xray data for 2 FeO.SiO$_2$

## Mo. Radiation Zr. Filter

| Author's Sample | | 2FeO.SiO$_2$ (ASTM Card 20-1139) | |
|---|---|---|---|
| 'd' spacing Å | Comparative Intensity I/I$_I$ | 'd' spacing Å | Comparative Intensity I/I$_I$ |
| 5.25 | W | 5.23 | 40 |
| 4.00 | M | 3.98 | 50 |
| 3.50 | VS | 3.55 | 80 |
| 2.80 | S | 2.828 | 90 |
| 2.64 | W | 2.630 | 50 |
| 2.56 | S | 2.565 | 70 |
| 2.50 | VS | 2.501 | 100 |
| 2.40 | W | 2.410 | 50 |
| 2.30 | S | 2.307 | 60 |
| 1.84 | S | 1.838 | 60 |
| 1.78 | VS | 1.777 | 90 |

VS - very strong
S - strong
M - medium
W - weak

## Table 2

## $CaO-2\ FeO.SiO_2$ in argon

### Results from hot filament microscope and cone fusion tests

| Ratio of Lime to Fayalite | Hot Filament Microscope | Cone Fusion Tests | | Remarks |
|---|---|---|---|---|
| | Initial Liquidus Temperature oC | Initial Bending Temperature oC | Final Collapse Temperature oC | |
| 0-10 | 1170-1200 | 1150 | 1220 | Gradual collapse after initial deformation of the tip |
| 1-9 | 1100-1120 | 1100 | 1170 | |
| 2-8 | 1100-1125 | 1140 | 1200 | |
| 3-7 | 1090-1120 | 1090 | 1240 | |
| 4-6 | 1070-1100 | 1080 | 1425 | Collapse ceased after initial deformation - resumed 20°C before final collapse |
| 5-5 | 1070-1100 | 1080 | >1500 | |
| 6-4 | 1130-1150 | 1140 | >1500 | |

## Table 3

## $CaO-2\ FeO.SiO_2$ heated in air

### Results from hot filament microscope and cone fusion tests

| Ratio of Lime to Fayalite | Hot Filament Microscope | Cone Fusion Tests | | Remarks |
|---|---|---|---|---|
| | Initial Liquidus Temperature oC | Initial Bending Temperature oC | Final Collapse Temperature oC | |
| 0-10 | 1550-1570 | >1500 | >1500 | Collapse temperature decreased with additions of lime |
| 1-9 | 1200-1240 | 1190 | >1500 | |
| 2-8 | 1190-1220 | 1180 | 1340 | |
| 3-7 | 1170-1200 | 1170 | 1270 | |
| 4-6 | 1170-1200 | 1150 | 1250 | |
| 5-5 | 1230-1250 | 1240 | 1350 | |
| 6-4 | 1300-1320 | 1270 | 1500 | |

## Table 4

The average thickness of the dicalcium silicate layer precipitated around small lime pellets during immersion in fayalite and fayalite + 10 Wt% manganese oxide

| Immersion Time min. | $2\ FeO.SiO_2$ | | $2\ FeO.SiO_2$+10 Wt% MnO | |
|---|---|---|---|---|
| | Thickness of $2CaO.SiO_2$ rim µm | | Thickness of $2CaO.SiO_2$ rim µm | |
| | static | rotated | static | rotated |
| 1 | 5 | 27 | 10 | 17 |
| 2 | 10 | 47 | 12 | 35 |
| 3 | 17 | 70 | 15 | 50 |
| 4 | 40 | 90 | 27 | 62 |
| 5 | 28 | 10 | 5 | 20 |
| 6 | 14 | 5 | 7 | 5 |
| 7 | 10 | 5 | 5 | 5 |
| 8 | 5 | | 5 | |
| 9 | 5 | | 5 | |

## Table 5

The average thickness of the dicalcium silicate layer precipitated around large lime pellets during immersion in fayalite and fayalite + 10 Wt% manganese oxide

| Immersion Time min. | $2\ FeO.SiO_2$ | | $2\ FeO.SiO_2$+10Wt% MnO | |
|---|---|---|---|---|
| | Thickness of $2CaO.SiO_2$ rim µm | | Thickness of $2CaO.SiO_2$ rim µm | |
| | static | rotated | static | rotated |
| 1 | 5 | 7 | 6 | 3 |
| 2 | 5 | 5 | 6 | 3 |
| 3 | 7 | 10 | 5 | 4 |
| 4 | 5 | 7 | 4 | 4 |
| 5 | 5 | 5 | 4 | 4 |
| 6 | 5 | 5 | 4 | 4 |
| 7 | 5 | 5 | 5 | 5 |

## Table 6

## Dissolution of small lime pellets in fayalite and fayalite + 10 Wt% manganese oxide

| Immersion Time min. | $2\ FeO.SiO_2$ vol. loss $cm^3\ cm^{-2}$ |  | $2\ FeO.SiO_2 + 10\ Wt\%\ MnO$ vol. loss $cm^3\ cm^{-2}$ |  |
|---|---|---|---|---|
|  | static | rotated | static | rotated |
| 0.5 | 0.0155 | 0.021 | 0.009 | 0.012 |
| 1 | 0.026 | 0.034 | 0.017 | 0.020 |
| 2 | 0.043 | 0.058 | 0.029 | 0.034 |
| 3 | 0.058 | 0.081 | 0.043 | 0.049 |
| 4 | 0.062 | 0.105 | 0.051 | 0.065 |
| 5 | 0.067 | 0.129 | 0.057 | 0.074 |
| 6 | 0.070 | 0.140 | 0.062 | 0.082 |
| 7 | 0.074 |  | 0.068 | 0.091 |
| 8 | 0.079 |  | 0.075 |  |
| 9 | 0.084 |  | 0.081 |  |

## Table 7

## Dissolution of small lime pellets in fayalite + 10 Wt% calcium fluoride

| Immersion Time sec. | $2\ FeO.SiO_2 + 10\ Wt\%\ CaF_2$ vol. loss $cm^3\ cm^{-2}$ |  |
|---|---|---|
|  | static | rotated |
| 7.5 | 0.022 | 0.054 |
| 15 | 0.04 | 0.079 |
| 22.5 | 0.060 | 0.105 |
| 30 | 0.074 |  |
| 45 | 0.11 |  |

## Table 8

### Dissolution of large lime pellets in fayalite and fayalite + 10 Wt% manganese oxide

| Immersion Time min. | $2\,FeO.SiO_2$ vol. loss $cm^3\ cm^{-2}$ | | $2\,FeO.SiO_2$+10 Wt% MnO vol. loss $cm^3\ cm^{-2}$ | |
|---|---|---|---|---|
| | static | rotated | static | rotated |
| 0.5 | 0.008 | 0.017 | 0.006 | 0.012 |
| 1 | 0.015 | 0.028 | 0.012 | 0.020 |
| 1.5 | 0.020 | 0.037 | 0.015 | 0.025 |
| 2 | 0.026 | 0.049 | 0.021 | 0.031 |
| 3 | 0.035 | 0.073 | 0.027 | 0.045 |
| 4 | 0.044 | 0.086 | 0.035 | 0.059 |
| 5 | 0.053 | | 0.044 | 0.075 |
| 6 | 0.064 | | 0.049 | |
| 7 | 0.073 | | 0.055 | |

## Table 9

### Dissolution of large lime pellets in fayalite + 10 Wt% calcium fluoride

| Immersion Time sec. | $2\,FeO.SiO_2$ + 10 Wt% $CaF_2$ vol. loss $cm^3\ cm^{-2}$ | |
|---|---|---|
| | static | rotated |
| 7.5 | 0.009 | 0.029 |
| 15 | 0.015 | 0.052 |
| 22.5 | 0.021 | 0.070 |
| 30 | 0.025 | 0.085 |
| 60 | 0.039 | |
| 90 | 0.061 | |
| 120 | 0.079 | |
| 150 | 0.099 | |

## Table 10

### Dissolution of large lime pellets with different preheat temperatures in fayalite

| Immersion Time min. | Pellet Preheat Temperature | | |
|---|---|---|---|
| | 1300°C vol. loss cm$^3$ cm$^{-2}$ | 1000°C vol. loss cm$^3$ cm$^{-2}$ | 600°C vol. loss cm$^3$ cm$^{-2}$ |
| 1 | 0.015 | 0.010 | 0.001 |
| 2 | 0.025 | 0.0193 | 0.009 |
| 3 | 0.035 | 0.030 | 0.0193 |
| 4 | 0.044 | 0.0375 | 0.0282 |

## Table 11

### Dissolution rates of small and large lime pellets in different melts

| Pellet | 2 FeO.SiO$_2$ cm$^3$ cm$^{-2}$ min$^{-1}$ | | 2 FeO.SiO$_2$+MnO cm$^3$ cm$^{-2}$ min$^{-1}$ | | 2FeO.SiO$_2$+CaF$_2$ cm$^3$ cm$^{-2}$ min$^{-1}$ | |
|---|---|---|---|---|---|---|
| | static | rotated | static | rotated | static | rotated |
| Small Lime | 0.0185<br>0.0045 × | 0.0275<br>0.0140 × | 0.0125<br>0.006 × | 0.0150<br>0.009 × | 0.150 | 0.30 |
| Large Lime | 0.010 | 0.0210 | 0.0075 | 0.0140 | 0.037 | 0.188 |

× Figures represent the rates before and after the inflexion in the graphs (Fig. 13) of volume loss plotted against time.

## Table 12

## CaO - 2 FeO.$SiO_2$ + 10 Wt% MnO in argon

## Results from hot filament microscope and cone fusion tests

| Ratio of Lime to Fayalite | Hot Filament Microscope | Cone Fusion Tests | | Remarks |
|---|---|---|---|---|
| | Initial Liquidus Temperature oC | Initial Bending Temperature oC | Final Collapse Temperature oC | |
| 0-10 | 1190-1220 | 1160 | 1240 | Manganese oxide increased the total collapse temperatures of all the lime-melt mixtures |
| 1-9 | 1110-1130 | 1090 | 1170 | |
| 2-8 | 1150-1170 | 1180 | 1230 | |
| 3-7 | 1130-1150 | 1140 | 1300 | |
| 4-6 | 1100-1130 | 1110 | >1500 | |
| 5-5 | 1120-1140 | 1100 | >1500 | |
| 6-4 | 1170-1200 | 1170 | >1500 | |

## Table 13

## CaO - 2 FeO.$SiO_2$ + 20 Wt% MnO in argon

## Results from hot filament microscope and cone fusion tests

| Ratio of Lime to Fayalite | Hot Filament Microscope | Cone Fusion Tests | | Remarks |
|---|---|---|---|---|
| | Initial Liquidus Temperature oC | Initial Bending Temperature oC | Final Collapse Temperature oC | |
| 0-10 | 1220-1250 | 1230 | 1300 | Manganese oxide increased the collapse temperature of the melt - but decreased the final collapse temperature of lime rich mixtures |
| 1-9 | 1170-1200 | 1170 | 1200 | |
| 2-8 | 1140-1170 | 1150 | 1310 | |
| 3-7 | 1150-1170 | 1140 | 1460 | |
| 4-6 | 1130-1150 | 1110 | 1460 | |
| 5-5 | 1130-1150 | 1110 | 1460 | |
| 6-4 | 1230-1250 | 1220 | >1500 | |

## Table 14

### CaO - 2 FeO.SiO$_2$ + 10 Wt% MnO heated in air

### Results from filament microscope and cone fusion tests

| Ratio of Lime to Fayalite | Hot Filament Microscope | Cone Fusion Tests | | Remarks |
|---|---|---|---|---|
| | Initial Liquidus Temperature oC | Initial Bending Temperature oC | Final Collapse Temperature oC | |
| 0-10 | 1390-1420 | 1400 | 1450 | Gradual collapse of cones except 1-9 cone which did not collapse completely below 1500°C |
| 1-9 | 1290-1310 | 1180 | >1500 | |
| 2-8 | 1270-1290 | 1180 | 1300 | |
| 3-7 | 1260-1270 | 1160 | 1240 | |
| 4-6 | 1280-1300 | 1190 | 1270 | |
| 5-5 | 1230-1240 | 1220 | 1340 | |
| 6-4 | 1220-1240 | 1220 | 1430 | |

## Table 15

### CaO - 2 FeO.SiO$_2$ + 20 Wt% MnO heated in air

### Results from hot filament microscope and cone fusion tests

| Ratio of Lime to Fayalite | Hot Filament Microscope | Cone Fusion Tests | | Remarks |
|---|---|---|---|---|
| | Initial Liquidus Temperature oC | Initial Bending Temperature oC | Final Collapse Temperature oC | |
| 0-10 | 1350-1370 | 1340 | 1390 | Gradual collapse of cones except 1:9 cone which did not collapse completely below 1500°C |
| 1-9 | 1190-1210 | 1170 | > 1500 | |
| 2-8 | 1170-1190 | 1180 | 1320 | |
| 3-7 | 1180-1200 | 1180 | 1280 | |
| 4-6 | 1180-1200 | 1180 | 1250 | |
| 5-5 | 1220-1240 | 1250 | 1270 | |
| 6-4 | 1250-1270 | 1250 | 1350 | |

### Table 16

### $CaO - 2 FeO.SiO_2 + 10 Wt\% CaF_2$ in argon

### Results from hot filament microscope and cone fusion tests

| Ratio of Lime to Fayalite | Hot Filament Microscope | Cone Fusion Tests | | Remarks |
|---|---|---|---|---|
| | Initial Liquidus Temperature oC | Initial Bending Temperature oC | Final Collapse Temperature oC | |
| 0-10 | 1080-1110 | 1120 | 1130 | Very rapid collapse after initial deformation of the tip |
| 1-9 | 1040-1070 | 1050 | 1100 | |
| 2-8 | 1090-1120 | 1080 | 1140 | |
| 3-7 | 1090-1120 | 1090 | 1180 | |
| 4-6 | 1080-1110 | 1080 | 1230 | |
| 5-5 | 1080-1110 | 1080 | 1200 | |
| 6-4 | 1150-1170 | 1100 | 1290 | |

### Table 17

### $CaO - 2 FeO.SiO_2 + 10 Wt\% B_2O_3$ in argon

### Results from hot filament microscope and cone fusion tests

| Ratio of Lime to Fayalite | Hot Filament Microscope | Cone Fusion Tests | | Remarks |
|---|---|---|---|---|
| | Initial Liquidus Temperature oC | Initial Bending Temperature oC | Final Collapse Temperature oC | |
| 0-10 | 1040-1070 | 1000 | 1070 | Very rapid collapse after initial deformation of the tip |
| 1-9 | 900- 930 | 920 | 970 | |
| 2-8 | 800- 830 | 860 | 920 | |
| 3-7 | 800- 830 | 820 | 880 | |
| 4-6 | 800-830 | 800 | 830 | |
| 5-5 | 800- 830 | 820 | 860 | |
| 6-4 | 870- 900 | 830 | 900 | |

## Table 18

## Dissolution of dicalcium silicate pellets in fayalite

| Immersion Time sec. | Volume Loss $cm^3 \ cm^{-2}$ |
|---|---|
| 15 | 0.066 |
| 22.5 | 0.108 |
| 30 | 0.135 |

Fig. 1

Bardenheuer's (56) pseudo ternary diagram showing the change in slag composition during a blow

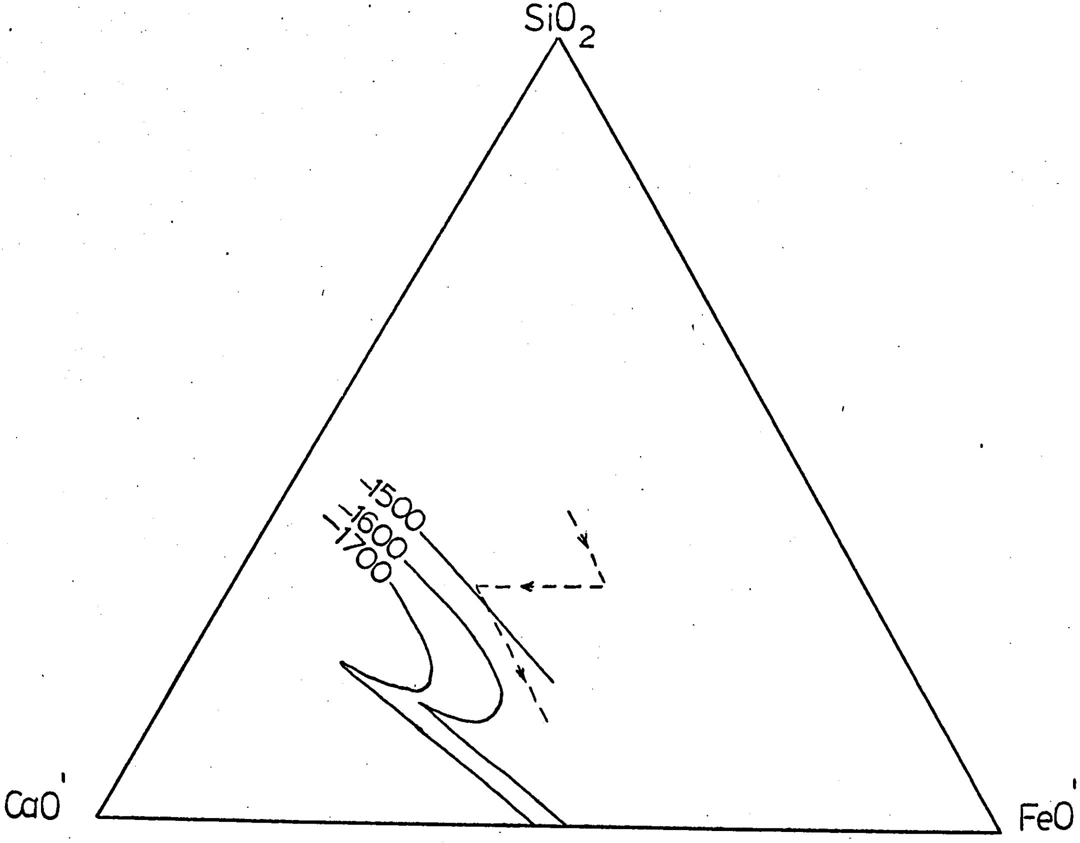
SiO$_2'$
CaO'
FeO'
1500
1600
1700

Fig. 2

Apparatus used in the determination of bulk density of compacts and pellets

a - test piece

b - mercury

c - weight

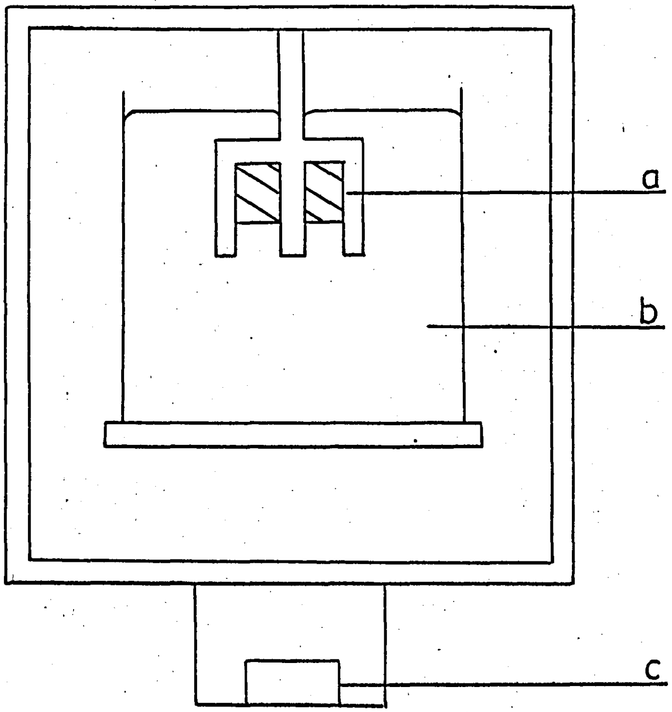
a
b
c

Fig. 3

Cross-section through the immersion furnace

a - water cooled copper tubing
b - alumina work tube
c - Pt/5%Rh-Pt/20% Rh control thermocouple
d - ceramic plug
e - spiral heating element
f - alumina support tube
g - aluminium head
h - Pt - Pt/13% Rh thermocouple

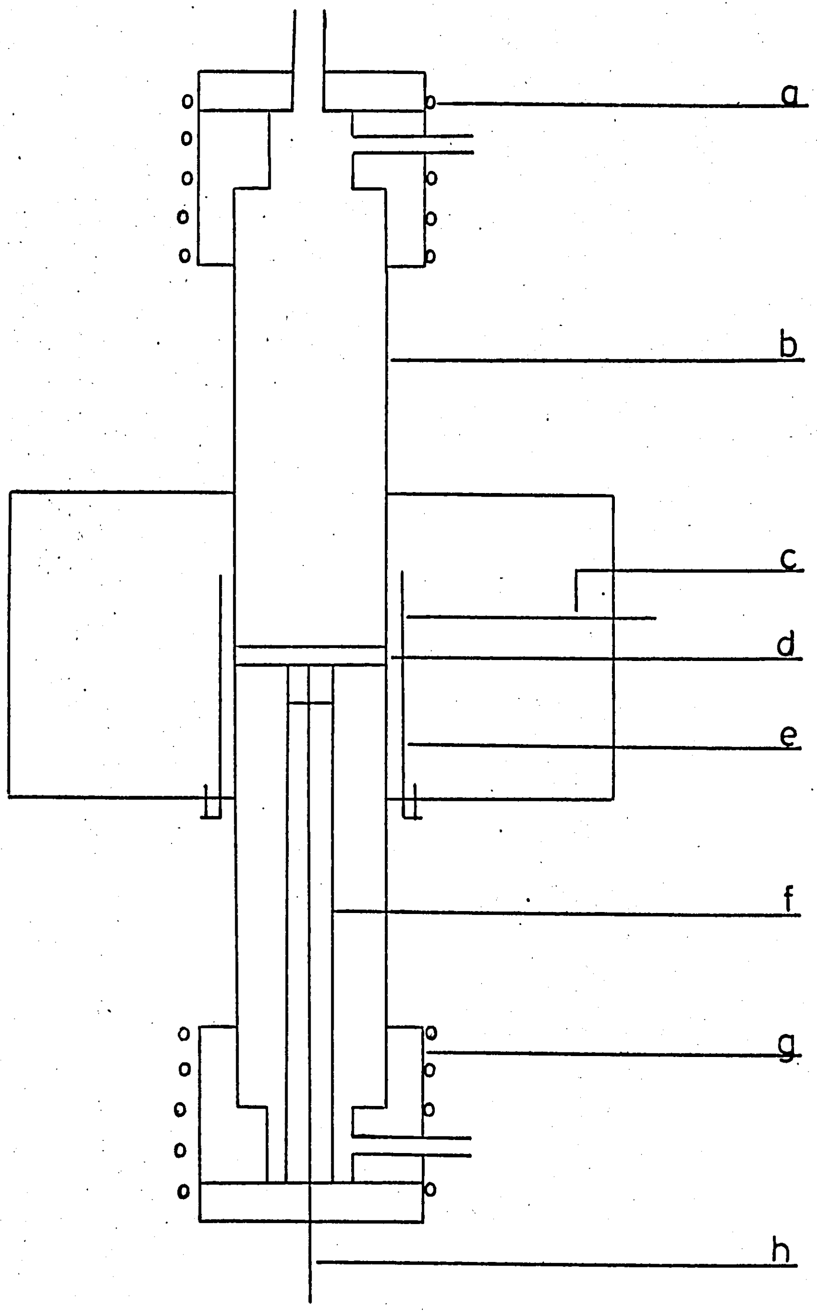
a
b
c
d
e
f
g
h

Fig. 4

Cone fusion results and initial liquidus temperatures of various lime - fayalite mixtures plotted on the CaO - 2 FeO.$SiO_2$ isopleth

— — — initial bending temperature

------ final collapse temperature

I initial liquidus temperature range

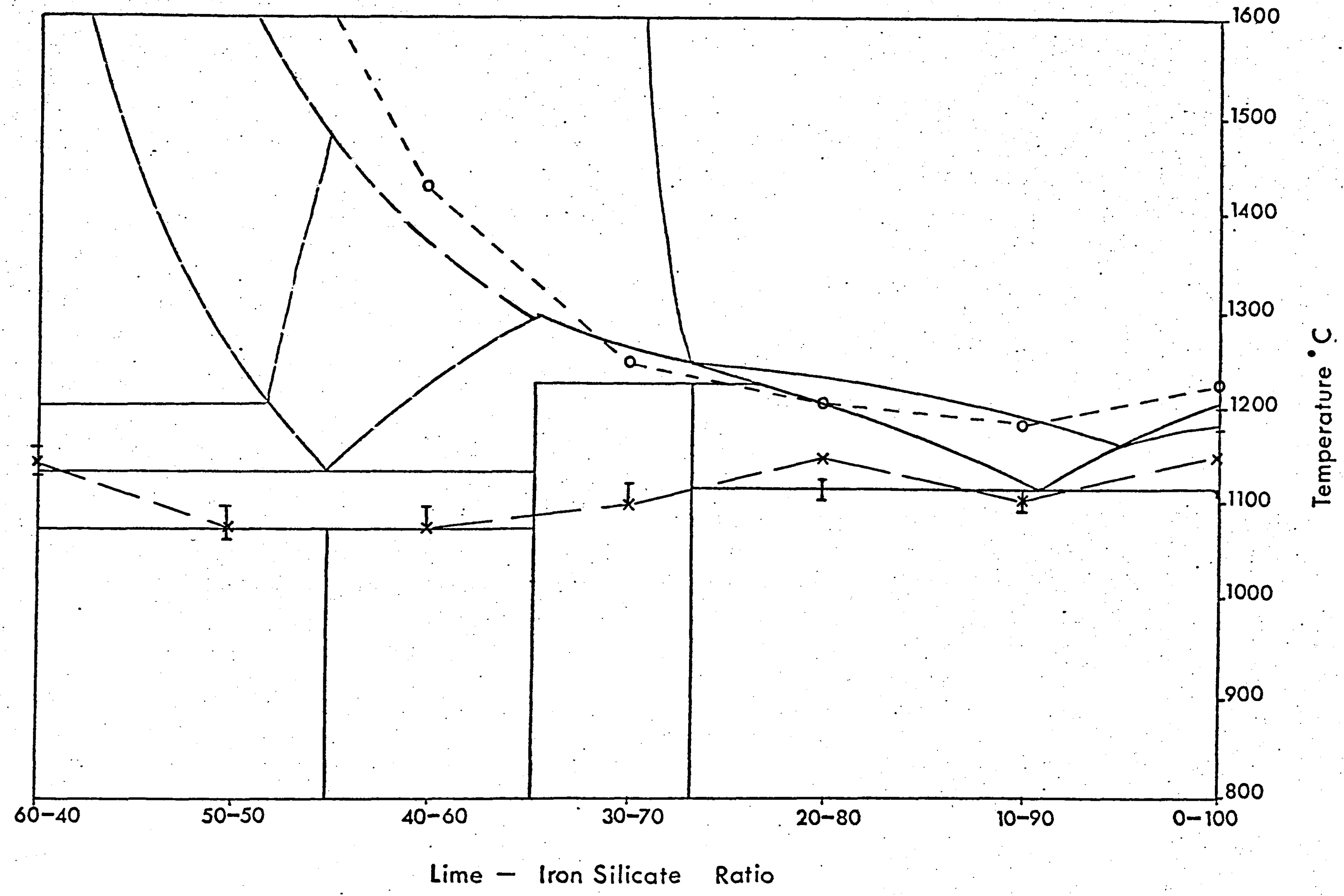
1600
1500
1400
1300
1200
1100
1000
900
800
Temperature °C
60–40
50–50
40–60
30–70
20–80
10–90
0–100
Lime — Iron Silicate Ratio

Fig. 5

The $CaO$ - 2 $FeO.SiO_2$ isopleth from the $CaO$-$FeO$-$SiO_2$ ternary diagram

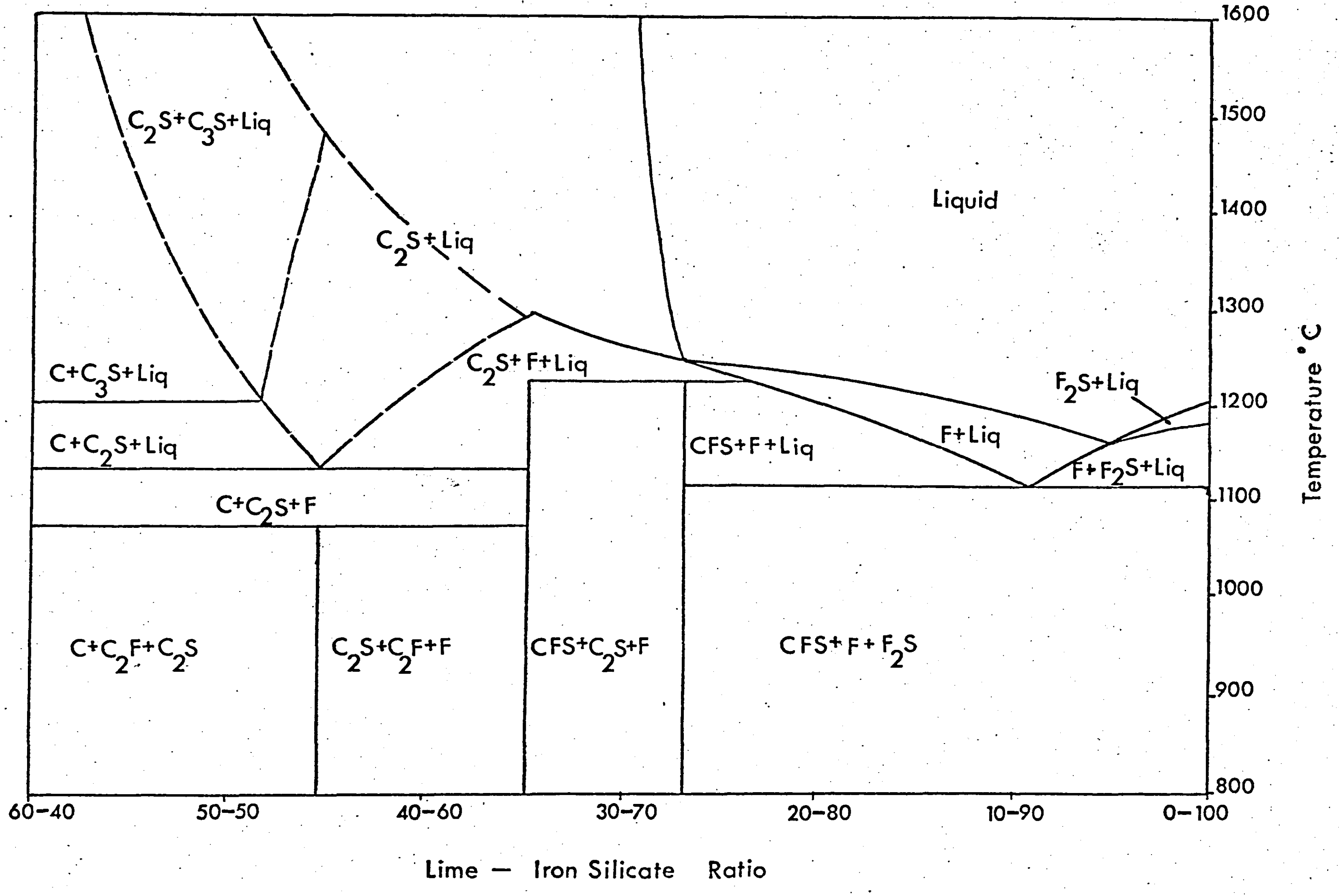
Liquid
$C_2S+C_3S+Liq$
$C_2S+Liq$
$C_2S+F+Liq$
$C+C_3S+Liq$
$C+C_2S+Liq$
$C+C_2S+F$
$C+C_2F+C_2S$
$C_2S+C_2F+F$
$CFS+C_2S+F$
$CFS+F+Liq$
$CFS+F+F_2S$
$F+Liq$
$F_2S+Liq$
$F+F_2S+Liq$
1600
1500
1400
1300
1200
1100
1000
900
800
Temperature °C
60–40
50–50
40–60
30–70
20–80
10–90
0–100
Lime — Iron Silicate Ratio

Fig. 6

The equilibrium percentage liquid of compositions along the CaO-2 $FeO.SiO_2$ isopleth present at various temperatures

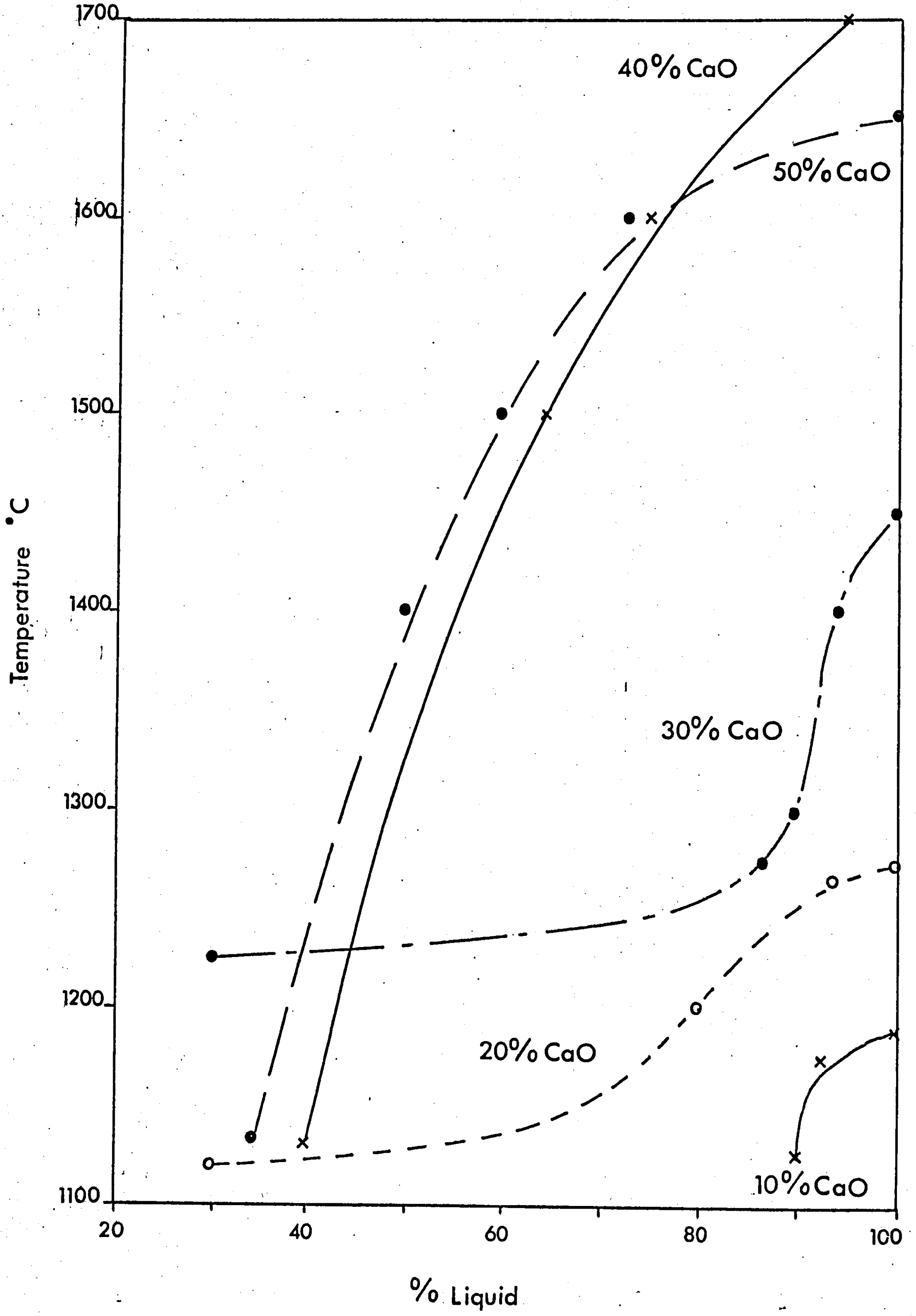
1700
1600
1500
1400
1300
1200
1100
Temperature °C
20
40
60
80
100
% Liquid
40% CaO
50% CaO
30% CaO
20% CaO
10% CaO

Fig. 7

The cone fusion results and initial liquidus temperatures of various lime - fayalite mixtures (heated in air) plotted on a section from the $CaO - Fe_2O_3 - SiO_2$ phase diagram

| | |
|---|---|
| — — — | initial bending temperature |
| -------- | final collapse temperature |
| I | initial liquidus temperature range |

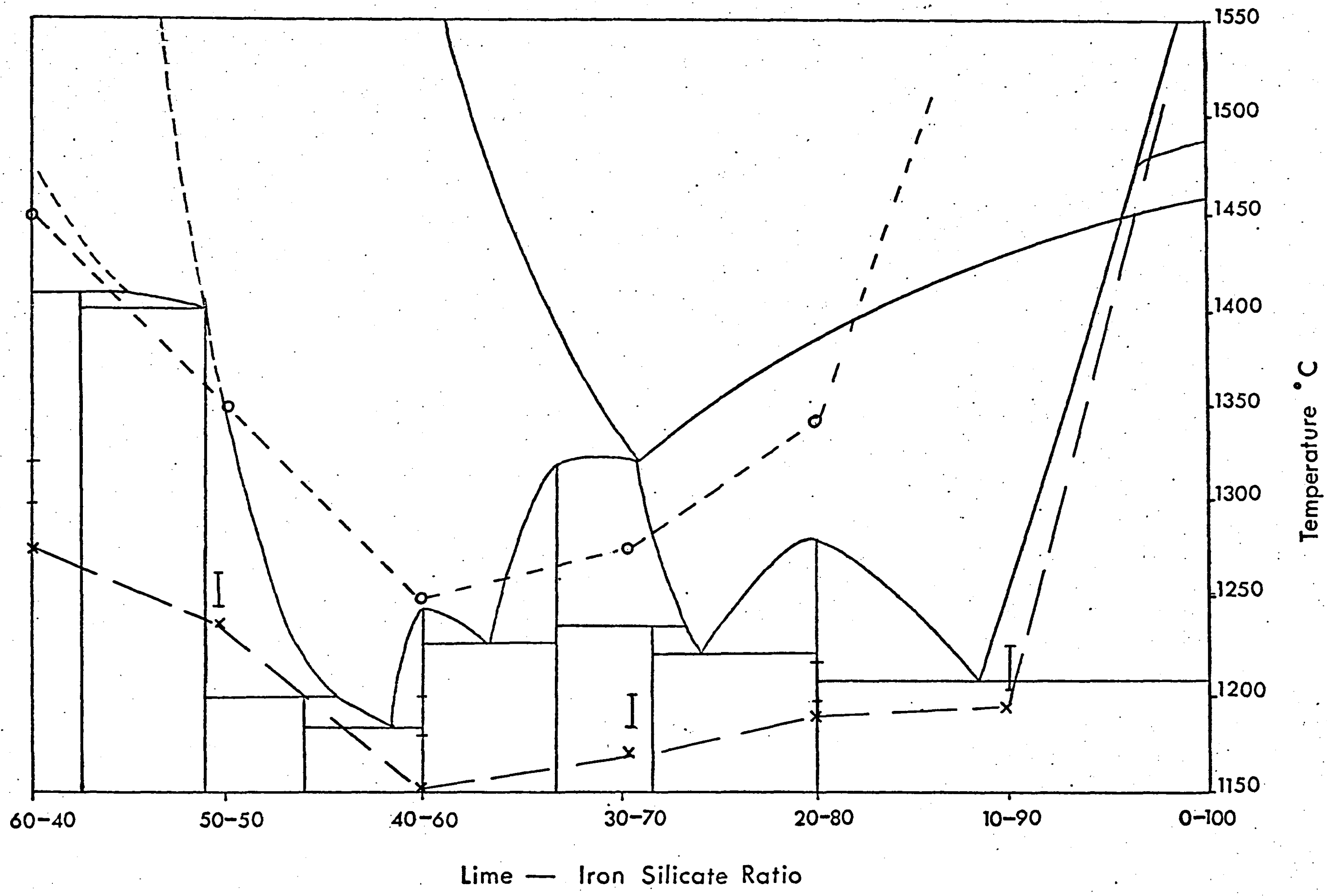
1550
1500
1450
1400
1350
1300
1250
1200
1150
Temperature °C
60–40
50–50
40–60
30–70
20–80
10–90
0–100
Lime — Iron Silicate Ratio

Fig. 8

The equilibrium percentage liquid of compositions along the CaO - $Fe_2O_3.SiO_2$ isopleth present at various temperatures

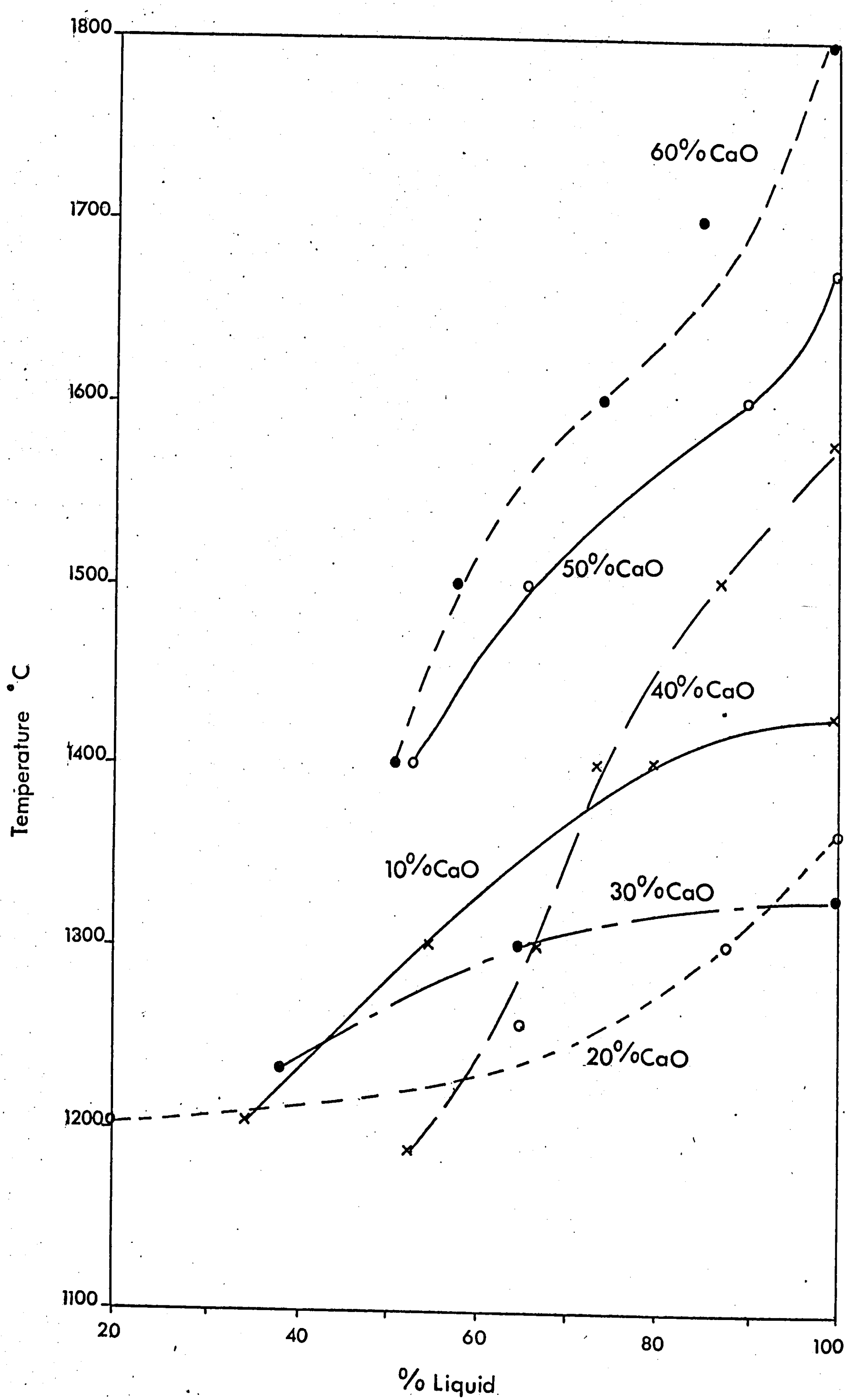
1800
1700
1600
1500
1400
1300
1200
1100
Temperature °C
20
40
60
80
100
% Liquid
60% CaO
50% CaO
40% CaO
10% CaO
30% CaO
20% CaO

Fig. 9

The width of the 2 $CaO.SiO_2$ rim around small lime pellets plotted against immersion time

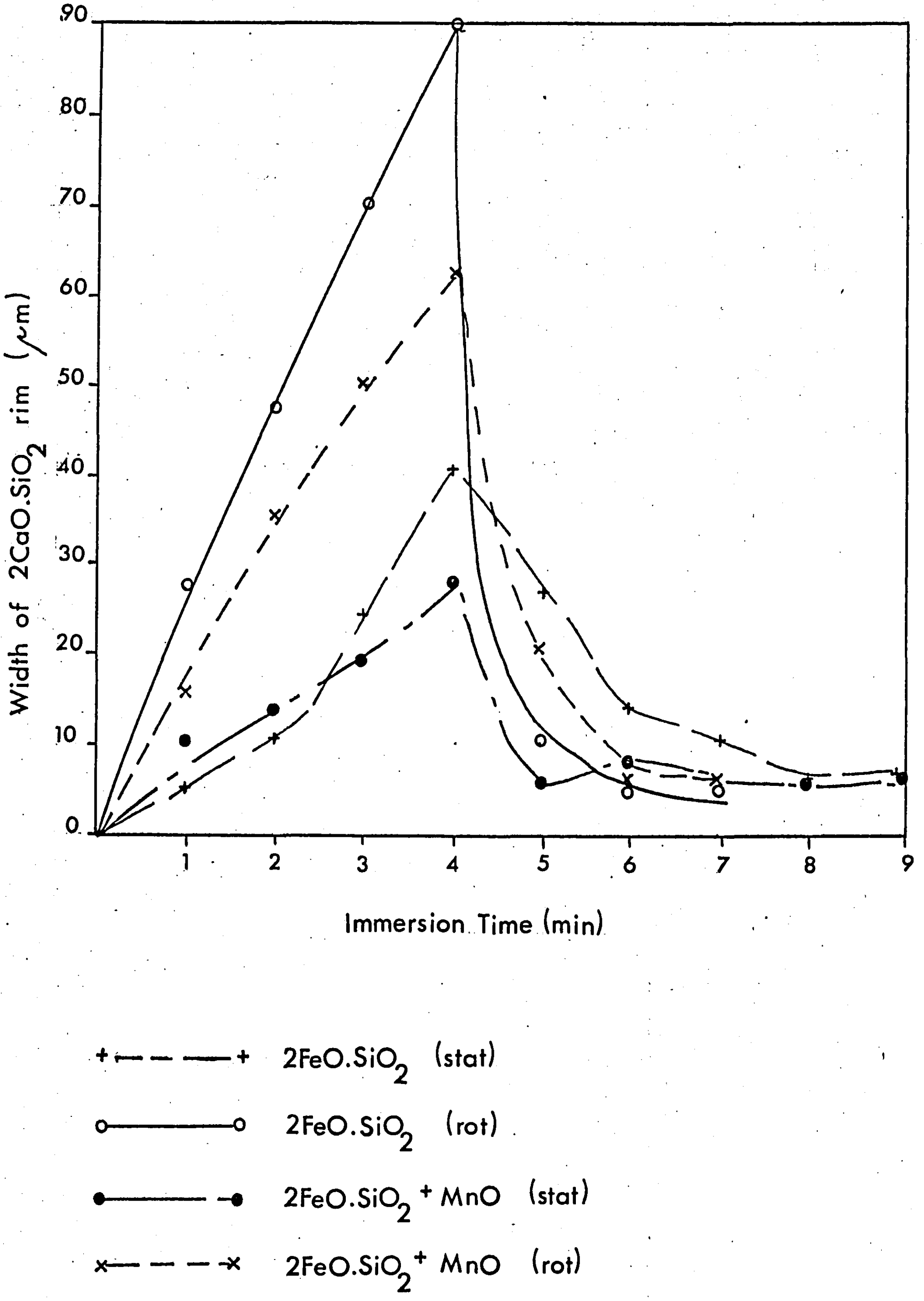
Width of 2CaO.SiO$_2$ rim (μm)
0
10
20
30
40
50
60
70
80
90
1
2
3
4
5
6
7
8
9
Immersion Time (min)
2FeO.SiO$_2$ (stat)
2FeO.SiO$_2$ (rot)
2FeO.SiO$_2$ + MnO (stat)
2FeO.SiO$_2$ + MnO (rot)

Fig. 10

The distribution of oxides across the reaction interface between CaO and 2 FeO.$SiO_2$ after an immersion time of 5 minutes

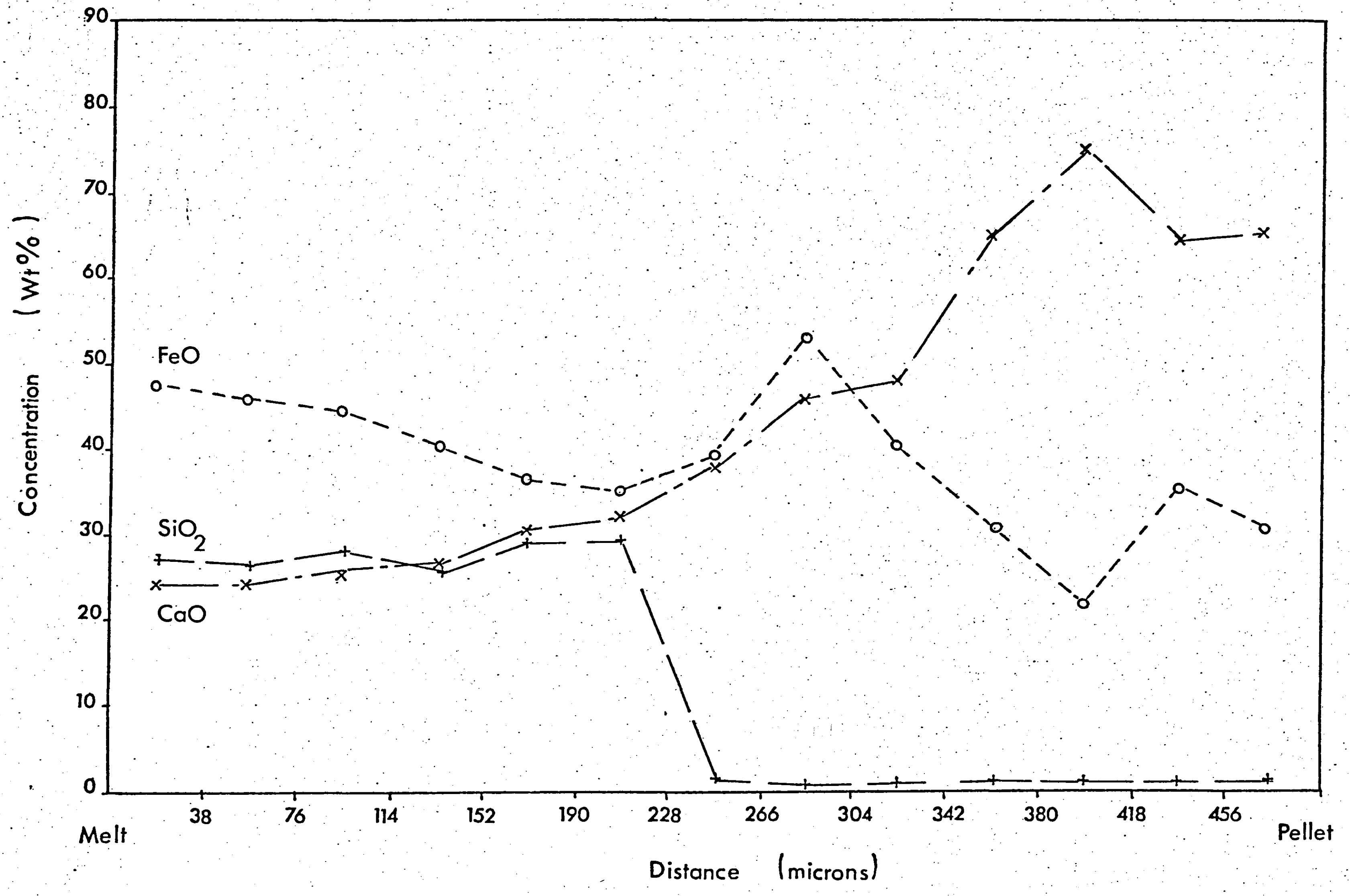

FeO
SiO$_2$
CaO
Concentration (Wt%)
90
80
70
60
50
40
30
20
10
0
Melt
38
76
114
152
190
228
266
304
342
380
418
456
Pellet
Distance (microns)

Fig. 11

The distribution of oxides across the reaction interface between CaO and 2 $FeO.SiO_2$ plotted on the 1300°C isotherm section of the $CaO-FeO-SiO_2$ ternary

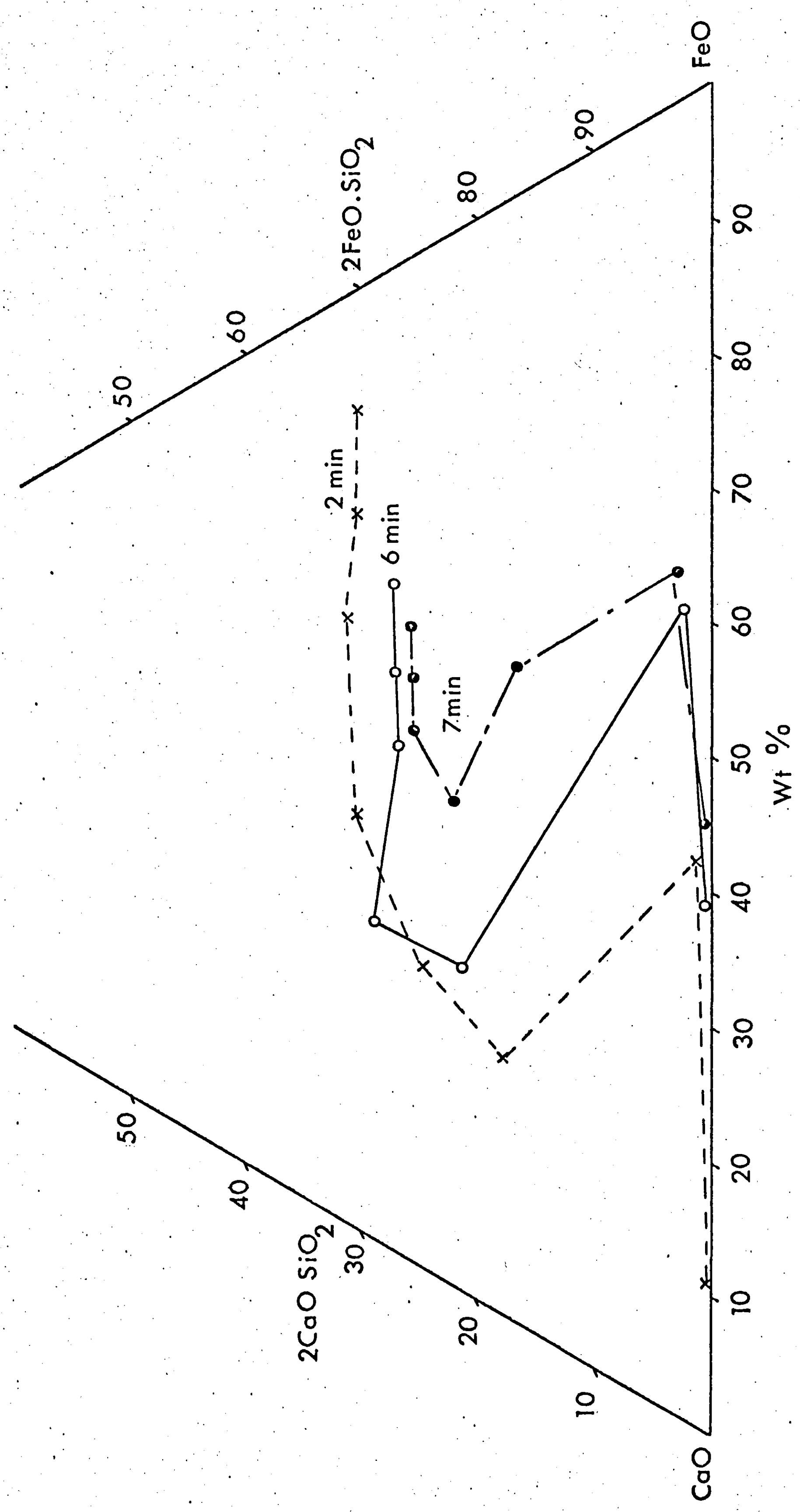
FeO
2FeO.SiO$_2$
50
60
80
90
2 min
6 min
7 min
2CaO SiO$_2$
10
20
30
40
50
CaO
10
20
30
40
50
60
70
80
90
Wt %

Fig. 12

The width of the 2 $CaO.SiO_2$ rim around large lime pellets plotted against immersion time

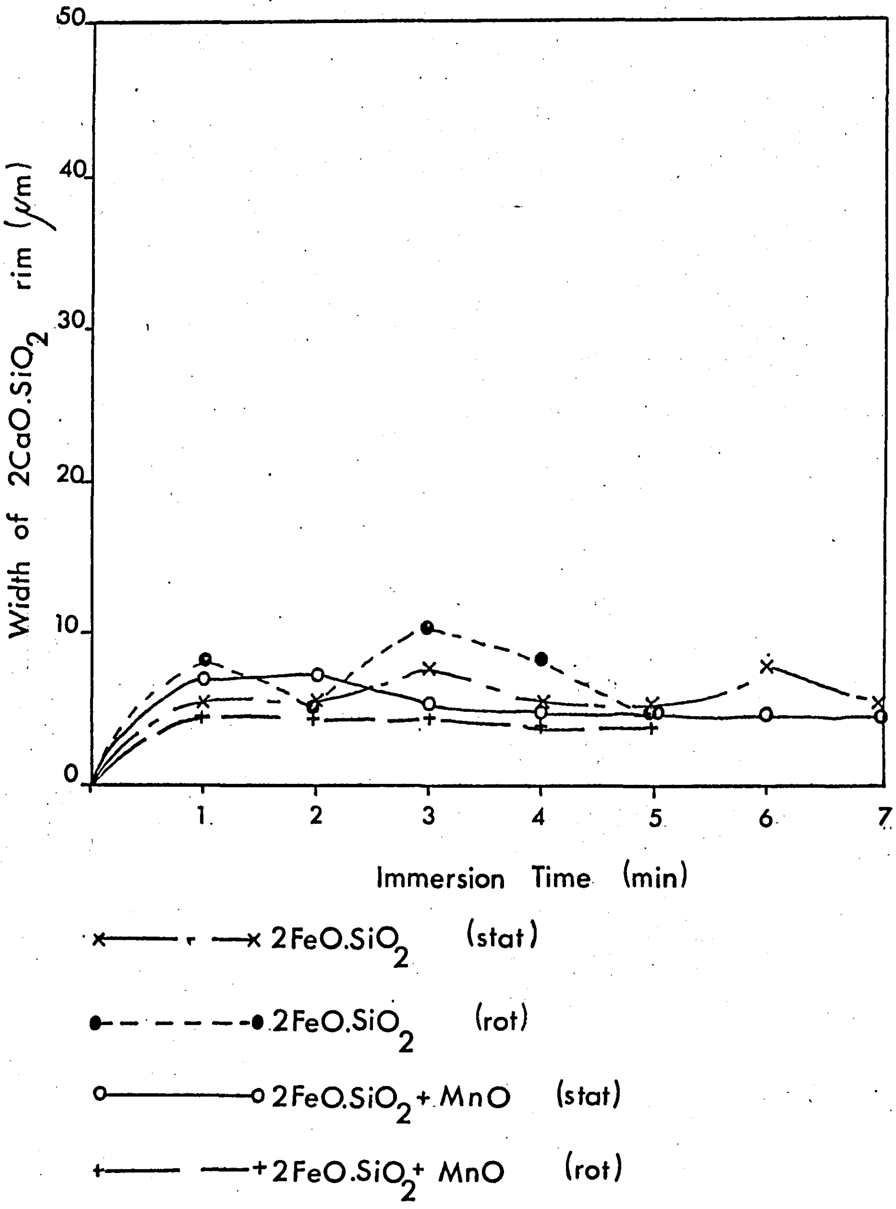

Width of 2CaO.SiO2 rim (μm)
50
40
30
20
10
0
1
2
3
4
5
6
7
Immersion Time (min)
2FeO.SiO2 (stat)
2FeO.SiO2 (rot)
2FeO.SiO2 + MnO (stat)
2FeO.SiO2 + MnO (rot)

## Fig. 13

The volume loss of small lime pellets in different melts plotted against immersion time

melt

1 - 2 $FeO.SiO_2$ (static)
2 - 2 $FeO.SiO_2$ (rotated)

3 - 2 $FeO.SiO_2$ + MnO (static)
4 - 2 $FeO.SiO_2$ + MnO (rotated)

5 - 2 $FeO.SiO_2$ + $CaF_2$ (static)
6 - 2 $FeO.SiO_2$ + $CaF_2$ (rotated)

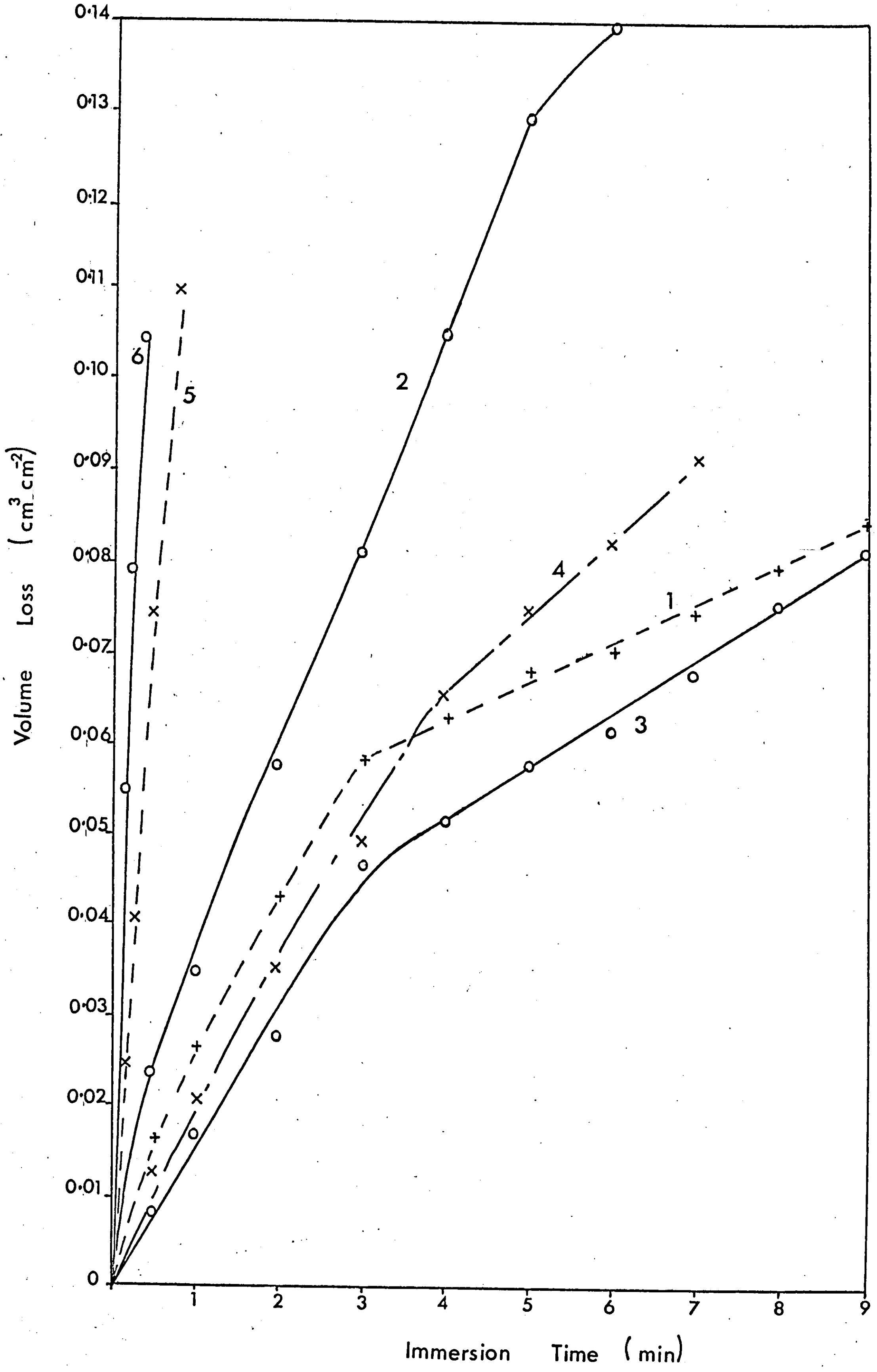
0·14
0·13
0·12
0·11
0·10
0·09
0·08
0·07
0·06
0·05
0·04
0·03
0·02
0·01
0
Volume Loss (cm$^3$.cm$^{-2}$)
1
2
3
4
5
6
7
8
9
Immersion Time (min)
6
5
2
4
1
3

## Fig. 14

The volume loss of large lime pellets in different melts plotted against immersion time

melt

1 - 2 $FeO.SiO_2$ (static)
2 - 2 $FeO.SiO_2$ (rotated)

3 - 2 $FeO.SiO_2$ + MnO (static)
4 - 2 $FeO.SiO_2$ + MnO (rotated)

5 - 2 $FeO.SiO_2$ + $CaF_2$ (static)
6 - 2 $FeO.SiO_2$ + $CaF_2$ (rotated)

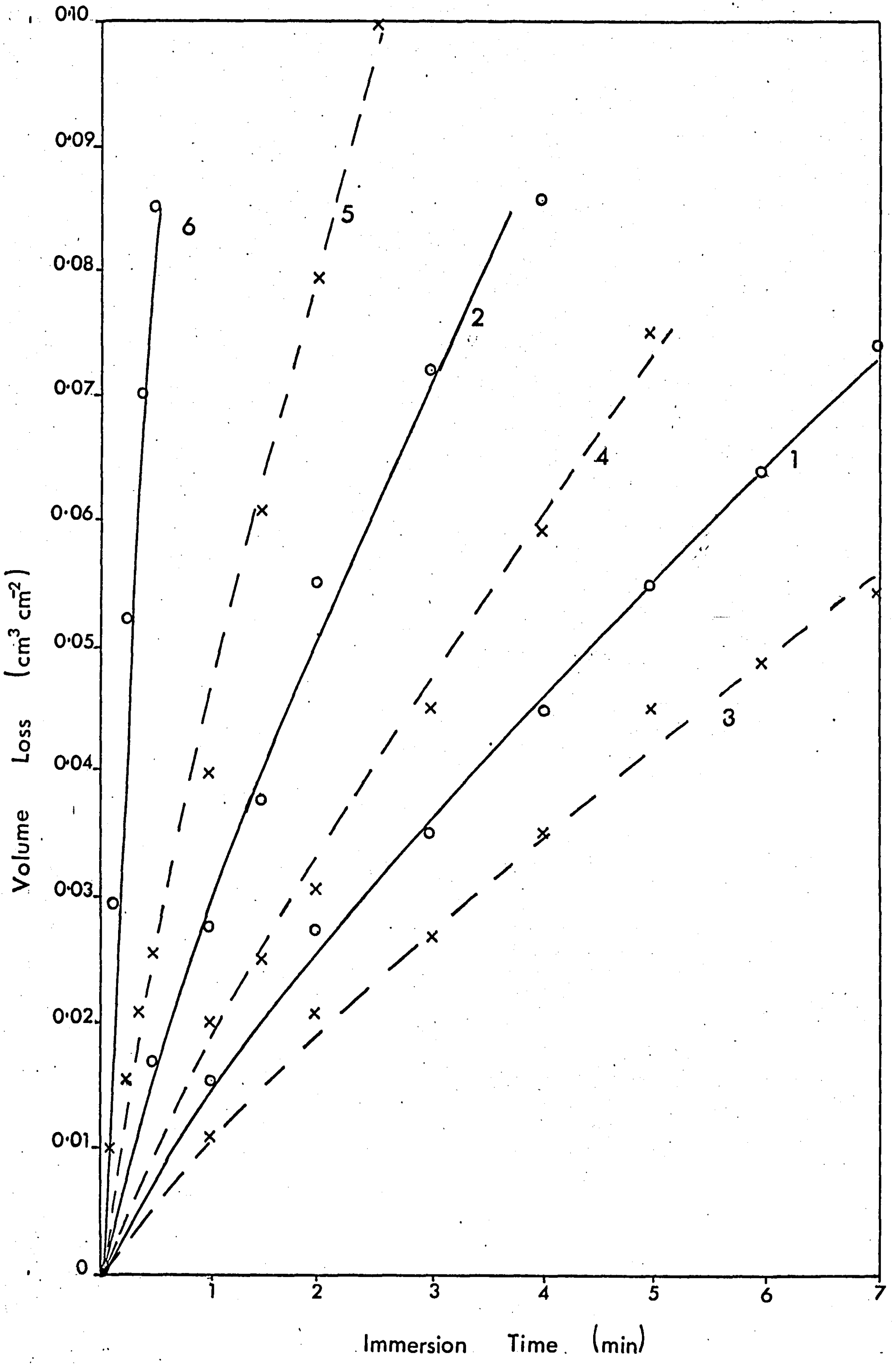

0·10
0·09
0·08
0·07
0·06
0·05
0·04
0·03
0·02
0·01
0
Volume Loss (cm$^3$ cm$^{-2}$)
1
2
3
4
5
6
7
Immersion Time (min)
6
5
2
4
1
3

Fig. 15

The volume loss of large lime pellets with various preheat temperatures in fayalite plotted against immersion time

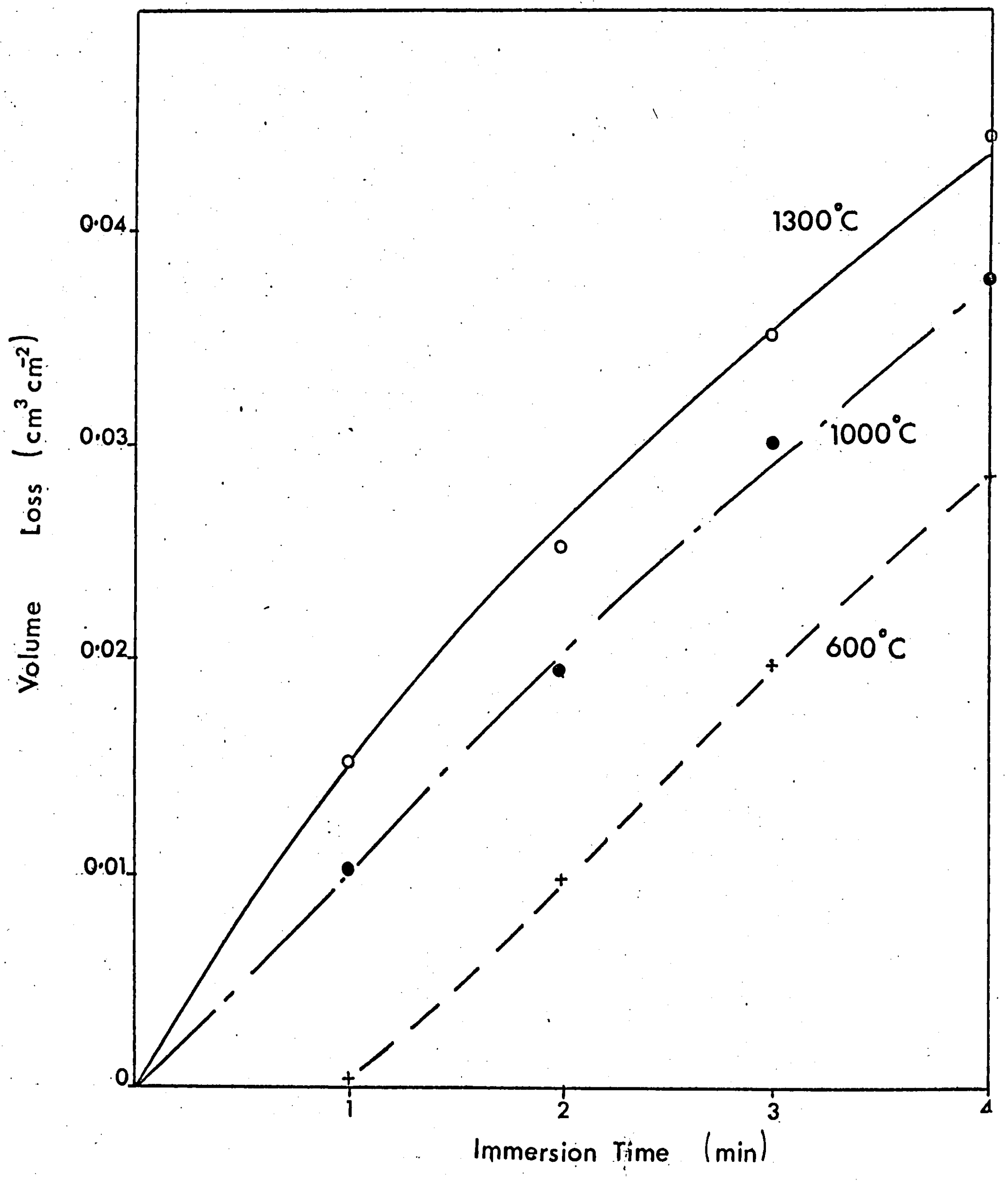

Volume Loss (cm$^3$ cm$^{-2}$)
0·04
0·03
0·02
0·01
0
1
2
3
4
Immersion Time (min)
1300°C
1000°C
600°C

Fig. 16

The cone fusion results and initial liquidus temperatures of various lime - fayalite + 10 Wt% manganese oxide mixtures plotted on the CaO - 2 $FeO.SiO_2$ isopleth

| | |
|---|---|
| – – – – – – – | initial bending temperature |
| ----------- | final collapse temperature |
| I | initial liquidus temperature range |

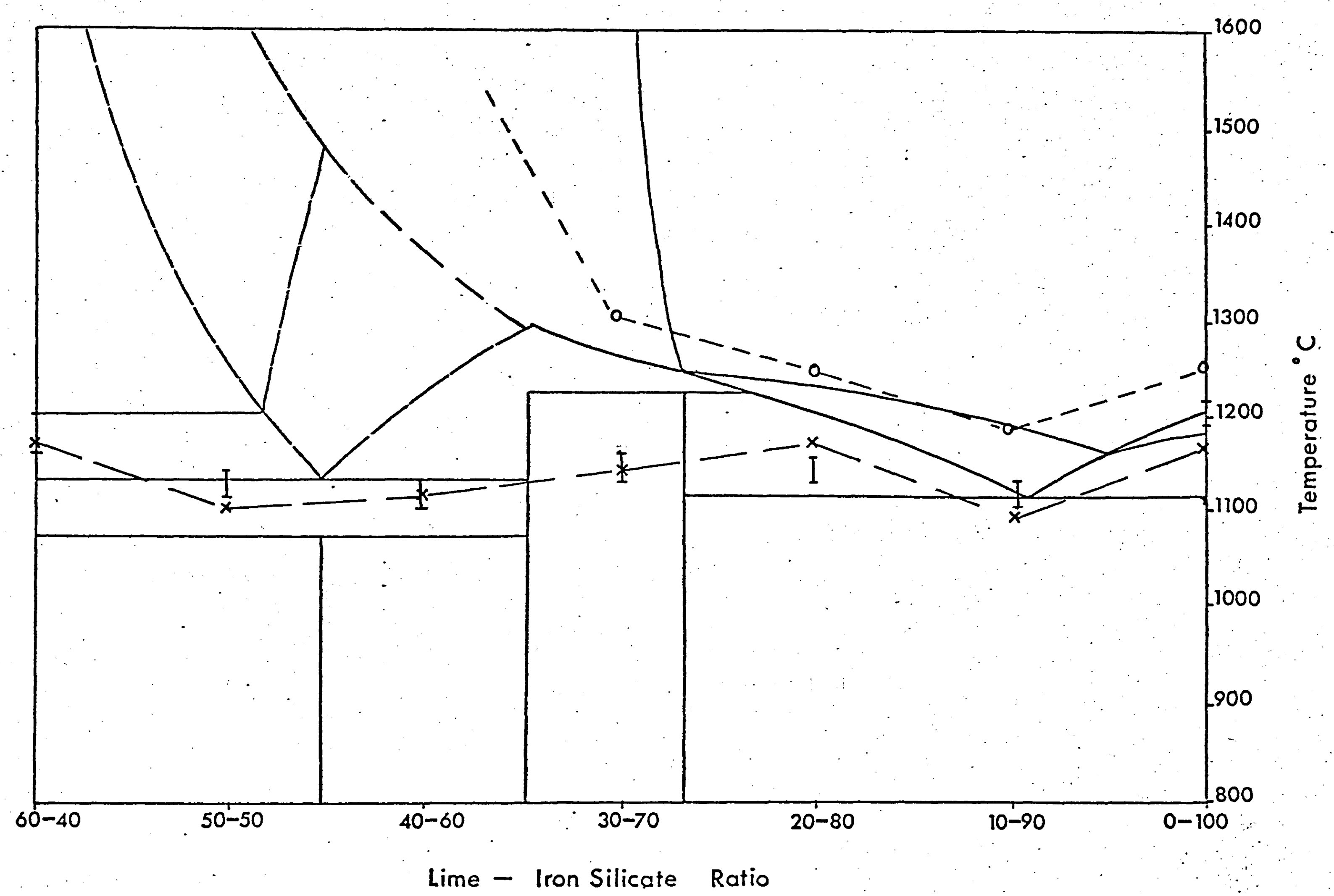
1600
1500
1400
1300
1200
1100
1000
900
800
Temperature °C
60–40
50–50
40–60
30–70
20–80
10–90
0–100
Lime — Iron Silicate Ratio

Fig. 17

The cone fusion results and initial liquidus temperatures of various lime - fayalite + 20Wt% manganese oxide mixtures plotted on the CaO - 2 FeO.SiO$_2$ isopleth

| | |
|---|---|
| — — — — | initial bending temperature |
| -------- | final collapse temperature |
| I | initial liquidus temperature range |

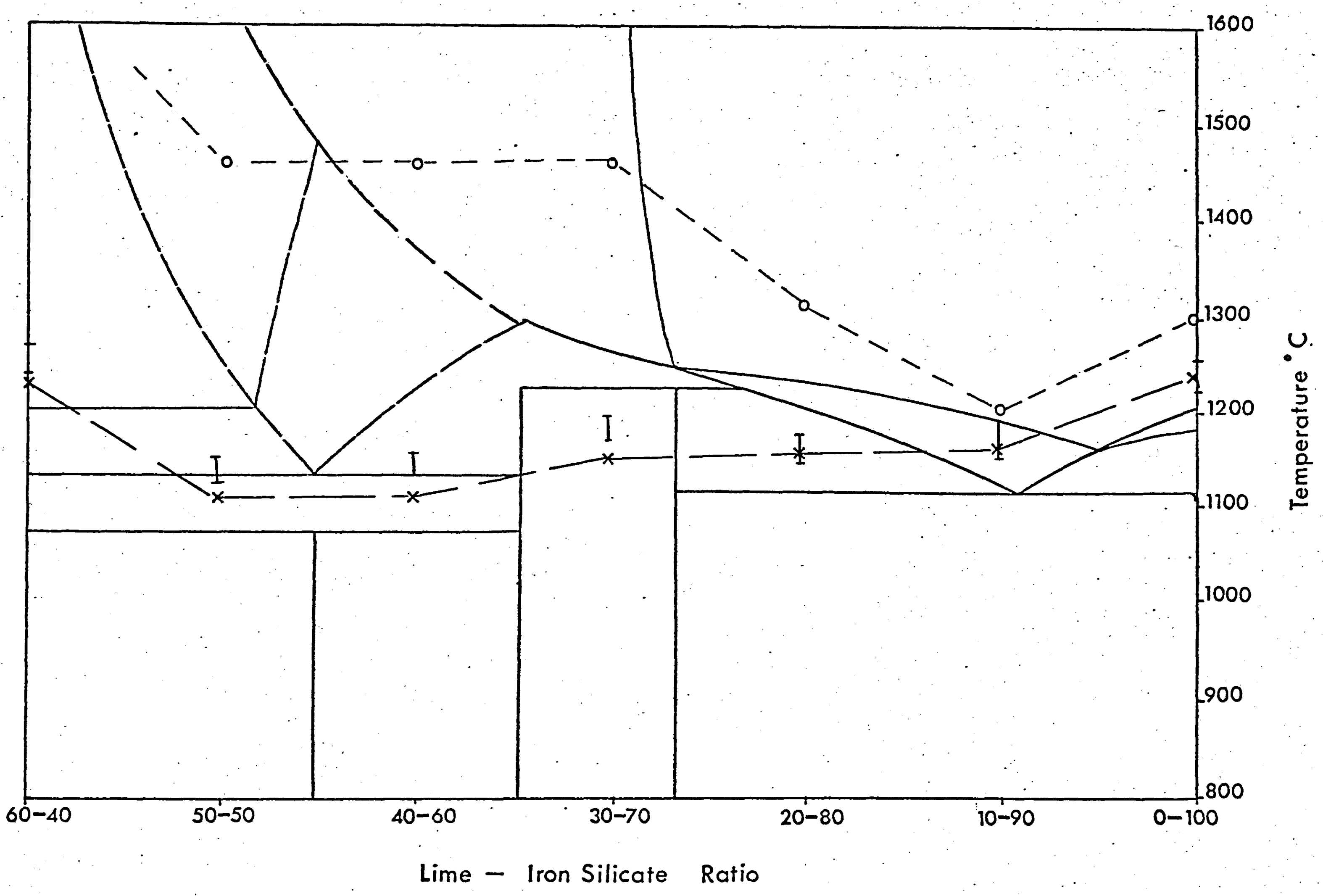
1600
1500
1400
1300
1200
1100
1000
900
800
Temperature °C
60–40
50–50
40–60
30–70
20–80
10–90
0–100
Lime — Iron Silicate Ratio

Fig. 18

The cone fusion results and initial liquidus temperatures of various lime - fayalite + 10Wt% manganese oxide mixtures (heated in air) plotted on a section from the $CaO - Fe_2O_3 - SiO_2$ phase diagram

| | |
|---|---|
| — — — — — | initial bending temperature |
| - - - - - - - - - | final collapse temperature |
| I | initial liquidus temperature range |

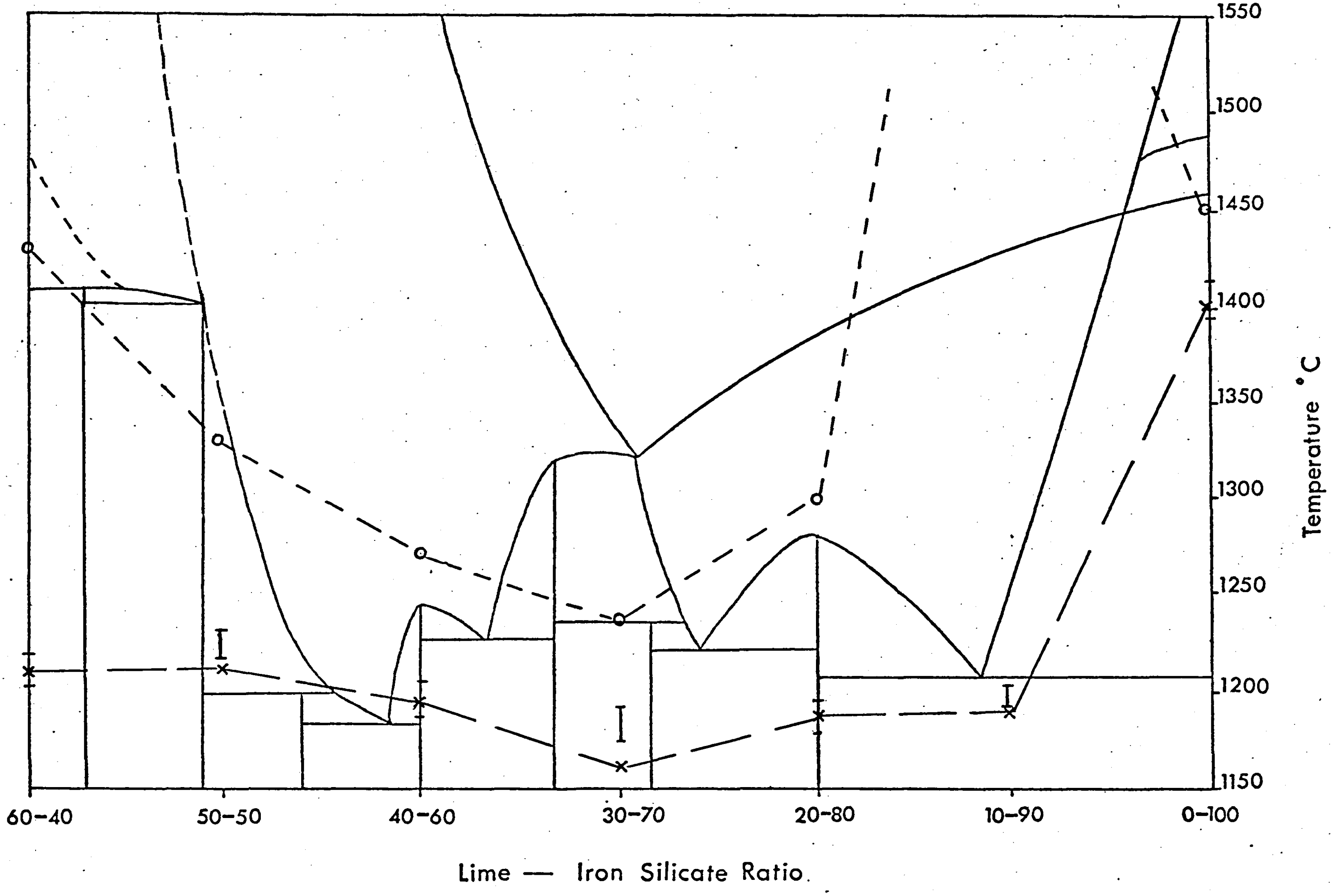
1550
1500
1450
1400
1350
1300
1250
1200
1150
Temperature °C
60–40
50–50
40–60
30–70
20–80
10–90
0–100
Lime — Iron Silicate Ratio

Fig. 19

The cone fusion results and initial liquidus temperatures of various lime - fayalite + 20Wt% manganese oxide mixtures (heated in air) plotted on a section from the $CaO - Fe_2O_3 - SiO_2$ phase diagram

| | |
|---|---|
| — — — — — | initial bending temperature |
| --------- | final collapse temperature |
| I | initial liquidus temperature range |

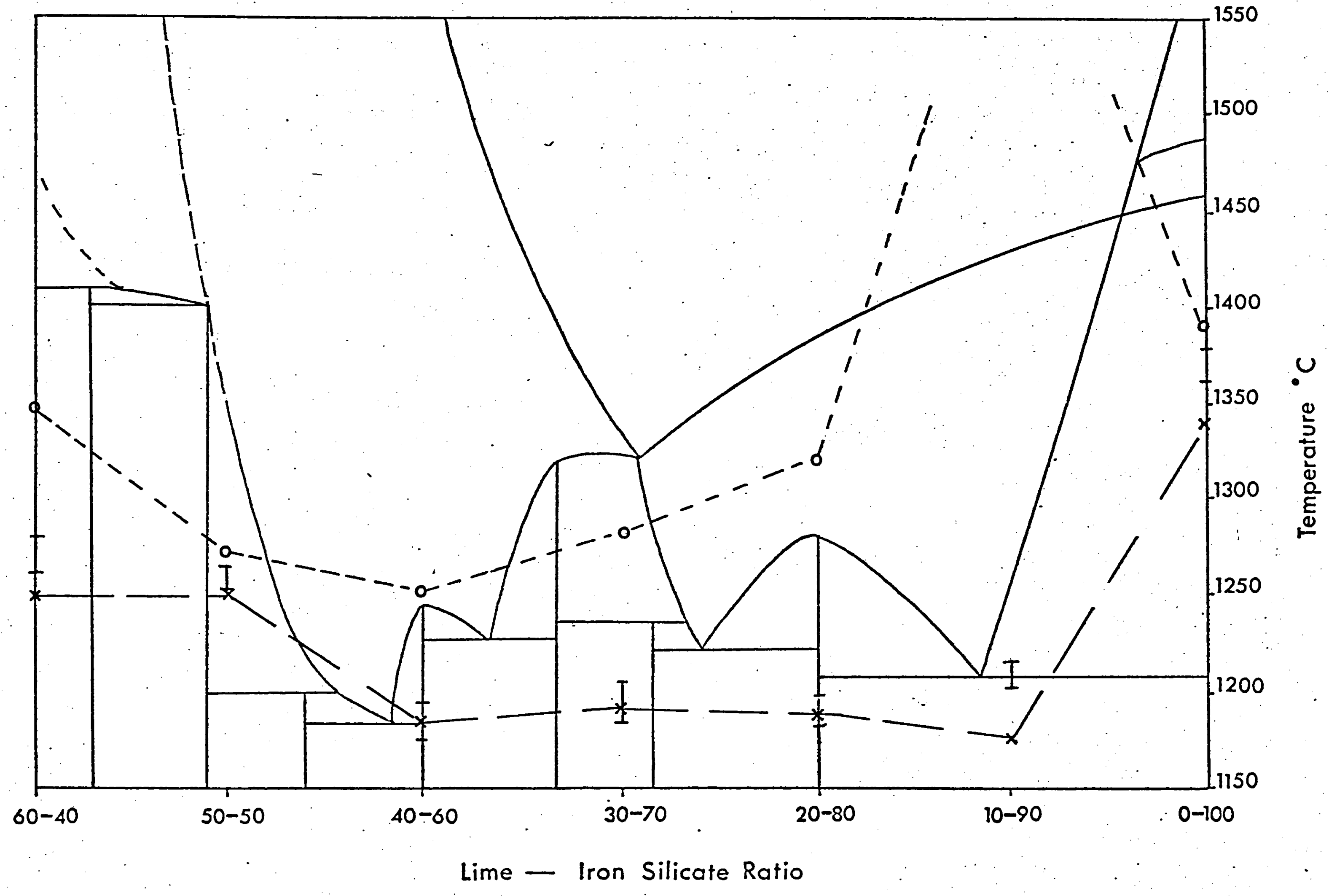
1550
1500
1450
1400
1350
1300
1250
1200
1150
Temperature °C
60–40
50–50
40–60
30–70
20–80
10–90
0–100
Lime — Iron Silicate Ratio

Fig. 20

The distribution of oxides across the reaction interface between CaO and 2 FeO.SiO$_2$ + 10 Wt% MnO after an immersion time of 3 minutes

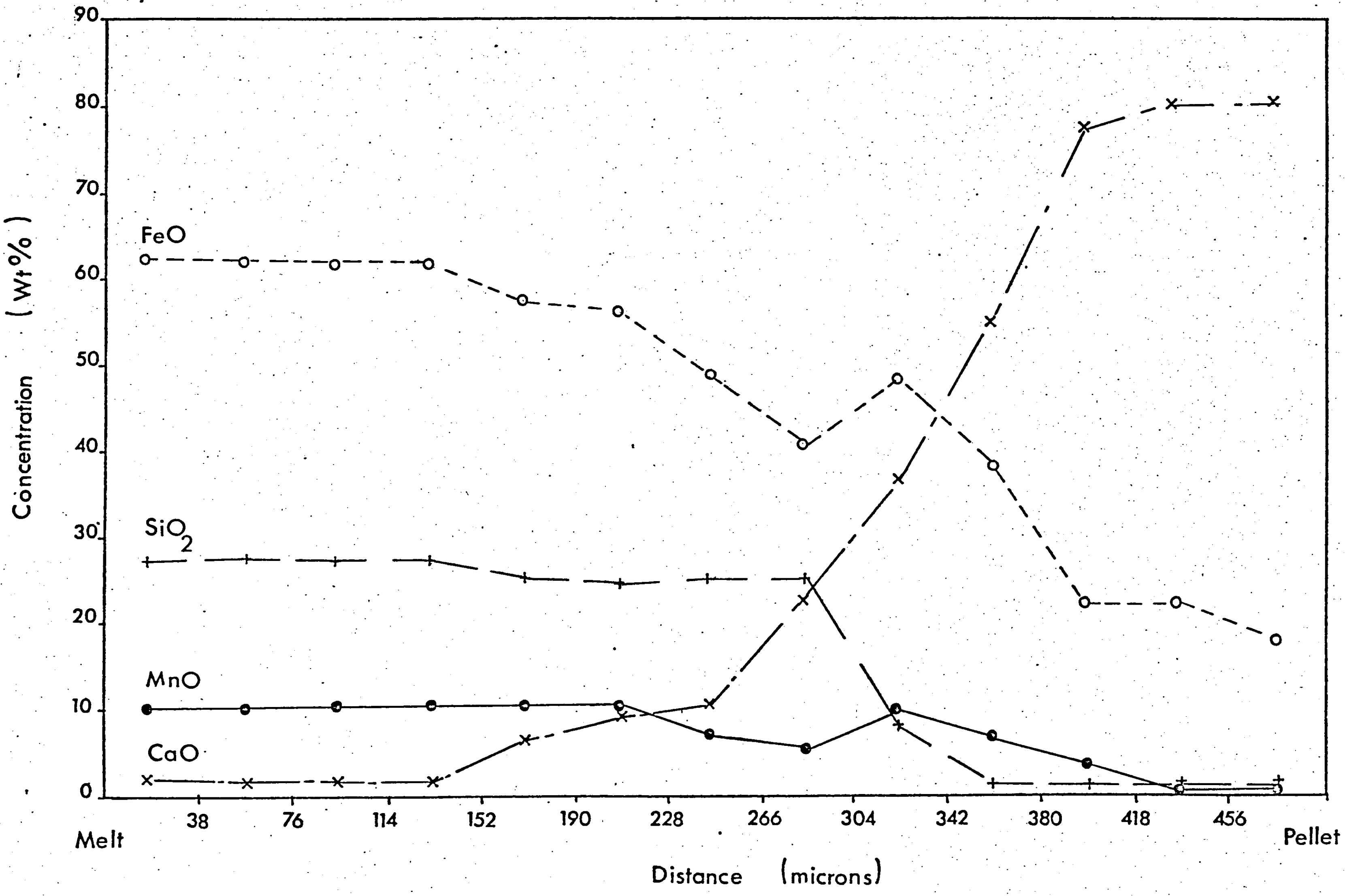
FeO
SiO$_2$
MnO
CaO
Concentration (Wt%)
90
80
70
60
50
40
30
20
10
0
Melt
38
76
114
152
190
228
266
304
342
380
418
456
Pellet
Distance (microns)

Fig. 21

The distribution of oxides across the reaction interface between CaO and 2 $FeO.SiO_2$ + 10 Wt% MnO plotted on the 1300°C isothermal section of the CaO - FeO - $SiO_2$ ternary

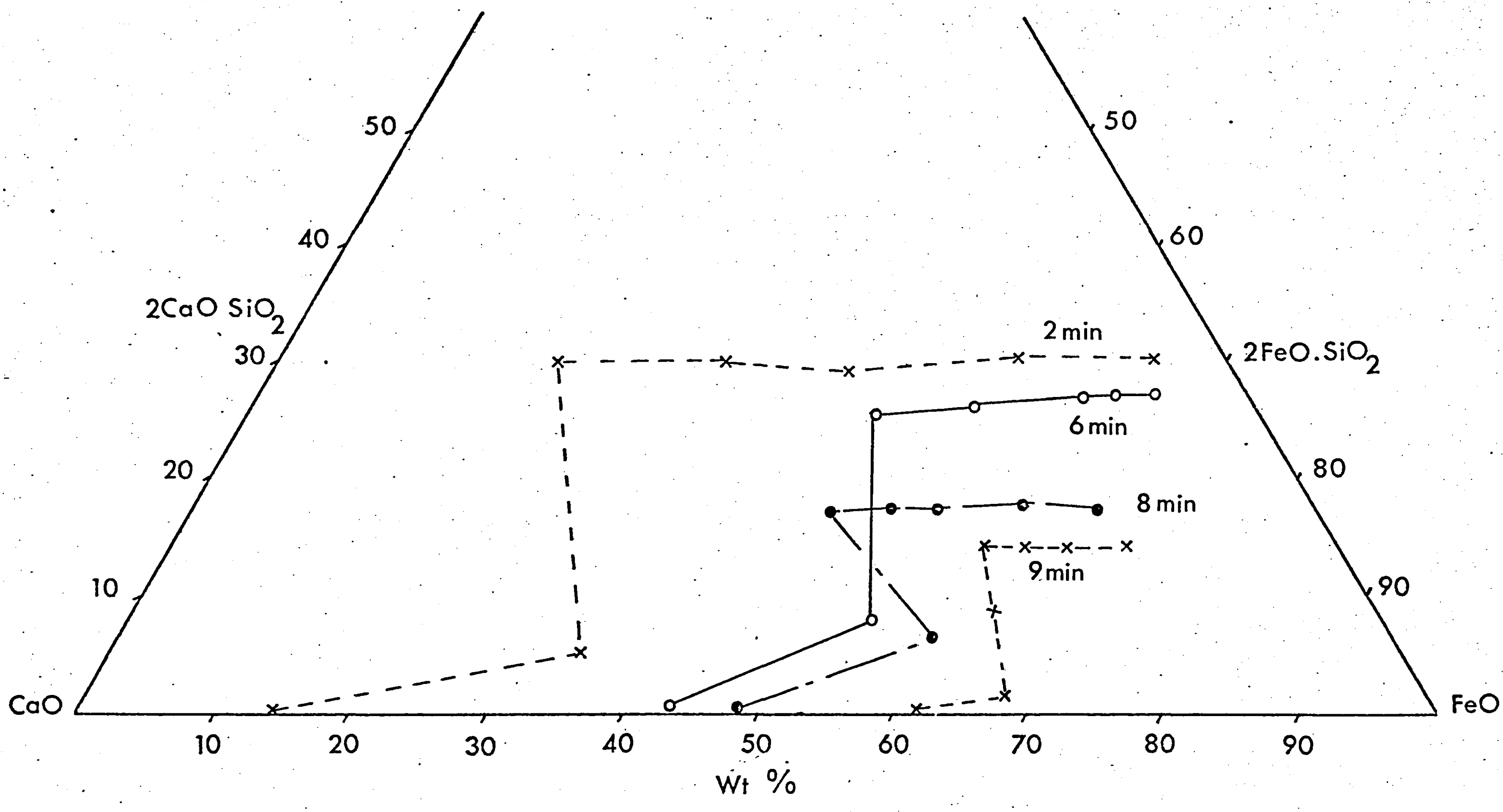
50
40
2CaO SiO$_2$
30
20
10
CaO
50
60
2FeO.SiO$_2$
80
90
FeO
2 min
6 min
8 min
9 min
10
20
30
40
50
60
70
80
90
Wt %

Fig. 22

The cone fusion results and initial liquidus temperatures of various lime - fayalite + 10 Wt% calcium fluoride mixtures plotted on the CaO - 2 FeO.$SiO_2$ isopleth

— — — — — initial bending temperature

--------- final collapse temperature

I initial liquidus temperature range

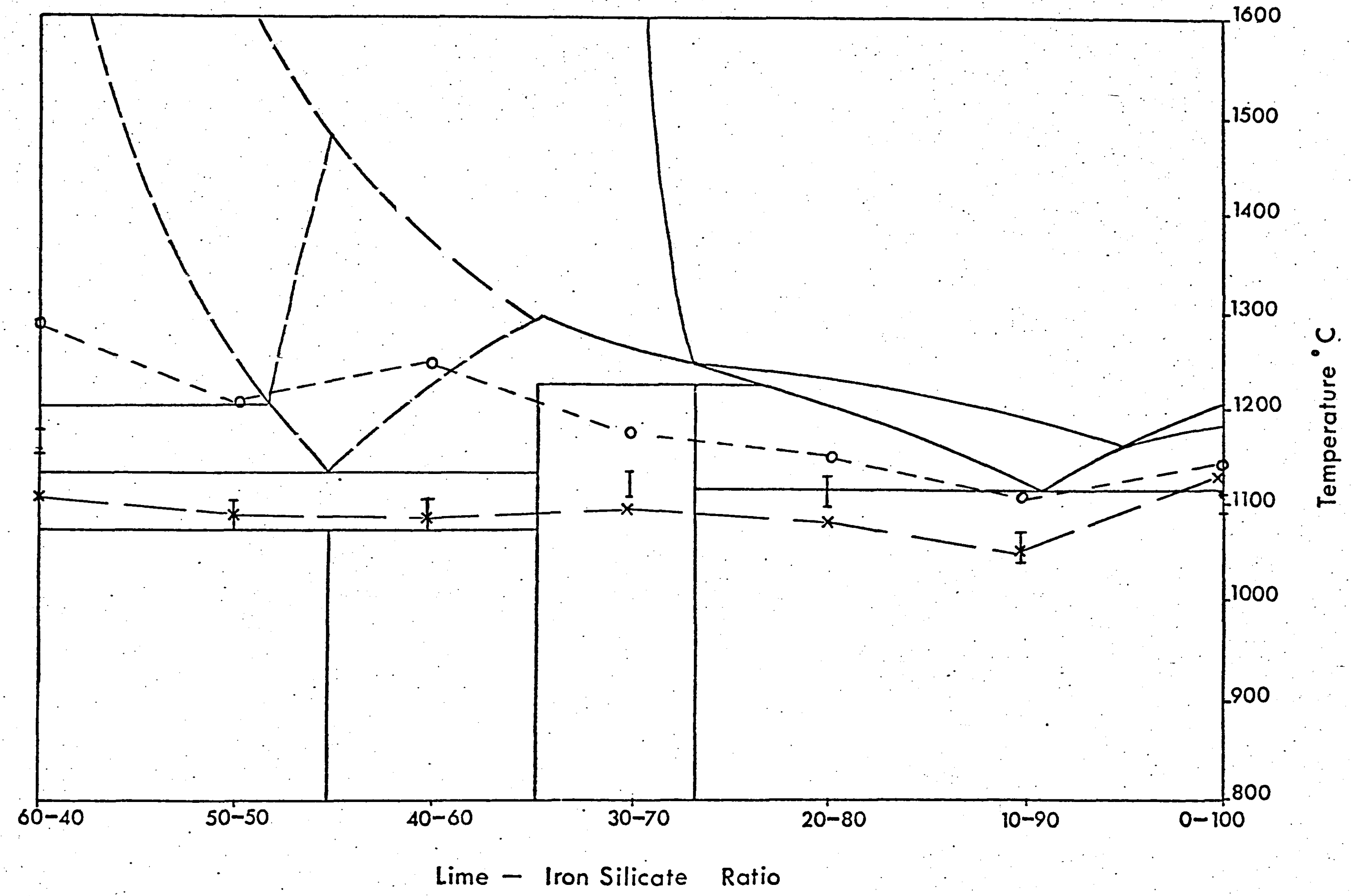
1600
1500
1400
1300
1200
1100
1000
900
800
Temperature °C
60–40
50–50
40–60
30–70
20–80
10–90
0–100
Lime — Iron Silicate Ratio

Fig. 23

The distribution of oxides across the reaction interface between CaO and 2 FeO.$SiO_2$ + 10 Wt% $CaF_2$ after an immersion time of 30 seconds

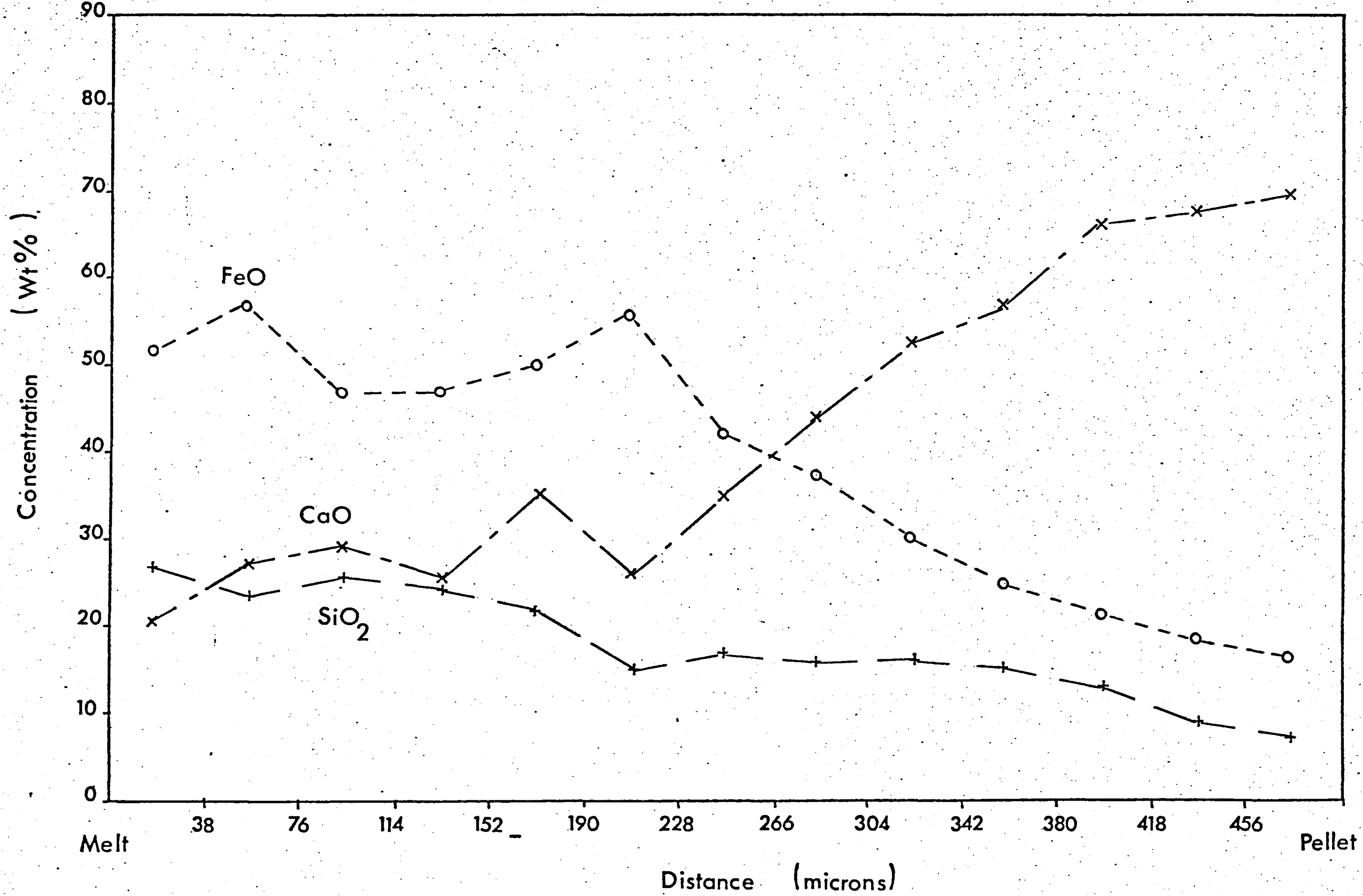
90
80
70
60
50
40
30
20
10
0
Concentration (Wt%)
FeO
CaO
SiO2
Melt
38
76
114
152
190
228
266
304
342
380
418
456
Pellet
Distance (microns)

Fig. 24

The distribution of oxides across the reaction interface between CaO and 2 FeO.$SiO_2$ + 10 Wt% $CaF_2$ plotted on the 1300°C isothermal section of the CaO - FeO - $SiO_2$ ternary

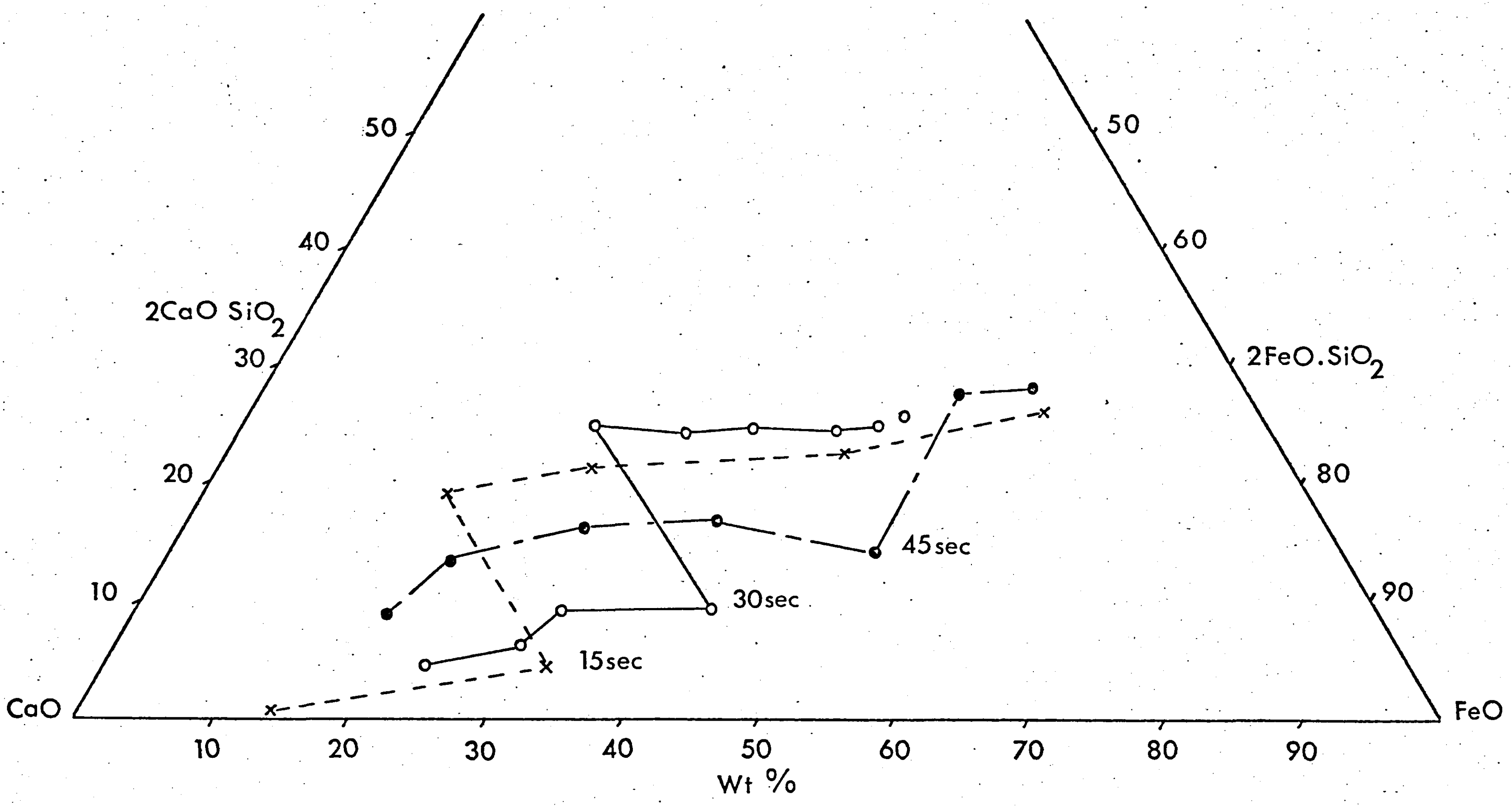
2CaO SiO2
50
40
30
20
10
2FeO.SiO2
50
60
80
90
CaO
FeO
10
20
30
40
50
60
70
80
90
Wt %
15sec
30sec
45sec

Fig. 25

The cone fusion results and initial liquidus temperatures of various lime - fayalite + 10 Wt% boric oxide mixtures plotted on the CaO - 2 FeO.$SiO_2$ isopleth

| | |
|---|---|
| – – – – – | initial bending temperature |
| --------- | final collapse temperature |
| I | initial liquidus temperature range |

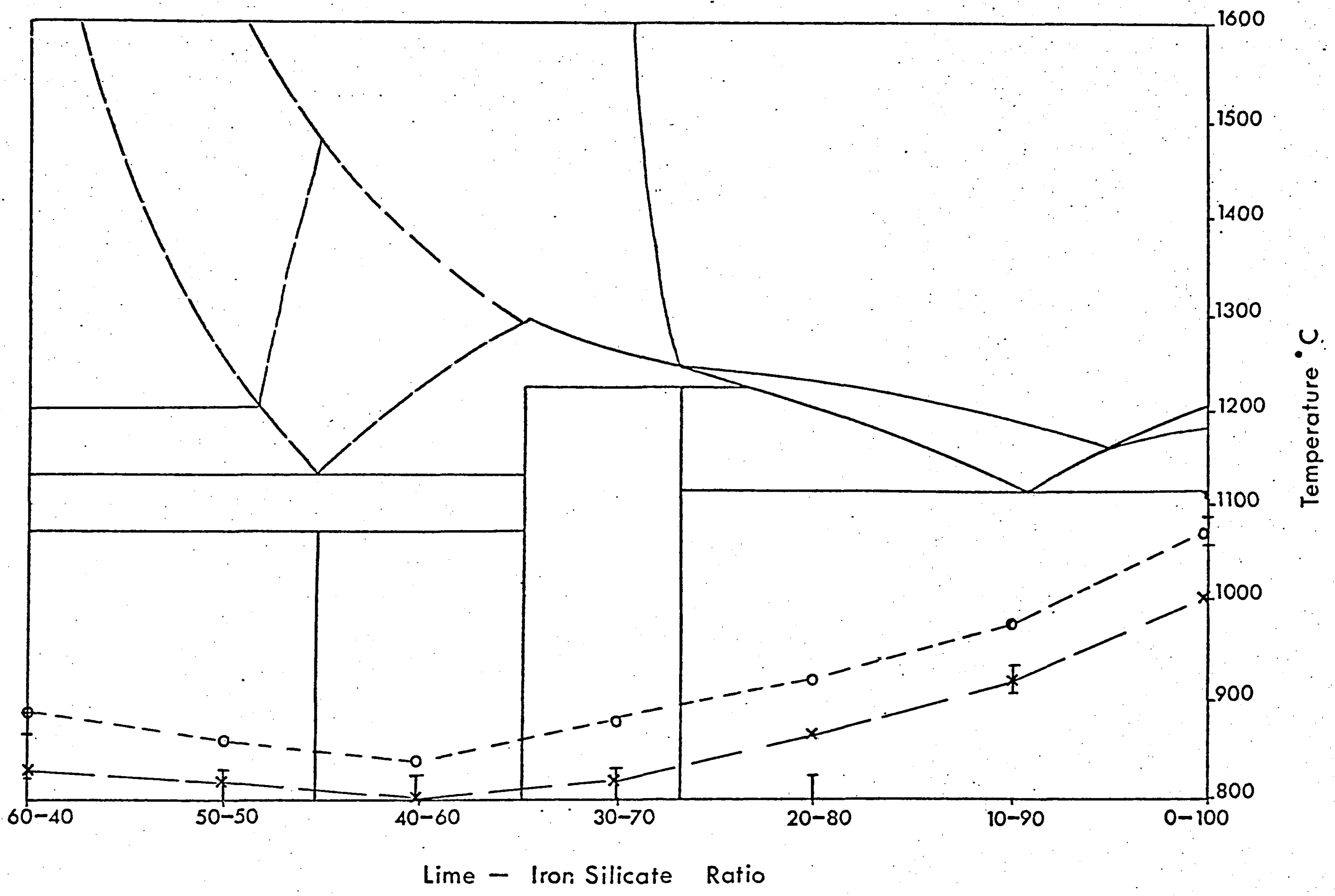1600
1500
1400
1300
1200
1100
1000
900
800
Temperature °C
60–40
50–50
40–60
30–70
20–80
10–90
0–100
Lime — Iron Silicate Ratio

Fig. 26

The distribution of oxides across the reaction interface between CaO and 2 $FeO.SiO_2$ + 10 Wt% $B_2O_3$ after an immersion time of 45 seconds

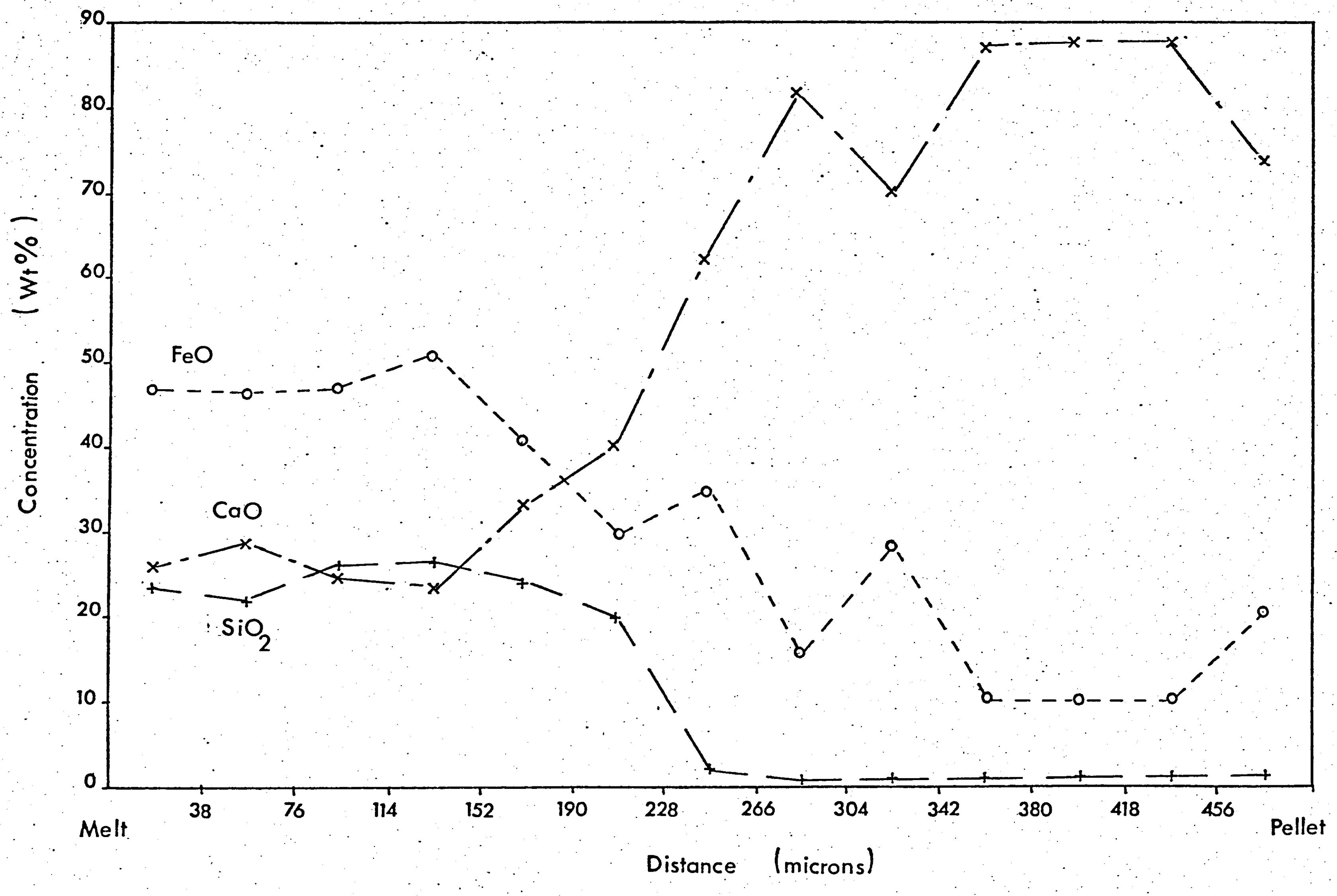
FeO
CaO
SiO₂
Concentration (Wt%)
90
80
70
60
50
40
30
20
10
0
Melt
38
76
114
152
190
228
266
304
342
380
418
456
Pellet
Distance (microns)

Fig. 27

The distribution of oxides across the reaction interface between $CaO$ and 2 $FeO.SiO_2$ + 10 Wt% $B_2O_3$ plotted on the 1300°C isothermal section of the $CaO$ - $FeO$ - $SiO_2$ ternary

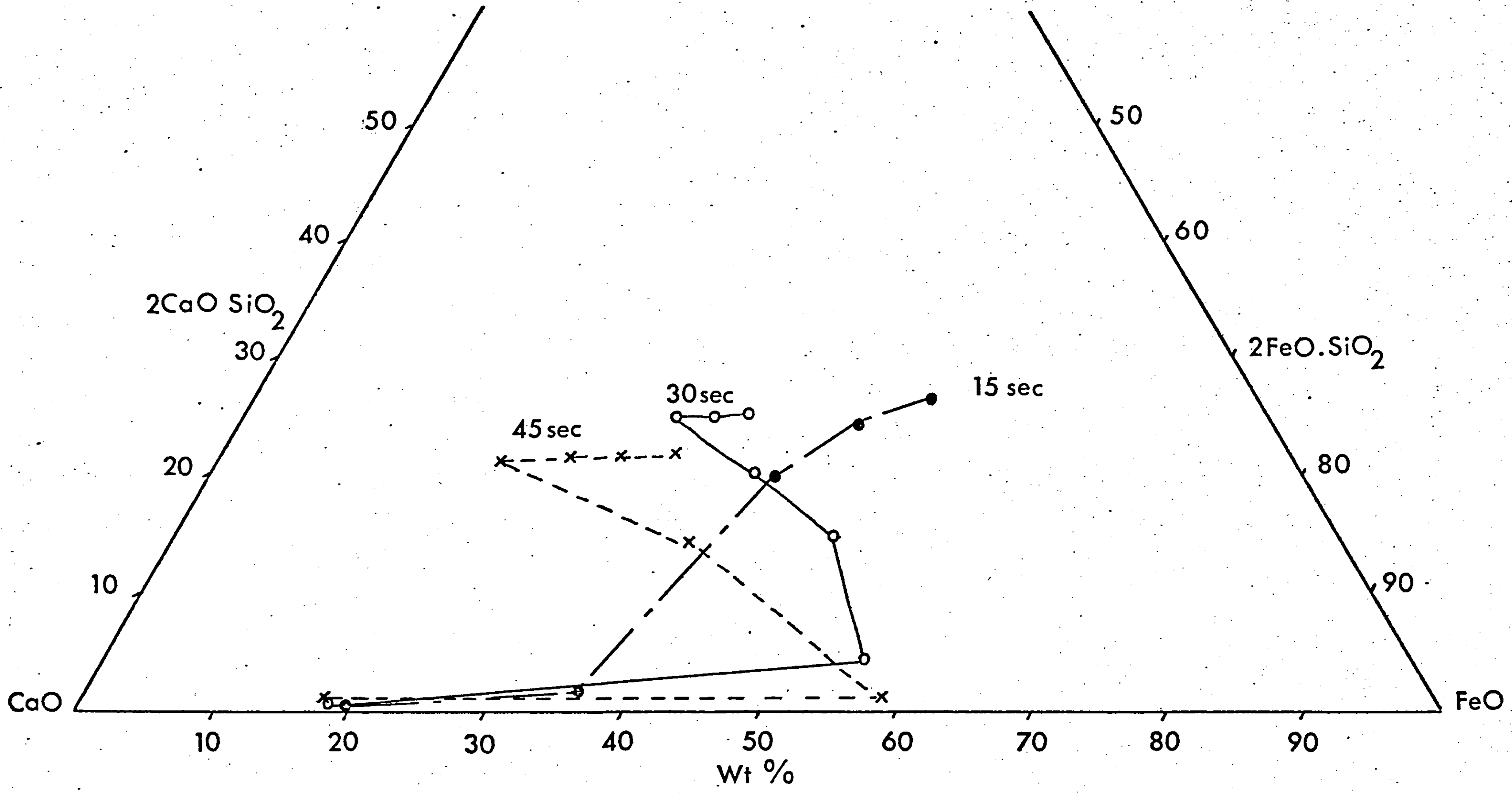
2CaO SiO$_2$
2FeO.SiO$_2$
CaO
FeO
10
20
30
40
50
50
60
80
90
10
20
30
40
50
60
70
80
90
Wt %
15 sec
30sec
45sec

Fig. 28

The distribution of oxides across the reaction interface between 2 $CaO.SiO_2$ and 2 $FeO.SiO_2$ after an immersion time of 30 seconds

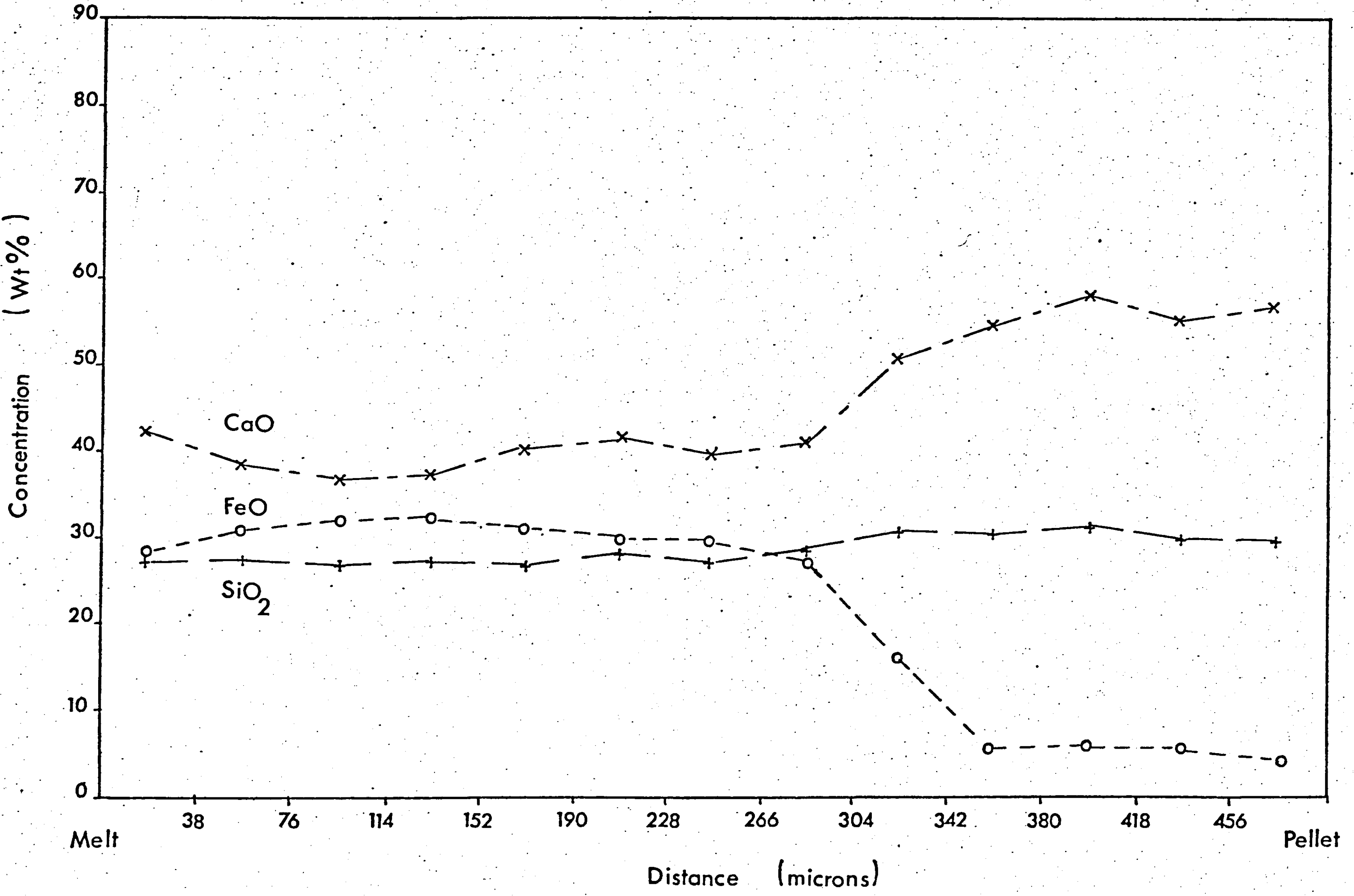
Concentration (Wt%)
90
80
70
60
50
40
30
20
10
0
CaO
FeO
SiO$_2$
Melt
38
76
114
152
190
228
266
304
342
380
418
456
Pellet
Distance (microns)

Fig. 29

The volume loss of static dicalcium silicate pellets (1) and static small lime pellets (2) in fayalite plotted against immersion time

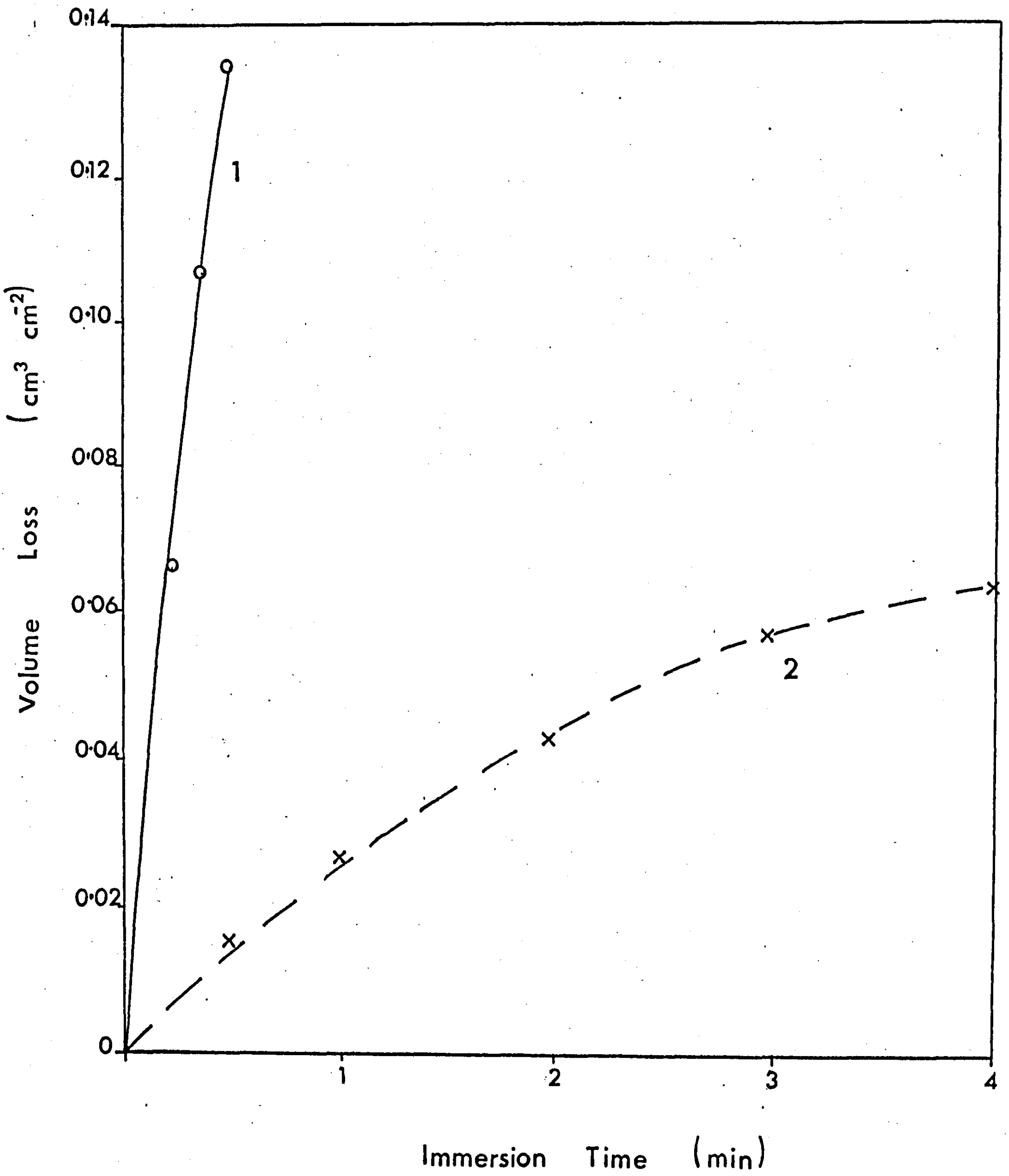
0·14
0·12
0·10
0·08
0·06
0·04
0·02
0
Volume Loss (cm³ cm⁻²)
1
2
3
4
Immersion Time (min)
1
2

Fig. 30

The 1300°C isotherm of the $CaO - FeO - SiO_2$ ternary diagram

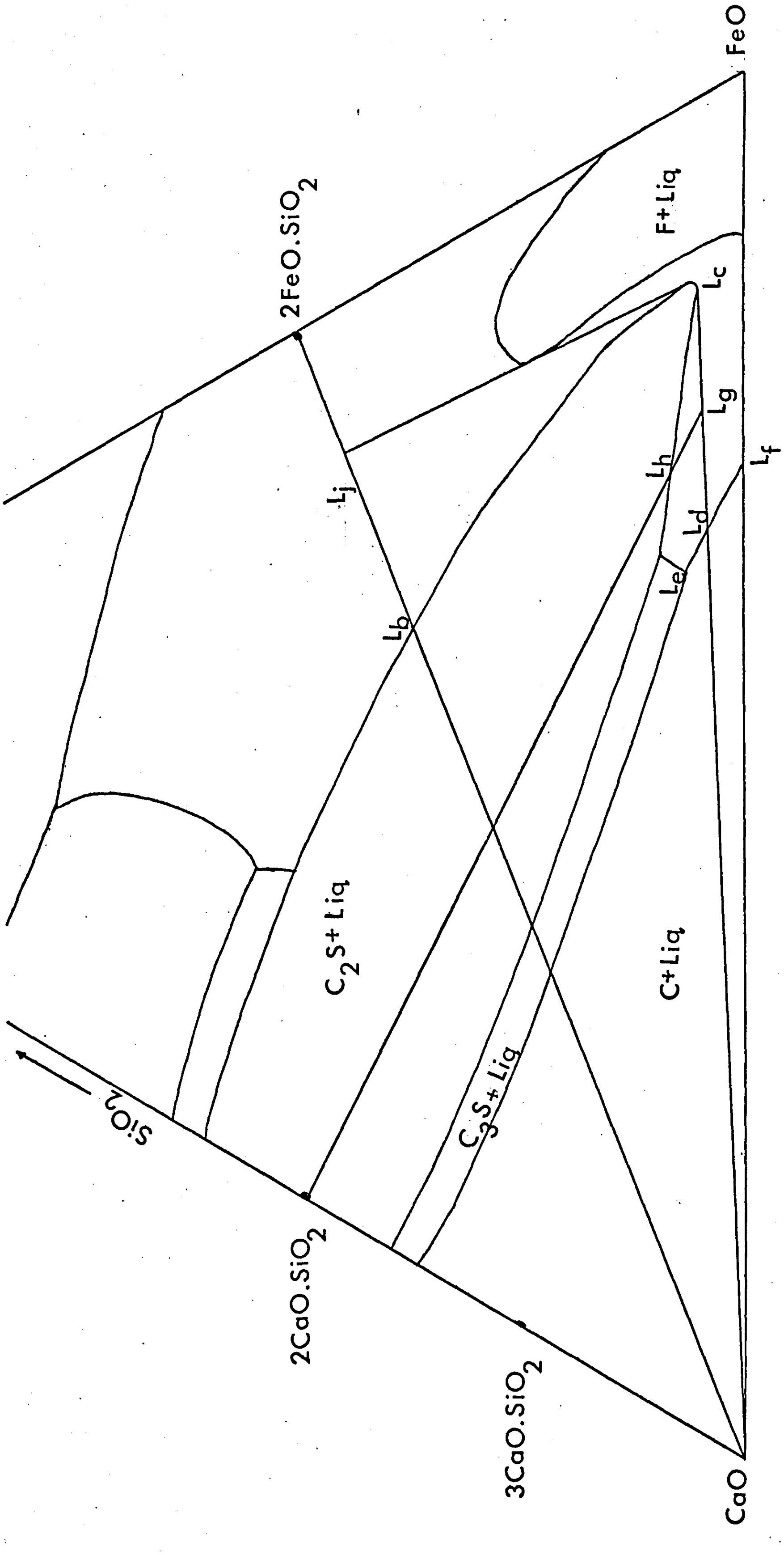
FeO
$2FeO.SiO_2$
F+Liq
$L_c$
$L_g$
$L_f$
$L_h$
$L_j$
$L_d$
$L_e$
$L_b$
$C_2S$+Liq
C+Liq
$C_3S$+Liq
$SiO_2$
$2CaO.SiO_2$
$3CaO.SiO_2$
CaO

Fig. 31

Iso-viscosity lines (poise) at 1400°C in the $FeO - MnO - SiO_2$ system (138)

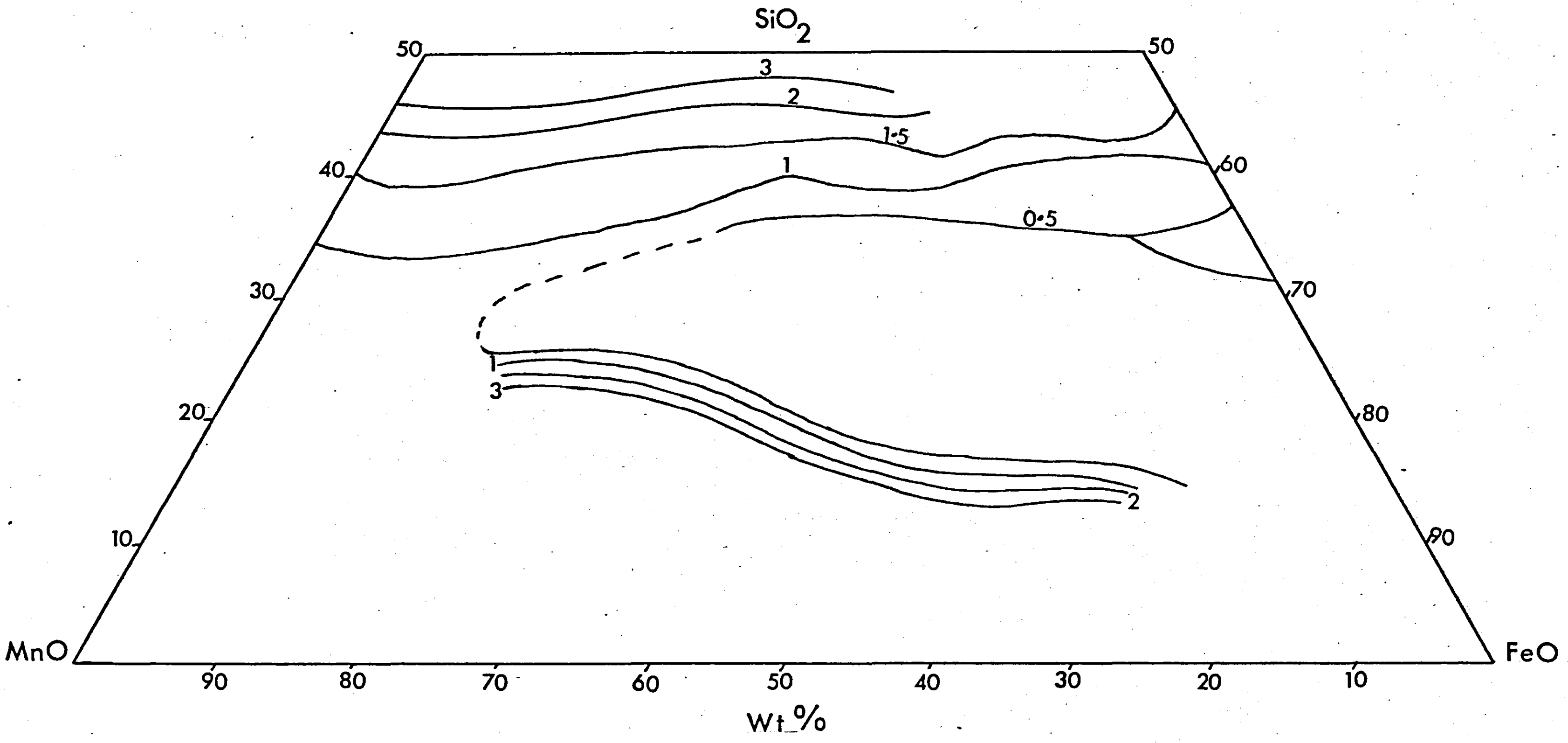
SiO$_2$
50
50
3
2
1·5
1
0·5
1
3
2
40
30
20
10
60
70
80
90
MnO
FeO
90
80
70
60
50
40
30
20
10
Wt_%

## General Information on the Following Micrographs

1. The negatives were printed directly onto photographic paper with no enlarging of the image.
2. All the micrographs are of specimens etched in Nital with the melt always on the L.H.S.
3. The large pores and voids found on all specimens are almost certainly the result of mechanical damage during preparation for microscopic examination.
4. The different combinations of pellet, melt and immersion time which were studied are listed overleaf.

## Melt-Pellet-Immersion Time Combinations

| Melt | Pellet | Immersion Time | Static-Rotated | Plate Number | Remarks |
|---|---|---|---|---|---|
| $2FeO.SiO_2$ | Small | 10sec. | static | 18 | |
| | Lime | 1min. | | 13 | |
| | | 2 " | | | $2CaO.SiO_2$ layer starting to buckle |
| | | 3 " | | 14,17 | |
| | | 4 " | | 20 | |
| | | 5 " | | 15,19,29,36 | |
| | | 6 " | | 16 | |
| | | 7 " | | 21,22 | |
| | | 8 " | | | ) very thin |
| | | 9 " | | | ) precipitated layer |
| | | 1 " | rotated | 23 | |
| | | 2 " | | | |
| | | 3 " | | 24 | |
| | | 4 " | | 25 | |
| | | 5 " | | 26, 37 | |
| | | 6 " | | 27,28 | |
| | | 7 " | | | very thin $2CaO.SiO_2$ layer |
| | Large | 1min. | static | 30 | |
| | Lime | 2 " | | | buckled $2CaO.SiO_2$ layer |
| | | 3 " | | 31 | |
| | | 4 " | | | entrapment of melt |
| | | 5 " | | 63 | |
| | | 6 " | | 32 | |
| | | 7 " | | | $2CaO.SiO_2$ precipitated on cooling |
| | | 1 " | rotated | 33 | |
| | | 2 " | | 34 | |
| | | 3 " | | | very thin $2CaO.SiO_2$ layer |
| | | 4 " | | 35 | |
| | | 5 " | | | very thin $2CaO.SiO_2$ layer |

| Melt | Pellet | Immersion Time | Static-Rotated | Plate Number | Remarks |
|---|---|---|---|---|---|
| $2FeO.SiO_2$ +MnO | Small Lime | 1min. | static | 40 | |
| | | 2 " | | 43 | |
| | | 3 " | | 41,44 | |
| | | 4 " | | 45 | |
| | | 5 " | | 46,57 | |
| | | 6 " | | 42,47,56 | |
| | | 7 " | | 48 | |
| | | 8 " | | 49 | |
| | | 9 " | | | long liquid breakouts in the melt |
| | | 1min. | rotated | 50 | |
| | | 2 " | | | liquid breakouts |
| | | 3 " | | 51,52 | |
| | | 4 " | | | $2CaO.SiO_2$ starting to dissolve on the inside surface |
| | | 5 " | | 38,53,57 | |
| | | 6 " | | 54 | |
| | | 7 " | | 55 | |
| | Large Lime | 1min. | static | 58 | |
| | | 2 " | | | very thin $2CaO.SiO_2$ layer |
| | | 3 " | | | |
| | | 4 " | | 59 | |
| | | 5 " | | 63 | |
| | | 6 " | | | very thin $2CaO.SiO_2$ layer |
| | | 7 " | | | |
| | | 1min. | rotated | 60 | |
| | | 2 " | | | thin $2CaO.SiO_2$ layer |
| | | 3 " | | 61 | |
| | | 4 " | | | corrugated $2CaO.SiO_2$ layer |
| | | 5 " | | 62,64 | |

| Melt | Pellet | Immersion Time | Static-Rotated | Plate Number | Remarks |
|---|---|---|---|---|---|
| $2FeO.SiO_2$ + $CaF_2$ | Small Lime | 15sec. | static | 39,65,66,67 | |
| | | 30 " | | 68,69,72 | |
| | | 45 " | | | individual $2CaO.SiO_2$ particles |
| | | 15 " | rotated | 70 | |
| | | 30 " | | 71 | |
| | Large Lime | 30sec. | static | 73 | |
| | | 1min. | | 75 | FeO dendrites in the melt |
| | | 1.5min | | 76 | |
| | | 15sec | rotated | 77 | |
| | | 30sec | | 78,79 | |
| $2FeO.SiO_2$ + $B_2O_3$ | Small Lime | 15sec. | static | 80,81,82 | liquid breakouts |
| | | 30 " | | 83,84 | |
| | | 45 " | | 85 | |
| | Large Lime | 15 " | static | 86 | |
| | | 30 " | | 87,88 | $2CaO.SiO_2$ dissolving on both interfaces |
| 2 $FeO.SiO_2$ | $2CaO.SiO_2$ | 15sec. | static | 89,90,92 | |
| | | 30 " | | 91 | horseshoe grains |
| $2FeO.SiO_2$ | Commercial Lime | 2min. | static | 93 | $2CaO.SiO_2$ precipitated on cooling |
| | | 4 " | | 94,95 | |
| | | 6 " | | 96 | |
| $2FeO.SiO_2$ +MnO | Commercial Lime | 2min. | static | 97 | |
| | | 4 " | | 98 | liquid breakouts |
| | | 6 " | | 99 | |

## Plate 1

The change in concentration of
various elements during a L.D. blow

## Plate 2

The $CaO$-$FeO$-$SiO_2$ ternary phase diagram

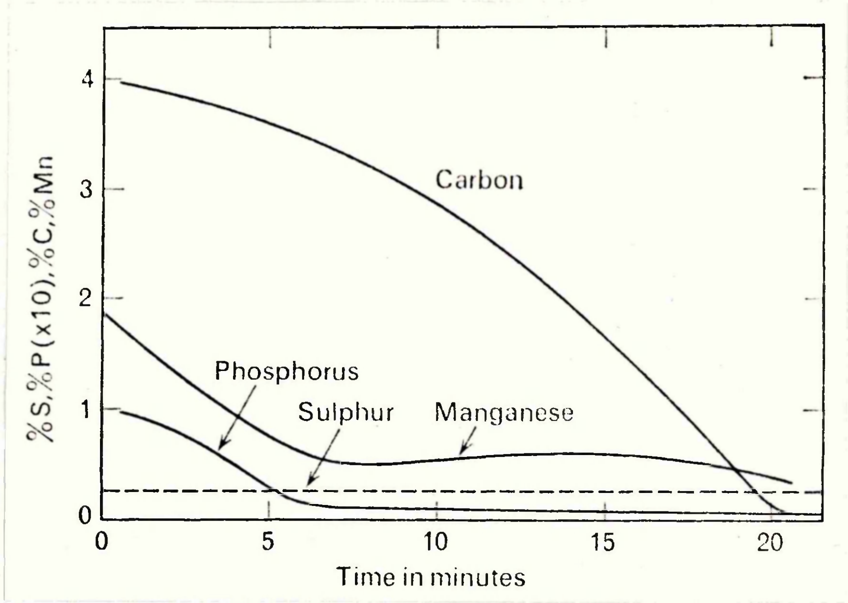

**$CaO$–$FeO$–$SiO_2$**

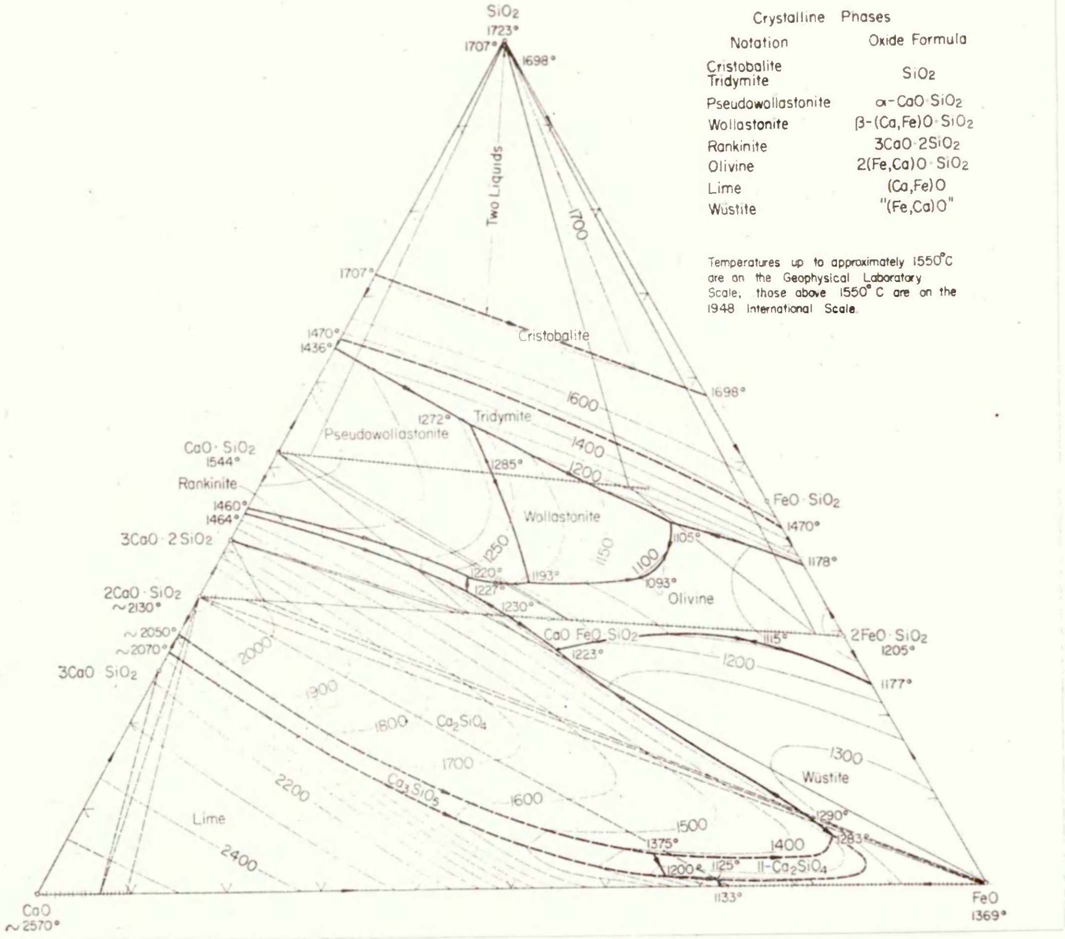

$SiO_2$
1723°
1707°
1698°
Two Liquids
1700
1707°
Cristobalite
1698°
1470°
1436°
1600
Tridymite
1272°
Pseudowollastonite
1400
1285°
1200
$CaO \cdot SiO_2$
1544°
Rankinite
1460°
1464°
$3CaO \cdot 2SiO_2$
Wollastonite
$FeO \cdot SiO_2$
1470°
1105°
1178°
1250
1150
1100
1220°
1227°
1193°
1093°
Olivine
$2CaO \cdot SiO_2$
~2130°
1230°
~2050°
~2070°
$CaO \cdot FeO \cdot SiO_2$
1223°
1115°
$2FeO \cdot SiO_2$
1205°
1177°
1200
$3CaO \cdot SiO_2$
2000
1900
1800
$Ca_2SiO_4$
1700
1300
Wüstite
2200
$Ca_3SiO_5$
1600
1290°
Lime
1500
1283°
1375°
1400
2400
1200°
1125°
II-$Ca_2SiO_4$
1133°
CaO
~2570°
FeO
1369°

Crystalline Phases

| Notation | Oxide Formula |
|---|---|
| Cristobalite<br>Tridymite | $SiO_2$ |
| Pseudowollastonite | $\alpha$-$CaO \cdot SiO_2$ |
| Wollastonite | $\beta$-$(Ca,Fe)O \cdot SiO_2$ |
| Rankinite | $3CaO \cdot 2SiO_2$ |
| Olivine | $2(Fe,Ca)O \cdot SiO_2$ |
| Lime | $(Ca,Fe)O$ |
| Wüstite | "$(Fe,Ca)O$" |

Temperatures up to approximately 1550°C are on the Geophysical Laboratory Scale, those above 1550° C are on the 1948 International Scale.

## Plate 3

The standard free energy of formation of a number of silicates at temperatures in the range 0°C to 1700°C

Silicates

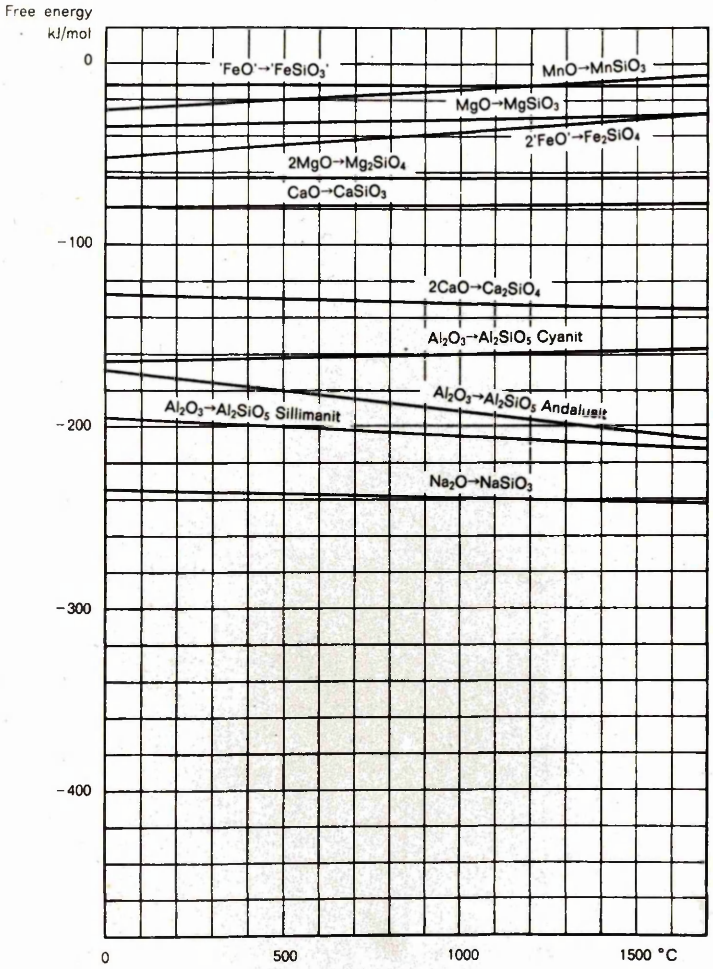
Free energy kJ/mol
0
-100
-200
-300
-400
0
500
1000
1500 °C
'FeO'→'FeSiO$_3$'
MnO→MnSiO$_3$
MgO→MgSiO$_3$
2'FeO'→Fe$_2$SiO$_4$
2MgO→Mg$_2$SiO$_4$
CaO→CaSiO$_3$
2CaO→Ca$_2$SiO$_4$
Al$_2$O$_3$→Al$_2$SiO$_5$ Cyanit
Al$_2$O$_3$→Al$_2$SiO$_5$ Andalusit
Al$_2$O$_3$→Al$_2$SiO$_5$ Sillimanit
Na$_2$O→NaSiO$_3$

## Plate 4

a. 20 mm. diameter $Ca(OH)_2$ compacts before and after sintering at 1450°C for 3 hours

b. 10 mm. diameter $Ca(OH)_2$ compacts before and after sintering at 1250°C for 3 hours

c. 10 mm. diameter $2\ CaO.SiO_2$ compact

## Plate 5

Hot filament microscope

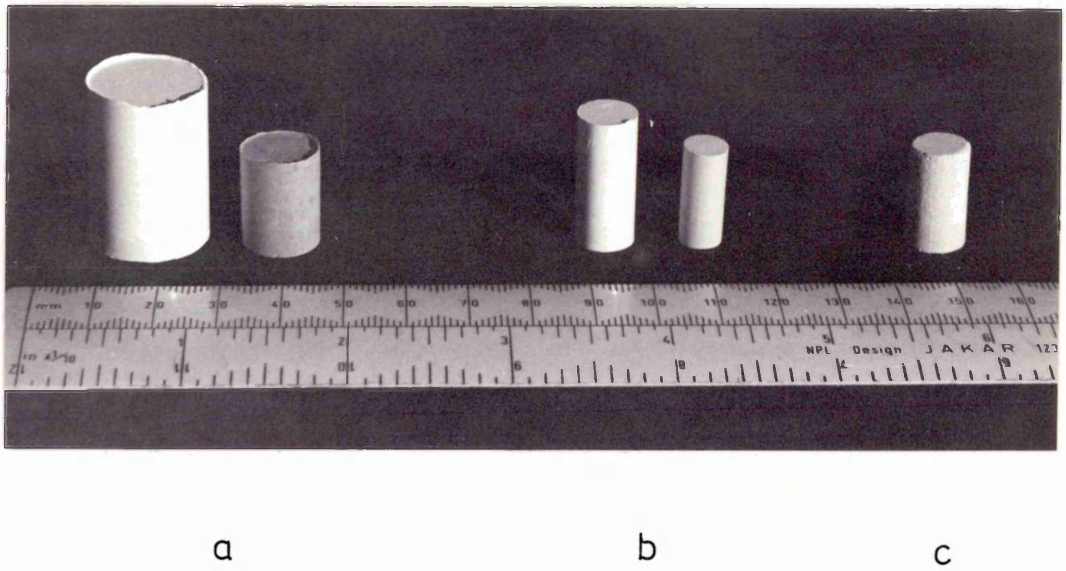
a
b
c

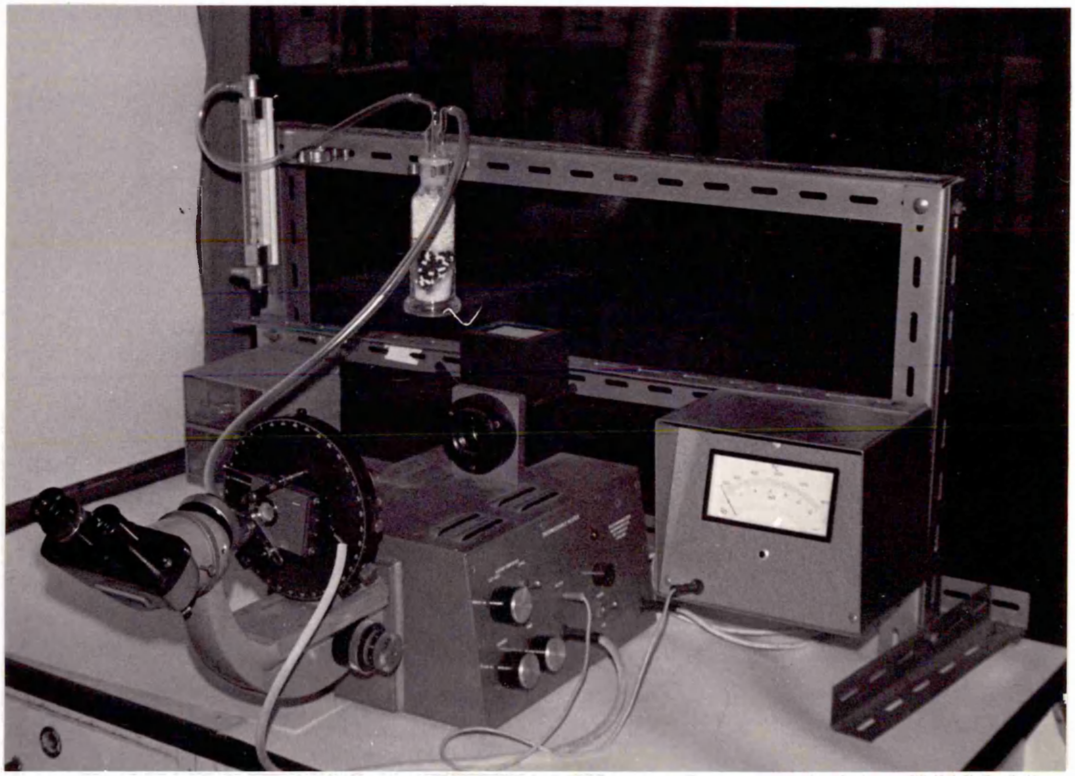

Plate 6

Tubular Crusilite D.M. type heating element

Plate 7

Immersion furnace

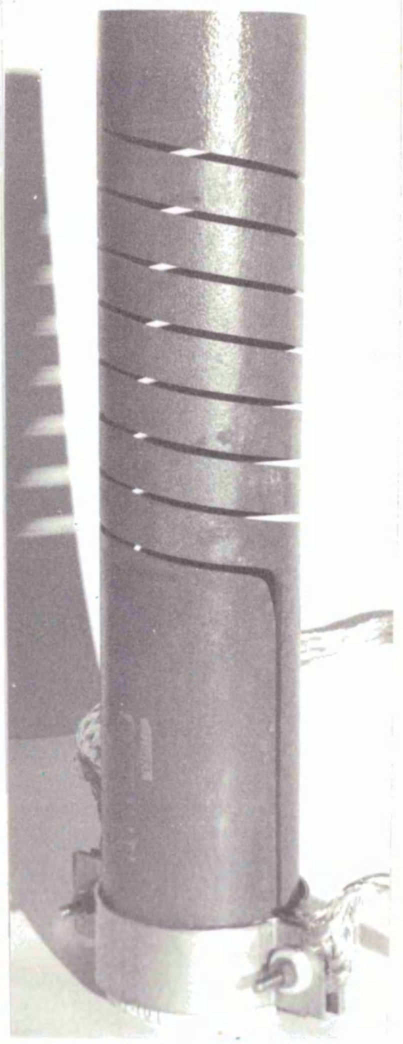

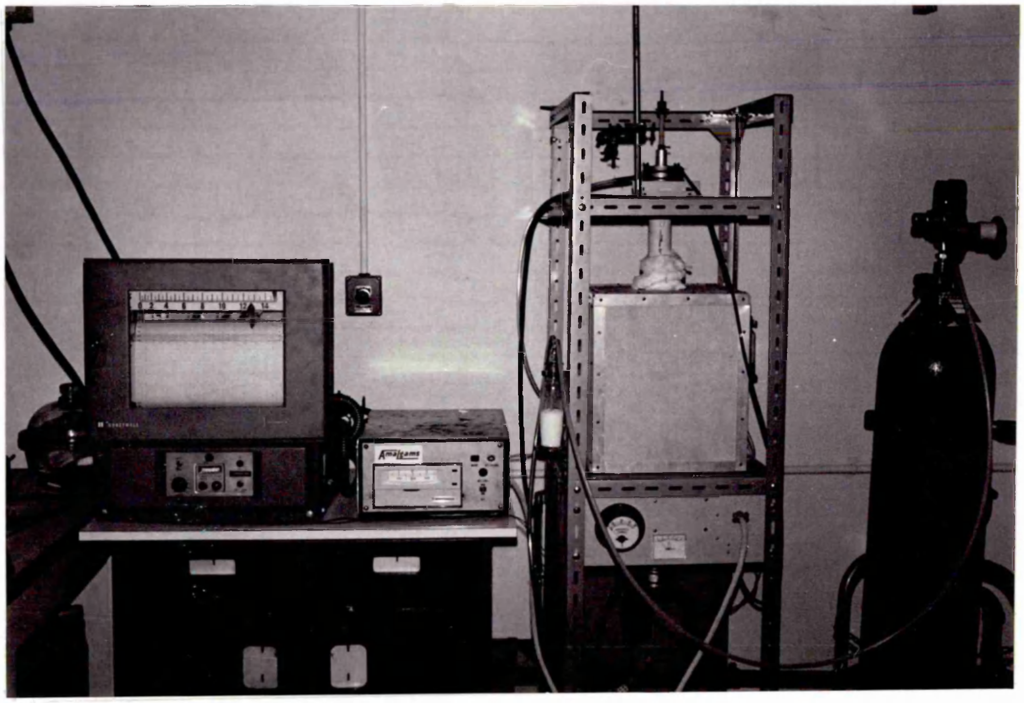
Amalgams

Plate 8

Cone mounted on an alumina cement base

Plate 9

Cone fusion furnace with silica glass viewing window

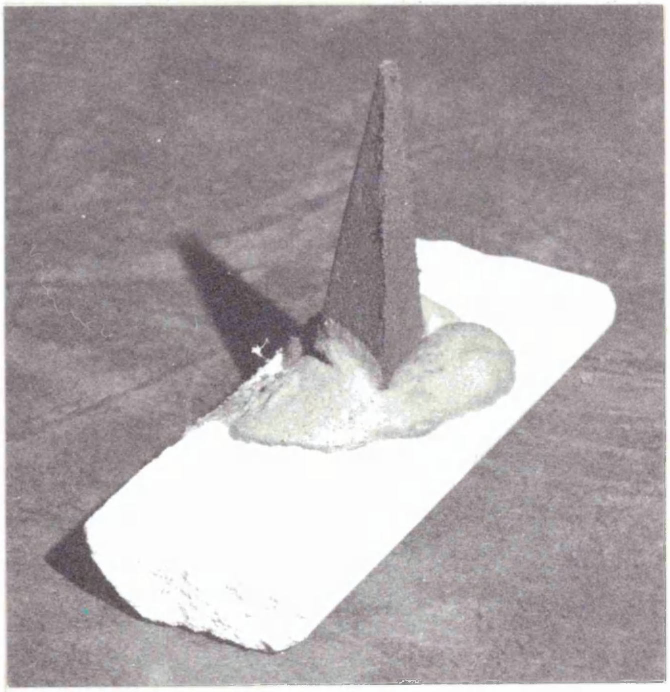

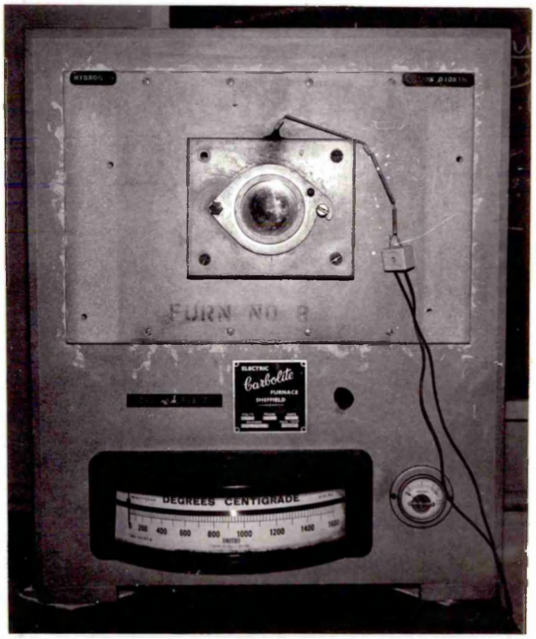
FURN NO 8
ELECTRIC
Carbolite
FURNACE
SHEFFIELD
DEGREES CENTIGRADE
200 400 600 800 1000 1200 1400 1600

## Plate 10

Pellet attached to a hollow alumina spindle

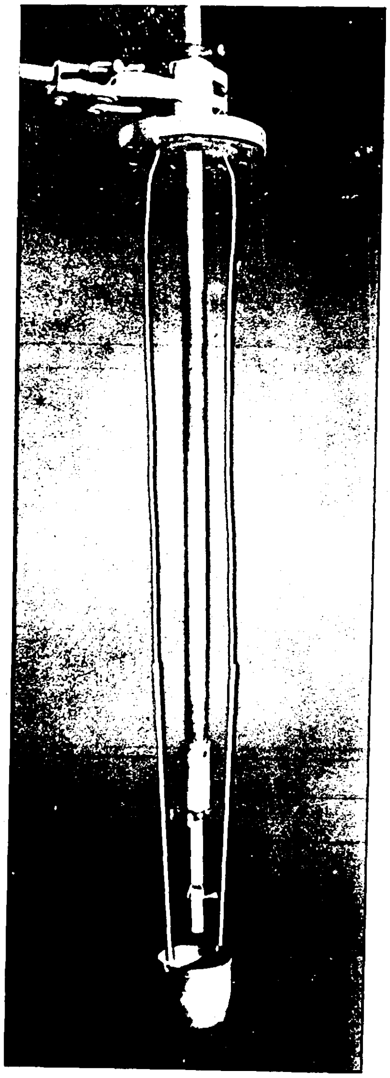

## Plate 11

Stirrer motor connected by 'flexidrive'
to the top of the alumina spindle

## Plate 12

Density bottles used in the
quantitative experiments

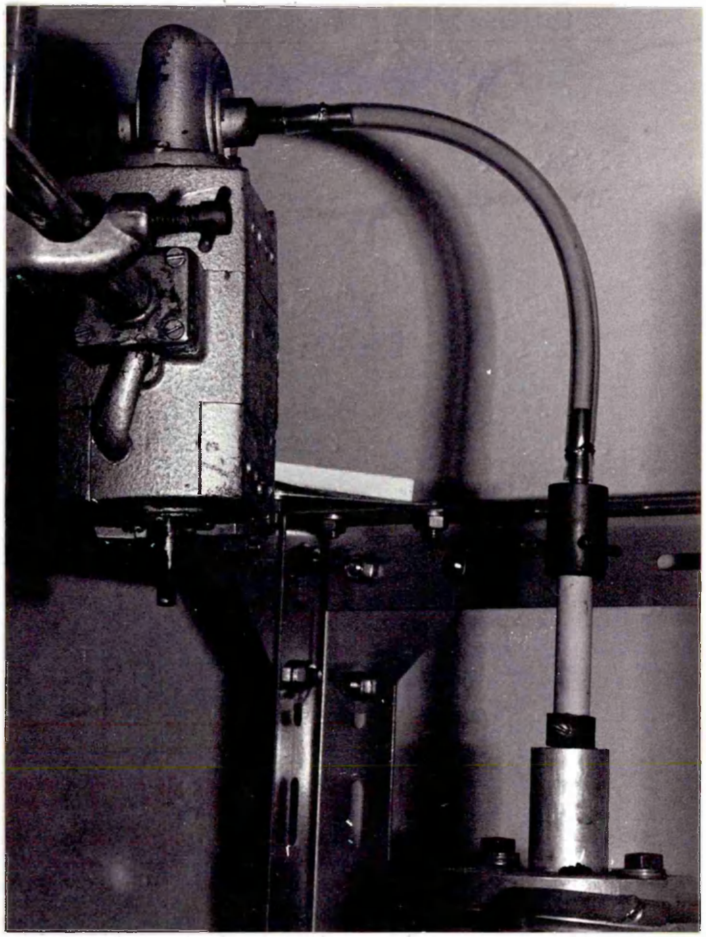

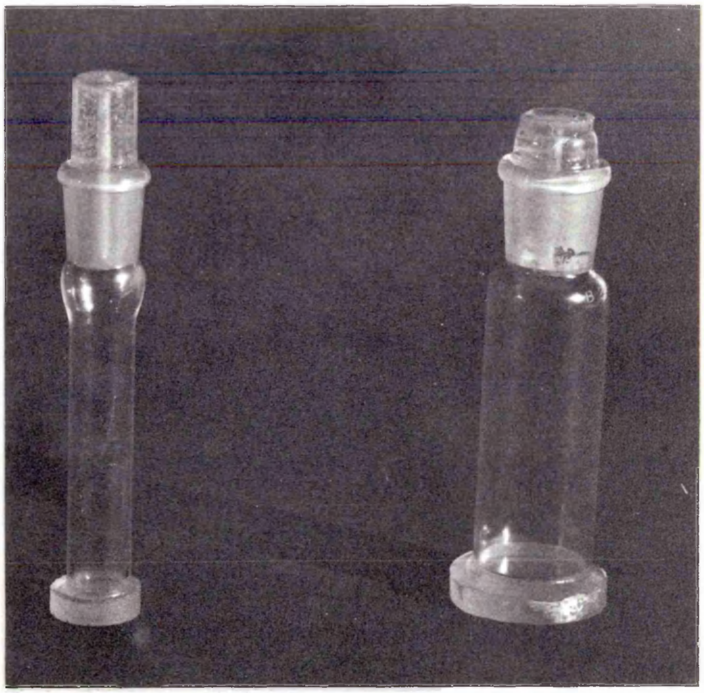

## Plate 13

Static small lime pellet 1 minute immersion

$2\ FeO.SiO_2$ melt x 400

The lime pellet was separated from the melt by solid $2\ CaO.SiO_2$ (etched dark) and an iron oxide (etched white) rich phase which was liquid at the reaction temperature

## Plate 14

Static small lime pellet 3 minutes immersion

$2\ FeO.SiO_2$ melt x 400

Penetration of the lime pellet by the iron oxide rich liquid phase

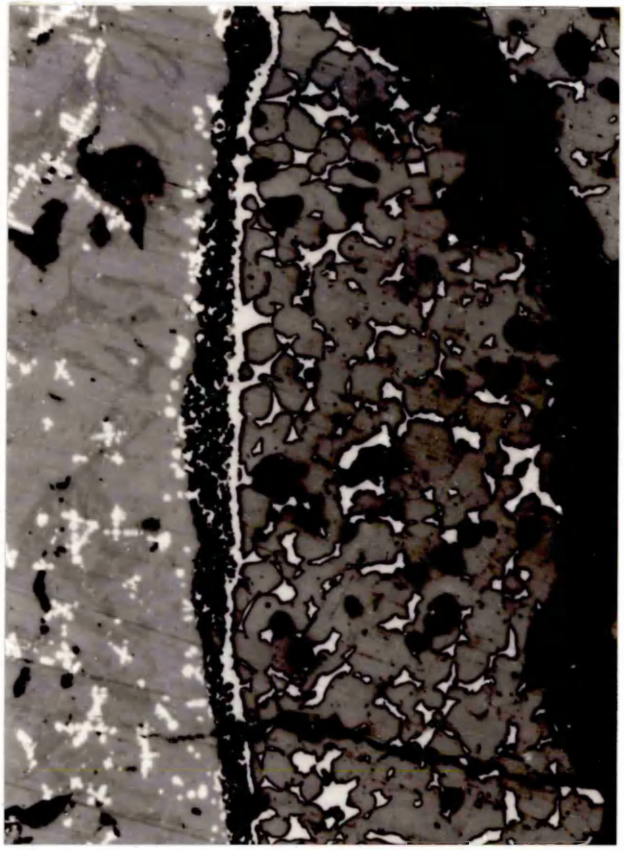

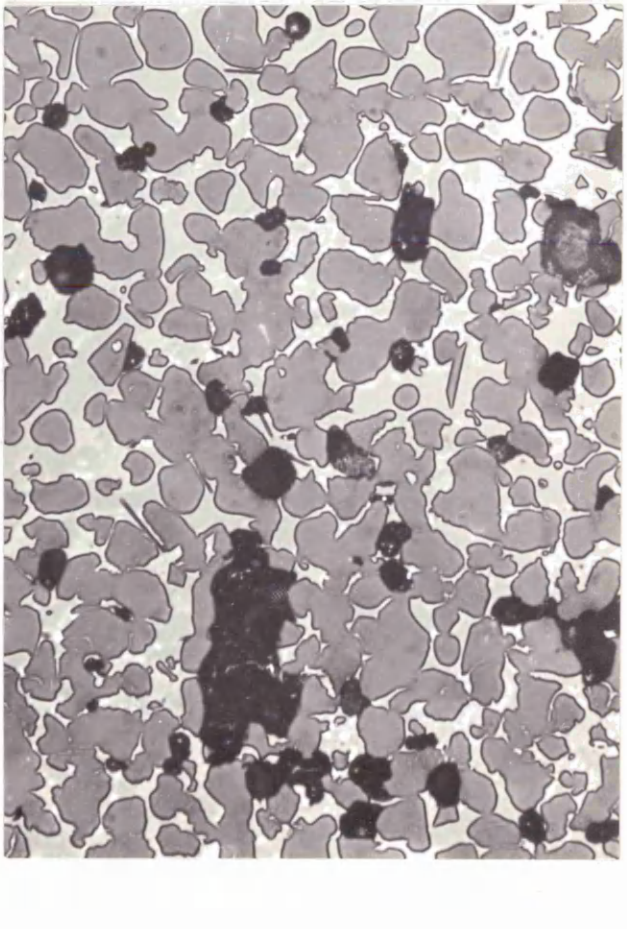

## Plate 15

Static small lime pellet    2 FeO.SiO$_2$ melt
5 minutes immersion    x 400

Particles of iron (etched white in Nital) adjacent to the lime grains

## Plate 16

Static small lime pellet    2 FeO.SiO$_2$ melt
6 minutes immersion    x 400

Needles of 3 CaO.SiO$_2$ precipitated on cooling with isothermally precipitated 3 CaO.SiO$_2$ appearing as large angular crystals. The large rounded grains are lime with iron oxide in solid solution

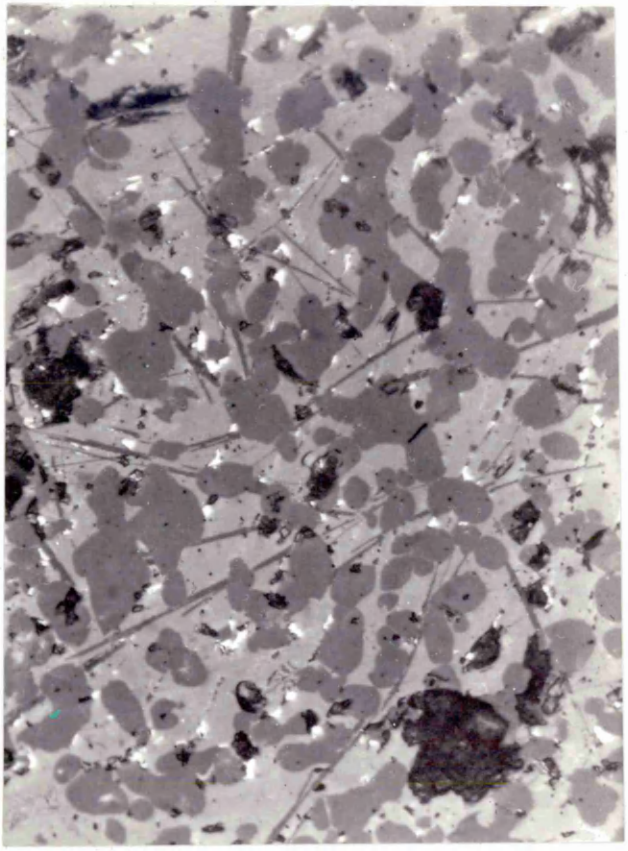

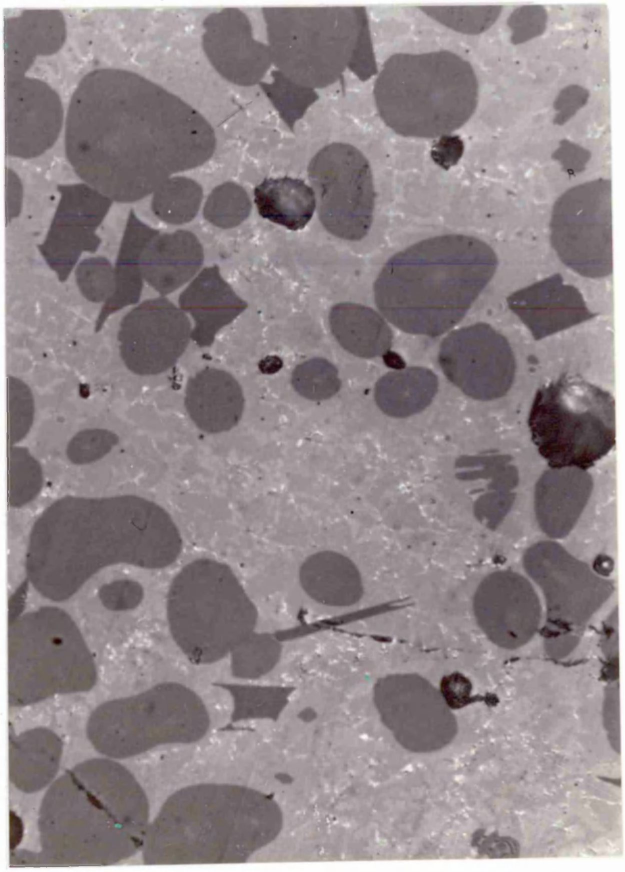

## Plate 17

Static small lime pellet $2\ FeO.SiO_2$ melt
3 minutes immersion x 400

The structure of the white phase is wustite dendrites surrounded by a eutectic matrix

## Plate 18

Static small lime pellet $2\ FeO.SiO_2$ melt
10 seconds immersion x 1000

Particles of $2\ CaO.SiO_2$ (etched dark) agglomerating in the iron oxide rich liquid

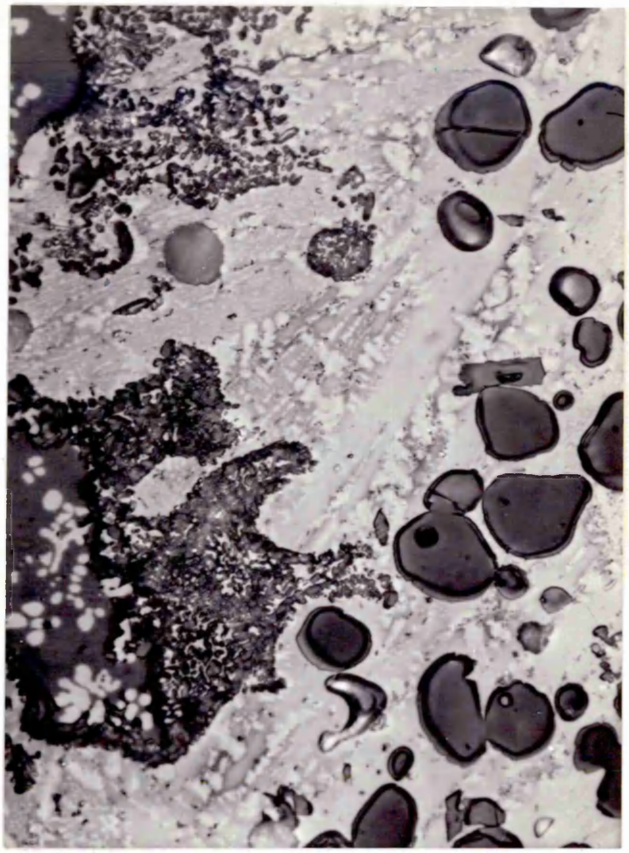

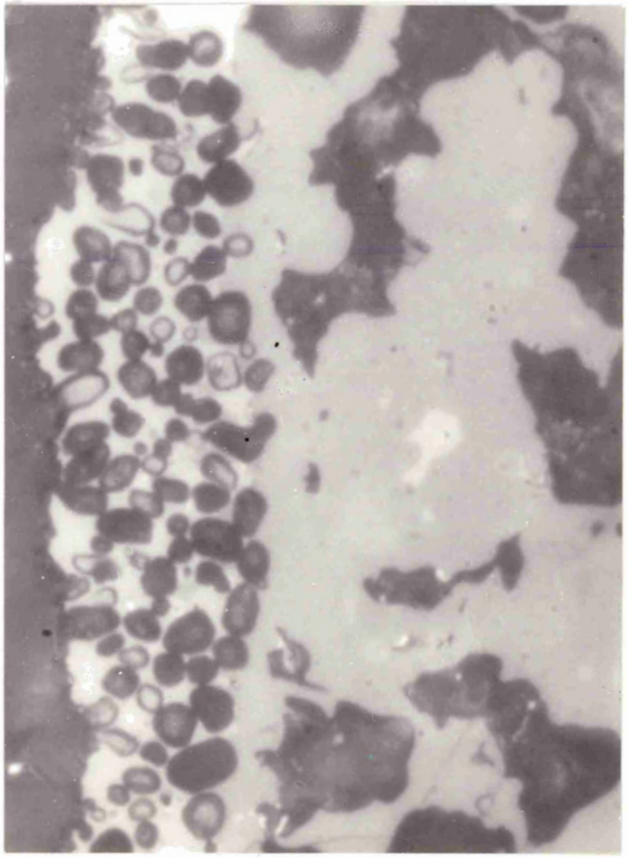

## Plate 19

Static small lime pellet 2 FeO.$SiO_2$ melt
5 minutes immersion x 400

Large aggregates of 2 CaO.$SiO_2$ breaking away into the iron oxide rich liquid phase

## Plate 20

Static small lime pellet 2 FeO.$SiO_2$ melt
4 minutes immersion x 400

Dissolving 3 CaO.$SiO_2$ crystals (angular) adjacent to the 2 CaO.$SiO_2$ rim

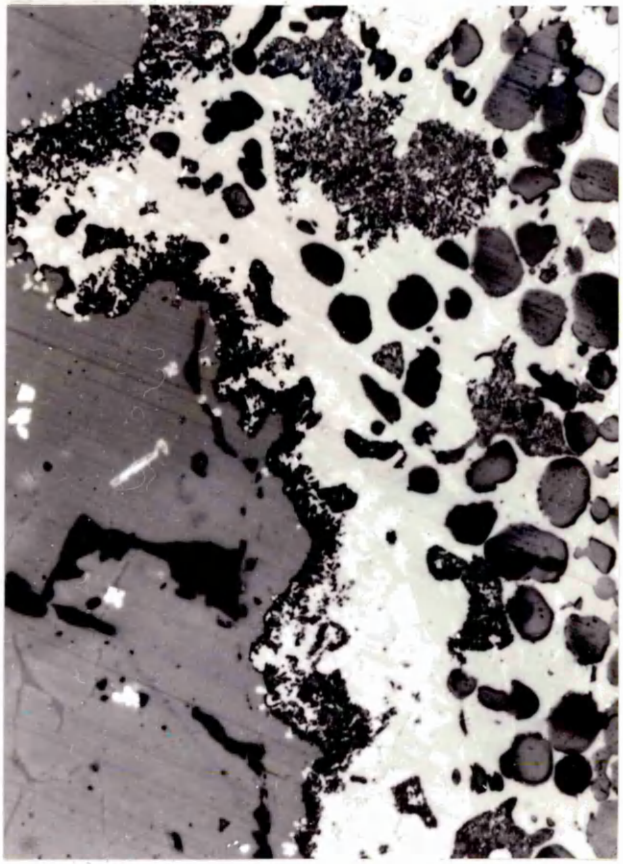

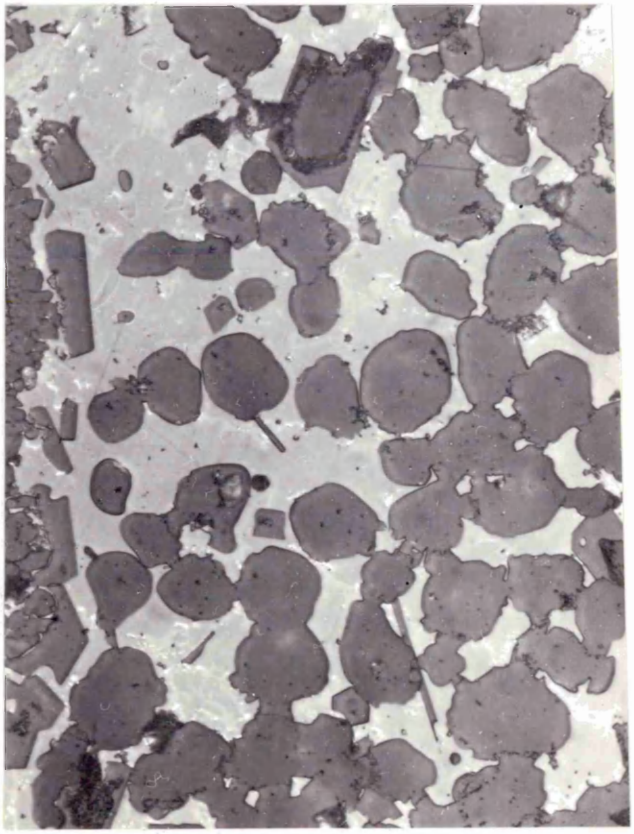

## Plate 21

Static small lime pellet 2 $FeO.SiO_2$ melt
7 minutes immersion x 40

The 2 $CaO.SiO_2$ – melt interface has 'moved' inwards as the lime pellet receded

## Plate 22

Static small lime pellet 2 $FeO.SiO_2$ melt
7 minutes immersion x 1000

Wustite dendrites (etched white) precipitated from the melt during freezing

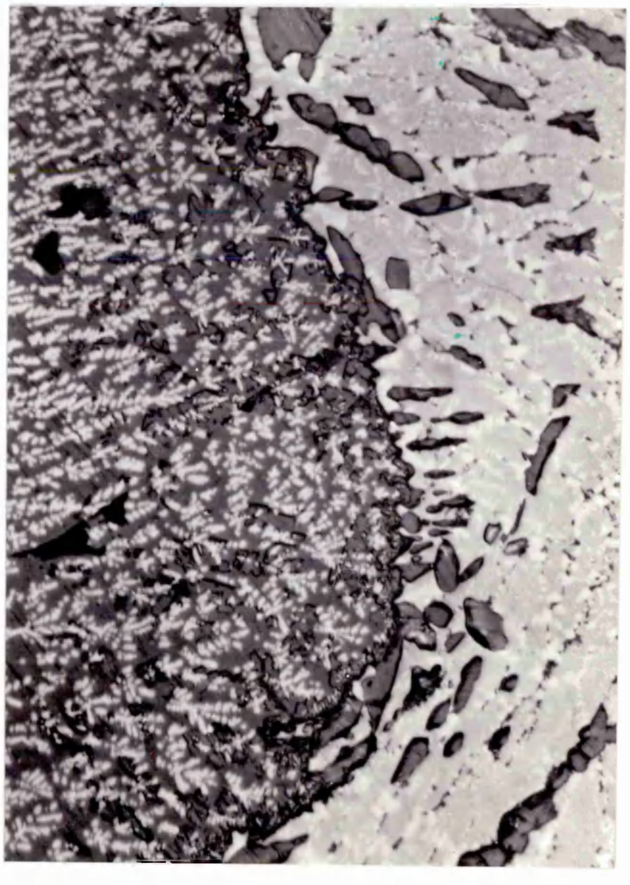

## Plate 23

| | |
|---|---|
| Rotated small lime pellet | 2 FeO.$SiO_2$ melt |
| 1 minute immersion | x 400 |

Corrugated layer of 2 CaO.$SiO_2$

## Plate 24

| | |
|---|---|
| Rotated small lime pellet | 2 FeO.$SiO_2$ melt |
| 3 minutes immersion | x 400 |

Liquid breakouts (etched white) in the melt

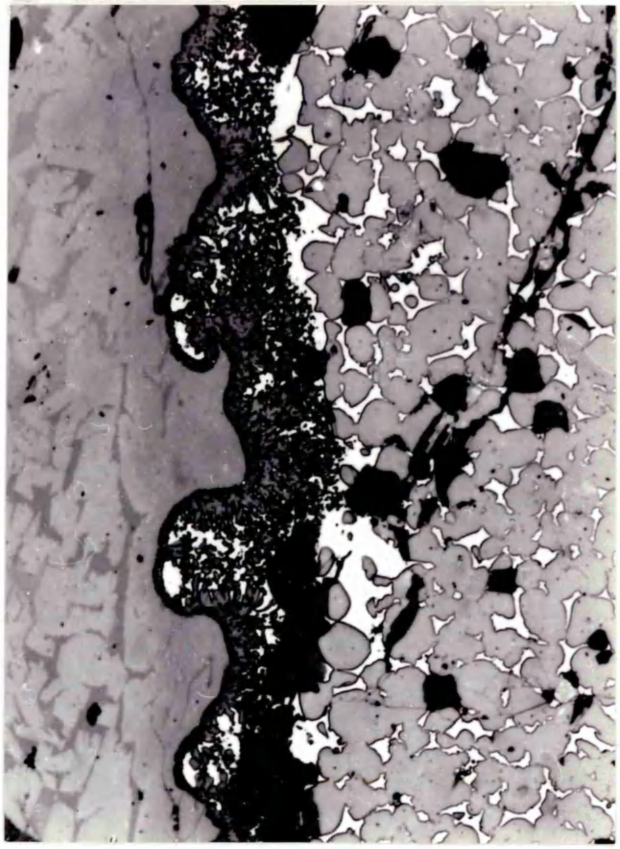

## Plate 25

| | |
|---|---|
| Rotated small lime pellet | 2 $FeO.SiO_2$ melt |
| 4 minutes immersion | x 400 |

A region of melt partially isolated in the liquid phase

## Plate 26

| | |
|---|---|
| Rotated small lime pellet | 2 $FeO.SiO_2$ melt |
| 5 minutes immersion | x 400 |

Relatively thin layer of 2 $CaO.SiO_2$ along the melt boundary

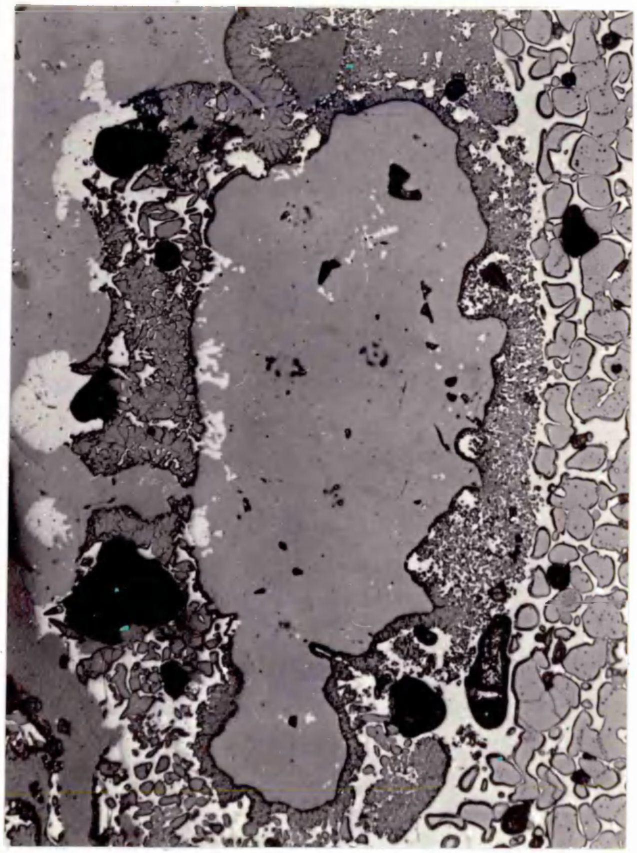

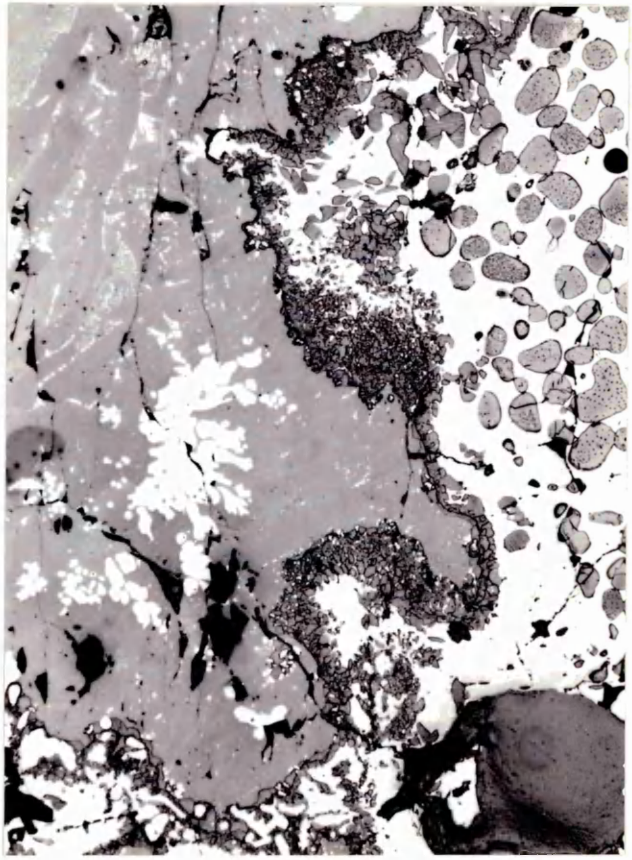

## Plate 27

Rotated small lime pellet  
6 minutes immersion

2 FeO.$SiO_2$ melt  
x 400

Particles of 2 CaO.$SiO_2$ forming a network in the liquid phase

## Plate 28

Rotated small lime pellet  
6 minutes immersion

2 FeO.$SiO_2$ melt  
x 800

Sintered groups of 2 CaO.$SiO_2$ particles

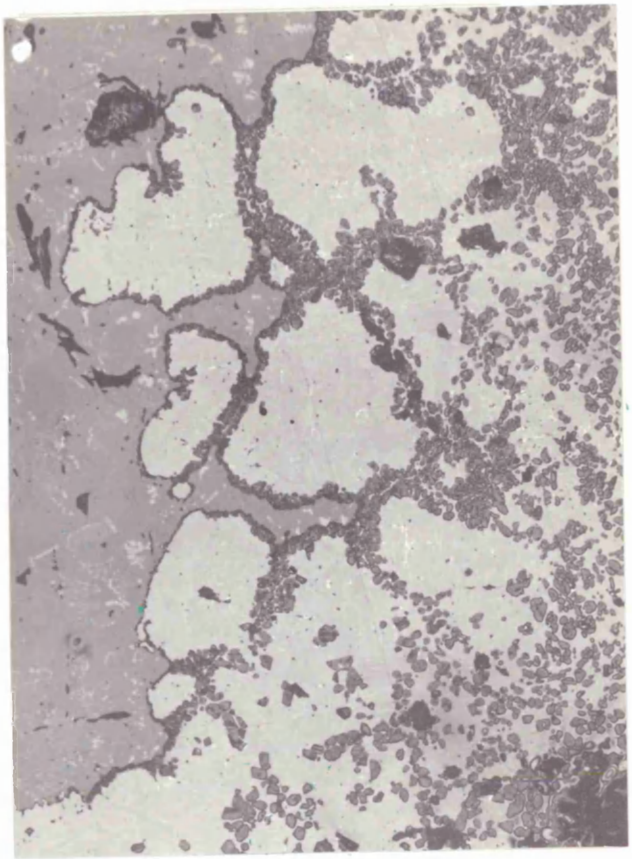

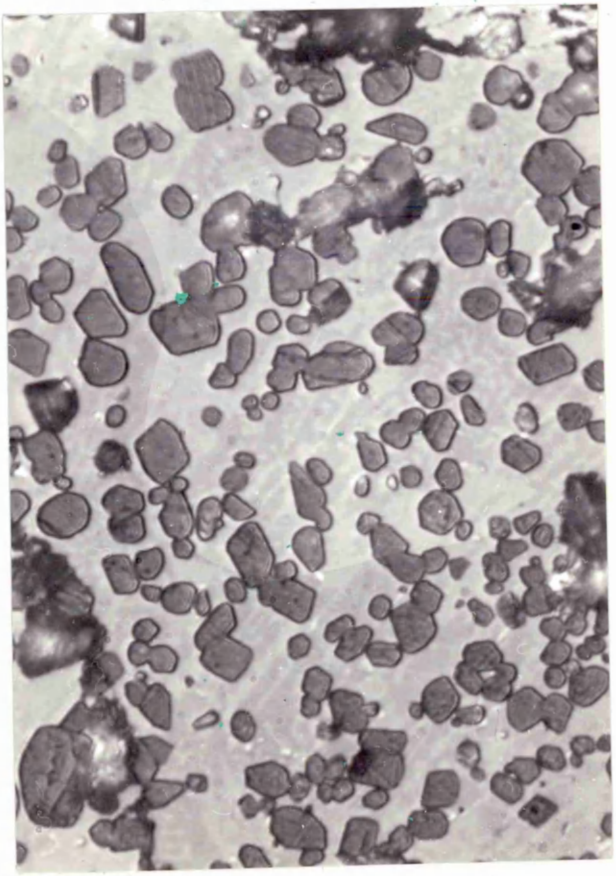

## Plate 29

5 minutes immersion

Section from the reaction zone between CaO and 2 $FeO.SiO_2$

a. Electron Image
b. Calcium
c. X ray image for Silicon
d. Iron

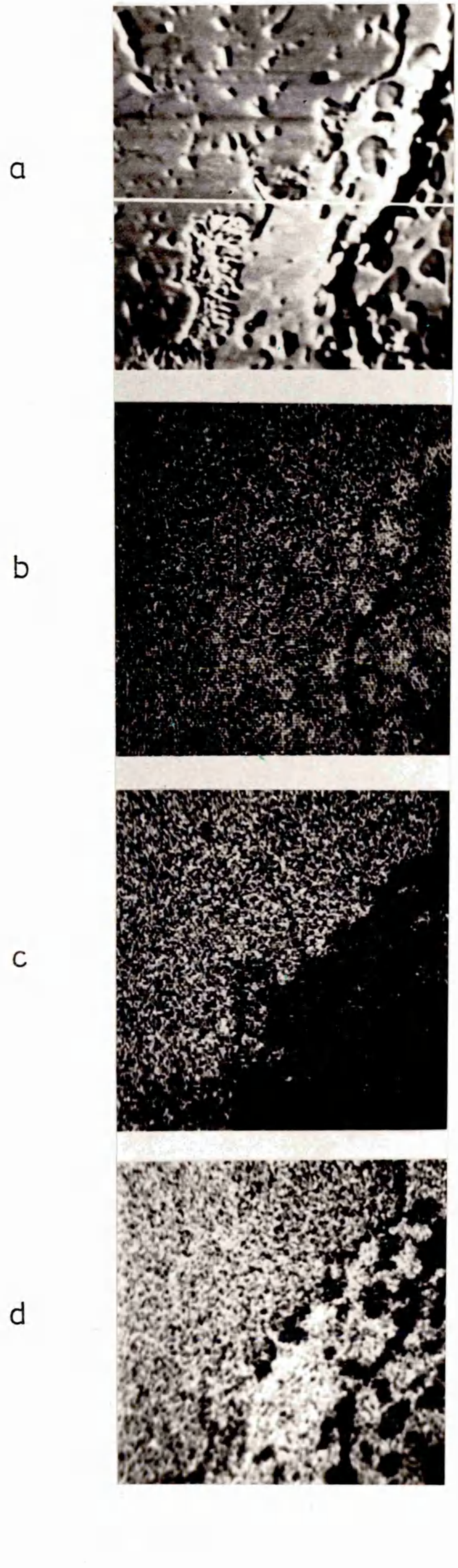
a
b
c
d

## Plate 30

Static large lime pellet $2\ FeO.SiO_2$ melt
1 minute immersion x 400

Thin layer of $2\ CaO.SiO_2$ with additional $2\ CaO.SiO_2$ (precipitated as dendrites) in the melt.

## Plate 31

Static large lime pellet $2\ FeO.SiO_2$ melt
3 minutes immersion x 400

A continuous layer of $2\ CaO.SiO_2$ along the melt boundary

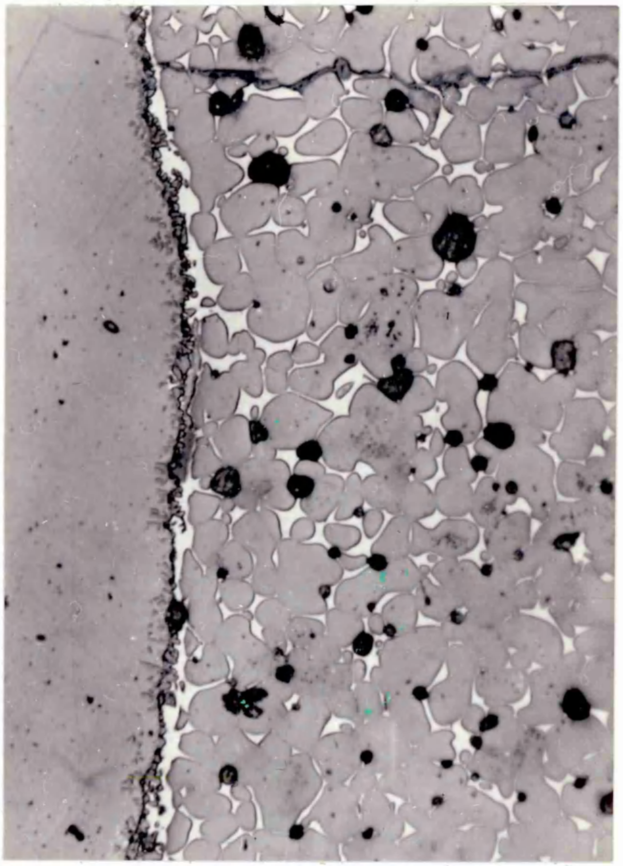

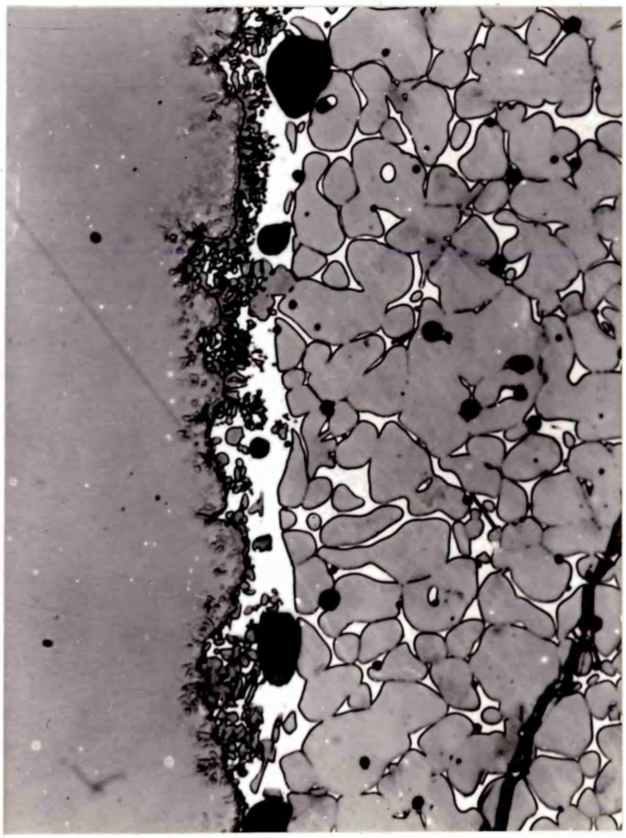

## Plate 32

| | |
|---|---|
| Static large lime pellet | 2 $FeO.SiO_2$ melt |
| 6 minutes immersion | x 400 |

A crack in the pellet infiltrated by the melt. The structure is 2 $CaO.SiO_2$ surrounded by large angular crystals of 3 $CaO.SiO_2$. These two phases being separated from the pellet by an iron oxide liquid phase.

## Plate 33

| | |
|---|---|
| Rotated large lime pellet | 2 $FeO.SiO_2$ melt |
| 1 minute immersion | x 400 |

Corrugated layer of 2 $CaO.SiO_2$ along the melt boundary

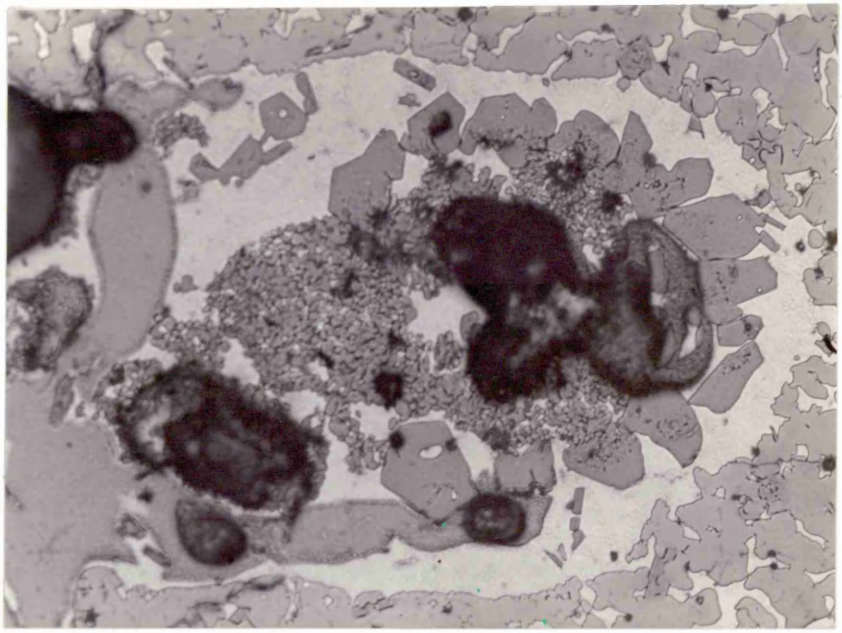

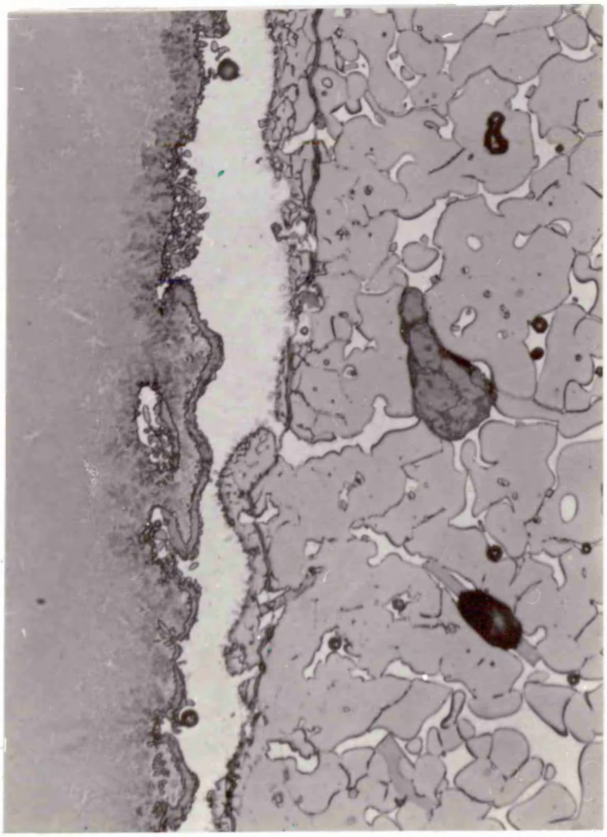

## Plate 34

Rotated large lime pellet
2 minutes immersion

$2\ FeO.SiO_2$ melt
x 400

Dendrites of $2\ CaO.SiO_2$ in the melt adjacent to the isothermally precipitated layer.

## Plate 35

Rotated large lime pellet
4 minutes immersion

$2\ FeO.SiO_2$ melt
x 400

Isolated region of melt with $2\ CaO.SiO_2$ on the lime pellet side only

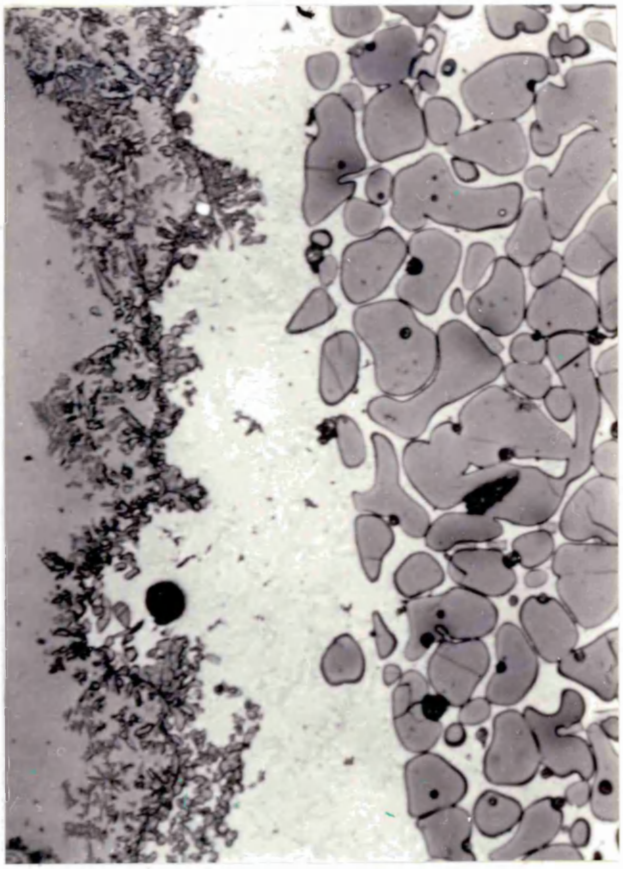

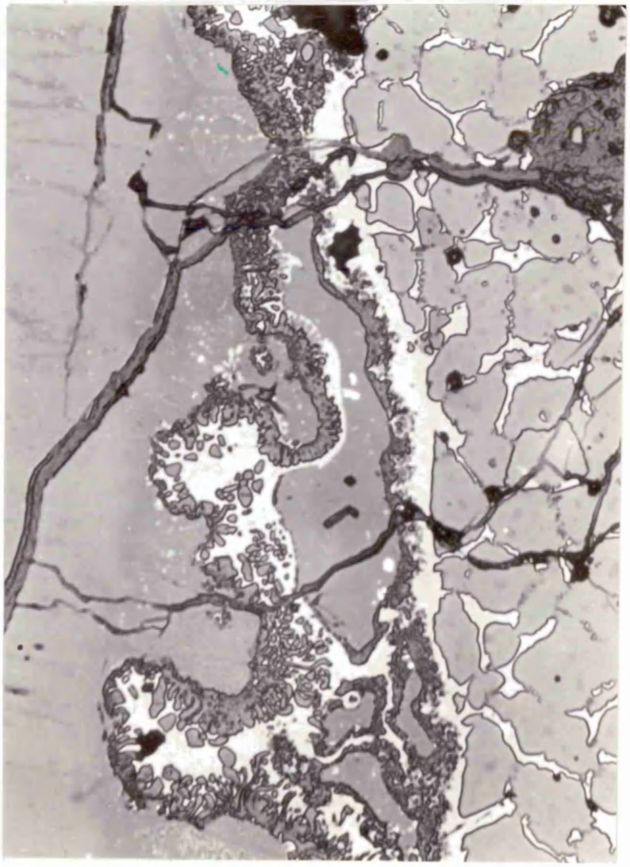

x 3

Plate 36

5 minutes static
in 2 $FeO.SiO_2$

Plate 37

5 minutes rotated
in 2 $FeO.SiO_2$

Plate 38

5 minutes rotated
in 2 $FeO.SiO_2$ + 10% MnO

Plate 39

15 seconds static
in 2 $FeO.SiO_2$ + 10% $CaF_2$

## Plate 40

Static small lime pellet 2 $FeO.SiO_2$ + MnO melt
1 minute immersion x 400

A layer of 2 $CaO.SiO_2$ separating the melt and liquid phases

## Plate 41

Static small lime pellet 2 $FeO.SiO_2$ + MnO melt
3 minutes immersion x 400

Infiltration of the porous pellet by the liquid phase

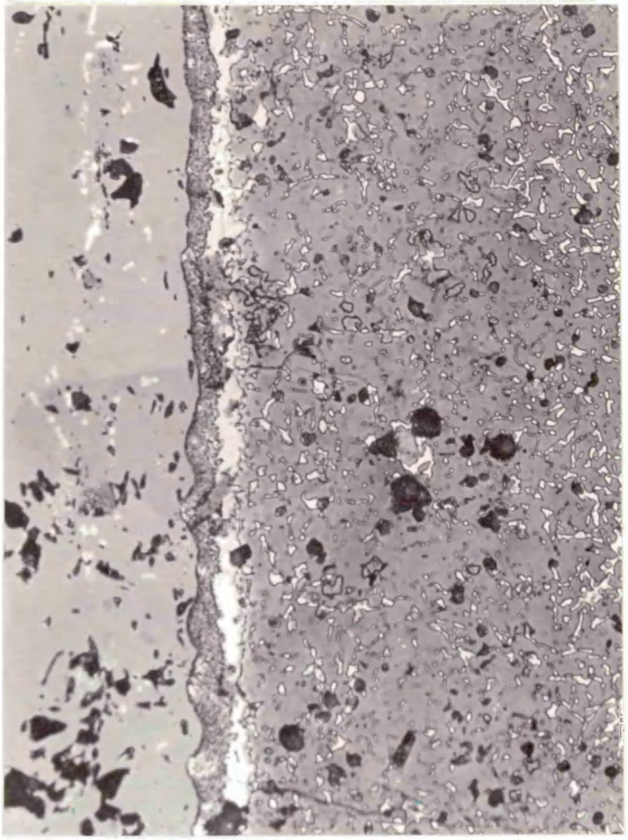

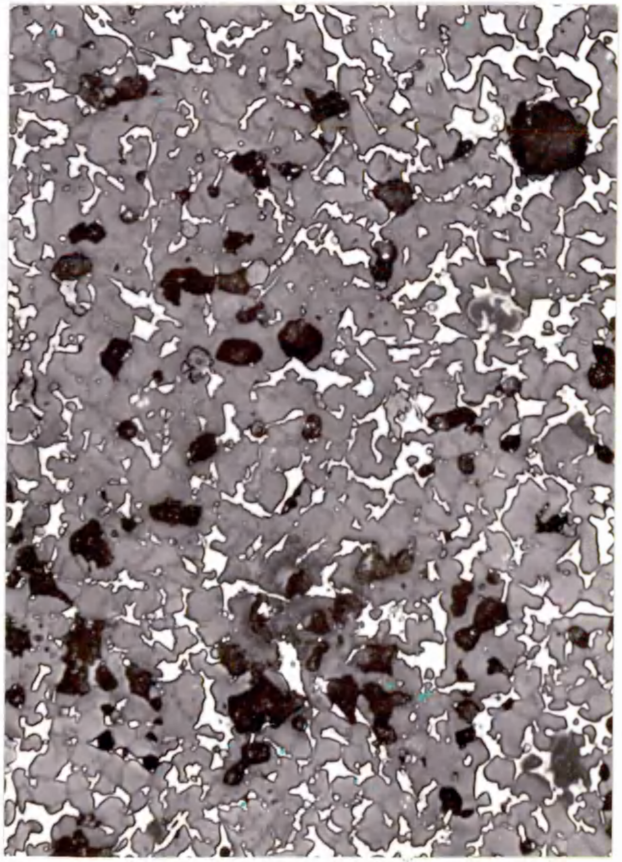

## Plate 42

Static small lime pellet
6 minutes immersion

$2\ FeO.SiO_2 + MnO$ melt
x 400

Direct bonding still present between some of the lime grains

## Plate 43

Static small lime pellet
2 minutes immersion

$2\ FeO.SiO_2 + MnO$ melt
x 400

Variation in the distribution of $2\ CaO.SiO_2$ particles along the melt boundary

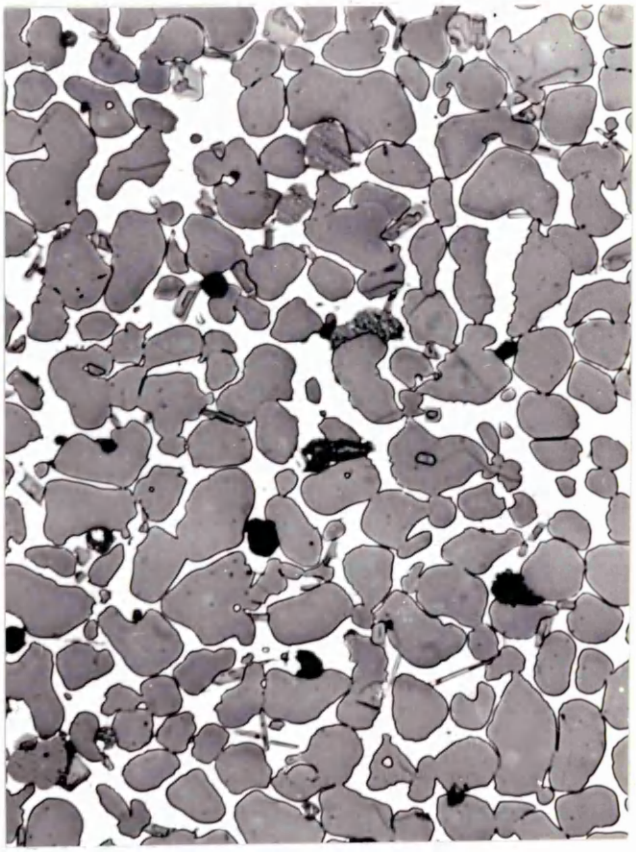

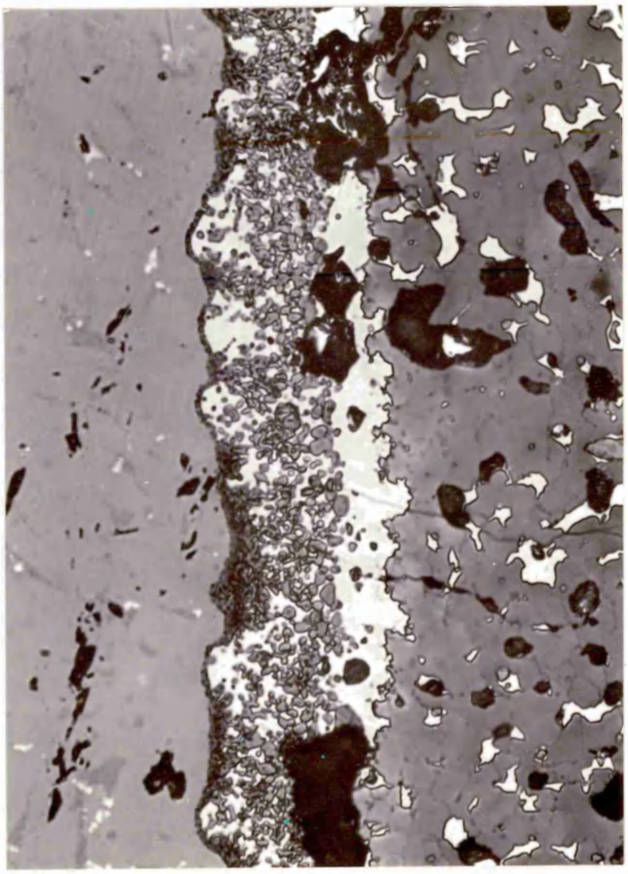

## Plate 44

Static small lime pellet $2\ FeO.SiO_2$ + MnO melt
3 minutes immersion x 400

The corrugations in the $2\ CaO.SiO_2$ rim becoming V shaped

## Plate 45

Static small lime pellet $2\ FeO.SiO_2$ + MnO melt
4 minutes immersion x 400

Breakout of liquid in the melt

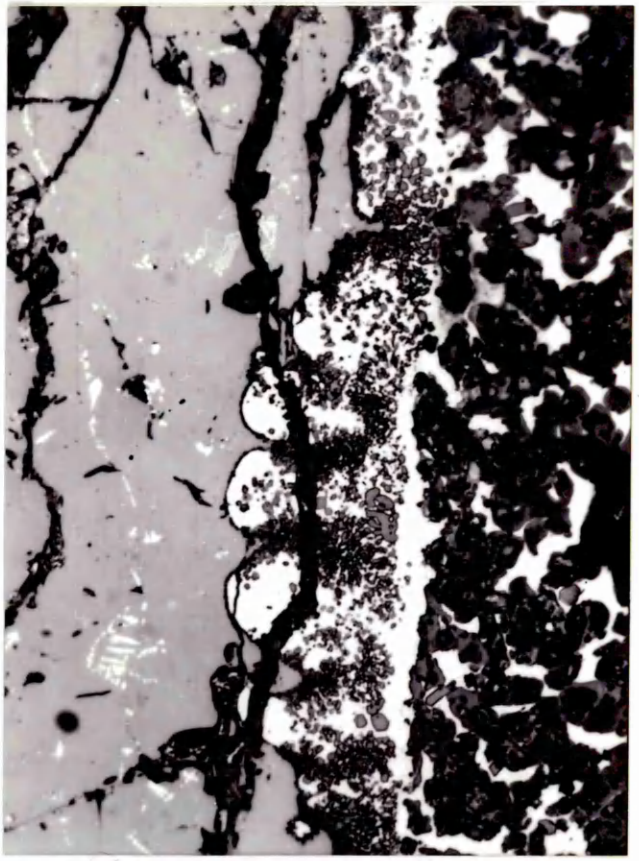

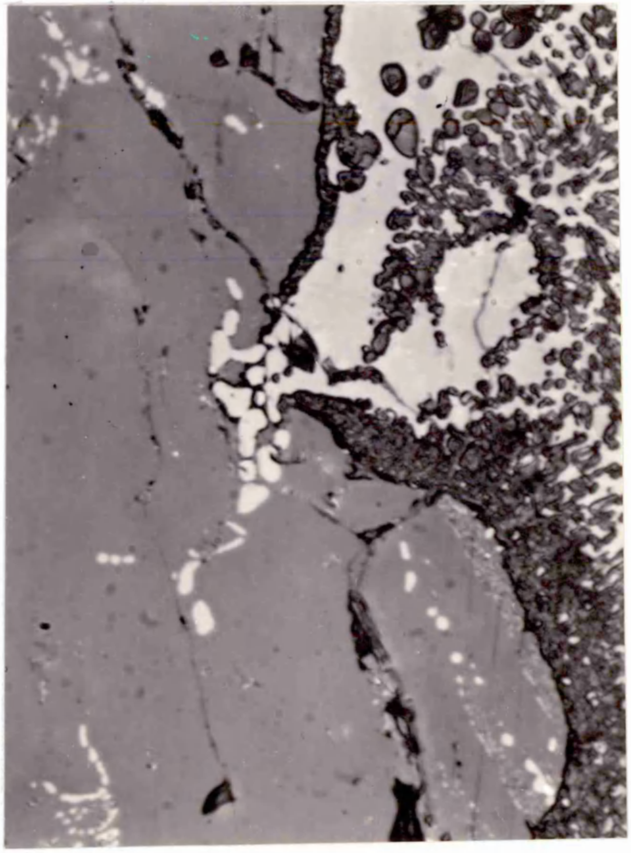

## Plate 46

Static small lime pellet
5 minutes immersion

$2\ FeO.SiO_2 + MnO$ melt
x 400

Large breakout of liquid in the melt. The breakout appeared single phased whilst the parent has a duplex structure on cooling

## Plate 47

Static small lime pellet
6 minutes immersion

$2\ FeO.SiO_2 + MnO$ melt
x 400

Two breakouts of liquid

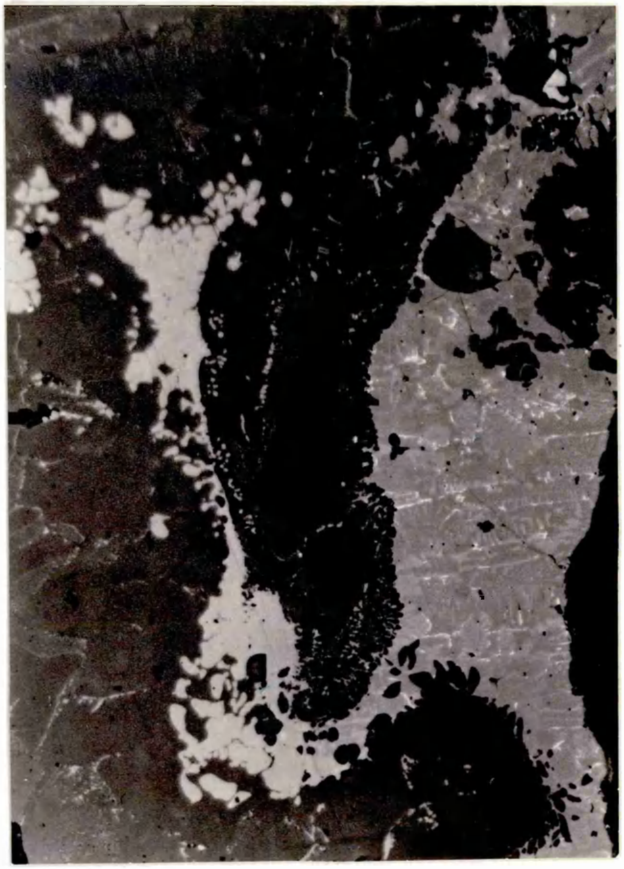

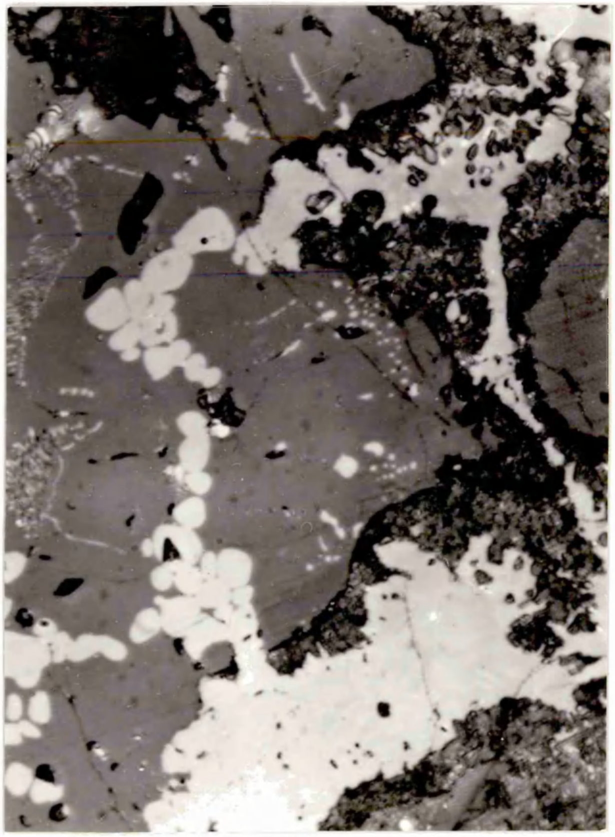

## Plate 46

Static small lime pellet $2\ FeO.SiO_2 + MnO$ melt
5 minutes immersion x 400

Large breakout of liquid in the melt. The breakout appeared single phased whilst the parent has a duplex structure on cooling

## Plate 47

Static small lime pellet $2\ FeO.SiO_2 + MnO$ melt
6 minutes immersion x 400

Two breakouts of liquid

## Plate 48

Static small lime pellet $\quad$ 2 $FeO.SiO_2$ + MnO melt
7 minutes immersion $\quad$ x 400

An elongated region of melt isolated in the liquid phase

## Plate 49

Static small lime pellet $\quad$ 2 $FeO.SiO_2$ + MnO melt
8 minutes immersion $\quad$ x 400

Spherical regions of melt surrounded by a 2 $CaO.SiO_2$ rim

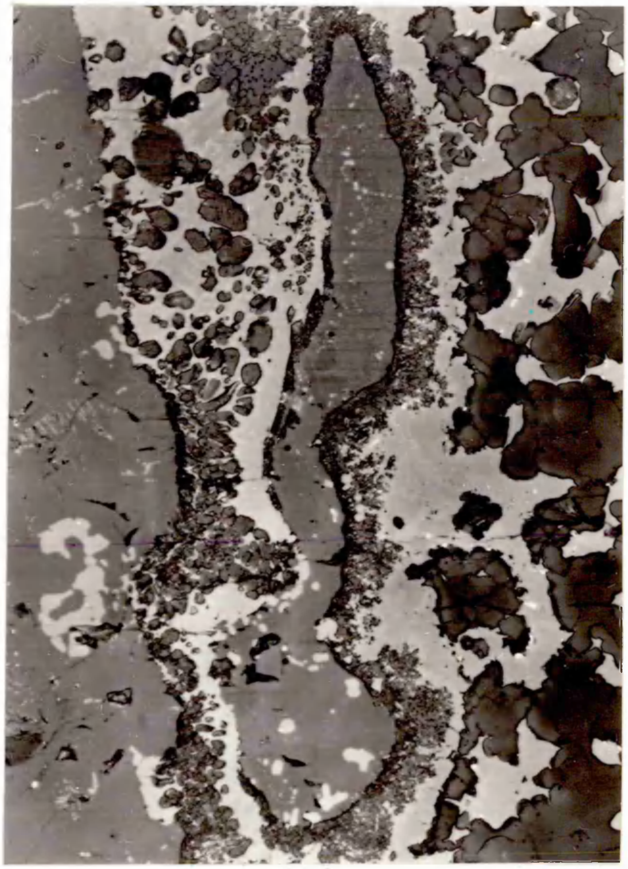

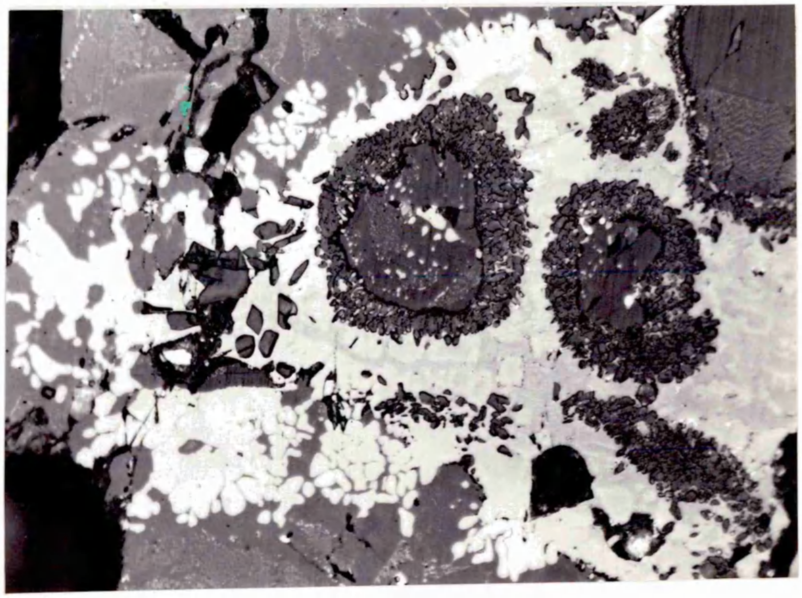

## Plate 50

| | |
|---|---|
| Rotated small lime pellet | 2 $FeO.SiO_2$ + MnO melt |
| 1 minute immersion | x 400 |

Corrugated 2 $CaO.SiO_2$ layer

## Plate 51

| | |
|---|---|
| Rotated small lime pellet | 2 $FeO.SiO_2$ + MnO melt |
| 3 minutes immersion | x 400 |

Disproportional distribution of 2 $CaO.SiO_2$ particles along the melt boundary

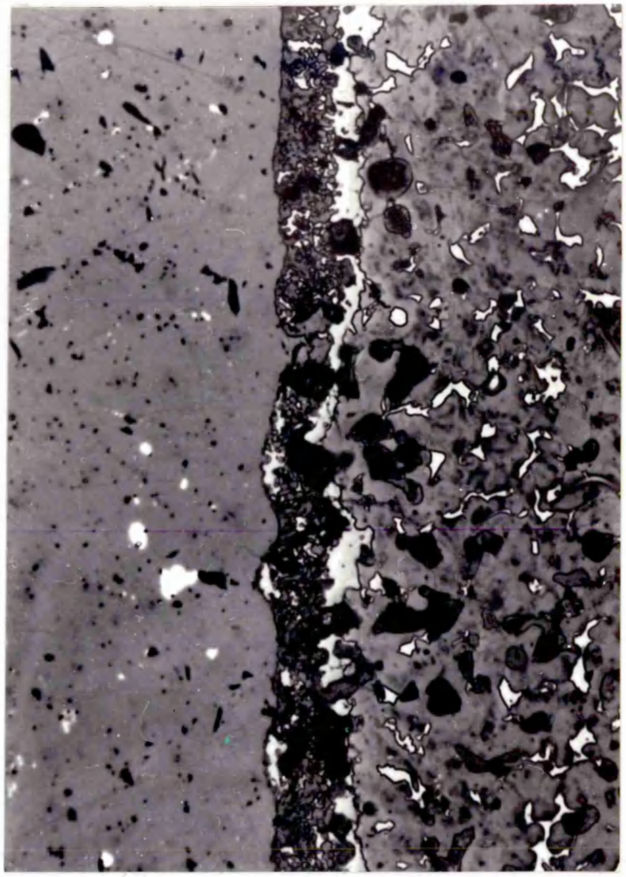

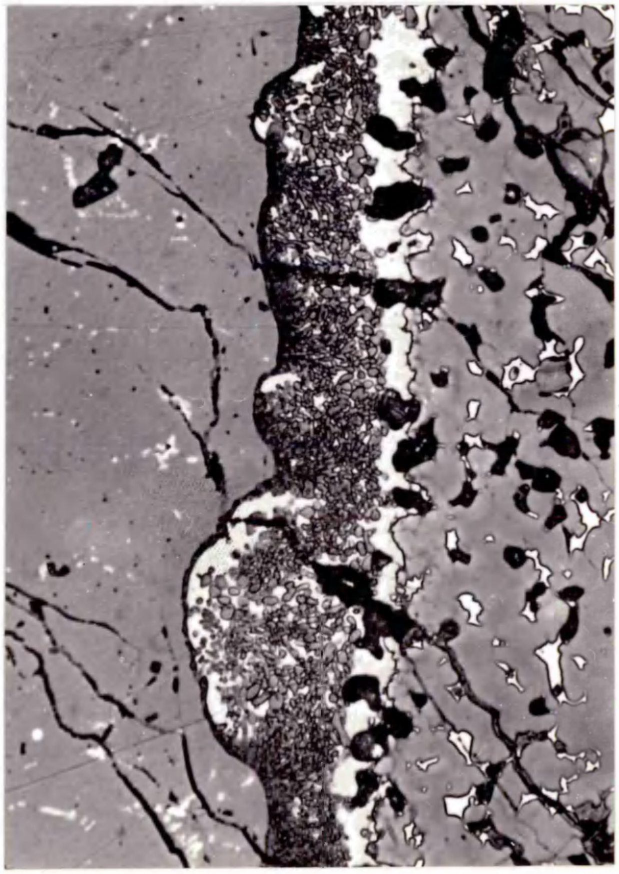

## Plate 52

Rotated small lime pellet  $2\,FeO.SiO_2 + MnO$ melt
3 minutes immersion  x 400

A region of liquid isolated by a large mass of $2\,CaO.SiO_2$

## Plate 53

Rotated small lime pellet  $2\,FeO.SiO_2 + MnO$ melt
5 minutes immersion  x 400

Large breakout of liquid in the melt. Note there was no $2\,CaO.SiO_2$ precipitate along the melt-breakout interface

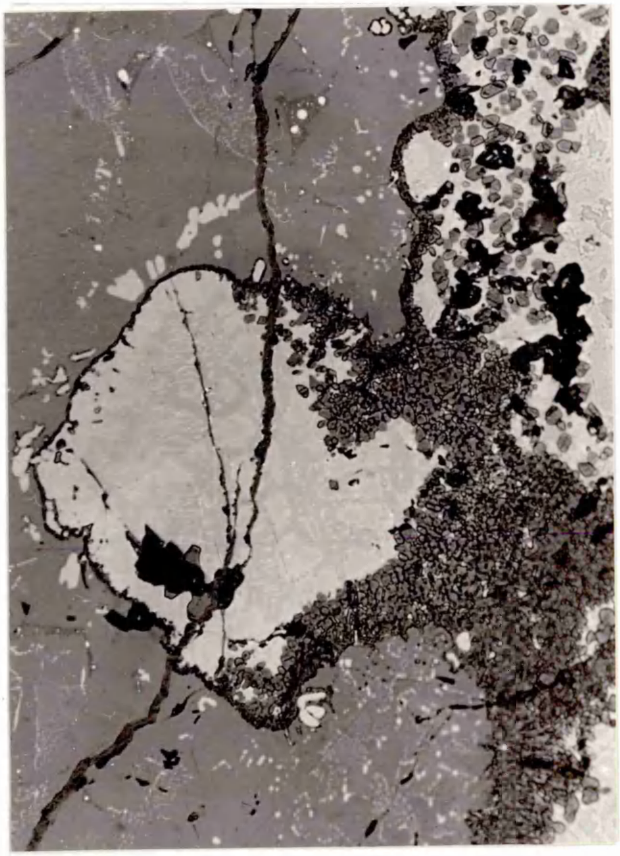

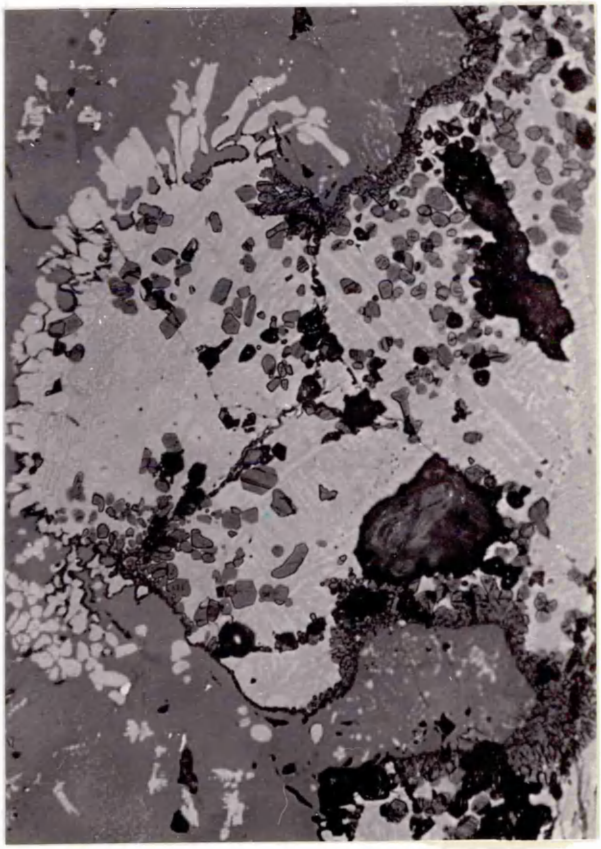

## Plate 54

Rotated small lime pellet $2\ FeO.SiO_2$ + MnO melt
6 minutes immersion x 400

Isolated region of melt

## Plate 55

Rotated small lime pellet $2\ FeO.SiO_2$ + MnO melt
7 minutes immersion x 400

Dissolving crystals of $3\ CaO.SiO_2$ (etched dark)

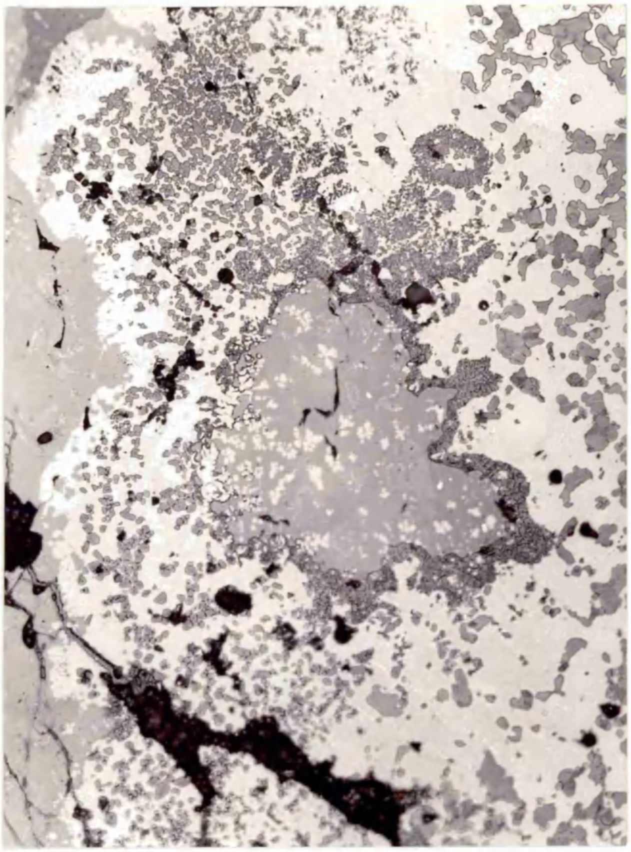

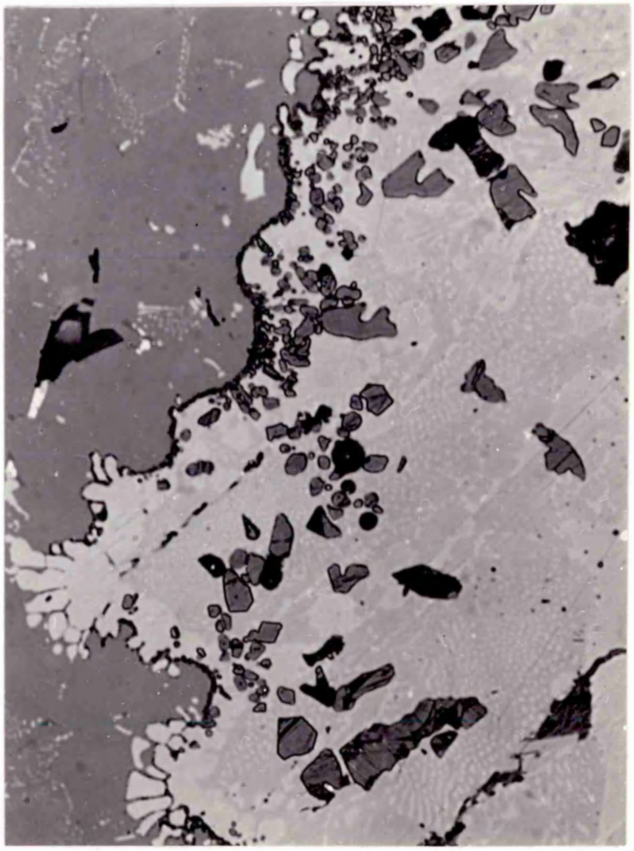

## Plate 56

5 minutes immersion

Section from the reaction zone between CaO and 2 $FeO.SiO_2$ + MnO

a. Electron Image

b. Calcium

c. X ray image for Silicon

d. Iron

e. Manganese

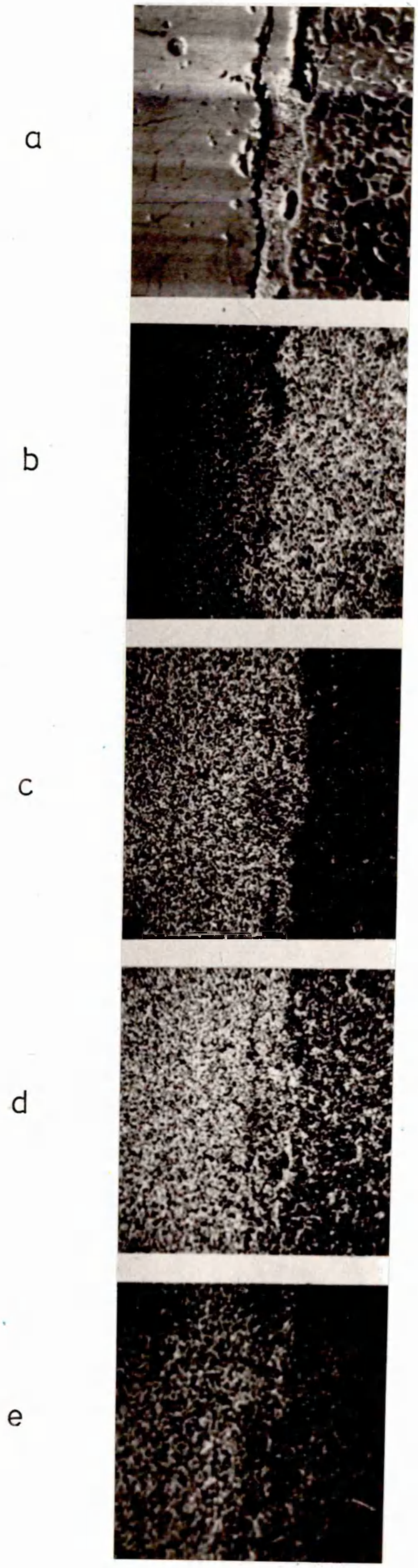
a
b
c
d
e

## Plate 57

5 minutes immersion

Breakout of liquid in the CaO - 2 $FeO.SiO_2$ + MnO system

a. Electron Image
b. Calcium
c. X ray image for Silicon
d. Iron
e. Manganese

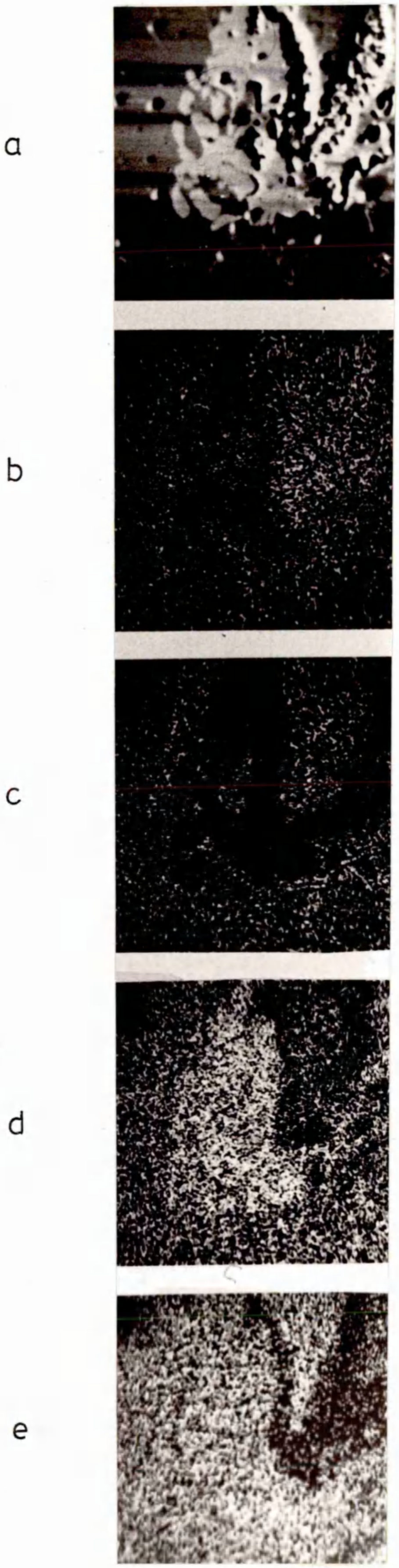
a
b
c
d
e

## Plate 58

Static large lime pellet — $2\ FeO.SiO_2 + MnO$ melt
1 minute immersion — x 400

Corrugated $2\ CaO.SiO_2$ layer along the melt boundary

## Plate 59

Static large lime pellet — $2\ FeO.SiO_2 + MnO$ melt
4 minutes immersion — x 400

Precipitation of $2\ CaO.SiO_2$ dendrites in the melt adjacent to the $2\ CaO.SiO_2$ layer

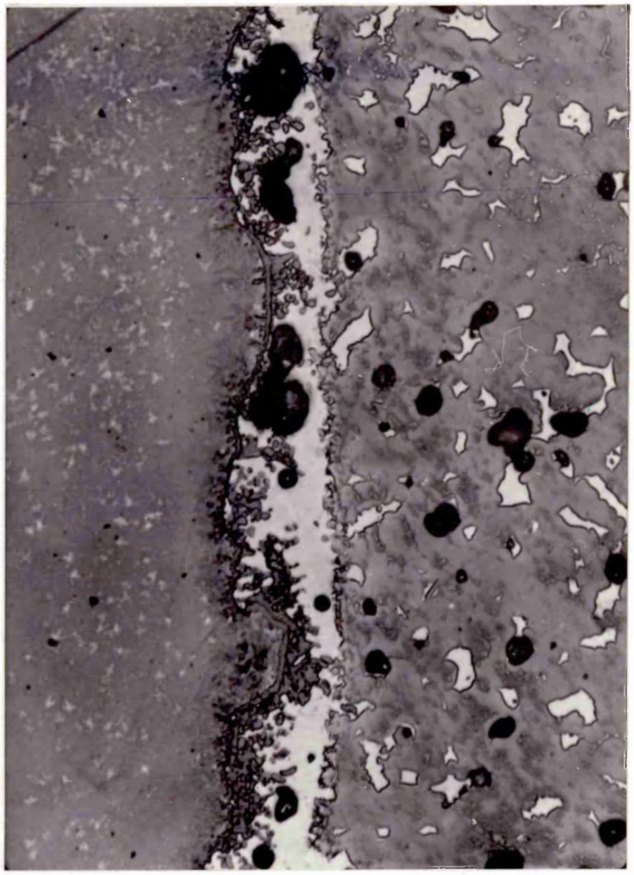

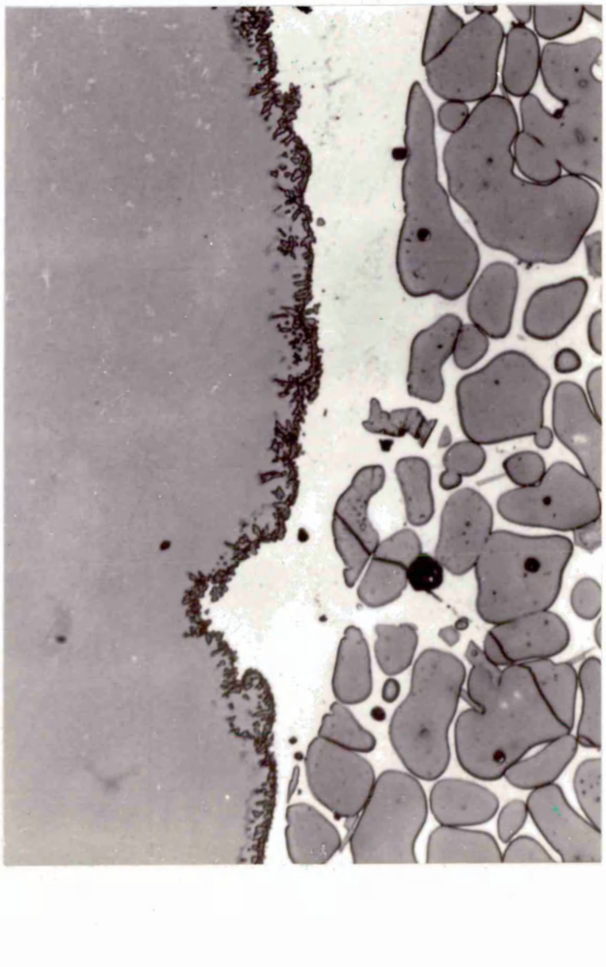

## Plate 60

Rotated large lime pellet — $2\ FeO.SiO_2$ + MnO melt
1 minute immersion — x 400

Corrugated layer of $2\ CaO.SiO_2$

## Plate 61

Rotated large lime pellet — $2\ FeO.SiO_2$ + MnO melt
3 minutes immersion — x 400

A continuous $2\ CaO.SiO_2$ rim with no liquid breakouts

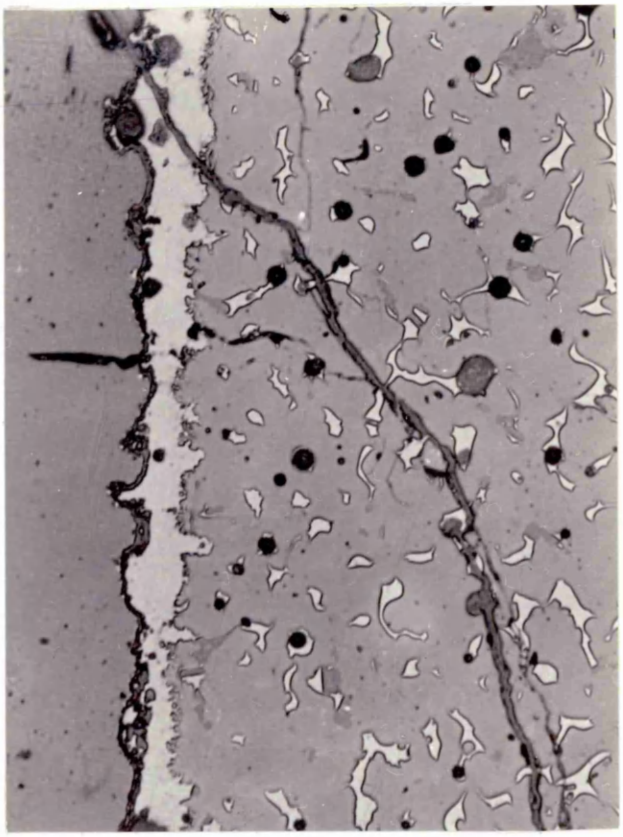

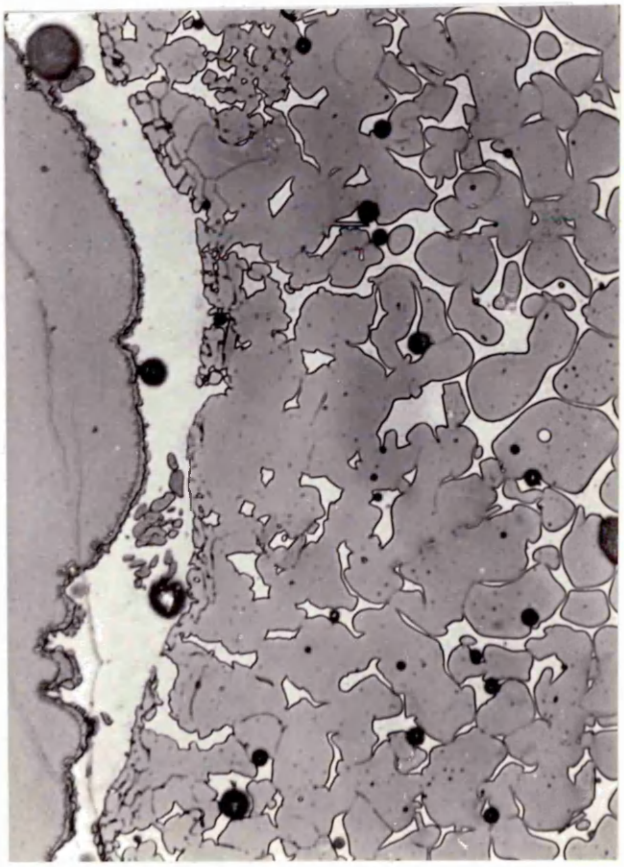

## Plate 62

| | |
|---|---|
| Rotated large lime pellet | 2 FeO.$SiO_2$ + MnO melt |
| 5 minutes immersion | x 400 |

Thin layer of 2 CaO.$SiO_2$ along the melt boundary

## Plate 63

| | |
|---|---|
| Static large lime pellet | 2 FeO.$SiO_2$ melt |
| 5 minutes immersion | x 400 |

The photomicrograph shows the reaction interface inside a longitudinal groove. Although the 2 CaO.$SiO_2$ layer had corrugated, therewere no breakouts

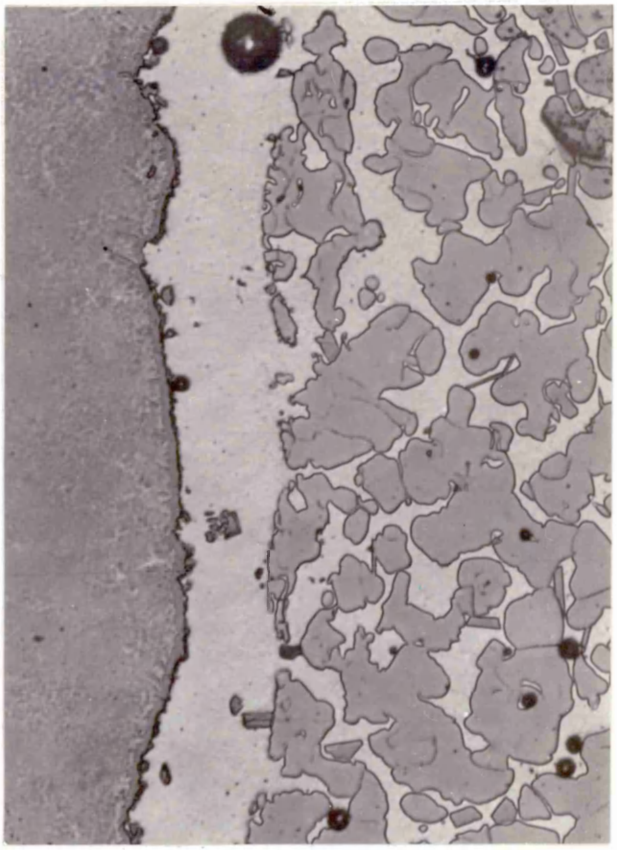

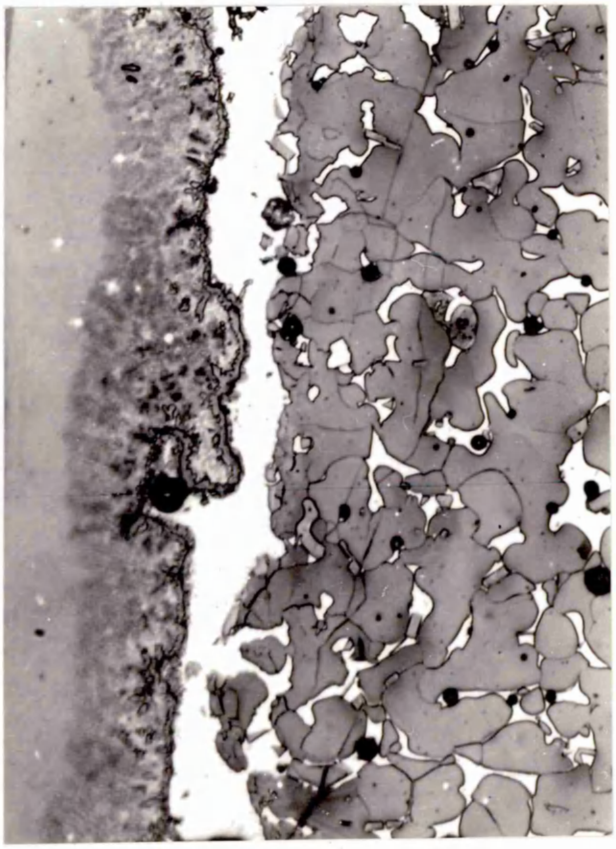

## Plate 64

Static large lime pellet
5 minutes immersion

$2\ FeO.SiO_2 + MnO$ melt
x 400

The photomicrograph shows the reaction interface inside a longitudinal groove. There were numerous breakouts of liquid through a discontinuous $2\ CaO.SiO_2$ layer

## Plate 65

Static small lime pellet
15 seconds immersion

$2\ FeO.SiO_2 + CaF_2$ melt
x 160

$2\ CaO.SiO_2$ (etched dark) appeared as individual horseshoe shaped particles in the liquid phase

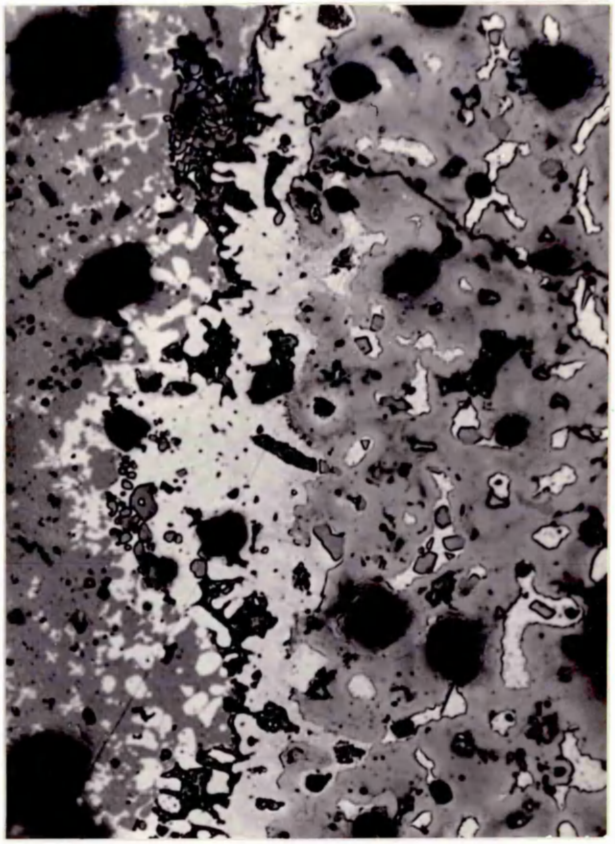

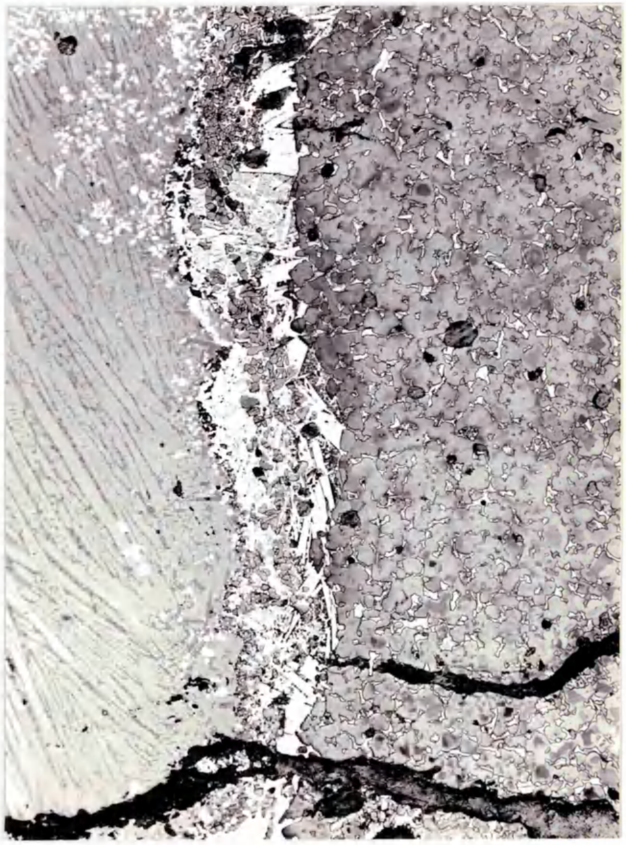

## Plate 66

Static small lime pellet — $2\,FeO.SiO_2 + CaF_2$ melt
15 seconds immersion — x 400

Higher magnification of area in Plate 65

## Plate 67

Static small lime pellet — $2\,FeO.SiO_2 + CaF_2$ melt
15 seconds immersion — x 400

Increasing proportion of lime-iron oxide eutectic towards the centre of the specimen

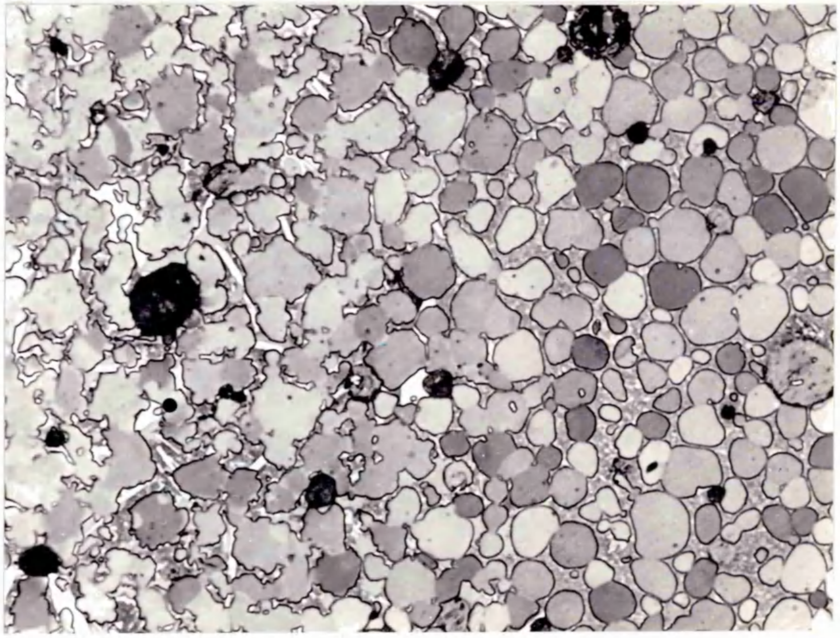

## Plate 68

Static small lime pellet
30 seconds immersion

2 $FeO.SiO_2 + CaF_2$ melt
x 400

Precipitation of 2 $CaO.SiO_2$ dendrites during cooling

## Plate 69

Static small lime pellet
30 seconds immersion

2 $FeO.SiO_2 + CaF_2$ melt
x 800

Dendrites of wustite in the melt. There was also horseshoe shaped crystals of an another phase (marked X). 2 $CaO.SiO_2$ is etched black on the R.H.S. of the photomicrograph

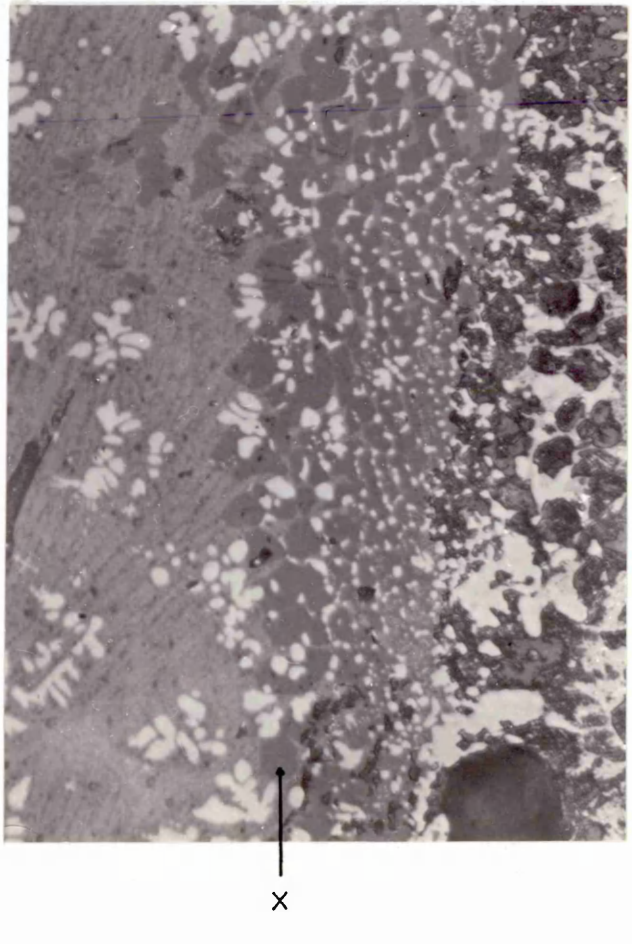
X

## Plate 70

| | |
|---|---|
| Rotated small lime pellet | 2 $FeO.SiO_2$ + $CaF_2$ melt |
| 15 seconds immersion | x 150 |

Large number of 2 $CaO.SiO_2$ particles precipitated isothermally and athermally

## Plate 71

| | |
|---|---|
| Rotated small lime pellet | 2 $FeO.SiO_2$ + $CaF_2$ melt |
| 30 seconds immersion | x 150 |

2 $CaO.SiO_2$ dendrites precipitated during cooling

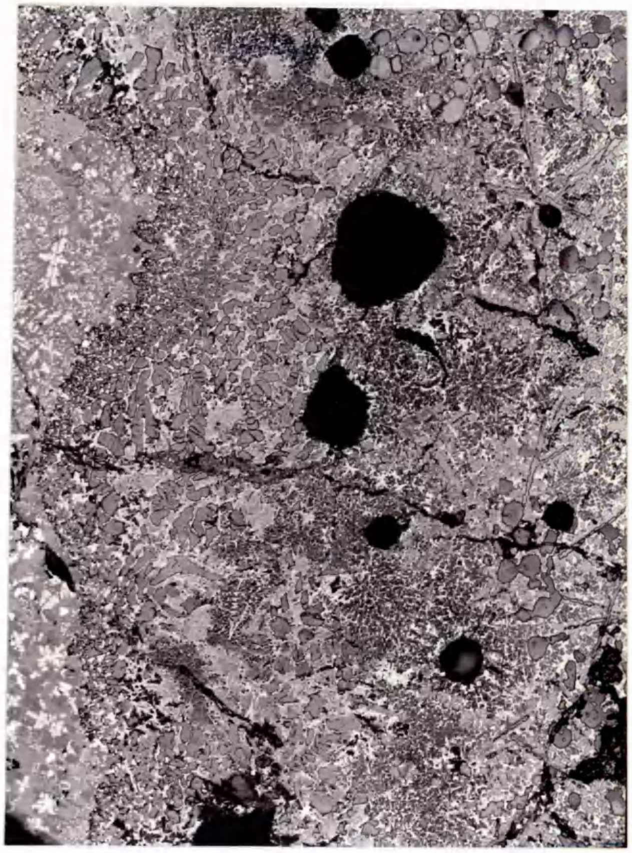

# Plate 72

30 seconds immersion

Section of the reaction zone between CaO and $2\ FeO.SiO_2 + CaF_2$

a. Electron Image

b. ⎡ Calcium
c. X ray image for ⎨ Silicon
d. ⎣ Iron

a

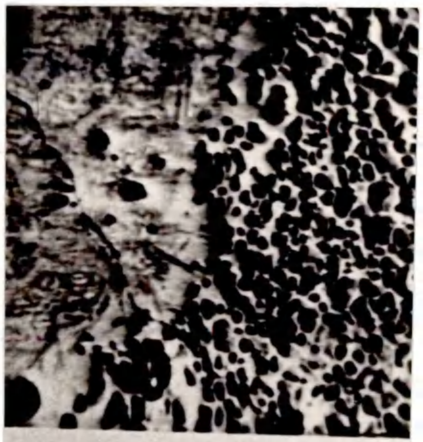

b

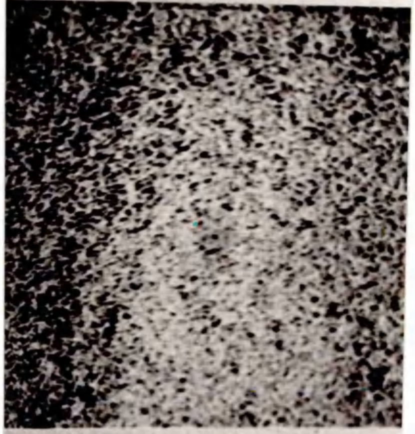

c

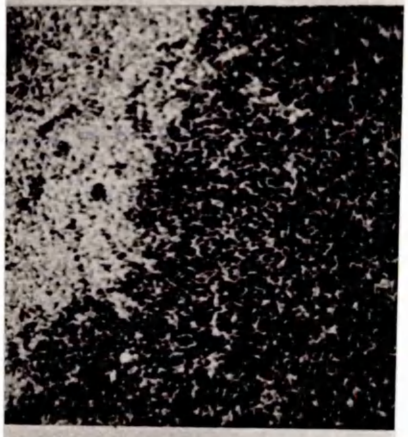

d

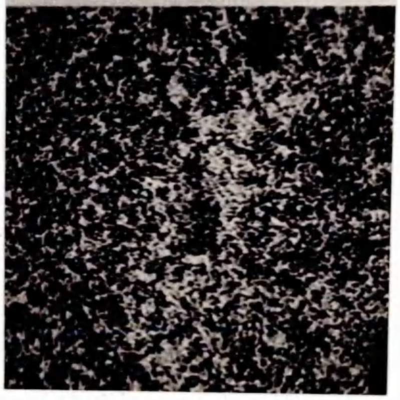

## Plate 73

Static large lime pellet $\quad$ $2\ FeO.SiO_2 + CaF_2$ melt
30 seconds immersion $\quad$ x 400

Rounded particles of $2\ CaO.SiO_2$ and angular crystals of $3\ CaO.SiO_2$ undergoing resolution

## Plate 74

Cross - section of static large lime pellets x 3

a. immersed for 30 seconds in $2\ FeO.SiO_2 + CaF_2$ melt

b. immersed for 4 minutes in $2\ FeO.SiO_2$ - showing unreacted core of free lime

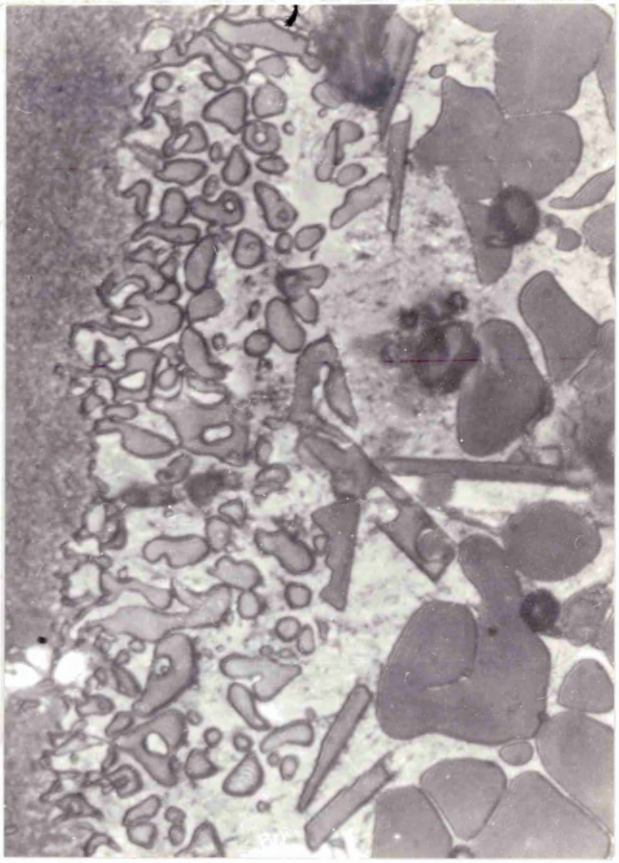

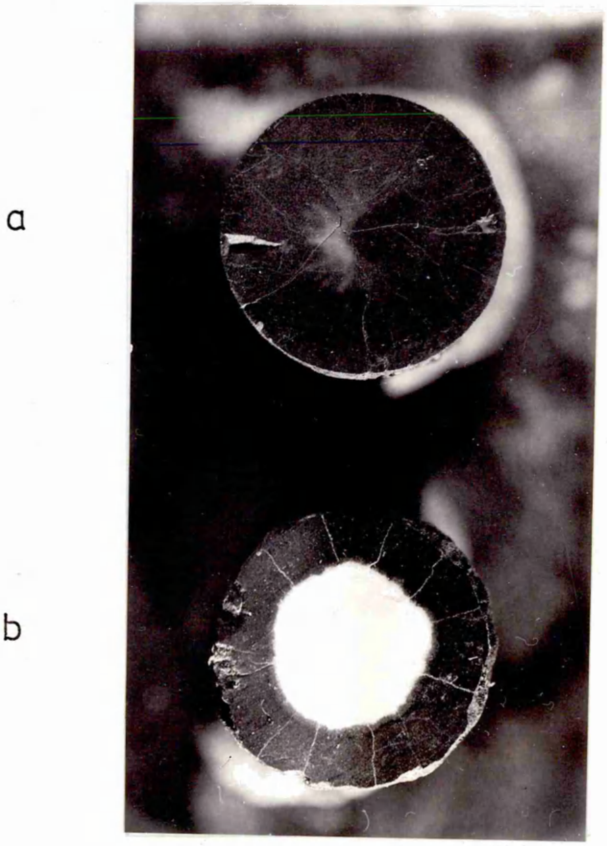
a
b

## Plate 75

Static large lime pellet
1 minute immersion

$2\ FeO.SiO_2 + CaF_2$ melt
x 400

Wustite dendrites in the melt

## Plate 76

Static large lime pellet
1.5 minutes immersion

$2\ FeO.SiO_2 + CaF_2$ melt
x 400

Increasing proportion of wustite dendrites in the melt

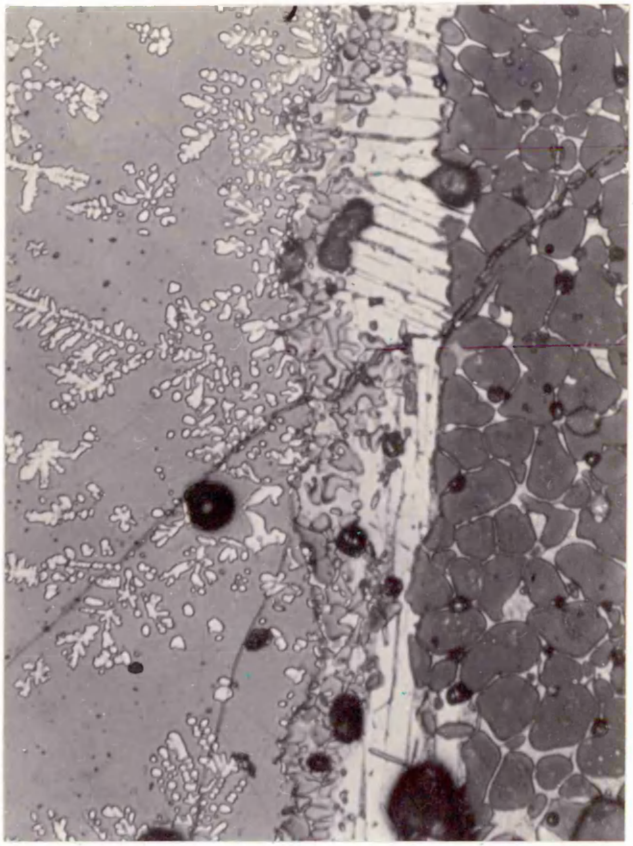

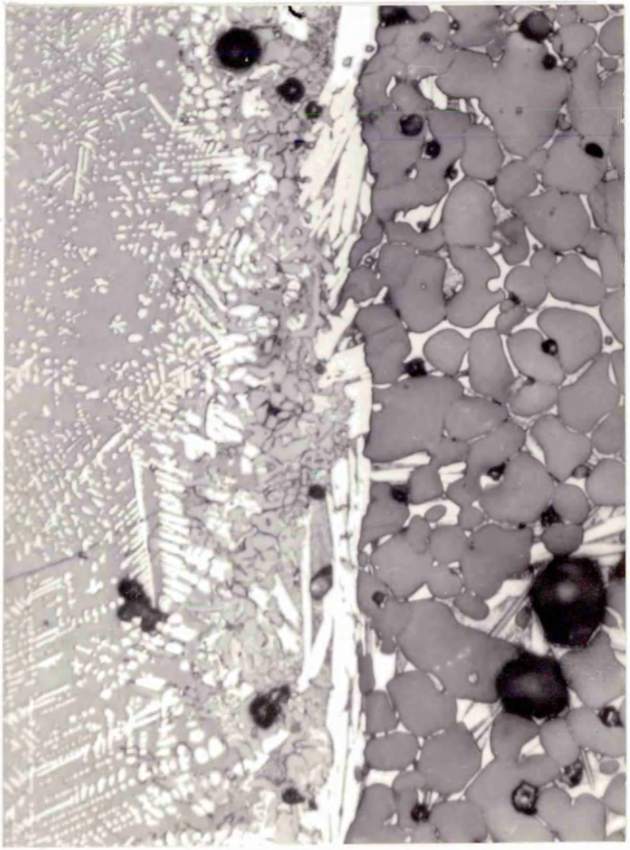

# Plate 77

| | |
|---|---|
| Rotated large lime pellet | 2 $FeO.SiO_2$ + $CaF_2$ melt |
| 15 seconds immersion | x 100 |

Horseshoe shaped particles of 2 $CaO.SiO_2$ and 3 $CaO.SiO_2$ dissolving in the liquid phase

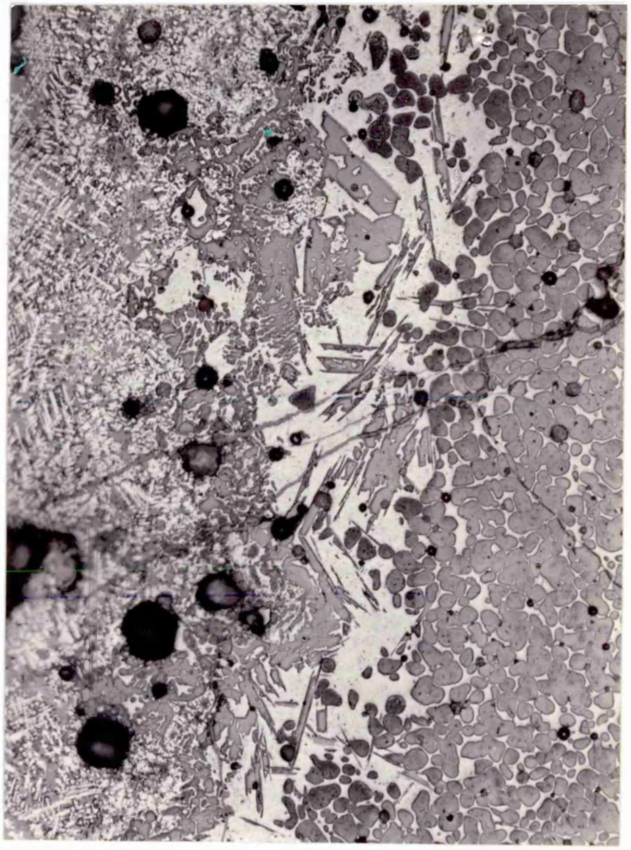

## Plate 78

Rotated large lime pellet 30 seconds immersion

$2\ FeO.SiO_2 + CaF_2$ melt x 1000

The characteristic twinning of $2\ CaO.SiO_2$ associated with the $\alpha' \longrightarrow \beta$ transformation

## Plate 79

Rotated large lime pellet 30 seconds immersion

$2\ FeO.SiO_2 + CaF_2$ melt x 1000

Angular crystals of $3\ CaO.SiO_2$ dissolving in the liquid phase. The solid surfaces acting as sites for nucleation and growth processes during cooling

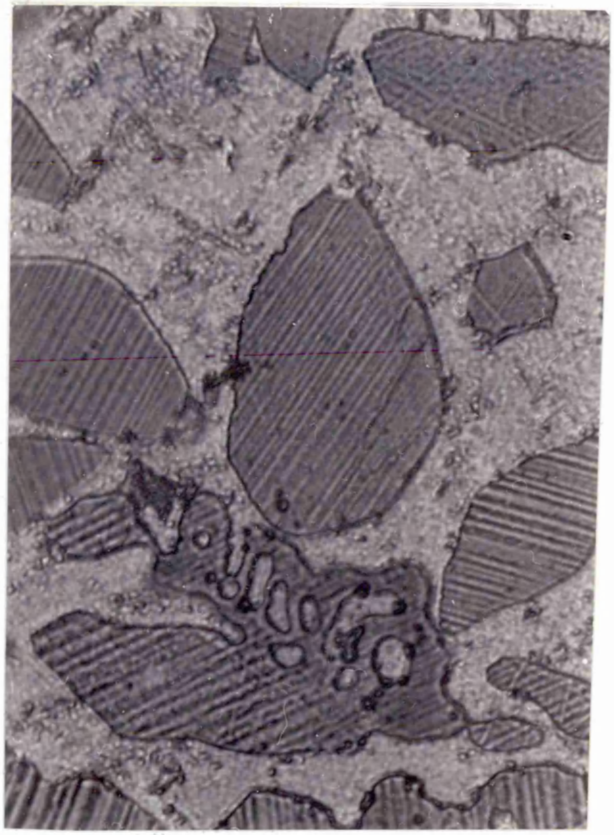

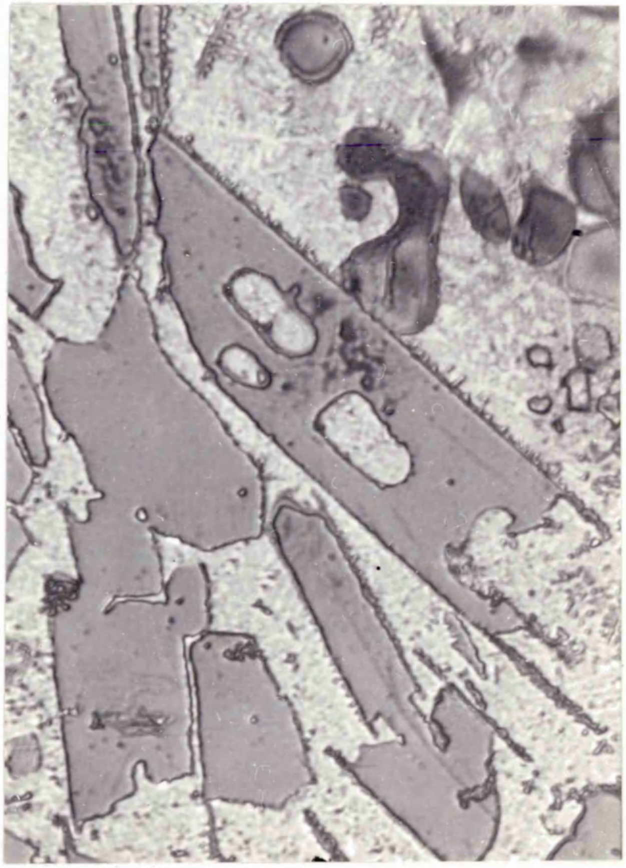

## Plate 80

Static small lime pellet
15 seconds immersion

$2\ FeO.SiO_2 + B_2O_3$ melt
x 400

Thick layer of $2\ CaO.SiO_2$ along the melt boundary

## Plate 81

Static small lime pellet
15 seconds immersion

$2\ FeO.SiO_2 + B_2O_3$ melt
x 400

Liquid breakout in the melt

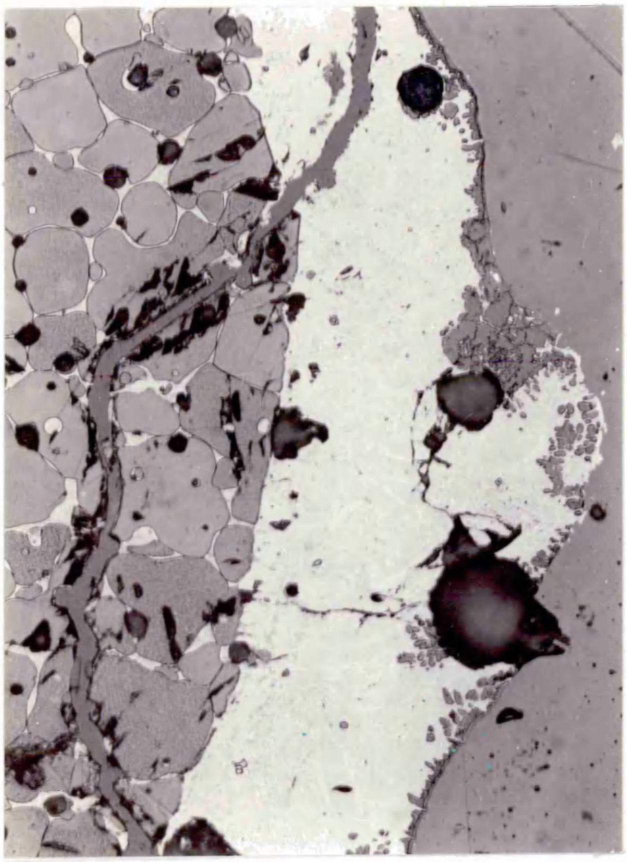

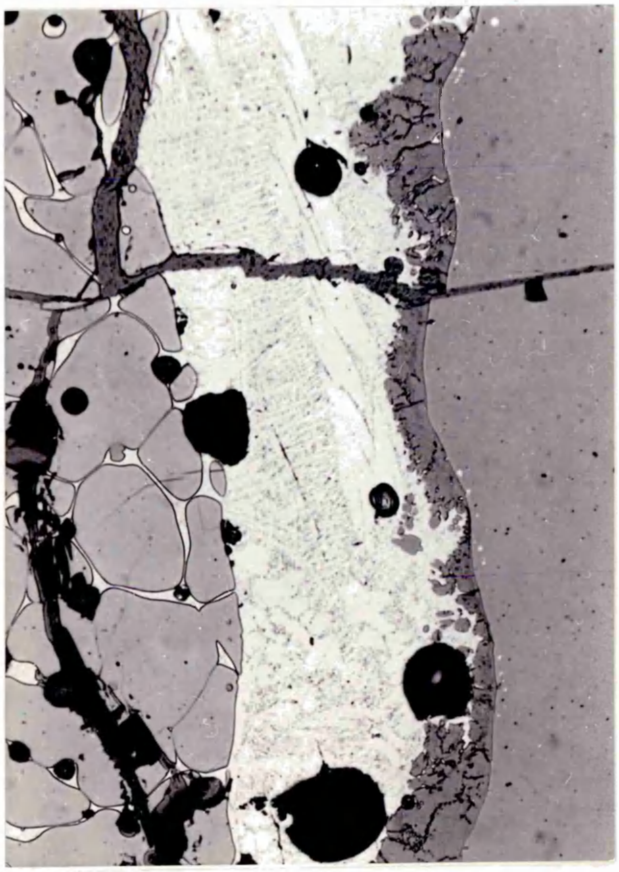

## Plate 82

Static small lime pellet — $2\ FeO.SiO_2 + B_2O_3$ melt
15 seconds immersion — x 400

Rapid infiltration and dissolution of the pellet by the iron oxide rich liquid

## Plate 83

Static small lime pellet — $2\ FeO.SiO_2 + B_2O_3$ melt
30 seconds immersion — x 400

Dissolution of $2\ CaO.SiO_2$ by the melt and the liquid phase

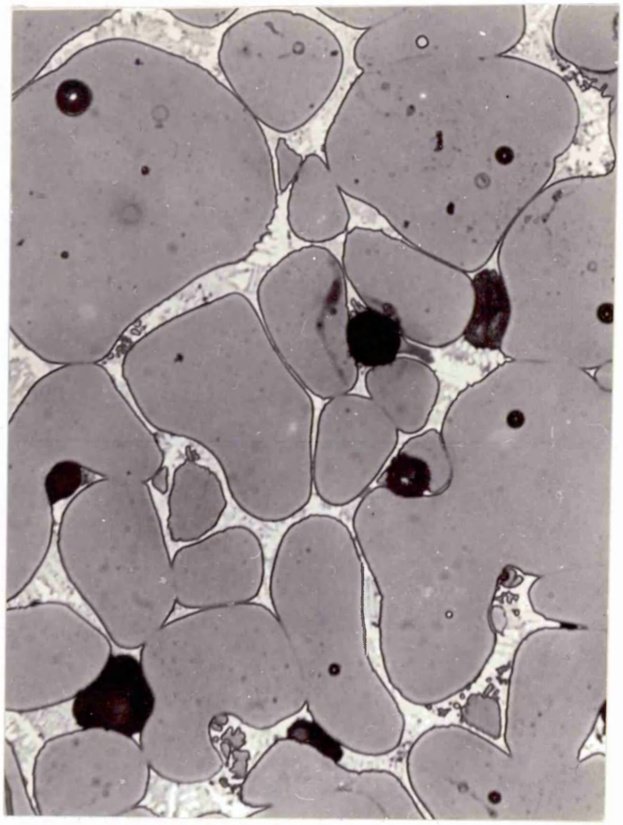

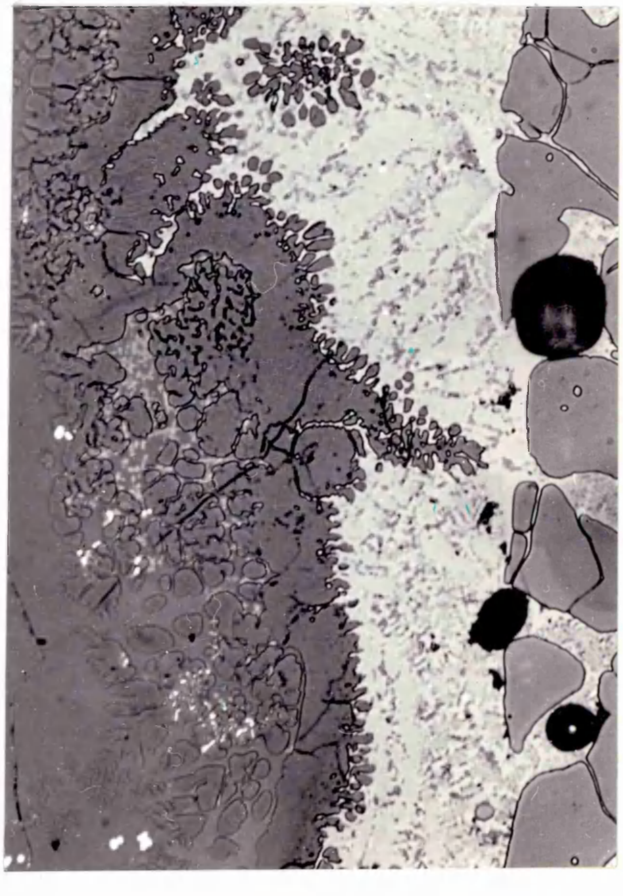

## Plate 84

Static small lime pellet / 30 seconds immersion — $2\ FeO.SiO_2 + B_2O_3$ melt, x 250

Encapsulated region of melt

# Plate 85

45 seconds immersion

Section from the reaction zone between CaO and 2 $FeO.SiO_2$ + $B_2O_3$

a. Electron Image

| | | |
|---|---|---|
| b. | X ray image for | Calcium |
| c. | | Silicon |
| d. | | Iron |

a

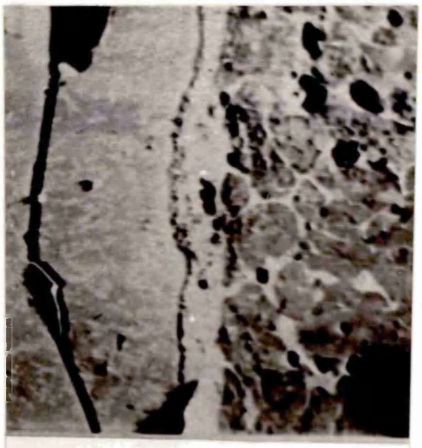

b

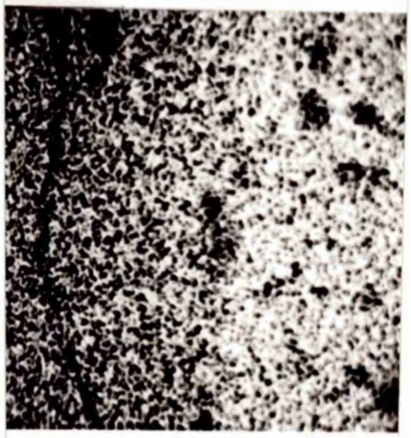

c

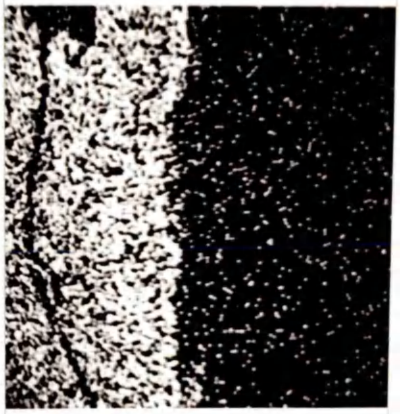

d

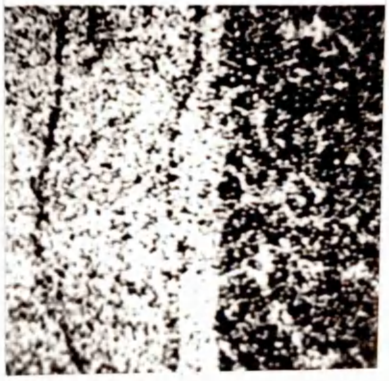

## Plate 86

Static large lime pellet
15 seconds immersion

2 $FeO.SiO_2 + B_2O_3$ melt
x 400

Large equiaxed particles of 2 $CaO.SiO_2$ along the melt boundary

## Plate 87

Static large lime pellet
30 seconds immersion

2 $FeO.SiO_2 + B_2O_3$ melt
x 400

Corrugated layer of 2 $CaO.SiO_2$ particles

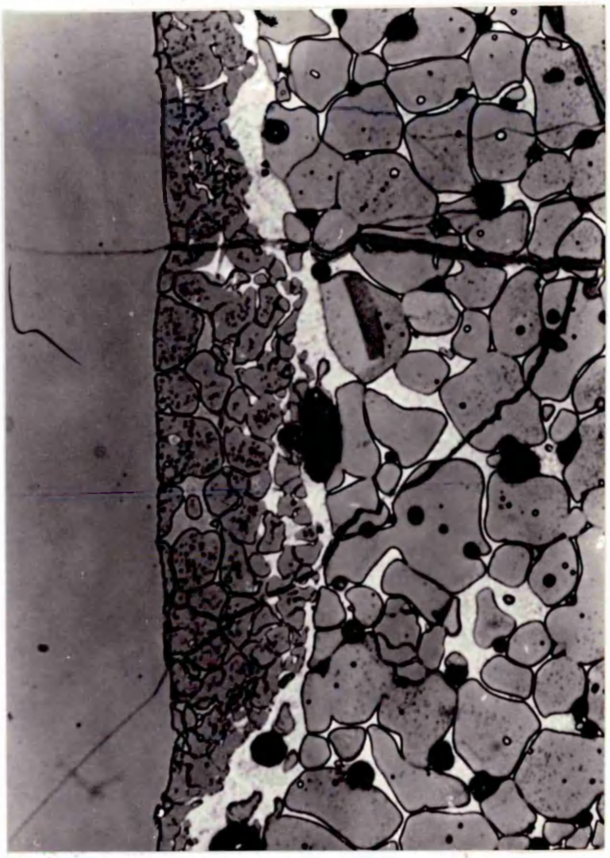

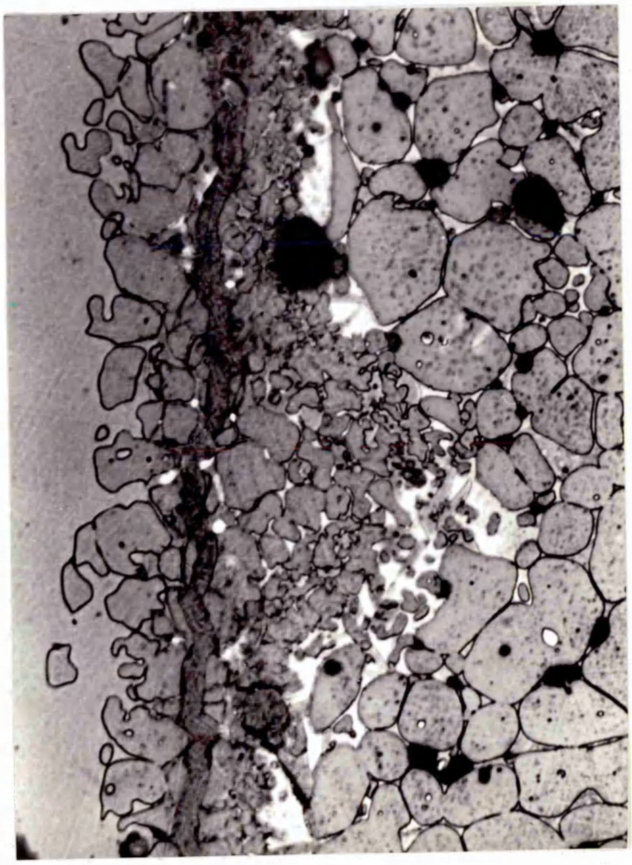

## Plate 88

Static large lime pellet
30 seconds immersion

2 $FeO.SiO_2 + B_2O_3$ melt
x 100

Liquid breakouts in the melt

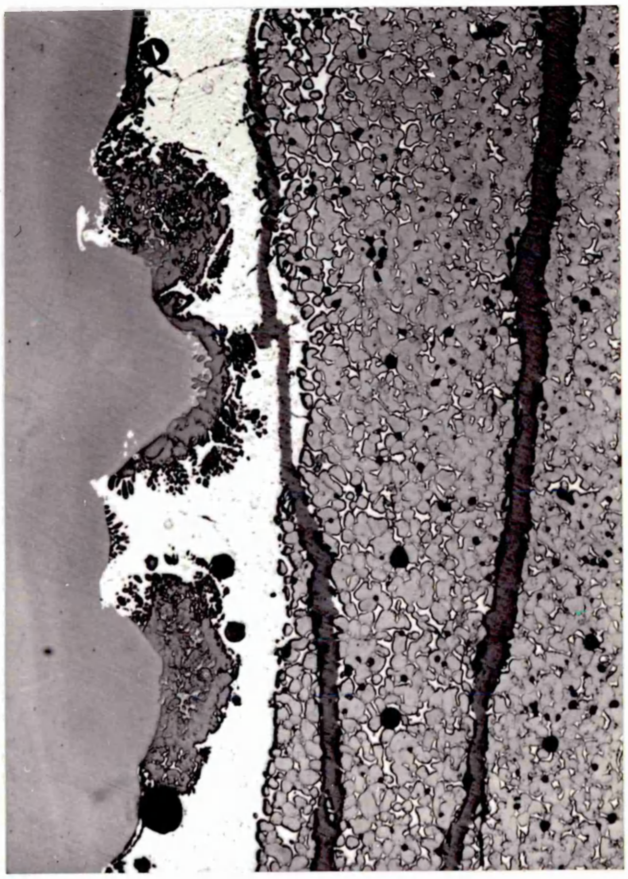

## Plate 89

Static pellet of $2\ CaO.SiO_2$ $2\ FeO.SiO_2$ melt
15 seconds immersion x 400

Rapid infiltration of the pellet by the melt

## Plate 90

Static pellet of $2\ CaO.SiO_2$ $2\ FeO.SiO_2$ melt
15 seconds immersion x 400

Grains showing the characteristic twinning of $2\ CaO.SiO_2$

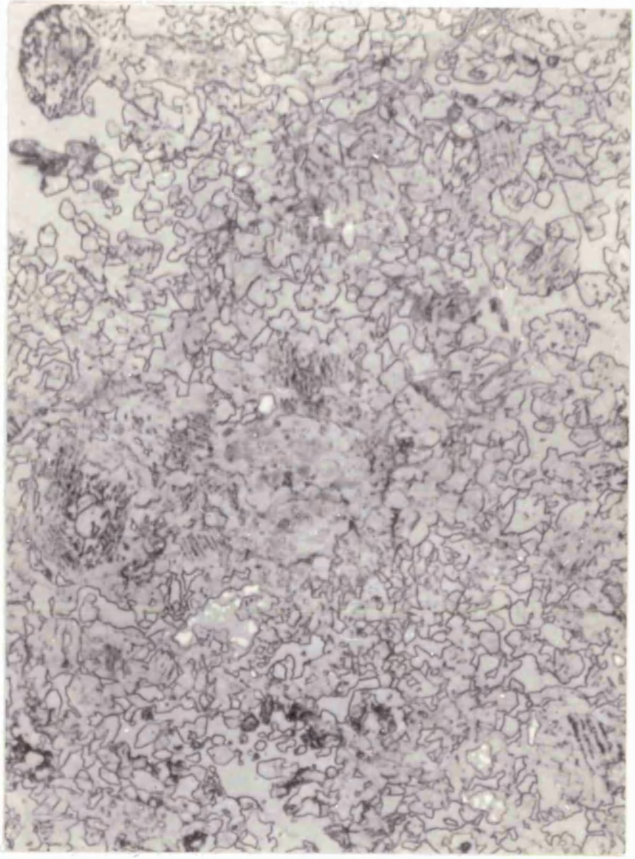

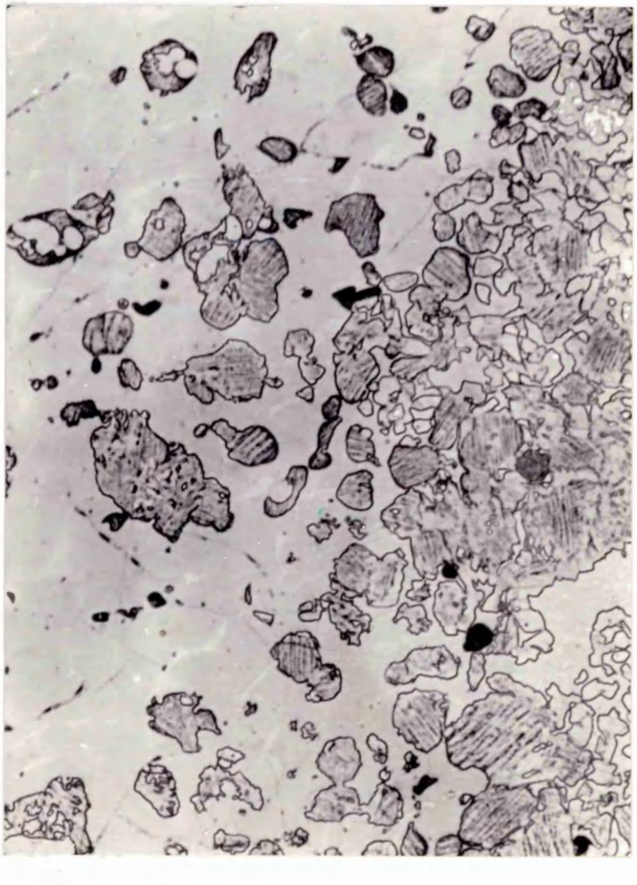

## Plate 91

Static pellet of 2 $CaO.SiO_2$ 2 $FeO.SiO_2$ melt
30 seconds immersion x 400

Large quantity of melt inside the pellet. The grains etched lighter than the melt

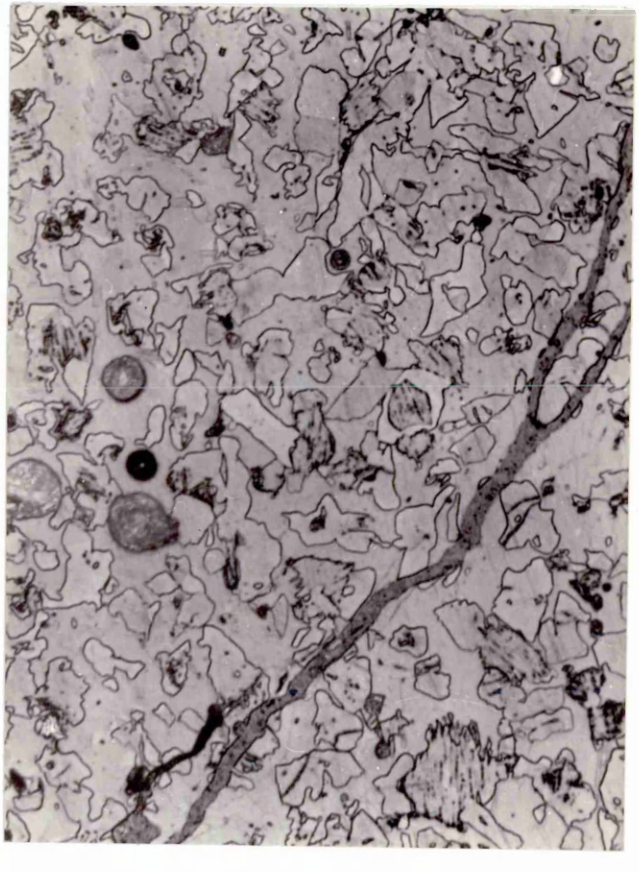

# Plate 92

15 seconds immersion

Section of reaction zone between 2 $CaO.SO_2$ and 2 $FeO.SiO_2$

a. Electron Image

b. Calcium

c. X ray image for Silicon

d. Iron

a

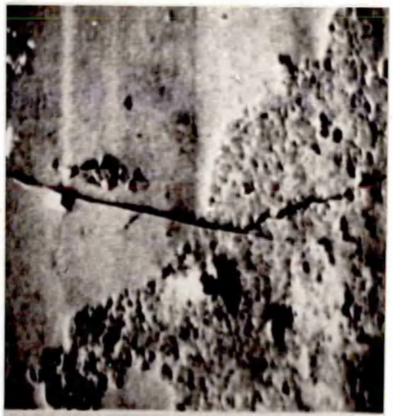

b

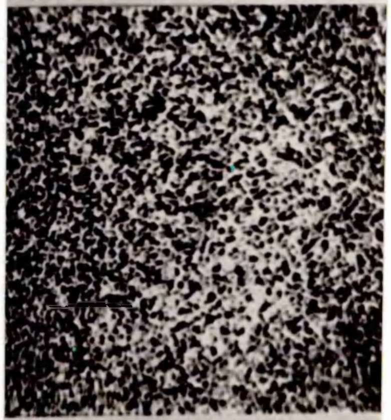

c

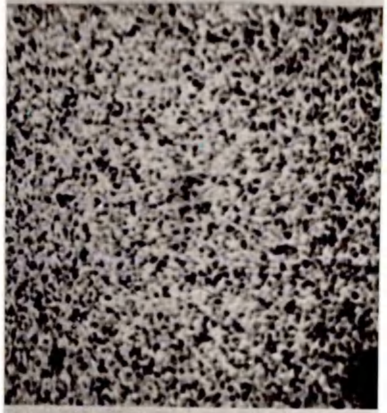

d

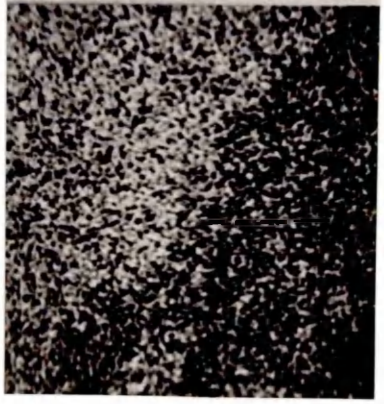

## Plate 93

Static commercial lime — 2 $FeO.SiO_2$ melt
2 minutes immersion — x 400

Dendrites of 2 $CaO.SiO_2$ along the melt boundary

## Plate 94

Static commercial lime — 2 $FeO.SiO_2$ melt
4 minutes immersion — x 400

Corrugated 2 $CaO.SiO_2$ layer with no discontinuities. The thick band running down the centre of the photomicrograph is mounting compound.

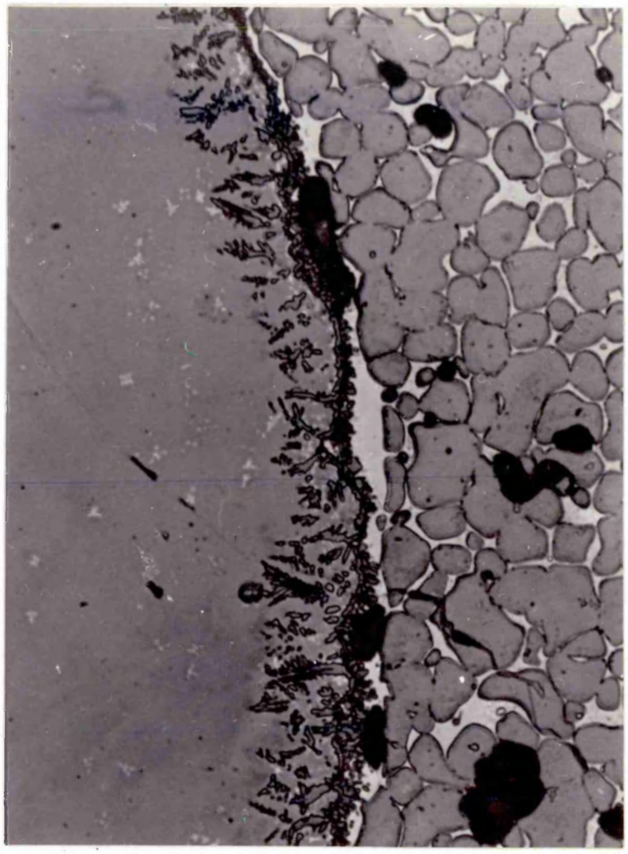

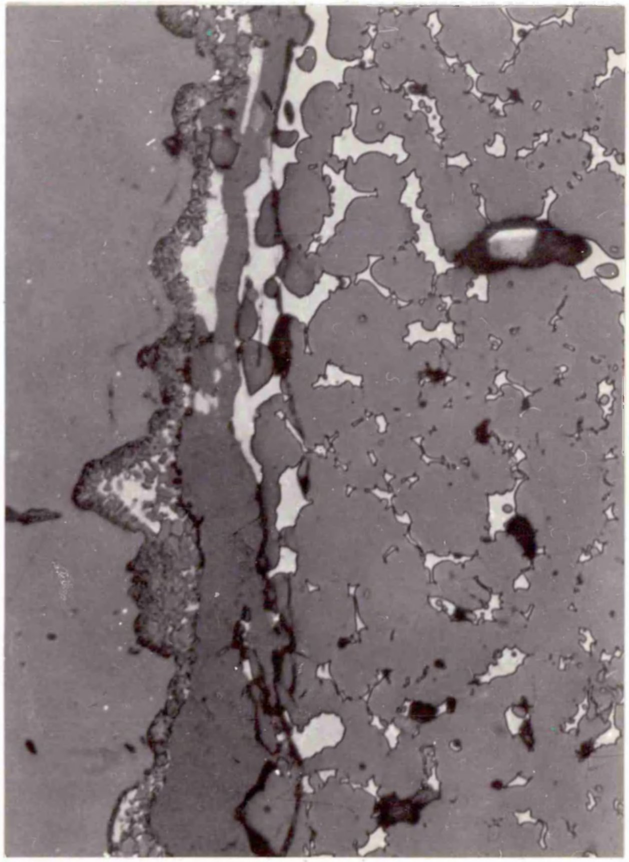

## Plate 95

Static commercial lime — 2 $FeO.SiO_2$ melt
4 minutes immersion — x 1000

The individual lime particleswere not dissolving uniformily

## Plate 96

Static commercial lime — 2 $FeO.SiO_2$ melt
6 minutes immersion — x 400

Corrugated 2 $CaO.SiO_2$ layer along the melt boundary

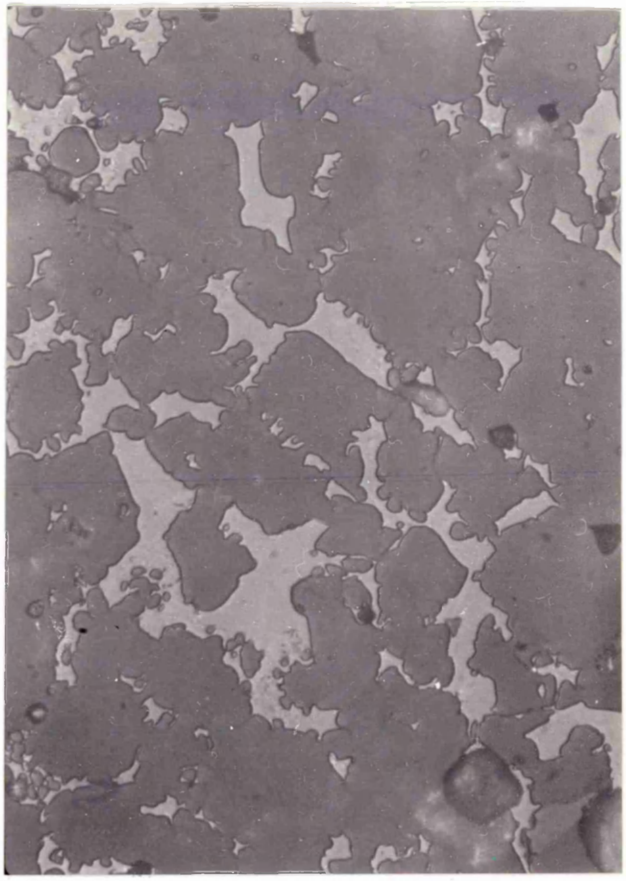

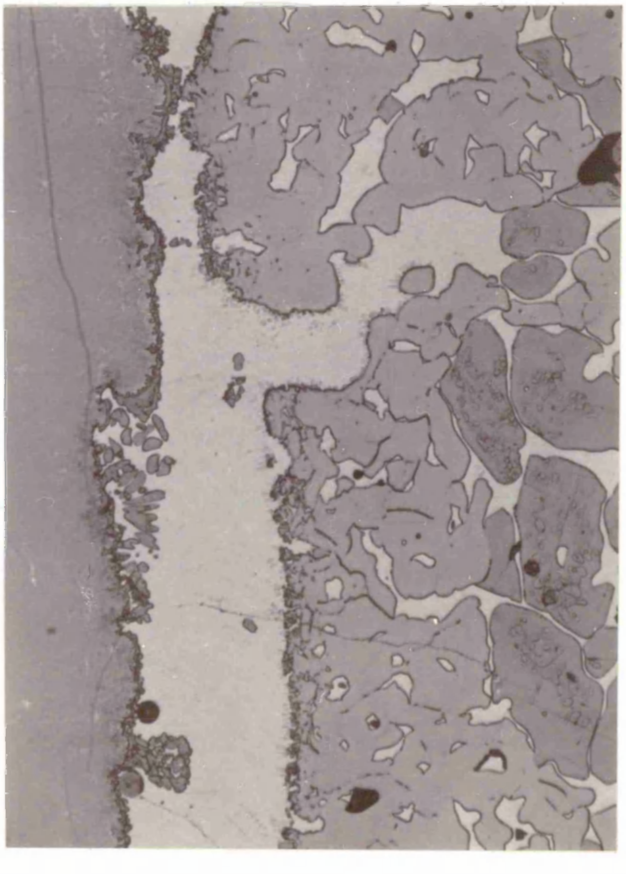

## Plate 97

Static commercial lime — $2\ FeO.SiO_2$ + MnO melt
2 minutes immersion — x 400

Therewere a large number of light coloured particles along the melt boundary. The white colour suggested theywere iron oxide rich.

## Plate 98

Static commercial lime — $2\ FeO.SiO_2$ + MnO melt
4 minutes immersion — x 400

A number of liquid breakouts in the melt

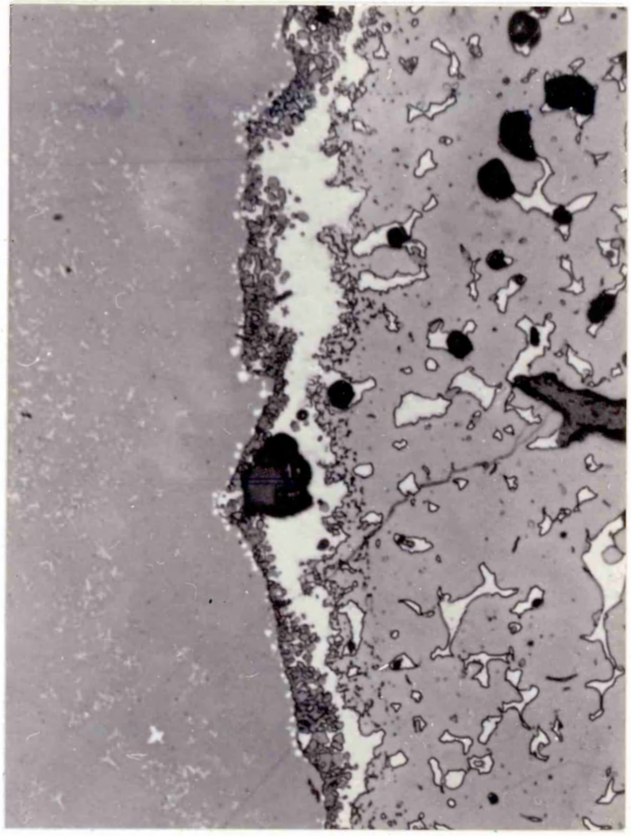

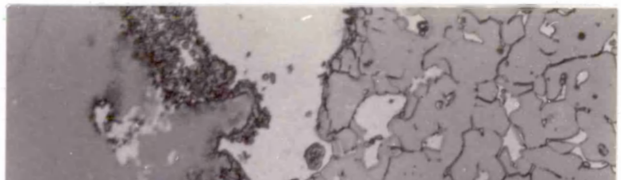

## Plate 99

Static commercial lime
6 minutes immersion

$2\ FeO.SiO_2 + MnO$ melt
x 400

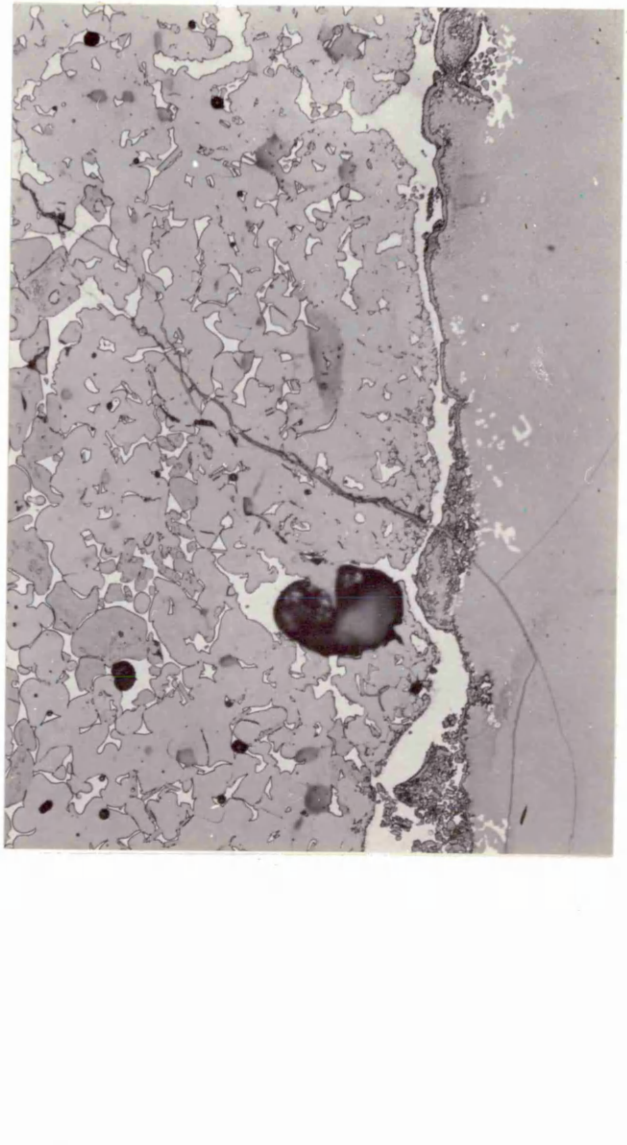Corrugated $2\ CaO.SiO_2$ layer with liquid breakouts